

UC Irvine

UC Irvine Electronic Theses and Dissertations

Title

Characterization of Aeroengine Lean Direct Injector Concept Adapted for Low NO_x Power Generation Using Hydrogen

Permalink

<https://escholarship.org/uc/item/5n1136z3>

Author

Tran, Britney Lam

Publication Date

2022

Peer reviewed|Thesis/dissertation

UNIVERSITY OF CALIFORNIA,
IRVINE

Characterization of Aeroengine Lean Direct Injector Concept Adapted for Low NO_x Power
Generation Using Hydrogen

THESIS

Submitted in partial satisfaction of the requirements
for the degree of

MASTER OF SCIENCE

in Mechanical and Aerospace Engineering

by

Britney L. Tran

Thesis Committee:
Professor Jack Brouwer, Chair
Professor Vincent McDonell
Professor Bihter Padak

2022

Table of Contents

List of Tables	iv
List of Figures	vi
Acknowledgements	xiii
ABSTRACT OF THE THESIS	xiv
1. Introduction	1
2. Literature Review	6
2.1 Pollutant Emissions from Combustion of Fuel and Air	6
2.1.1 Fuel NO _x Mechanism	6
2.1.2 Prompt NO _x Mechanism	7
2.1.3 Thermal NO _x Mechanism	8
2.1.4 NNH Pathway	8
2.1.5 N ₂ O Pathway	9
2.1.6 Other Pollutants	10
2.2 Hydrogen Advantages	11
2.3 Hydrogen Challenges	12
2.4 Strategies to Lower NO _x Emissions	14
2.4.1 Water Injection	15
2.4.2 Ultra-Lean Fuel Mixtures	15
2.4.3 Micromixers	16
2.4.4 Post Combustion Strategies	28
2.5 Remaining Research Questions	28
3. Approach	31
4. Methodology	36
4.1 Experimental Methods	36
4.1.1 Methodology for Effective Area Tests	41
4.1.2 Methodology for Emissions Measurement	46
4.2 Numerical Analysis	49
4.2.1 CRNs and CHEMKIN	49
4.2.3 CFD and ANSYS Fluent	51
4.2.4 ANOVA	52
5. Results and Discussion	55

5.1 ANOVA Analysis	57
5.1.1 CO Model	57
5.1.2 NO Model	64
5.1.3 NO _x Model	89
5.1.4 NO/NO _x Model	115
5.1.5 Lower Temperature (1100-1300K) Matrix.....	126
5.1.6 Optimization	134
5.2 CHEMKIN	139
5.2.1 Fully Premixed vs. Non Premixed.....	144
5.2.2 Heat Loss Study.....	146
5.2.3 Chemical Kinetics Analysis.....	147
6. Summary, Conclusions, and Recommendations	161
6.1 Summary	161
6.2 Conclusions	167
6.3 Recommendations	169
7. Appendices	171
7.1 Appendix A: Effective Area Tests	171
7.2 Appendix B: Emissions on a Volume vs. a Mass Basis.....	173
7.3 Appendix C: Volume/Confinement Study	176
7.4 Appendix D: Supplementary Tables and Figures	179
References	230

List of Tables

Table 1. Summary of NO _x Mechanisms.....	10
Table 2. Current Micromixing Technology	24
Table 3. Factors for Test Plan.....	34
Table 4. Responses for Test Plan.....	34
Table 5. Test configurations	45
Table 6. Comparison Between the NO and NO _x Model	104
Table 7. Predicted Emissions for Optimization Study with Flame Temperature Range 1500-1850K.....	135
Table 8. Predicted Emissions for Optimization Study with Flame Temperature Range 1500-1850K.....	136
Table 9. Optimization Model for Hydrogen for Various Flame Temperatures	137
Table 10. Optimization Model for Methane for Various Flame Temperature	137
Table 11. CHEMKIN Volume vs. Measured Volume.....	143
Table 12. Varying Heat Loss Assumptions with Accompanying Emissions Data.....	147
Table A- 1. Effective Areas for Air and Fuel Circuits.....	171
Table A- 2. Calibration Curves Used in Effective Area Tests.....	172
Table A- 3. Expected vs. Actual % O ₂ from Emissions Test.....	173
Table A- 4. Cylinder Characteristics	177
Table A- 5. Emissions Data for Volume/ Confinement Study	178
Table A- 6. Standard Order for Test Matrix	180
Table A- 7. Corresponding Air Flow Rates in SCFM at Specified Preheat Temperatures and Pressure Drops for Injector 3	182
Table A- 8. Actual Pressure Drops for Injector 1 with Respect to Injector 3.....	182
Table A- 9. Actual Pressure Drops for Injector 2 with Respect to Injector 3.....	182
Table A- 10. Actual Pressure Drops for Injector 4 with Respect to Injector 3.....	183
Table A- 11. Actual Pressure Drops for Injector 5 with Respect to Injector 3.....	183
Table A- 12. Actual Pressure Drops for Injector 8 with Respect to Injector 3.....	183
Table A- 13. Actual Pressure Drops for Injector 10 with Respect to Injector 3.....	183
Table A- 14. Flow Rates for Test Matrix.....	184
Table A- 15. Emissions Results for Injector 1	185

Table A- 16. Emissions Results for Injector 2	187
Table A- 17. Emissions Results for Injector 3	189
Table A- 18. Emissions Results for Injector 4	190
Table A- 19. Emissions Results for Injector 5	192
Table A- 20. Emissions Results for Injector 6	194
Table A- 21. Emissions Results for Injector 7	196
Table A- 22. Emissions Results for Injector 8	197
Table A- 23. Emissions Results for Injector 9	199
Table A- 24. Emissions Results for Injector 10	201
Table A- 25. Emissions Results for Injector 11	202
Table A- 26. Emissions Results for Injector 12	204
Table A- 27. Emissions Results for Injector 13	206
Table A- 28. Emissions Results for Injector 14	207
Table A- 29. Emissions Results for Injector 15	209
Table A- 30. Emissions Results for Injector 16	211
Table A- 31. CO Emissions Experimental vs. CHEMKIN, 15% O2 ppmvd	215
Table A- 32. NO Emissions Experimental vs. CHEMKIN, 15% O2 ppmvd	217
Table A- 33. NOx Emissions Experimental vs. CHEMKIN, 15% O2 ppmvd	219
Table A- 34. CO Emissions Experimental vs. CHEMKIN Model, ng/J	220
Table A- 35. NO Emissions Experimental vs. CHEMKIN Model, ng/J	222
Table A- 36. NOx Emissions Experimental vs. CHEMKIN Model, ng/J	224
Table A- 37. Perfectly Premixed CHEMKIN Results	225

List of Figures

Figure 1. Smog in Los Angeles on July 15, 1978 [4]	1
Figure 2. Mitsubishi’s Dry Low NOx Combustor [9]	17
Figure 3. Parker Hannifin’s Micromixing Injector [44]	17
Figure 4. (Left) Swirl Radial Cup [43] and (Right) Mixed Axial and Swirl Cup [50].....	18
Figure 5. Honeywell’s Garrett GTCP 36-300 [48]	19
Figure 6. GE’s F Class Engines Multi-Tube Concept [36].....	20
Figure 7. Mitsubishi’s Plate Flat (Left) and Convex (Right) Plate [8]	21
Figure 8. Kawasaki’s Micromixing Gas Turbine [57].....	22
Figure 9. Solar Turbine’s Micromixing Injector [59].....	23
Figure 10. Top Collins Injector Plate.....	37
Figure 11. Bottom Heater Plate	37
Figure 12. Airbox with Side Ports	38
Figure 13. Yor Lok Fittings	38
Figure 14. Completed Airbox Setup on the Test Stand	39
Figure 15. Pressure Transducer Routed to the Airbox.....	40
Figure 16. Heater with Connections	41
Figure 17. Heater Controller Box	41
Figure 18. Airline Connections.....	43
Figure 19. (a) Plate Configuration 1, (b) Plate Configuration 2, (c) Plate Configuration 3	44
Figure 20. Injectors 1-16 (Left to Right)	46
Figure 21. PG 350 Emissions Analyzer Machine.....	47
Figure 22. ANOVA Results for CO Model	58
Figure 23. CO Model	59
Figure 24. Predicted vs. Actual for CO Model.....	59
Figure 25. Flame Temperature vs. Fuel Composition for CO Model.....	61
Figure 26. CO Emissions vs. Air Splits	63
Figure 27. CO Emissions vs. Air Swirl.....	63
Figure 28. CO Emissions vs. Preheat Temperature. (No Squared Terms)	63
Figure 29. CO Emissions vs. Fuel Composition. (No Squared Terms).....	63
Figure 30. CO Emissions vs. Flame Temperature	63

Figure 31. NO Emissions vs. Run Number, Sorted by Injector Number.....	65
Figure 32. ANOVA Results for the NO Model	67
Figure 33. NO Model.....	68
Figure 34. Predicted vs. Actual for NO Model.....	69
Figure 35. Higher Air Split Injectors by Run Number	71
Figure 36. Higher Air Split Injectors by Injector Number.....	72
Figure 37. Higher Air Swirl Angle Injectors by Run Number	72
Figure 38. Higher Air Swirl Angle Injectors by Injector Number.....	73
Figure 39. NO Emissions vs. Air Splits.....	74
Figure 40. NO Emissions vs. Fuel Swirl.....	74
Figure 41. NO Emissions vs. Air Swirl	74
Figure 42. NO Emissions vs. Pressure Drop.....	75
Figure 43. NO Emissions vs. Preheat Temperature	75
Figure 44. NO Emissions vs. Fuel Composition	76
Figure 45. NO Emissions vs. Flame Temperature.....	76
Figure 46. NO Emissions for Air Split and Fuel Swirl Interaction. (Red-Higher Fuel Swirl, Black-Lower Fuel Swirl)	77
Figure 47. NO Emissions for Air Split and Pressure Drop Interaction. (Red-Higher Pressure Drop, Black-Lower Pressure Drop)	78
Figure 48. NO Emissions for Preheat Temperature vs. Air Split Interaction (Middle Fuel Swirl)	79
Figure 49. NO Emissions for Preheat vs. Air Split Interaction (Lower Fuel Swirl).....	80
Figure 50. NO Emissions for Preheat vs. Air Split Interaction (Higher Fuel Swirl).....	80
Figure 51. NO Emissions for Fuel Composition vs. Air Splits Interaction	81
Figure 52. NO Emissions for Flame Temperature vs. Air Splits Interaction	82
Figure 53. NO Emissions for Air Swirl vs. Fuel Swirl Interaction.....	83
Figure 54. NO Emissions for Fuel Swirl vs. Pressure Drop Interaction. (Red-Higher Pressure Drop, Black-Lower Pressure Drop)	84
Figure 55. NO Emissions for Preheat Temperature vs. Air Swirl Interaction (Middle Air Split))	85
Figure 56. NO Emissions for Preheat Temperature vs. Air Swirl Interaction (Lower Air Split). 85	

Figure 57. NO Emissions for Preheat Temperature vs. Air Swirl Interaction (Higher Air Split)	85
Figure 58. NO Emissions for Flame Temperature vs. Preheat Temperature Interaction	87
Figure 59. NO Emissions for Fuel Composition vs. Flame Temperature Interaction	88
Figure 60. NOx Emissions vs. Run Number, Sorted by Injector Number.....	90
Figure 61. NOx Emissions vs. %H2 for Injector 1	92
Figure 62. NOx Emissions vs. %H2 for Injector 2	92
Figure 63. NOx Emissions vs. %H2 for Injector 3	93
Figure 64. NOx Emissions vs. %H2 for Injector 4.....	93
Figure 65. NOx Emissions vs. %H2 for Injector 5	94
Figure 66. NOx Emissions vs. %H2 for Injector 6.....	94
Figure 67. NOx Emissions vs. %H2 for Injector 7	95
Figure 68. NOx Emissions vs. %H2 for Injector 8.....	95
Figure 69. NOx Emissions vs. %H2 for Injector 9.....	96
Figure 70. NOx Emissions vs. %H2 for Injector 10.....	96
Figure 71. NOx Emissions vs. %H2 for Injector 11	97
Figure 72. NOx Emissions vs. %H2 for Injector 12.....	97
Figure 73. NOx Emissions vs. %H2 for Injector 13.....	98
Figure 74. NOx Emissions vs. %H2 for Injector 14.....	98
Figure 75. NOx Emissions vs. %H2 for Injector 15.....	99
Figure 76. NOx Emissions vs. %H2 for Injector 16.....	99
Figure 77. ANOVA Results for NOx Model	101
Figure 78. NOx Model.....	102
Figure 79. Predicted vs. Actual for NOx Model.....	103
Figure 80. NOx Emissions vs. Pressure Drop.....	105
Figure 81. NOx Emissions for Air Splits vs. Fuel Swirl Interaction. (Red-Higher Fuel Swirl, Black-Lower Fuel Swirl)	106
Figure 82. NO Emissions for Flame Temperature vs. Air Splits Interaction (Higher Fuel Swirl)	107
Figure 83. NOx Emissions for Flame Temperature vs. Air Splits Interaction (Higher Fuel Swirl)	107

Figure 84. NO _x Model for Fuel Swirl vs. Pressure Drop Interaction. (Red-Higher Pressure Drop, Black-Lower Pressure Drop)	108
Figure 85. NO _x Emissions for Fuel Composition vs. Air Swirl Interaction.....	109
Figure 86. NO _x Emissions for Air Swirl vs. Flame Temperature Interaction. (Red-Higher Flame Temperature, Black-Lower Flame Temperature)	110
Figure 87. NO _x Emissions for Flame Temperature vs. Pressure Drop Interaction (Middle Air Swirl).....	111
Figure 88. NO _x Emissions for Flame Temperature vs. Pressure Drop Interaction (Lower Air Split).....	111
Figure 89. NO _x Emissions for Flame Temperature vs. Preheat Temperature Interaction (Middle Air Split)	112
Figure 90. NO _x Emissions for Flame Temperature vs. Preheat Temperature Interaction (Lower Air Split)	113
Figure 91. NO _x Emissions for Flame Temperature vs. Preheat Temperature Interaction (Lower Air Swirl)	113
Figure 92. NO _x Emissions for Flame Temperature vs. Fuel Composition Interaction (Higher Air Swirl).....	114
Figure 93. ANOVA Results for NO/NO _x Model	116
Figure 94. Predicted vs. Actual for NO/NO _x Model	116
Figure 95. NO/NO _x vs. Air Splits	118
Figure 96. NO/NO _x vs. Fuel Swirl	118
Figure 97. NO/NO _x vs. Air Swirl.....	118
Figure 98. NO/NO _x vs. Pressure Drop	119
Figure 99. NO/NO _x vs. Preheat Temperature	119
Figure 100. NO/NO _x vs. Fuel Composition	120
Figure 101.NO/NO _x vs. Flame Temperature	120
Figure 102. NO/NO _x Ratio for Fuel Swirl vs. Splits Interaction	121
Figure 103. NO/NO _x for Air Splits vs. Air Swirl Interaction. (Red-Higher Air Swirl, Black-Lower Air Swirl).....	122
Figure 104. NO/NO _x for Fuel Swirl vs. Pressure Drop (Higher Air Split).....	123
Figure 105. NO/NO _x for Fuel Composition vs. Preheat Temperature Interaction.....	124

Figure 106. NO/NO _x for Preheat Temperature vs. Fuel Composition Interaction. (Red-100% H ₂ , Black-100% CH ₄) (a) Flame Temperature of 1500K (b) Flame Temperature of 1850K. All other factors are at the middle of the design space.	124
Figure 107. NO/NO _x for Fuel Composition vs. Flame Temperature Interaction. (Red-High Flame Temperature, Black-Low Flame Temperature)	125
Figure 108. NO Model, 1100K Flame Temperature.....	127
Figure 109. NO Model, 1300K Flame Temperature.....	127
Figure 110. NO Model, 1500K Flame Temperature.....	128
Figure 111. NO Model, 1675K Flame Temperature.....	128
Figure 112. NO Model, 1850K Flame Temperature.....	129
Figure 113. NO _x Model, 1100K Flame Temperature.....	131
Figure 114. NO _x Model, 1300K Flame Temperature.....	131
Figure 115. NO _x Model, 1500K Flame Temperature.....	132
Figure 116. NO _x Model, 1675K Flame Temperature.....	132
Figure 117. NO _x Model, 1850K Flame Temperature.....	133
Figure 118. CHEMKIN Model	139
Figure 119. Normal Distribution Curve.....	140
Figure 120. (a) STD 13 0% H ₂ , (b) STD 25 50% H ₂ , (c) STD16 100% H ₂ . Black and white images were captured with a Dynacolor camera and colored images with a Nikon camera.	142
Figure 121. NO ng/J vs. Flame Temperature (CHEMKIN Fully Mixed)	145
Figure 122. NO ng/J vs. Flame Temperature (CHEMKIN Fully Mixed)	146
Figure 123. NO Normalized Sensitivity for STD 13 (100% CH ₄) for PSR 2.....	149
Figure 124. NO Normalized Sensitivity for STD 16 (100% H ₂) for PSR 2	149
Figure 125. NO ₂ Normalized Sensitivity for STD 13 (100% CH ₄) in PSR 2	150
Figure 126. NO ₂ Normalized Sensitivity for STD 16 (100% H ₂) in PSR 2	150
Figure 127. Main CH ₄ Pathways to NO in PSR 2, STD 13. The colors represent different side species that are involved in a reaction line that connect two species in the diagram.	152
Figure 128. Main H ₂ Pathways to NO in PSR 2, STD 16. The colors represent different side species that are involved in a reaction line that connect two species in the diagram.	153
Figure 129. NO Normalized Sensitivity for STD 7 (100% CH ₄) for PSR 2.....	156
Figure 130. NO Sensitivity for STD 8 (100% H ₂) in PSR 2.....	156

Figure 131. NO ₂ Sensitivities for STD 7 (100% CH ₄) in PSR 2.....	157
Figure 132. NO ₂ Sensitivities for STD 8 (100% H ₂) in PSR 2	157
Figure 133. Main CH ₄ Pathways to NO in PSR 2, STD 7. The colors represent different side species that are involved in a reaction line that connect two species in the diagram.	159
Figure 134. Main H ₂ Pathways to NO in PSR 2, STD 7. The colors represent different side species that are involved in a reaction line that connect two species in the diagram.	159
Figure A- 1. NO 15% O ₂ ppmvd. vs. Flame Temperature.....	175
Figure A- 2. NO _x 15% O ₂ ppmvd. vs. Flame Temperature.....	175
Figure A- 3. NO ng/J vs. Flame Temperature	176
Figure A- 4. NO _x ng/J vs. Flame Temperature	176
Figure A- 5. Rectangular Configuration, Case 2	177
Figure A- 6. Tall Cylinder Configuration, Case 3	178
Figure A- 7. Solidworks Drawing of Airbox with Heater Plate Interface	179
Figure A- 8. Solidworks Drawing of Airbox with Injector Plate Interface and Side Profiles	180
Figure A- 9. Normal Plot of Residuals for CO Model.....	213
Figure A- 10. Residuals vs. Predicted for CO Model.....	213
Figure A- 11. Residuals vs. Run for CO Model	213
Figure A- 12. Normal Plot of Residuals for NO Model	213
Figure A- 13. Residuals vs. Predicted for NO Model.....	214
Figure A- 14. Residuals vs. Run for NO Model	214
Figure A- 15. Normal Plot of Residuals for NO _x Model	214
Figure A- 16. Residuals vs. Predicted for NO _x Model.....	214
Figure A- 17. Residuals vs. Run for NO _x Model	215
Figure A- 18. Normal Plot of Residuals for NO/NO _x Model.....	215
Figure A- 19. Residuals vs. Predicted for NO/NO _x Model.....	215
Figure A- 20. Residuals vs. Run for NO/NO _x Model	215
Figure A- 21. NO Normalized Sensitivity for STD 13 (100% CH ₄) for PFR.....	228
Figure A- 22. NO ₂ Normalized Sensitivity for STD 13 (100% CH ₄) for PFR.....	228
Figure A- 23. NO Normalized Sensitivity for STD 16 (100% H ₂) for PFR	228
Figure A- 24. NO ₂ Normalized Sensitivity for STD 16 (100% H ₂) for PFR	228
Figure A- 25. NO Normalized Sensitivity for STD 7 (100% CH ₄) for PFR.....	228

Figure A- 26. NO Normalized Sensitivity for STD 7 (100% CH ₄) for PFR.....	228
Figure A- 27. NO ₂ Normalized Sensitivity for STD 8 (100% H ₂) for PFR	229
Figure A- 28. NO ₂ Normalized Sensitivity for STD 8 (100% H ₂) for PFR	229

Acknowledgements

I would like to thank my committee members Professor Jack Brouwer, Professor Vince McDonell, and Professor Bihter Padak for taking the time to review the work presented here. I greatly appreciate all of your support and all that you do for APEP. With your leadership, open communication and collaborative efforts among its students, even when working on different projects, were easily arranged.

I would like to express the deepest appreciation to my advisor, Professor Vince McDonell, who has guided me over the past year as a graduate student researcher. Your advice and knowledge are truly invaluable. You always offered many avenues of solutions whenever a problem was presented. Without your support, this achievement and future endeavors would not be possible.

Lastly, I would like to thank my family, friends, research partner (Iker G. Escudero), and Collins Aerospace for their support. The late nights and long weekends to meet deadlines would not have been accomplished without all of you.

ABSTRACT OF THE THESIS

Characterization of Aeroengine Lean Direct Injector Concept Adapted for Low NO_x Power
Generation Using Hydrogen

By

Britney L. Tran

Master of Science in Mechanical and Aerospace Engineering

University of California, Irvine, 2022

Professor Jack Brouwer, Chair

As decarbonization of our society becomes more important, gas turbine manufacturers are investigating the utilization of hydrogen as a fuel in their systems. In parallel, a need exists to minimize pollutant emissions associated with power generation. Traditionally, gas turbine manufacturers have adopted lean premixed strategies to minimize pollutant emissions. However, the consideration of hydrogen as a fuel while using traditional premixing strategies for low emissions requires one to consider hydrogen's unique combustion features compared to natural gas including 1) high flame speed and associated flashback risk, 2) high diffusivity, and 3) high adiabatic flame temperatures for a given fuel/air mixture. "Micromixing" technology is a current promising fuel injection strategy under development for low emission hydrogen fueled ground-based engines to 1) avoid challenges with flashback found in premixed systems by rapidly mixing fuel and air together at a small spatial scale and 2) to produce compact reactions with short residence times which help minimize NO_x formation. The general goal of micromixing is to attain premixed conditions and compact reactions using small fuel and air passages immediately upstream of the combustion zone.

A relatively new approach is derived from successful low emissions technology developed for aeroengines. The highly transient operation of aeroengines and the need for passenger safety require an even more robust combustion system performance compared to power generation. “Lean direct injection” (LDI) involves larger physical scales (order of 0.1-0.2 in² effective area) compared to the typical 0.01-0.02 in² micromixers) and seeks to attain rapid mixing of the fuel and air. In the present effort, an LDI concept developed by Collins Aerospace for liquid fuel applications is adapted for a ground-based turbine system to be operated on hydrogen. Of particular interest in the present effort is the fuel flexibility of these injectors (e.g., Can they operate on a range of natural gas and hydrogen mixtures?) as well as the emissions performance. A set of carefully designed injectors were fabricated to allow air flow splits, air swirl strength, fuel swirl strength to be studied. In addition, operating conditions controlled via the pressure drop, preheat temperature, fuel composition, and adiabatic flame temperature were investigated. With seven factors, a statistical test matrix was designed using a Box-Behnken approach to yield 43 test points per injector for a total of 688 test points for 16 injectors.

Analysis of variance was used to develop response surface correlations for the pollutant emissions produced. The analysis identified that the geometric parameters had some influence, on emissions, but that fuel composition, air preheat, and flame temperature were most significant. Optimization identified that a higher air pressure drop, higher air swirl, and more air into the inner part of the injector with low fuel swirl yielded the best emissions performance regardless of fuel composition or calculated adiabatic flame temperature. The results indicate that the Collins injector concept rivals other manufacturers’ micromixing injectors by producing NO_x levels below 10 ng/J while having the flexibility to operate on methane and hydrogen.

A chemical kinetics study using a reactor network with the GRI Mech 3.0 mechanism was also conducted to understand differences between NO_x formed by hydrogen and methane. The network was developed with the ability to account for some unmixedness expected for the LDI configuration. The results identified the NNH (nitrogen-nitrogen-hydrogen) pathway as the main cause for NO emissions when using hydrogen for all conditions studied. Whereas hydroxyl (OH) leads to the direct formation of NO when hydrogen is burned, the bulk of this intermediate species forms carbon dioxide (CO₂) rather than NO when methane is combusted. For methane fuel, at reaction temperatures below 1675K, NO is formed mainly through the nitrous oxide (N₂O) intermediate mechanism route. At temperatures above 1800K, NO is mainly formed through the Zeldovich (or thermal) mechanism route for both fuels as expected.

1. Introduction

In response to environmental concerns, the United States Environmental Protection Agency (EPA) enacted the Clean Air Act to regulate emissions in 1970 [1], [2]. Over the span of ten years, several more laws and actions were implemented to further improve the environment which included the Clean Water Act (1972), phasing out leaded gasoline (1973), revoking aid to polluters (1975), and phasing out CFCs (1978) [3]. From 1980-2000, emphasis was placed on banning and cleaning up of hazardous wastes. It was not until 2000-2010s that pollutant emissions from the transportation sector were heavily regulated. Regarding aircraft, many regulations were adapted from the United Nations' International Civil Aviation Organization (ICAO) [2]. The goal was to keep pace with international efforts to address environmental concerns.



Figure 1. Smog in Los Angeles on July 15, 1978 [4]

As part of this effort, the University of California, Irvine Combustion Laboratory (UCICL) was founded by Scott Samuelsen in 1970 to address conflicts regarding environmental

and energy concerns. Since then, UCICL has been engaged in sustainable and alternative fuel research. Every few years, the EPA issues increasingly stringent regulations regarding emissions entering the atmosphere. NO_x emissions are given special attention as they are toxic and an important ozone precursor contributing to air pollution in the urban air shed. NO_x emissions are produced from burning fuels with air at high temperatures [5].

Regarding strategies towards decarbonization to reduce greenhouse gas emissions, hydrogen has been receiving increased interest. Hydrogen is a promising solution in that it does not contain carbon, can be extracted via various sources, is versatile, and has wide flammability limits. Yet, to maximize benefits from combustion systems, it is essential that pollutants, especially oxides of nitrogen, be minimized. Thereby, combustion systems derived for hydrogen must be able to produce little to no NO_x emissions.

As proven by previous research, hydrogen can be used in many applications. In the context of current gas turbine applications and research, the industry has been using hydrogen as a fuel for over 30 years [6], [7]. Many of these examples are associated with use of hydrogen as a waste gas. Furthermore, these systems generally do not focus on attaining low pollutant emissions performance. For applications like base load power generation using renewable hydrogen, it is imperative that a low pollutant emissions solution be developed. Gas turbine manufacturers including Solar Turbines Incorporated, Mitsubishi, Kawasaki, and General Electric have already completed demonstrations projects with various models of gas turbines for which mixtures of hydrogen and natural gas have been used. In some cases, pollutant emissions have been minimized using diluent addition (e.g., water injection) and post combustion clean up (e.g., selective catalytic reduction of the pollutants in the exhaust stream). But eventually these systems need to attain low emissions performance that are on par with their current state of the

art natural gas systems. To accomplish this, technologies derived from natural gas systems while accounting for features of hydrogen such as high flame speed and high diffusivity are needed. Current low emissions systems for natural gas rely on premixing of the fuel and air at overall lean mixtures in order to help reduce reaction temperatures and thus minimize NO_x formation via the Zeldovich (or thermal) mechanism. However, the reactive nature of hydrogen and high flame speeds of hydrogen/air reactions leads to a technical risk with this approach.

To address this concern, industry has adopted strategies which minimize the time which the fuel and air is premixed. This is being accomplished through “micromixing” strategies in which many small reactions are held on injector arrays in place of a traditional larger swirl stabilized injector. In one example, Mitsubishi is developing a micromixing model that has a total of 36 injector holes for which the air will be injected to surround the fuel profile for mixing [8], [9]. This current configuration only runs on blends of syngas fuels and small mixtures of hydrogen fuel. Mitsubishi has plans for a gas turbine model that runs on 100% hydrogen to be completed in 2025 [10]. More examples of this micromixing strategy are discussed in section 2.4.3.

In the current effort, a type of injector that minimizes the time during which the fuel and air are mixed is investigated. This “lean-direct injection” approach seeks to attain rapid mixing of fuel and air to lean conditions. Collins Aerospace has successfully utilized the LDI approach for low emissions operation on liquid fuels for aeroengines and the current study assesses if this approach can be successful as adapted to inject hydrogen and air into the combustor. The goal of the LDI approach is to simultaneously avoid any chance of flashback and minimizing pollutant emissions by operating fuel lean to attain low temperatures during combustion and by having compact reactions to reduce the time of the reactions occurring. To explore the sensitivity of the

injector configuration, the test hardware varied the effect of air flow split, air and fuel swirl strength, air pressure drop, air preheat temperature, fuel composition, and flame temperature. The results set the foundation for further development of combustion systems for gas turbines operating with high hydrogen fuel content. The research effort in this thesis will address the following:

1. Assess emissions for all 16 injectors and create a predictive model for the factors in question.
 - a. What factors and factor interactions are significant to the injector performance?
 - i. Which combination of factors minimizes pollutant emissions?
 - ii. From 1ai, does the desired combination of factors change with the different fuels?
 - b. What modifications to the current injector design can be suggested to further improve performance?
2. How does Collins Aerospace's LDI design perform compared to current micromixing designs?
3. Does the current design of injectors produce higher or lower NO_x emissions when operating on hydrogen fuel compared to natural gas?
 - a. Can the current design operate on mixtures of hydrogen and natural gas up to 100%?
 - b. Which blend of fuel achieves the lowest emissions?
 - i. How does the NO_x formation mechanism change, if at all, as a function of fuel composition?

4. How do the ANOVA and CHEMKIN models compare to the experimental results? How can the ANOVA and CHEMKIN models be modified to better fit experimental data?

The following tasks are executed to answer the research questions:

Task 1: Design the Airbox/Test Stand Apparatus

Task 2: Determine Effective Areas for the Air Circuit for the Injectors

Task 3: Determine Effective Areas for the Fuel Circuit for the Injectors

Task 4: Develop Test Matrix

Task 5: Evaluate and Analyze Experimental Results

Task 6: Verify Experimental Results with a Theoretical Model on CHEMKIN

Task 7: Establish the Optimal Configuration

In Chapter 2, various NO_x mechanisms present during the combustion of fuel and air are discussed. Focused is placed on methane and hydrogen as these two fuels are used to conduct this experiment. Then, a brief overview of hydrogen advantages and challenges are discussed. This is followed by methods to reduce NO_x emissions. This includes a summary of existing efforts regarding micromixing injection technologies for hydrogen to help center it on the research goal. Chapter 3 presents the approach and Chapter 4 presents the methods used during the experiment. Chapter 5 presents the results and discusses the important findings. Finally, a comprehensive summary is provided in Chapter 6.

2. Literature Review

In this chapter, a brief review of the mechanisms resulting in pollutant emissions from combustion of air and fuels, specifically methane and hydrogen, are presented. While the majority of discussions center on NO and NO_x emissions, other pollutants such as CO also exist and are examined. Next, specific advantages and challenges of hydrogen as a fuel are reviewed. Current strategies to overcome the challenges are then presented. While strategies like water injection and ultra-lean fuel mixtures are discussed, emphasis is given to current fuel/air injection strategies for hydrogen air combustion in gas turbines. The literature review concludes with remaining research questions that are investigated in the current thesis.

2.1 Pollutant Emissions from Combustion of Fuel and Air

Beginning in the 1970s, laws concerning the environment, especially pollution, were enacted by the Environmental Protection Agency. These regulations catapulted a series of stricter thresholds for pollutant emissions as the public's environmental concerns increased. Of all combustion system emissions, oxides of nitrogen (NO_x) are perhaps the most critical as they are toxic and are important ozone precursors. There are three main mechanisms from which NO_x emissions originate from: the fuel nitrogen mechanism, the prompt NO_x mechanism, and the thermal NO_x (or Zeldovich) mechanism [11], [12].

2.1.1 Fuel NO_x Mechanism

Any atomic nitrogen contained with the fuel molecule itself will rapidly form NO once oxidation starts. An example that is gaining interest as a carbon free fuel is ammonia (NH₃) [13]. Fuel NO_x is more prevalent in liquid and solid fuels as they can contain higher levels of fuel-bound nitrogen. For instance, coal and crude oil can contain up to 2% and 0.5% nitrogen,

respectively, by mass. An obvious solution to combat fuel-based NO_x is to use fuels that do not contain atomic nitrogen. In the context of ground-based gas turbines operating on hydrogen, NO_x from fuel bound nitrogen is inherently eliminated because it does not contain atomic nitrogen.

2.1.2 Prompt NO_x Mechanism

The second form of NO_x emissions is through the “prompt” NO_x mechanism [14]. Prompt NO_x forms when hydrocarbon radicals (CH_x) react rapidly with the nitrogen in the air to form nitrogen oxide (NO) and hydrogen [12], [13]. Typically, prompt NO_x is most prevalent in the earliest stages of the combustion reaction and does not play a role until temperatures are below 1600 K. The representative reactions involved in the prompt NO_x mechanism include:



The conversion from HCN to NO formation is described below:



Some have suggested that NO_x emissions through the prompt NO_x mechanism are only found in rich hydrocarbon flames and are not a significant concern for pure hydrogen combustion [15]. This is because hydrocarbon radicals cannot be formed during the combustion hydrogen.

2.1.3 Thermal NO_x Mechanism

Thermal NO_x, also known as the Zeldovich mechanism, is formed when nitrogen and oxygen combine to form NO and NO₂ [12], [16]. As the temperature increases, the thermal NO_x mechanism produces NO_x at exponentially higher levels and becomes prominent above 1900K [17]. Increases in residence time and pressure for temperatures above 1900K further increases emissions. Thus, shorter combustor designs are favored. Thermal NO_x will exist in both hydrogen and methane combustion as long as the combustion temperatures are above 1900K.

The equations for the thermal NO_x mechanism include:



2.1.4 NNH Pathway

Other than the three main NO_x mechanisms, there are other pathways such as the NNH pathway. The NNH pathway occurs in flame regions with high hydrogen or H radicals (e.g., in the flame zone), especially at gas turbine operating conditions and for long-chain hydrocarbon fuels [18]. NNH forms when nitrogen reacts with hydrogen, which then reacts with oxygen to form NO [19]. As a result, the NNH pathway is one of interest when using hydrogen as a fuel. The NNH pathway is most significant at low temperatures and at conditions where the residence times are short [19].

The reactions for the NNH mechanism are:

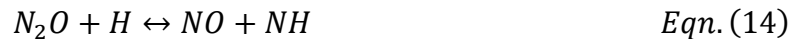




2.1.5 N₂O Pathway

Another pathway is through the N₂O intermediate pathway. N₂O first forms when nitrogen reacts with oxygen. Then from N₂O, NO is formed. This intermediate mechanism can contribute up to 90% of the NO_x emissions under elevated pressures and oxygen rich conditions [20], [21]. For gas turbines, the contribution drops to 30% [21]. At lower temperatures, where the Zeldovich pathway is not as dominant, N₂O becomes more important. It has been shown that N₂O production rates increase with increased pressures and can occur at the flame-front and post flame-front [20]. It is important to note that the pressure dependency is still debated in literature. In some cases, the pressure dependency was found to be neutral [22]. The disagreement could be due to the uncertainty in the destruction of N₂O to N₂ and O [20]. Although this thesis did not investigate higher pressures, it is still important to note the N₂O pathway. The N₂O pathway is not specific to a fuel type and could be found in both methane and hydrogen combustion.

The reactions for the N₂O mechanism are defined below [20].



Here, M represents a chemically unchanged third species. Table 1 summarizes the NO_x mechanisms discussed in section 2.1.1 – 2.1.5.

Table 1. Summary of NO_x Mechanisms

Fuel NO _x Mechanism	<p>Methane:</p> <ul style="list-style-type: none"> • Nonexistent since nitrogen is not part of the fuel composition <p>Hydrogen:</p> <ul style="list-style-type: none"> • Nonexistent since nitrogen is not part of the fuel composition
Prompt NO _x Mechanism	<p>Methane:</p> <ul style="list-style-type: none"> • Typically present in the earliest stages of combustions and at combustion temperatures lower than 1600K <p>Hydrogen:</p> <ul style="list-style-type: none"> • Nonexistent since hydrocarbon radicals cannot form
Thermal NO _x Mechanism	<p>Methane:</p> <ul style="list-style-type: none"> • Dominates at temperatures above 1900K <p>Hydrogen:</p> <ul style="list-style-type: none"> • Dominates at temperatures above 1900K.
NNH Pathway	<p>Methane:</p> <ul style="list-style-type: none"> • Dominates in regions of high hydrogen radicals like the flame zone • Significant at low temperatures and at conditions where the residence times are short <p>Hydrogen:</p> <ul style="list-style-type: none"> • Dominates in regions of high hydrogen radicals like the flame zone • Especially important to hydrogen fuel due as H₂ breaks down to H radicals • Significant at low temperatures and at conditions where the residence times are short
N ₂ O Pathway	<p>Methane:</p> <ul style="list-style-type: none"> • Dominates when the thermal NO_x mechanism is not present or below 1900K • Pressure dependency is still debated in literature <p>Hydrogen:</p> <ul style="list-style-type: none"> • Dominates when the thermal NO_x mechanism is not present or below 1900K • Pressure dependency is still debated in literature

2.1.6 Other Pollutants

While much focus is on NO_x emissions, other emissions exist, such as carbon monoxide, or CO. CO is an odorless, colorless, and poisonous gas that forms during incomplete combustion

of fuels. As a result, it becomes a primary concern at lower temperatures [15], [23]. It is nearly impossible to achieve complete combustion in any combustion scenario as there is a wide range of both major and minor species that are present [24]. CO emissions can range around 1-5 ppmvd (parts per million on a volume basis, dried) even when near complete combustion is achieved. The EPA estimates 0.5-5 ppm of CO emissions are present in ambient conditions indoors [25]. Vehicles and machinery that burn fossil fuels are currently one of the biggest sources that contribute to CO emissions in the atmosphere. As CO is ubiquitous, it poses a serious health hazard and should be considered when evaluating emissions. Fortunately, with the use of hydrogen, CO emissions should be eliminated since no carbon exists in the fuel composition.

Unburned hydrocarbons are another pollutant that exists in the vapor phase at flue gas temperatures [26]. Hydrocarbons are a class of chemical compounds that are comprised of entirely carbon and hydrogen atoms. The combustion of these compounds emits some hydrocarbons into the air and are noted as unburned hydrocarbon emissions. They are also typically formed as a result of incomplete combustion. Some examples of these emissions include alkanes, alkenes, aldehydes, carboxylic acids, and substituted benzenes [26]. With hydrogen fuel, these compounds do not exist. However, for hydrogen, there could be some unburned hydrogen due to inefficiencies of the combustion project. In the current project, unburned hydrogen is unmeasured due to limitations of the PG 350 gas analyzer.

2.2 Hydrogen Advantages

Hydrogen has garnered wide interest for its myriad of benefits. First, using hydrogen as a fuel will eliminate the fuel NO_x and prompt NO_x mechanisms. Additionally, with hydrogen fuel there exists no CO emissions or unburned hydrocarbon emissions. Moreover, hydrogen was

wider flammability limits compared to methane. Hydrogen has a flammability range of 0.1 -7.1 (expressed in equivalence ratios) whereas methane has a flammability range of 0.5-1.7 [27]. The increased range of flammability, combined with high flame speed, allows hydrogen to have inherently more stable combustion than methane. Hydrogen enrichment also produces more compact flames which can allow combustion systems to be shorter and compact [28], [29].

2.3 Hydrogen Challenges

The challenges with hydrogen as a fuel include its flame and energy characteristics. Gas turbines operating on hydrogen have been studied since the 1990s yet some of the earliest documented challenges still exist today. The following challenges are often cited when using hydrogen as a fuel: possible higher nitrogen oxide emissions, higher flame speeds, and flashback [30], [28], [31], [32], [33]. Potentially higher NO_x emissions are one of the primary drivers behind carrying out the combustion research to understand and mitigate this feature. In one study, Lantz et al. reported an increase in NO_x emissions with increased hydrogen content due to increased flame speeds which increase local flame temperatures [34]. Lantz's experiment was not perfectly premixed which could also be the reason for the increased local temperatures for hydrogen. Moreover, Lantz hypothesized that the increase in NO_x emissions when adding hydrogen could be due to the larger post combustion zone since the flame reactions start further upstream [34]. Kim et al. also report higher NO emissions for increased hydrogen content due to less recirculated gases that contribute to higher flame temperatures [35]. Kim's experiment was conducted on the assumption that it was a perfectly premixed system. However, there are also other studies that illustrate NO_x levels do not increase or even drop compared to natural gas. York et al showed that additions of hydrogen up to 100% reported lower emissions when compared to methane H₂ [36]. However, a 60%H₂/40%N₂ fuel mixture produced the lowest

NO_x emissions compared to 100% H₂ [36]. Mohammad et al. conducted their study on a fully premixed system and showed essentially no difference in NO_x emissions if the adiabatic flame temperature was constant [23]. Their results were validated with experimental results; however, it should be noted that above 50% hydrogen, the difference between the chemical kinetics model and experimental results increased dramatically. The takeaway from this discussion is the fact that whether increasing hydrogen content in fuel mixtures causes an increase or decrease in NO and NO_x emissions is still being debated.

The other two challenges are higher flame speeds and flashback. Due to higher flame speeds, hydrogen is more affected by the level of mixedness because the fluid momentum of hydrogen is higher than methane [37]. While higher flame speeds can help with flashback and flame holding, the mixing profile becomes more center peaked with hydrogen which causes hot spots that can give rise to higher NO_x emissions [37]. Hydrogen is cited to be more prone to flashback due to its higher reactivity and high laminar burning velocity [38], [39]. However, with higher reactivity, hydrogen can operate at much lower equivalence ratios compared to methane which makes the system more stable overall [40]. The essence of this discussion was to show that the cited challenges of hydrogen can also be an advantage. Thus, much research on hydrogen is still required to fully understand its fuel characteristics.

Another point to note is that a lot of current gas turbine technology also retrofit or work on preexisting solutions that were optimized for natural gas. Perhaps, reinventing a new system entirely for the benefit of hydrogen is an overall better solution. It is difficult to address the challenges presented in this section in one neat solution. What is clear is that more research on hydrogen and its fuel characteristics are warranted. Regardless of the chosen method, the

objective is to lower NO_x emissions. Thus, it will be discussed first and given the highest significance. In the succeeding sections, strategies to lower NO_x emissions are discussed.

2.4 Strategies to Lower NO_x Emissions

Strategies aimed at solving the challenges presented in the previous section include 1) reducing peak temperatures 2) reducing residence time 3) oxy-fuel combustion 4) fuels that contain no nitrogen and 5) micromixing [11], [23], [41]. Reducing the peak temperatures, or method one, will lower emissions overall by limiting NO_x formation through the thermal NO_x mechanism. Reducing the residence time, or method two, can be done through injection timing or by limiting the length of the flame. This strategy lowers emissions by limiting the total amount of time the combustion chamber is actively at high temperatures. The third method, or oxy-fuel combustion, reduces NO_x emissions by eliminating nitrogen available to form NO by combusting in a pure oxygen environment. Using oxygen instead of air should be proceeded with caution as it produces more intense flames that must be diluted to maintain the operating temperatures of gas turbines. Method four is an easier approach as it utilizes ultra-low nitrogen fuel compositions, such as hydrogen, to nearly eliminate fuel and prompt NO_x [42]. Lastly, micromixing can be used to address both methods one and two in one combination. Micromixing reduces peak temperature by allowing fuel and air to premix rapidly and by allowing systems to operate leaner. It also reduces residence time by producing hundreds of small compact flames versus one larger flame. This method is discussed more in detail in section 2.4.3.

In reviewing all strategies, the most common and simplest is to reduce the peak combustion temperatures to reduce thermal NO_x emissions. These strategies include water injection, ultra-lean fuel mixtures, and micromixing. The first three strategies will be briefly

elaborated on in the next few sections. Micromixing will be focused on in detail as it corresponds with the thesis' objective.

2.4.1 Water Injection

Water injection allows for emissions control by lowering the peak temperatures through the injection of either water or steam [23]. This method is estimated to have 70-80% reduction in NO_x emissions and can produce emissions as low as 9.8 parts per million, dried on a volume basis and corrected to 15% O₂, or ppmvd 15% O₂ (parts per million on a volume basis, dried and corrected to 15% O₂) [41]. It should be emphasized that water injection is not typically seen as a standalone solution to achieve low NO_x emissions. For instance, it can be coupled with Selective Catalytic Reduction (SCR), where SCR and water injection act as the primary and post combustion method, respectively. It is also difficult to justify water injection as the system becomes reliant on water and may become a challenge to water resources.

2.4.2 Ultra-Lean Fuel Mixtures

In a study conducted by NASA, ultra-lean mixtures were used as a strategy to reduce local hot spots and average flame temperatures. This resulted in lower emissions levels, as much as a factor of two, compared to conventional gas turbine combustors [40]. The ultra-lean mixtures reduced peak combustion temperatures. Further, with the reactivity of hydrogen, flame temperatures below 1300 K can be sustained. At flame temperatures below 1300K, the NO_x concentrations were shown to be below 0.05ppmv [40]. Contrary to the study's successes, the experimental apparatus faced practicability and flashback challenges. The experimental apparatus ultimately had to be modified to include a high blockage to resolve the flashback; however, this is an impractical gas turbine design.

2.4.3 Micromixers

One of the many ground-breaking methods proposed was the concept of micromixing. Micromixing combined the benefit of having shorter residence time and lean premixed combustion into one system. Current micromixer designs have also been shown to reduce peak temperature and risks of autoignition [9], [43]. Due their small size, micromixers are able to produce smaller compact flames to reduce emissions significantly to below 3 ppm [44], [45], [46]. The benefits of micromixing are also already recognized in many industrial applications today, especially in gas turbines [44], [47], [48]. Even with various fuel blends, the engine operations during idling, startup, and acceleration were all proven to be stable without blowback or flashback [49]. The utility of this technology can be tailored to reach various desirable performance levels, making it one of the more compelling solutions to face the many challenges of emission stringent stipulations.

The fundamental advantage of micromixers is their reduced spatial scale at which they can mix. The diameter of the holes in these micromixer cups ranges from a few millimeters to a few nanometers. Traditional swirl mixers or a jet injection mixer typically have one fluid injected into the other and mixed via sprays or atomization. Micromixers, on the contrary, are comprised of hundreds of small-scale mixers that premix fuel and air before it enters the combustion chamber. As a result, a homogenous fuel and air mixture is easily achievable; it takes less time to mix over a shorter distance and mixes quicker in smaller quantities. This not only reduces peak temperatures, which lowers emissions as a result, but also allows for a more stable combustion process [28]. The added benefit of having multiple mixers is that the ability to stage the operations depending on usage is effortless [44]. Figure 2 and Figure 3 are examples of some micromixing concepts, which all have been tested and verified.

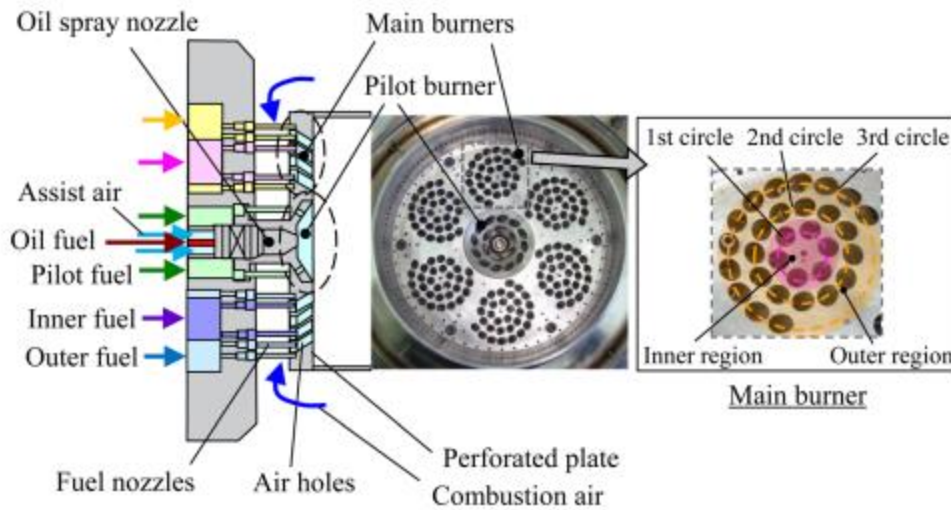


Figure 2. Mitsubishi's Dry Low NOx Combustor [9]

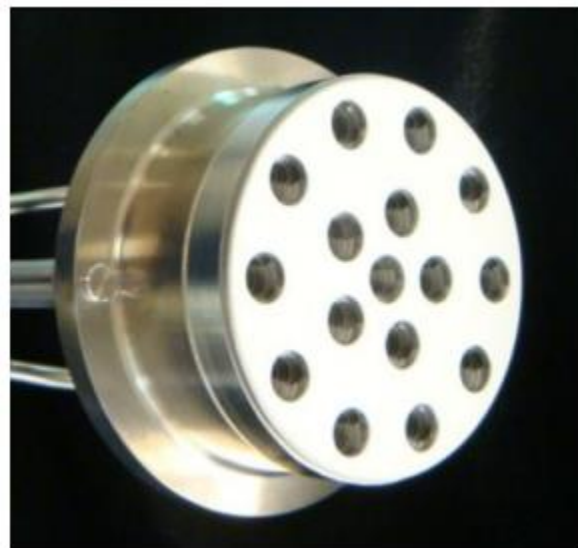


Figure 3. Parker Hannifin's Micromixing Injector [44]

In a series of studies, Parker Hannifin, spearheaded by Hollan et al. successfully demonstrated the use of micromixers on a full-scale 1.3 MW gas turbine at full range operating conditions, while retaining low NO_x emissions [44]. The study's success was driven with an axial and swirl micromixer cup design with side injection ports sandwiched in between layers as shown in Figure 4. The axial cup showed flashback resistance up to three atmospheres while the swirl cup reported lower emissions. This demonstrates the cup's inherent flexibility to tailor to

the gas turbines' application. More importantly, in both cases, NO_x emissions were lower than 5ppm. While tests were initially conducted at one atmosphere, the design was transitioned to the full scale at 12.4 bar or 180psi. Even so, NO_x emissions were below 3 ppm at 1750K. With robust and inherent flexibility, the findings of this study served as a model to similar micromixing technology.

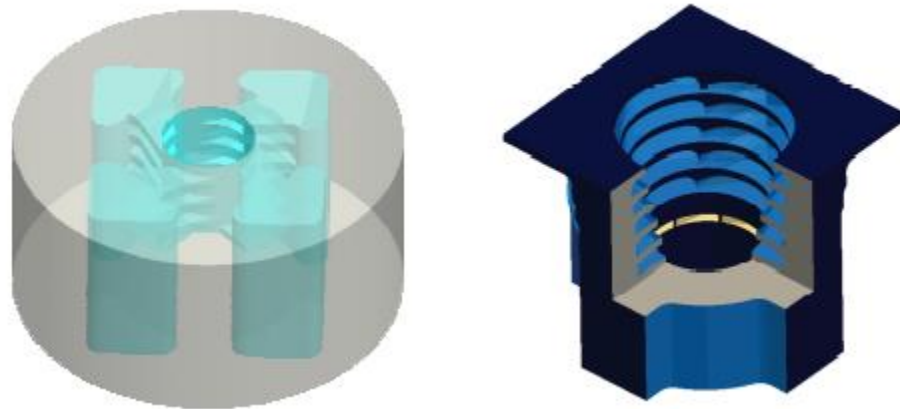


Figure 4. (Left) Swirl Radial Cup [43] and (Right) Mixed Axial and Swirl Cup [50]

For example, Honeywell's Garrett GTCP 36-300, consisted of 1,600 fuel and air ports with injection diameters of 0.3mm, reported 1.3 ppmv in NO_x emissions at an equivalence ratio of 0.4 [48]. In addition to pure hydrogen, the gas turbine was developed to interface with dual fuels on hydrogen and syngas as well as mixtures of hydrogen without any hardware changes [51]. To accommodate changes, the air gate size and the injection depth was adjusted. The air gate size directly influenced the velocity, which was helpful for retention time and subsequently, combustion efficiency. The injection depth was adjusted to an intermediate flame length to ensure flame stability while minimizing emissions. Other key findings of the study showed that while operating on syngas fuels led to peak temperatures being lowered by 100K, the combustion efficiency also decreased. The opposite was true hydrogen fuels which led to higher NO_x emissions, but combustion efficiencies exceeded 99%. Nevertheless, operating on 90%

hydrogen and 10% syngas fuel (CO), emissions levels were under 5ppm over the entire operating range at atmospheric conditions [51]. Honeywell's Garrett GTCP 36-300 is shown in Figure 5.

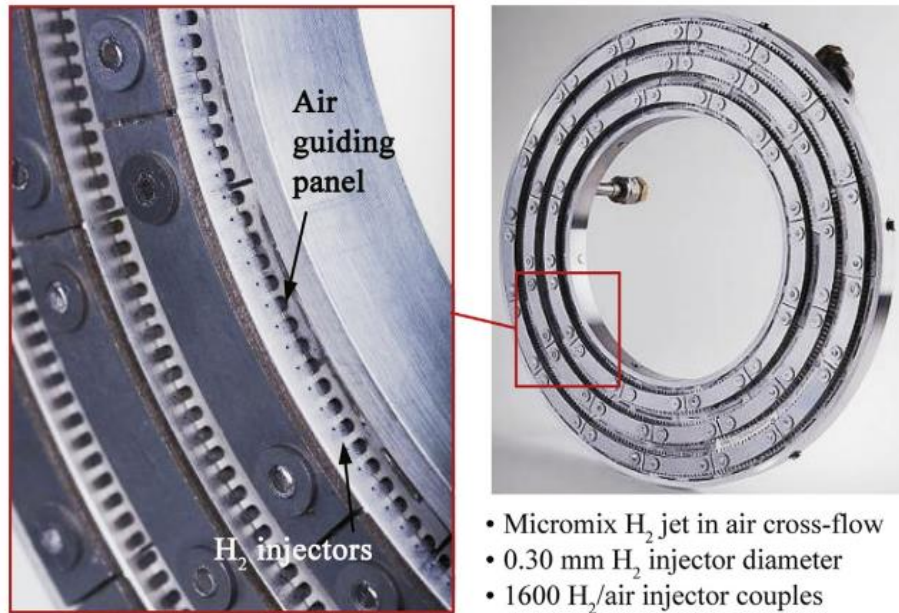


Figure 5. Honeywell's Garrett GTCP 36-300 [48]

Another industrial example is General Electric's F class engines which offer a unique multitube concept as shown in Figure 6. The advantage of this design allowed for ease of scalability without affecting the performance of the combustor. During the process of developing the F class engine, General Electric tested three fuel blends: 60/40 H₂/N₂, 100% H₂, and 60/30/10 H₂/N₂/CO. It was reported that nitrogen diluted hydrogen fuel (60/40 H₂/N₂) produced the lowest NO_x emissions due to the large amount of nitrogen that prohibits oxygen from forming NO_x. At full operating conditions up to 17 atm with 60/40 H₂/N₂ as a fuel, NO_x emissions remained lower than 10ppm (corrected at 15%- O₂) [36]. Other trends noted by researchers were that increasing the residence time led to increased emissions while decreasing pressure led to decreased emissions. Regardless, in all of the cases studied, stable conditions and no flashback were reported during nominal conditions. With the completion of this project, General Electric

currently has a variety of product lines that can operate reliably on hydrogen fuel. Their 7F and 9F engines can operate up to 65% and 80% hydrogen with the ability to go up to 100% hydrogen, respectively [52], [53]. Their 6F engines can currently operate on 100% hydrogen with NOx emissions less than 15ppm [54].

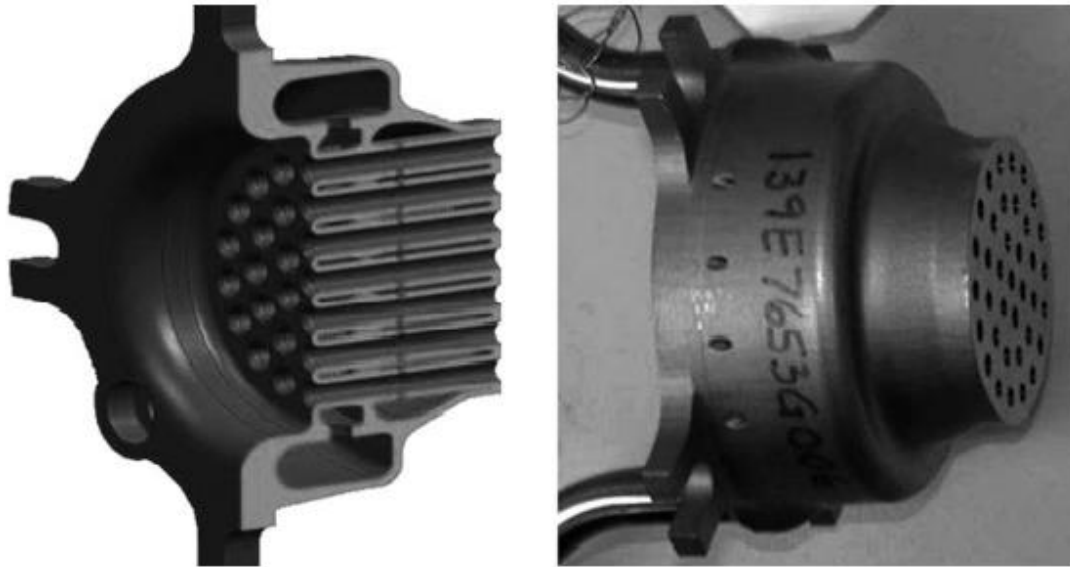


Figure 6. GE's F Class Engines Multi-Tube Concept [36]

In a separate study, Mitsubishi (conducted by Asai et al.) tested different fuel mixtures (consisting of CO, CH₄, hydrocarbons, N₂, CO₂) in combinations of mixtures of hydrogen on two different configurations as shown in Figure 7. The left plate is flat whereas the right plate is a convex injector design. In general, the convex plate had lower emissions and better combustion stability. The convex plate inhibits the flammable mixtures from igniting in the wake and the flame from attaching to the burner which are thought to be the primary cause for combustion oscillations [8]. It also has a longer mixing length which helps contribute to a homogenous fuel mixture, leading to lower NOx emissions. In all cases, NOx emissions lower than 10 ppmv for fuels ranging between 40-84% hydrogen [8]. Iterating on the convex plate, Mitsubishi successfully demonstrated staging ability on hydrogen rich syngas fuel. The micromixing

concept allowed the gas turbine to operate on a variety of fuels at different stages (idling, start up, acceleration, etc.) with ease [9]. With 50% CO, 20% H₂, and 20% N₂, NO_x emissions were near 10.9 ppm.



Figure 7. Mitsubishi's Plate Flat (Left) and Convex (Right) Plate [8]

Kawasaki, another industry leader, prototyped a 2 MW class gas turbine where both the flame ignitions and flames were stable throughout all operating conditions. Flashback also did not occur during operations and NO_x emissions remained lower than 45 ppm. The finalized design consisted of three hydrogen supply rings with over 400 injection points as shown in Figure 8. With the technology proven, Kawasaki continued to refine their work towards larger scaled demonstrations. In April 2018, they demonstrated the ability to supply heat and power to the Kobe City Port Island neighboring facilities using 100% hydrogen fuel. Then in May 2020, they were the first in the world to successfully demonstrate a full-scale gas turbine engine on micromixing technology [55]. The gas turbine could operate on either 100% H₂, 100% CH₄ or any combination of the fuels. With the addition of water injection, NO_x emissions were reported to be around 65 ppm [56]. The ground-breaking results proved the long years of research towards a hydrogen society was possible.

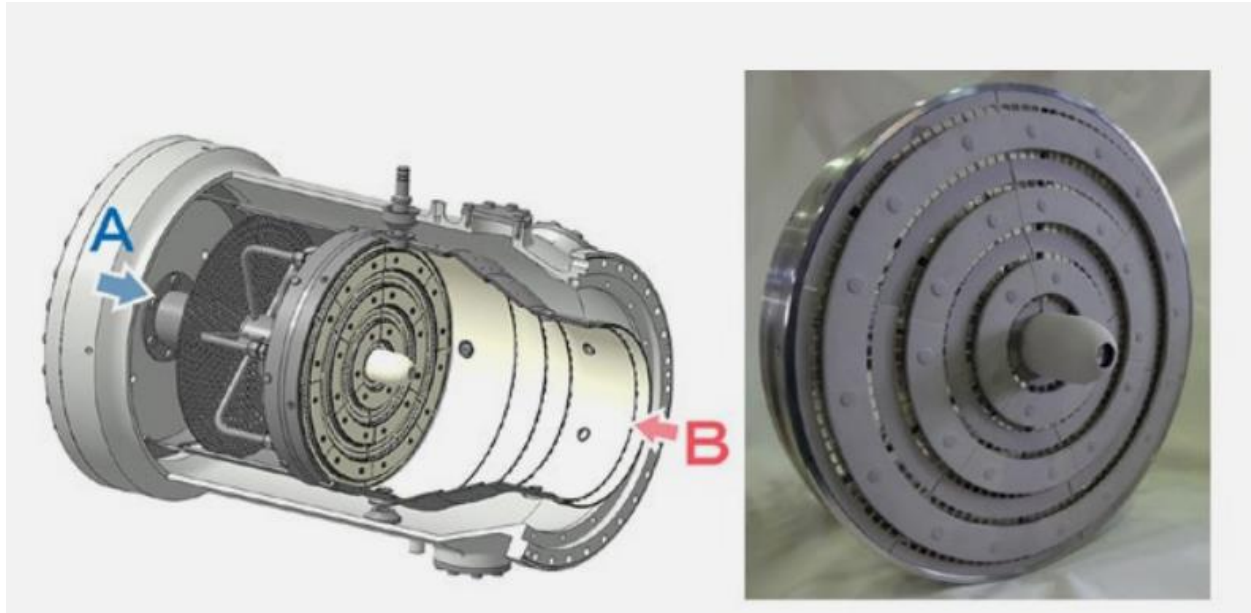


Figure 8. Kawasaki's Micromixing Gas Turbine [57]

Solar Turbines in partnership with Southwest Research Institute also developed their own micromixing gas turbine as shown in Figure 9. Their gas turbine was optimized to operate on using power generated from solar energy and high inlet temperatures starting at 1000°C [58]. Due to higher temperatures, autoignition and flashback was more prevalent. To address that, Solar Turbines developed a multibank micromixer design such that each individual mixing passage utilizes a single cross flow to pre-mix before entering the combustion chamber. Thus, each mixing passage can support its own independent flame. This allows the gas turbine to be adapted based on operating conditions. Due to this inherent design, at high temperatures, fuel banks that are turned off act as a buffer to reduce combustion temperatures at the wall. Currently, there is no reported experimental results for the design, but the numerical results show NO_x emissions lower than 10 ppm [59]. Moreover, while the results from this study were obtained assumed using a 1 MW combustor, autoignition and flashback physics are the same when applied to a 100 MW combustor.

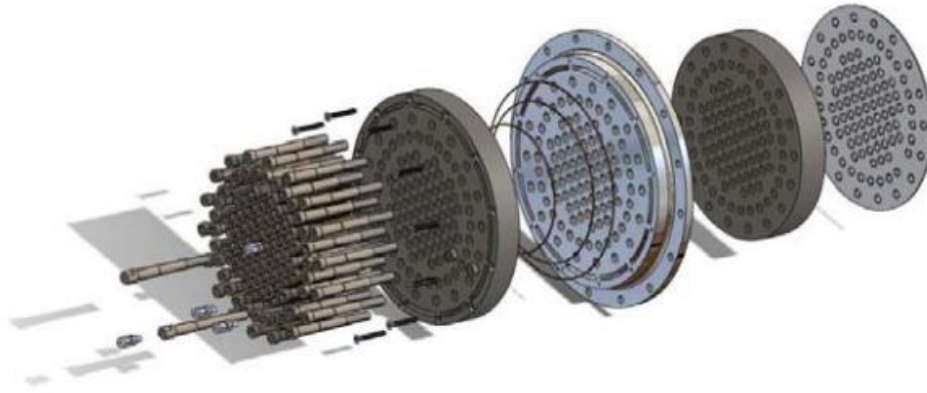


Figure 9. Solar Turbine's Micromixing Injector [59]

In another study, Hussain performed experiments with an oxygen-fuel mixture and showed that even without hydrogen enhancements, micromixing technology allowed operations to be sustained at oxy-methane flame at oxygen fraction 21% [47]. With hydrogen enrichment, the oxygen fraction drops to a record low of 13% with a 65% hydrogen fraction. Emission results were not disclosed in this study, but theory suggests that in an oxy-fuel operation, zero emissions can be achieved due to the emissions being comprised primarily of H_2O and the CO_2 which is ultimately captured [60]. Overall, while micromixing has cleared many great strides, there has still yet to be a gas turbine operating solely on hydrogen and at elevated pressures for commercial or industrial applications. Considering previously mentioned studies as well as Hussain's studies, micromixers have been proven repeatedly to be robust with large flexibility while remaining reliable and stable.

In the current study, Collins Aerospace is using a "premix" strategy where air and fuel are injected from two different streams and then mix inside the injector before entering the combustion chamber. While some studies already show fully operating gas turbines at 100% H_2 at high atmospheres (Kawasaki and General Electric), Collins Aerospace aims to retrofit and

adapt current aeroengines to become ground based gas turbines. Currently, most gas turbines studies are developed from the design phase rather than adapting existing current product lines. Moreover, Kawasaki, Mitsubishi, General Electric and Parker Hannifin used secondary strategies to lower emissions. Kawasaki used water injection methods whereas Mitsubishi, General Electric and Parker Hannifin used fuel dilution and only operated on high contents of hydrogen fuel as a method. General Electric was able to develop a gas turbine to operate with 100% H₂, but their design is very much different from Collins Aerospace. General Electric relied on a tube design to have air feeding through parallel structures inside a fuel plenum. Collins Aerospace design directly injects air and fuel separately but will premix rapidly based on the injector's geometry before entering the combustor. In regard to the other two studies (Hussain and Solar Turbines), they were more niche. Solar Turbines' gas mixer will operate using solar energy and so far, has only been in the developmental phase. Hussain's research also focused on oxy-fuel combustion rather than the conventional air and fuel combustion.

The table below summarizes current micromixing technology:

Table 2. Current Micromixing Technology


Gas Turbine Model	Key Features
<p data-bbox="203 1381 634 1451">Parker Hannifin 1.3 MW Injector [28], [43], [44], [50]</p> 	<ul style="list-style-type: none"> <li data-bbox="764 1381 1333 1451">• Using swirl and axial cups with different injection methods <li data-bbox="764 1465 1382 1535">• Even with natural gas, single digit emissions are achieved <li data-bbox="764 1549 1382 1696">• Full scale 1.3 MW injector with 16 cups was tested successfully <ul style="list-style-type: none"> <li data-bbox="862 1625 1382 1696">○ No flashback up to 100% H₂/N₂ at 8.1 bar <li data-bbox="764 1711 1382 1780">• 100% H₂ with 30% CO₂ dilution reported 3.6 ppmv in NO_x emissions

Table 2. Current Micromixing Technology



<p>Honeywell's Garrett GTCP 36-300 [48], [51]</p> 	<ul style="list-style-type: none"> • Dry Low Emissions (DLE) Combustor using crossflow mixing of air and hydrogen • 1600 miniature injectors • All test operations were done at 1 atm and NOx emissions were reported to be 1.3 ppmv @ 15% O₂ with equivalence ratio of 0.4 • When scaling to full scale conditions, hydrogen combustion was reported to be more than 99% efficient (90% H₂/10% CO) <ul style="list-style-type: none"> ○ Emissions were below 5 ppm for the entire operating range ○ 100% H₂ combustion reported higher emissions than when mixed with syngas
<p>General Electric's F Class Engines [36], [52], [53], [54]</p> 	<ul style="list-style-type: none"> • 65% H₂ capability with combustion efficiency greater than 60% • Compared to natural gas, pure hydrogen gave lower emissions below 5 ppmvd even at 17 atm • Use a multi-tube concept where fuel fills the plenum and air is feed through parallel channels <ul style="list-style-type: none"> ○ Pressure drop is low due to short length and straight path

Table 2. Current Micromixing Technology




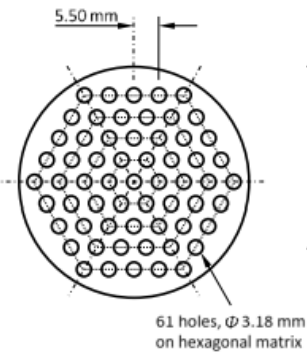

<p>Mitsubishi, [9], [8], [55]</p> 	<ul style="list-style-type: none"> • 30% hydrogen with premix configuration • Tested in high pressure facility with no flashback and NOx was within operating range • Air is injected to surround the fuel profile. A third air inlet is straight through the longest length of the flame • Tested up to 40-84% H₂, NOx emissions were lower than 10 ppm for all fuels at atmospheric conditions • Convex injector design had lower NOx than flat plate due to increase in mixing length • On Syngas fuel, (50% CO, 20% H₂, 20% N₂, 5% CO₂, 1.5 CH₄), emissions lower than 10.9 ppm at max load
<p>Kawasaki [56], [57], [61], [62]</p> 	<ul style="list-style-type: none"> • Dry Low Emission Combustion Technology using diffusion flame • Operates on 100% hydrogen and natural gas and mixtures all in between • Successfully demonstrated in Kobe City Port Island <ul style="list-style-type: none"> ○ 3 hydrogen supply rings with 400 injection holes ○ NOx emissions were below 65 ppm ○ Power output was 1635 kW
<p>Solar Turbines [59], [58]</p> 	<ul style="list-style-type: none"> • Air inlet temperature is 1000°C • Air flows through all the holes but controllers select which banks get fuel <ul style="list-style-type: none"> ○ Helps with varying load ○ At high temperatures, bypass helps with cooling combustion chamber • Scalable up to a 100 MW combustor with emissions lower than 20 ppm

Table 2. Current Micromixing Technology

<p>Hussain [47]</p> 	<ul style="list-style-type: none"> • Oxy-fuel combustion • Fuel is introduced to a mixing plenum for perfect pre-mixing • 61 jets, 3.18 mm in diameter • Peak temperatures all below 1700K up to 65% H₂ tested
<p>Collins Aerospace</p> 	<ul style="list-style-type: none"> • Modifying an aeroengine to be a gas turbine • 100% H₂ capability with no dilutants • Air and fuel are directly injected. No plenums or tubes

Overall, the objective that Collins Aerospace is trying to achieve has not been addressed yet. Adapting an aeroengine to a ground-based turbine that is specifically tailored to hydrogen will allow previous product lines to be salvaged and catapult the company quicker towards a hydrogen future. To do so, Collins Aerospace is utilizing a variety of combinations of flow splits, contraction, and swirl angles to fixate on the most optimal injector geometry. The unique geometry will facilitate mixing such that air and fuel can be injected as two separate lines and mix homogeneously before entering the combustion chamber. The design also hopes to achieve full operability up to ten atmospheres while being fueled 100% H₂ with no flashback. Furthermore, the gas turbine should be stable, and no combustion oscillations should occur during operating conditions.

2.4.4 Post Combustion Strategies

The previous strategies discussed were all in situ combustion strategies, however, there also exists methods to reduce NO_x emissions post combustion. For example, selective catalytic reduction (SCR) systems, which have been around since 1970s, can be designed to remove NO_x with an efficiency close to 90 percent [63]. Large scale demonstrations of SCR systems have already been in place in Europe and Japan since the 1990s [64]. SCR systems work to lower NO_x emissions by facilitating a reaction between the NO_x exhaust gases and a catalyst before it enters the atmosphere [65]. Ammonia is typically used as a catalyst such that NO_x emissions can be converted to nitrogen and water [63]. Another common catalyst is urea, but it is usually converted first into ammonia before injection. It is also easy to implement SCR systems since there are no moving parts; all that is required is an ammonia injection system and a catalyst bed [64]. Thus, the implementation of SCR technology into gas turbines are popular. Moreover, SCR systems are very flexible which allow this method to be suitable for any type of fuel.

2.5 Remaining Research Questions

As surveyed in literature, there are still many questions surrounding the implication of switching to hydrogen fuel. Hydrogen has apparent benefits in that it contains no nitrogen and can burn at leaner mixtures than natural gas. However, as discussed previously, some studies suggest increased hydrogen content leads to increased NO_x emissions, while others suggest the opposite. The role of hydrogen on NO_x emissions, still requires further study. While the question regarding how hydrogen content impacts NO_x emissions may be best addressed with fundamental premixed studies, the present effort also incorporates practical injection concepts that necessarily minimize risk of flashback through rapid direct injection schemes. As a result, the thesis investigates the following open questions in this context.

- How do you manufacture these injectors? What is the repeatability of the manufacturing process?
- Can the current design operate on mixtures of hydrogen and natural gas up to 100%?
- Which injector geometric factors and operating conditions are significant to the injector performance?
 - How does the ANOVA model for injector emissions performance compare with measured experimental results?
- What is the preferred configuration to attain desired performance?
- Does the current LDI design concept result in higher or lower NO_x emissions when operating on hydrogen fuel compared to natural gas? Why or why not?
 - Which chemical kinetic mechanism and pathway contributes to NO_x emissions the most?
 - What other chemical mechanisms and pathways are enabled, if any, as a result of using pure hydrogen?
- Does Collins Aerospace's micromixing design rival current micromixing designs?
- How does the CHEMKIN model compare to the measured experimental results?

The current research will focus on utilizing the micromixing strategy to lower emissions using Collins Aerospace's lean direct injection injector concept. As such, the results of the experiment will be compared to previous studies conducted by industry leaders and other researchers on other types of micromixers. The answer to these questions will immediately determine the feasibility and practicality of the design. At the conclusion of the pre-screening experiment, favorable factors (pressure drop, preheat temperatures, fuel composition, and flame temperatures) are selected to be refined. Finally, these questions will also help to assess the

validity of the numerical modelling of the injector through software programs like CHEMKIN and Design Expert by comparing it to the measured experimental results.

3. Approach

The overarching goal of the research is to adapt an aeroengine gas turbine injector to be used in a ground-based gas turbine that can operate on 100% hydrogen fuel. Without the knowledge of which injector characteristics are the most desirable for Collins Aerospace's application, four factors were tested. Each configuration was a different combination of flow splits, swirl angle, and contractions. At the conclusion of testing, one of 16 injectors will be selected as the most optimal to be used and scaled up for use in a full load gas turbine. The most optimal conditions are defined as one that produces the least amount of emissions while maintaining stability. Extending on stability, flashback and autoignition should not occur. Moreover, the design should allow for flexibility such as dual fuel and fuel mixture capabilities.

The 16 different configurations were decided and based on the Box Behnken approach. Rather than testing and determining the effect of one factor at a time (ex. flow splits, swirl angle, and contraction), these factors were mixed to reduce the number of tests required. This was achieved using Design Expert, a software to help design ideal experiments based on a combination of factors and parameters.

The following tasks were taken to determine the most optimal configuration:

Task 1: Design the Airbox/Test Stand Apparatus

Before testing can be conducted, the airbox and test stand must be designed to have an optical view for cameras, data logging devices for time analysis, and leak proof to minimize air and fuel losses throughout the pipes. In all aspects, flexibility, ease of assembly and speed of testing are also considered. The air box should be able to withstand temperature ranges from 500K to 800K for preheat and pressure drops of 2-6% at atmospheric conditions.

The test stand should accommodate auxiliary equipment for analysis such as the emissions analyzer, data acquisition devices, cameras mounted onto the table, mass flow controllers, and linear encoders.

Task 2: Determine Effective Area of the Air Circuit for the Injectors

The effective area is the driving factor for this experiment to be able to determine air flows for test conditions since the actual area of the injector is unknown. Additionally, due to additive manufacturing, surface finishes also affect the effective area and cannot be determined computationally. The equation for effective area is derived from the following assumptions.

First, for any flow field, mass continuity holds true.

$$\dot{m} = \rho_1 A_1 V_1 = \rho_2 A_2 V_2 \quad \text{Eqn. (17)}$$

where ρ is the fluid density, A is the cross-sectional area and V is the velocity. Subindices 1 and 2 represent upstream and downstream conditions, respectively. With the assumption that the flow is an ideal gas, Equation 18 can be used to relate density with pressure.

$$P = \rho RT \quad \text{Eqn. (18)}$$

where P is the pressure, R is the gas constant for a particular gas and T is the temperature.

Additionally, since no such flow can be truly frictionless, there are losses associated which can be calculated with Equation 19.

$$Q_{actual} = C Q_{ideal} \quad \text{Eqn. (19)}$$

where C is the discharge coefficient. Moreover, the energy equation for a reversible steady flow can be written as Equation 20 [66].

$$cpT_1 + \frac{V_1^2}{2g_c} = cpT_2 + \frac{V_2^2}{2g_c} \quad \text{Eqn. (20)}$$

where c_p is the specific heat at constant pressure. Finally, combining Equations 13-16, the effective area can be obtained in Equation 21.

$$\frac{Q_{actual}\rho}{\sqrt{2g_c \frac{\gamma}{\gamma-1} \frac{P_1^2}{RT_1} \left[\left(\frac{P_2}{P_1}\right)^{\frac{2}{\gamma}} - \left(\frac{P_2}{P_1}\right)^{\frac{\gamma+1}{\gamma}} \right]}} = CA_2 \quad Eqn. (21)$$

where γ is the specific heat ratio and g_c is a constant with a value of 1 kgm/(Ns²) when working with metric units.

Task 3: Determine Effective Area of the Fuel Circuit for the Injectors

Since the air and fuel are in separate circuits when entering the injector, the effective area of the fuel circuit must also be determined. Conveniently, Collins Aerospace was able to run tests of their own and estimated effective areas to be 0.006 in². The importance of Task 3 is to validate the test methods used in Task 2 to obtain the effective area. If the measured effective areas measured in UCICL's test facility matched Collins Aerospace's results, and the method used in Task 3 is the same as Task 2, then the method used in Task 2 is considered valid.

Task 4. Develop Test Matrix

Design Expert is used to develop the test matrix for testing conditions. To help limit the number of runs for time efficiency, a Box Behnken approach was taken. Pressure drop, preheat temperature, fuel composition, and the adiabatic flame temperature were defined as factors. 15% O₂-NO_x, NO and CO were all measured as responses. The upper and lower limits are expressed in Table 3 and Table 4.

Table 3. Factors for Test Plan

Factor	Units	Lower Limit	Upper Limit
Pressure Drop	%	2	6
Preheat Temperature	K	500	800
Fuel Composition	%H ₂	0	100
Adiabatic Flame Temperature	K	1500	1850

Table 4. Responses for Test Plan

Response	Units
NO _x	ng/J
NO	ng/J
CO	ng/J

With the effective areas known from Task 3, the air flow rates can be determined using Equation 13. Then with adiabatic flame temperatures, the equivalence ratios and subsequently, the fuel flow rates are defined. The test matrix was then applied to each of the various configurations. The originating test matrix is reported in Table A- 6 and its flow rates in Table A- 14 in the Appendix.

Task 5: Evaluate and Analyze Experimental Results

All values obtained from the experimental test runs were reported in Design Expert to be analyzed. Design Expert allows for ease of ANOVA analysis to report the significance of factors and their weight in the overall response. This is repeated for each of the 16 different configurations. The factor interactions between each case are studied to create a predictive

model. Other features in this software include numerical optimization and surface responses to aid in the selection of the most optimal configuration.

Task 6: Verify Experimental Results with Theoretical Model on CHEMKIN

To verify the experimental results, a numerical model was built in CHEMKIN in parallel with Task 4. CHEMKIN is a kinetic software that can give more insight into the contribution of each pathway (thermal, prompt, fuel, etc.) in the overall NO_x emissions. Cameras with temperature sensors are utilized to help determine temperature, reaction zones, and volumes to be used in the model. GRI Mech 3.0 is selected for the reaction mechanism in this study.

Task 7: Establish the Optimal Configuration

After gathering results experimentally and numerically, one final configuration is selected as the most optimal configuration. This configuration should produce the least amount of NO_x emissions, but still be stable such that autoignition and flashback are not concerns. The final configuration is then tested at a high atmospheric test facility to validate integration for use in a full-scale gas turbine.

4. Methodology

4.1 Experimental Methods

The experimental setup was designed according to desired operability requirements during testing:

1. The entire setup must be interchangeable to accommodate for different injectors
2. The airbox must accommodate for data logging devices
3. The combustion chamber must have an optical view for visual data
4. The airbox must be leakproof

Designing an airbox to be interchangeable to interface with different injectors required the airbox to be broken into multiple parts. First, a standard 6 in. stainless steel pipe was selected as the airbox. To seal the airbox, a top plate and bottom plate were added. The Collins injector interfaced with the top plate as shown in Figure 10. The injector is held in place with a tripod system with two 10-32 nuts on each prong. On the flip side, the bottom plate interfaced with the heater as shown in Figure 11. The heater is directly attached to the bottom plate which helps minimize any heat losses and allows for a quicker heating process for the experimental setup. Both plates have through holes which the threaded 10-32 screws go into to thread into the airbox. Gasket insulation material is installed in between the interfacing plates to prevent leakage.



Figure 10. Top Collins Injector Plate

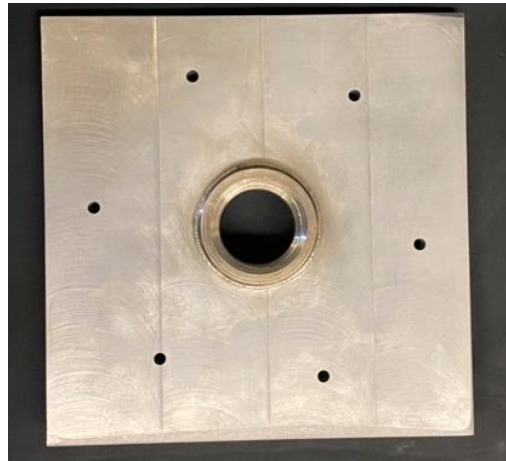


Figure 11. Bottom Heater Plate

To accommodate for pressure transducers and thermocouples, ports alongside the airbox are welded as shown in Figure 12. These ports are adapted with Yor Loks with front and back sleeves which allows them to be leakproof. When the nut threads onto the fitting, the front and back sleeves act as a lip mechanism that prevents any gas or liquid from escaping. A total of nine are installed in varying sizes and locations. Another advantage of having Yor Loks is their adaptability. The fittings can be swapped from a tee, straight connector, through wall, etc. since they are all the same size. This allows for ease of flexibility when accommodating data logging devices and for the air and fuel lines. An example of a Yor Lok fitting is shown in Figure 13.



Figure 12. Airbox with Side Ports

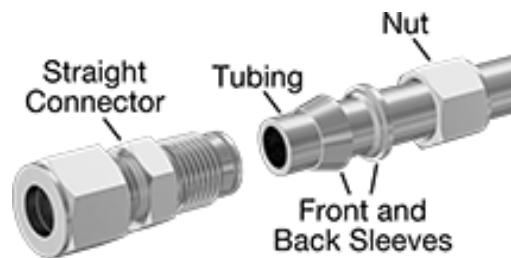


Figure 13. Yor Lok Fittings

To allow cameras to capture flame characteristics, a quartz tube was sandwiched between the injector and top plate with four threaded struts. The struts are held in place with 10-32 nuts that allow for the top plate's height to become adjustable. These struts are then thread directly into the airbox. At the top interface plate, there is a groove for the quartz cylinder to rest in place to minimize movement during testing (see Figure 14). To seal the interfaces between the various plates, high temperature paper gaskets were used. The finalized setup is shown in Figure 14. A total of three thermocouples are attached to the setup.

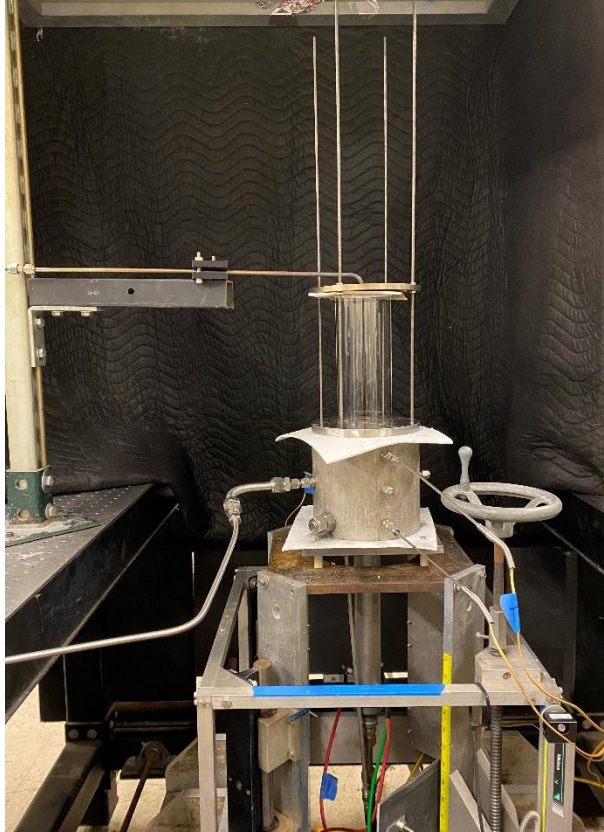


Figure 14. Completed Airbox Setup on the Test Stand

Auxiliary equipment is added to the airbox for data logging. Three type K thermocouples are used (model 3857K91 from McMaster Carr). The first two, shown in the front at the top and bottom in Figure 14, are used in LabView's NI 9213 with NI cRIO 9074. The two are strategically placed at the airbox inlet and outlet to monitor the temperature across the airbox. The third thermocouple is used for the temperature controller with the heater as part of a closed loop feedback system. The thermocouples have an accuracy of $\pm 0.75\%$. LabView's NI 9213 has a sample rate of 100S/s with an accuracy of $\pm 0.8^\circ\text{C}$.

A pressure transmitter (model Tek Bar 3120B with $\pm 0.0075\%$ of the full scale) is used to collect the pressure drop inside the airbox and is routed to NI 9203 for processing. NI 9203 has a sample rate of 200kS/s and an accuracy of $\pm 0.18\%$ of the reading). The pressure transmitter is shown in Figure 15. Lastly, a 6kW in line electric pipe heater (model 007-10137

from Convectronics) and a controller powered by 220V (model 006-10273 and 006-10290 from Convectronics), was selected for the supplied test conditions (see Figure 17). The Piccolo temperature controller has an accuracy of $\pm <1\%$ of the reading. The current test facility supplies 50 amps which is sufficient for the heater. 8AWG wires were used for all connections. The heater and its connections are shown in Figure 16.

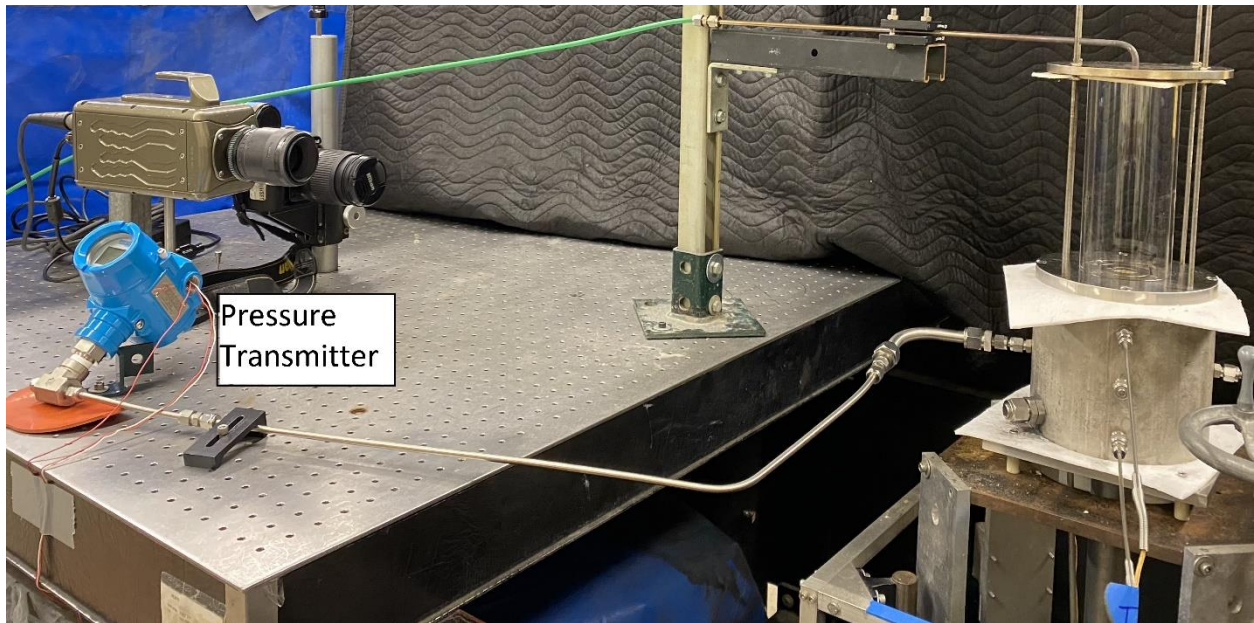


Figure 15. Pressure Transducer Routed to the Airbox

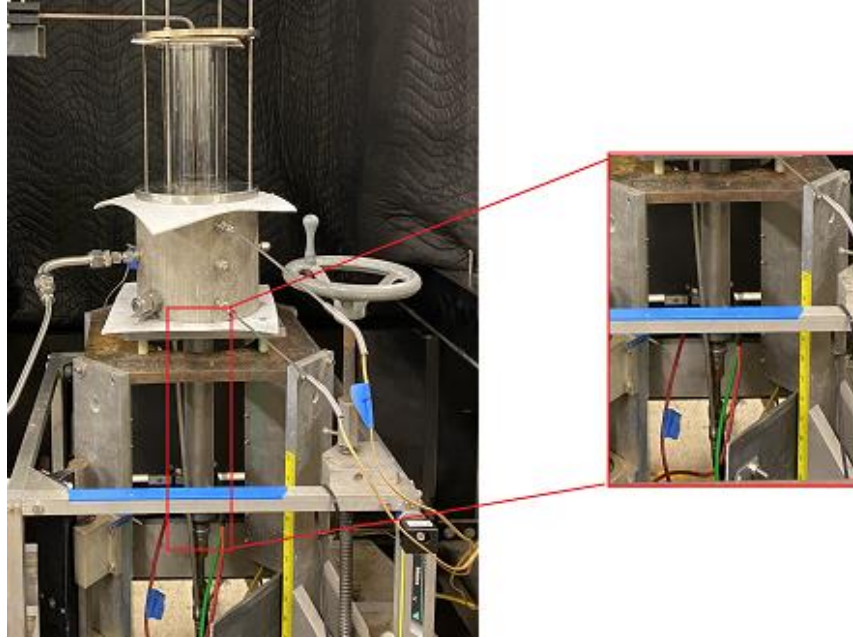


Figure 16. Heater with Connections



Figure 17. Heater Controller Box

4.1.1 Methodology for Effective Area Tests

To conduct the effective area test, the airbox was attached to the test stand with the heater attached. The air from the test facility is then routed directly and injected into the air box after

passing through the O'Keefe 0.125 in. sonic orifice as shown in Figure 18. The sonic orifice allows for convenient conversion from a pressure reading to a flow rate. It is important that there are no contractions smaller than the sonic orifice after the air passes through to avoid further choked flow.

To measure the pressure drop, a line is connected from the pressure transducer (model Tek Bar 3120B) to the air box. The pressure drop and supplied pressure are recorded to obtain the effective area from Equation 13. This procedure is repeated for the fuel circuit. The only difference is that the airline is 1/4 in., and the fuel line is 1/8 in. To avoid pressure drops along the 1/8 in. line, the pressure reading is taken directly before entering the injector with a tee attachment. When measuring the effective area of the fuel circuit, the injector does not need to be enclosed since the fuel is directly fed into the injector. It is important to note that the pressure transmitter and sonic orifice should be calibrated prior to data recordings.

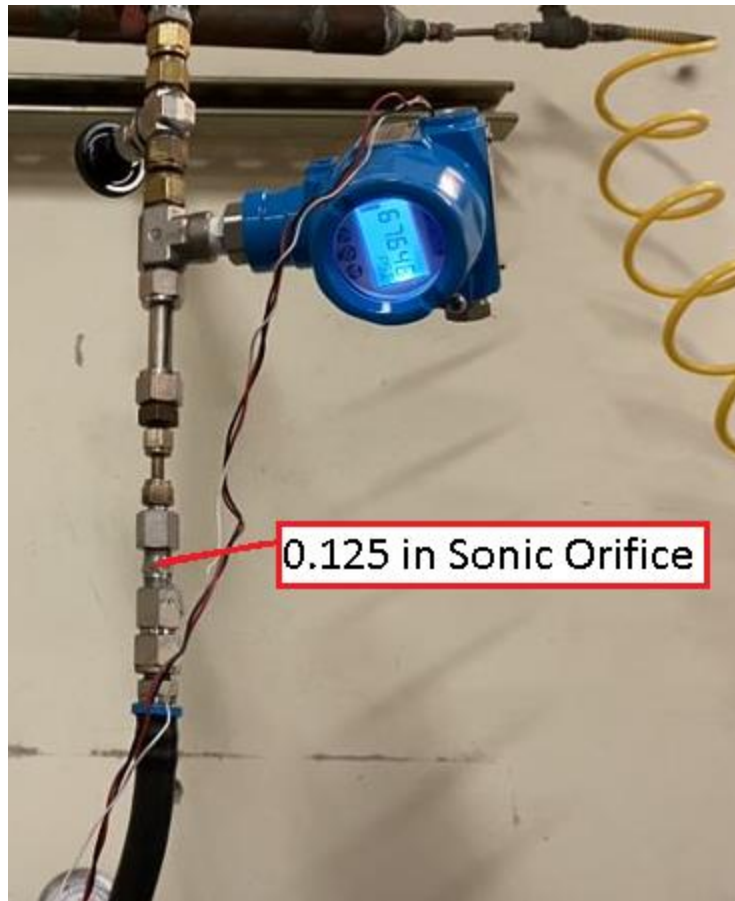
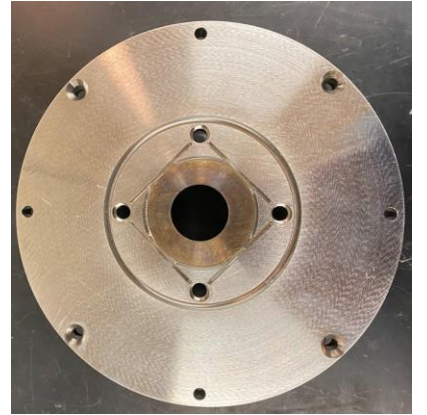
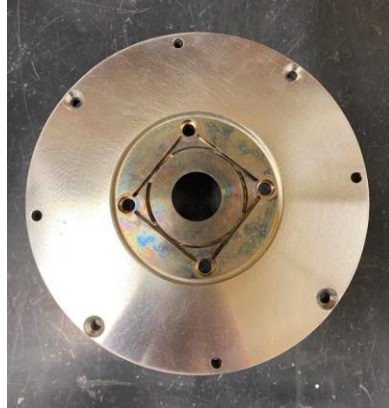
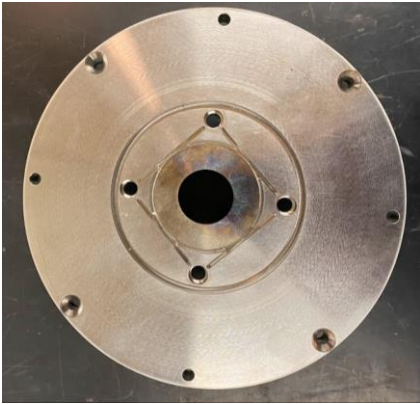
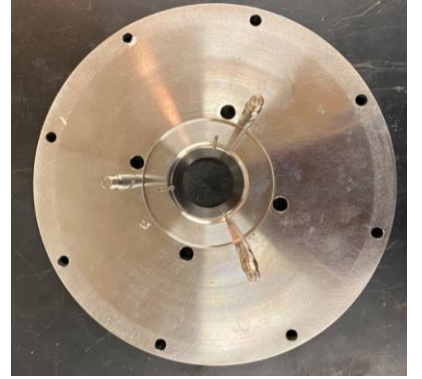
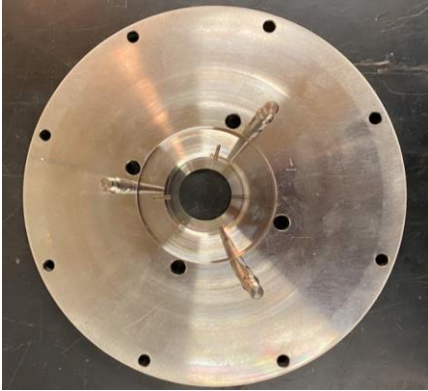


Figure 18. Airline Connections

The hardware for these tests is shown in

Figure 20 and the plates are shown in Figure 19. Each different pairing of a plate and injector is unique to a different flow split, swirl angle and contraction pattern. Table 5 summarizes the matching pairs of the injectors and plates.



(a)

(b)

(c)

Figure 19. (a) Plate Configuration 1, (b) Plate Configuration 2, (c) Plate Configuration 3

Table 5. Test configurations

Injector Number	Plate Number	Splits	Fuel Swirl	Air Swirl
1	2	0	-1	-1
2	3	-1	0	1
3	2	0	0	0
4	2	0	-1	1
5	3	-1	-1	0
6	1	1	1	0
7	1	1	0	1
8	2	0	1	-1
9	1	1	0	-1
10	2	0	1	1
11	3	-1	1	0
12	3	-1	0	-1
13	1	1	-1	0
14	1	1	1	1
15	1	1	1	-1
16	3	-1	1	1



Figure 20. Injectors 1-16 (Left to Right)

4.1.2 Methodology for Emissions Measurement

To measure emissions, a water-cooled probe was attached right at the exit of the combustion chamber (top of the top plate). The emissions line is then routed to the PG 350 gas

analyzer for measurement. The analyzer also can store emissions data over time. In conjunction, cameras were strategically placed on the table to accurately capture shadow effects and heat release zones. The analyzer has an accuracy of +/- 0.5% of the full scale. Emissions data is used to create a model in CHEMKIN and ANSYS CFD to compare with observations obtained during testing. The probe can be seen at the top of the exit plate in Figure 14.



Figure 21. PG 350 Emissions Analyzer Machine

The PG 350 analyzer can only measure on a volume dry basis. There are menu settings that allow the user to correct the value to 15% O₂, however as reported in literature, there are some biases when reporting in a volume dry basis for hydrogen than when compared to methane [67]. To resolve this, emissions in this thesis will be reported on two scales. The conversion from 15% O₂ ppmvd to ng/J can be obtained by first converting the measured emissions from a volume to a mass basis.

$$S_{m,raw} = S_v * \rho \quad \text{Eqn. (21)}$$

where $S_{m,raw}$ represents emissions converted to a mass basis without added correction factors, S_v is the measured emissions on a volume basis and ρ is the overall density. Units of density are in mg/m^3 since S_v are reported in parts per million and have a magnitude of 10^{-6} .

To account for differences in fuel composition, a fuel factor, F is required.

$$F = \frac{26854 * (3.64[H] + 1.53[C] + 0.57[S] + 0.14[N] - 0.46[O])}{Q_{gr}} \quad Eqn. (22)$$

where Q_{gr} is the gross heating value in Btu/lb. H, C, S, N, and O represent the corresponding elemental species by percentage of mass in the fuel mixture. Combined with the oxygen correction factor, the final conversion from a volume basis to a mass basis is shown in Equation 23. Units of F are in m^3/GJ but may be converted to m^3/MJ for a direct conversion to ng/J .

$$S_m = S_{m,raw} * F * \frac{20.9}{20.9 - \%O_2} \quad Eqn. (23)$$

When working with mixtures of fuels, the F factor is calculated differently. The F factor is the sum of each individual fuel and the prospective fraction of total heat input from each fuel, X , as shown in Equation 24.

$$F_{total} = \sum_{k=1}^n X_k F_k \quad Eqn. (24)$$

Similarly, the gross heating value for mixtures is calculated in Equation 25. It should be emphasized the gross heating value is based on percent mass. Z is the mass fraction of the total mass of the fuel from each individual fuel.

$$Q_{total} = \sum_{k=1}^n Z_k Q_k \quad Eqn. (25)$$

4.2 Numerical Analysis

After the collection and analysis of all experimental data, there is a need to validate the results with numerical analysis. There are a variety of software packages that exist to accurately predict and model emissions. These include but are not limited to ANSYS Fluent, ANSYS CHEMKIN and Design Expert. In the following sections these software methods and their niche are explained in detail.

4.2.1 CRNs and CHEMKIN

Many strategies have been developed to model emissions especially for NO_x pathways and formation. Some common strategies include Large Eddy Simulations (LES), Reynolds-averaged Navier Stokes equations (RANS) and the Eddy Dissipation Concept by Magnussen and Hjertager [68], [69]. However, all three strategies require ultra-fine meshes to capture effects of turbulent flows which is computationally costly. As a result, to obtain accurate yet quick results, chemical reactor networks (CRN) are used in tandem with computational fluid dynamics (CFD). In the following paragraphs, CRN will be discussed in detail while CFD is discussed in section 4.2.3.

As the name suggests, CRNs, are comprised of sets of idealized reactors in series or in parallel that represent an equivalent or simplified flow field to capture chemical reactions. S.L Bragg first introduced the concept in 1953 where he modeled a premixed flame using a perfectly stirred reactor (PSR) in series with a plug flow reactor (PFR) (also known as a Bragg Cell) [70]. The Bragg cell can be modified to simulate the kinetics of more complex flow fields such as

recirculation zones and pilot flames. This gives flexibility for some researchers to add as many as 20 different reactors to capture all minute details, but ultimately these reactions can be simplified down to less than ten reactors and still be able to accurately predict emissions. This methodology has been successfully implemented in different studies: [71], [72], [73].

In more detail, a PSR is 0-D homogenous, ideal reactor where perfect mixing is achieved inside the control volume. This makes it ideal to use when one is interested in modeling highly turbulent flows. The fundamental assumptions driving the PSR calculations are that it is assumed to be steady state and its residence time is computed by density multiplied by the volume which then is divided by the mass flow rate ($R = \frac{\rho V}{\dot{c}}$) [74]. Other limitations and assumptions are that the conversion rates from reactions to products are controlled by chemical reactions rates and that mass transport to the walls are infinitely fast. The following variables are required as inputs into CHEMKIN, a kinetics software, for a PSR: residence time, reaction volume, species of gas, mass flow of gas, initial guess for temperature, pressure, and heat losses.

A PFR, is an ideal reactor where no mixing in the axial direction exists, but perfect mixing in the traverse direction does. [74]. Without axial mixing, the maximum reaction conversion is achieved which implies that there are no mass transfer limitations. Moreover, since it is modeled as 1-ODE, the computational time is significantly reduced, and no transport properties are required. As a result, the governing equations are simplified forms of the conservation of mass, energy, and momentum. The following variables are required as inputs into CHEMKIN for a PFR: starting and ending axial position, initial guess for temperature, pressure, and reaction zone.

As alluded to previously, CRNs are very easily constructed in CHEMKIN. With the toolset provided, the researcher can build models to best match their experimental setup by adding gas mixers, inlets, exhausts (outlets), and numerous different reactors. It is also very flexible and can take specified outputs (i.e., percentages) from one reactor to another to better mimic recirculation flow fields. Moreover, the computational time for CRNs are orders of magnitudes less than other methods previously mentioned. For simple CRNs, it can take as little as one minute to complete a calculation.

CHEMKIN also allows for studies of different NO_x pathways and their contributions through different reaction mechanisms. The reaction mechanisms included are GRI Mech 3.0, Konnov, Galway III, USC Mech II. GRI Mech 3.0 is designed more for natural gas and consistently underpredicts NO_x emissions [71]. On the contrary, Konnov consistently overpredicts NO_x emissions, but it is more suited for smaller hydrocarbons which is good for studying hydrogen fuel mixtures. On the plus side, for both mechanisms, the nitrogen chemistry is already built in. For Galway III and USC Mech II, however, the nitrogen chemistry must be manually added into the list of reactions. USC Mech II was best suited for variable compositions that can include alkanes with the addition of hydrogen and carbon monoxide. For Galway III, like GRI Mech 3.0, it was designed for the combustion of natural gas with heavier alkanes like ethane, propane, and butane [71]. Overall, the Galway III mechanism was reported to best match experimental results. In this thesis, only GRI Mech 3.0 will be used for analysis due to its wide use in literature and most studied mechanism to date.

4.2.3 CFD and ANSYS Fluent

Computational Fluid Dynamics, or CFD, is used in tandem with CHEMKIN to lower computational costs. As a standalone software, CFD can predict emissions, but it is largely

inaccurate. The model ignores a large portion of chemical kinetics to reduce computational time [21]. Thus, while NO_x trends can be predicted, the details such as rates of formation cannot be obtained [71]. Nevertheless, CFD offers the ability to “look inside” the experimental setup by having the capability to model flow fields, simulate areas of heat release/reaction zones, peak temperatures, and flame structures. All of these parameters are important to incorporate into CHEMKIN to help refine the model. In this study, CFD studies are conducted with ANSYS Fluent. This thesis will not discuss CFD results as finite details of the injector are classified and complex. Collins Aerospace is hence responsible for the CFD analysis in the overall project.

4.2.4 ANOVA

Analysis of Variance (ANOVA) is used in Design Expert, a software that aids in determining significant factors by eliminating and filtering out variances in the experiment. Design Expert can also be used to design ideal experiments based on a combination of factors and parameters. ANOVA is based purely on normal distribution statistics. The user will specify factors that are predicted to affect the responses. The software then compares the experimental data to the normal probability distribution. The factors are deemed significant if the probability, or p, values fall below a certain threshold. For example, to be 95% confident that a certain population is different or significant, the p values should be less than 0.05. Any factors or interactions that have p values less than 0.05 have some contribution in the predictive model.

Design Expert also helps with designing a test matrix that can pull the most amount of data from the fewest number of runs. This works well for prescreening results. Examples of the included models are factorial designs, Box-Behnken, Central Composite, mixtures, etc. Factorial designs are the base design in Design Expert. They are simple and easy to implement, but the major drawback to their design is the large number of runs. Even when considering a fractional

factorial design, the large number of runs can be overwhelming. The Box Behnken and Central Composite design, however, work to limit the number of runs. There are slight differences between the two approaches.

In the Box Behnken approach, points lie within the operating ranges whereas in the Central Composite design, some design points lie outside of the upper specified limit. Furthermore, the Central Composite design also requires five levels whereas the Box Behnken only requires three. Some disadvantages to the Box Behnken approach are that it is sensitive to missing data points and that the design cube falls short on the corners. Despite this, in this research, the Box Behnken approach was taken given time and efficiency constraints. The software also has powerful tools for optimizations as well as for producing surface responses plots and interaction plots.

The current design matrix has 27 points for the original 4 factors and 3 levels (see Table 3) with three of them being repeated points to assess the lack of fit in the model. An additional 16 points were added to the design space to study hydrogen at lower flame temperatures of 1100K-1300K. The lower matrix is comprised of only 50% mixtures of hydrogen and pure methane since methane combustion are incomplete at these lower levels. The final test matrix is shown in Table A- 6. Each injector has a total of 43 points in the design space for a grand total of 688 test points. It is keen to point out that since each injector has its own effective area, the air and fuel flow rates will have to change for each injector to match the pressure drop factor of 2%, 4% and 6%. Changing each flow rate individually for each case would be too time consuming because determining the adiabatic flame temperatures is an iterative process. To resolve this issue, the actual pressure drops were recorded at a fixed air and fuel flow rate and was modified

in Design Expert accordingly. The results of the actual pressure drops are shown in Table A- 8-
Table A- 13.

5. Results and Discussion

The experimental results are first analyzed in section 5.1 by using Analysis of Variance (ANOVA). Four responses were analyzed: CO, NO, NO_x, and NO/NO_x to establish significant single factor and factor interactions. A lower adiabatic flame temperature matrix ranging from 1100K-1300K was also analyzed to compare hydrogen's emissions levels at low and high adiabatic flame temperatures. The four responses and the injector's geometric effect were then optimized using Design Expert's Numerical Optimization tool to minimize emissions. NO and NO_x pathways were then analyzed with CHEMKIN in section 5.2. Before analyzing pathways, premixed vs. non premixed and heat losses to validate the model are conducted in 5.2.1 and 5.2.2.

It is noted that, while the adiabatic flame temperature is an independent variable (fuel and air volumetric flow rates are varied instead) in this study, the true flame temperature is unknown. Further, the adiabatic flame temperature can only be estimated because the LDI system studied is not perfectly premixed. To elaborate, when the system is not perfectly premixed, there exists pockets of fuel/air burning with various local stoichiometries. Yet, for the purpose of analysis, the overall average equivalence ratio is used to estimate the average adiabatic flame temperature. Hence, the actual average temperature is lower than the adiabatic flame temperature used for analysis, and it varies over a range of temperatures rather than being a single value. While adiabatic flame may not be the best independent variable, it was used due to convenience and still offers valuable insight into how emissions change as a function of temperature. This also allows conclusions to be drawn on chemical kinetics such as thermal mechanisms. Moreover, most papers in literature compare and tabulate results using adiabatic flame temperatures so by performing an experiment where adiabatic flame temperature is an independent variable, it will

allow for direct comparison across multiple papers. As such, the estimated adiabatic flame temperature is used as an independent parameter for the context of this thesis.

While not a focus of this thesis, measurements of the injector effective areas were carried out. The goal of the design process was to establish a hardware set with identical effective areas for the fuel and air circuits but with varying air flow splits, air swirl angles and fuel swirl angles. The effective area of the air and fuel circuit were measured experimentally to be 0.15 in² and 0.007 in² (see Table A- 1 for details) with standard deviations of 0.003 and 0.0007, respectively. These results indicate a high-fidelity manufacturing process. More details regarding the effective areas are found in section 7.1 in the Appendix. Next, in section 7.2, the differences between reporting emissions on a volume or mass basis are discussed. Then, in section 7.3, the effects of volume confinement are studied with three geometric configurations for the combustion chamber. Lastly, Section 7.4 contains all supplementary graphs and tables that aid in discussions in the following sections.

All results are analyzed from experimental data which are recorded in Table A- 15-Table A- 30 in the Appendix. Emissions are tabulated on both a volume and a mass basis and the measured excess oxygen is used as a check for the air and fuel flows set during the test point. The calculated percent excess oxygen is obtained from Equation A-1 using the general combustion equation with hydrogen and methane as the fuel. The calculated value is then compared to the measured oxygen obtained from the PG 350 analyzer. All deviations from the calculated percent oxygen were less than 5%.

5.1 ANOVA Analysis

In the following sections, ANOVA (Analysis of Variance) results for the emissions models are obtained from Design Expert, a statistical software. CO, NO, NO_x, and NO/NO_x models are investigated and analyzed where each factor and factor interaction presented as significant were discussed. The significance level was based on a p value of less than 0.05 to be at least 95% confident the factor in question plays a role in the model. Factors and factor interaction that decreased emissions were noted. Next, a lower temperature (1100-1300K) test matrix was analyzed to determine if hydrogen can produce lower NO and NO_x emissions at lower adiabatic flame temperatures compared to the best-case scenarios for methane. Lastly, the analysis of each emissions model (CO, NO and NO_x), numerical optimization was performed where emissions were minimized and factors that minimized emissions were favored.

5.1.1 CO Model

The results of the ANOVA for the CO model are shown in Figure 22 and the CO model equation is shown in Figure 23. The results were selected based on a confidence interval of at least 95% or a p value of less than 0.05. Although the lack of fit is significant, this is due to the repeated points in the test matrix responses being nearly identical to one another. The lack of fit is comparing the significance of the difference in the actual and modeled values vs the variation in the repeats. Thus, any small deviations between the model and actual values will result in an indicated lack of fit from a purely statistical viewpoint. A better judgement of a good model would be to assess if the data are considered a normal distribution for statistical analysis and if residuals are randomized for each run. Figure 24 and Figure A- 9-Figure A- 11 in the Appendix show that the data are generally normally distributed and the residuals are randomized when the model is fitted to a natural log equation. For some test points, the PG 350 analyzer recorded

negative numbers. These numbers were interpreted to be zero since negative emissions cannot exist and certain models in Design Expert do not allow negative values. Moreover, cases with high CO were ignored due to incomplete combustion. It should be noted that levels of CO were constantly fluctuating +/-10ppm during data collection as the full scale was 500 ppm and the accuracy of the analyzer is +/-0.5% of the full scale. As a result, most CO numbers were rounded (e.g., 1214.33 was rounded to 1200).

Source	Sum of Squares	df	Mean Square	F-value	p-value	
Model	957.80	10	95.78	126.87	< 0.0001	significant
A-Splits	11.34	1	11.34	15.02	0.0001	
C-Air Swirl	27.88	1	27.88	36.93	< 0.0001	
E-Preheat Temperature	6.15	1	6.15	8.14	0.0045	
F-Fuel Composition	476.47	1	476.47	631.11	< 0.0001	
G-Flame Temperature	42.75	1	42.75	56.62	< 0.0001	
EF	4.06	1	4.06	5.37	0.0209	
FG	24.36	1	24.36	32.27	< 0.0001	
E ²	15.82	1	15.82	20.95	< 0.0001	
F ²	76.73	1	76.73	101.64	< 0.0001	
G ²	107.89	1	107.89	142.90	< 0.0001	
Residual	347.29	460	0.7550			
Lack of Fit	342.12	404	0.8468	9.18	< 0.0001	significant
Pure Error	5.17	56	0.0923			
Cor Total	1305.08	470				

Figure 22. ANOVA Results for CO Model

ln(CO-m)	=
+61.01456	
-0.191161	Splits
-0.298030	Air Swirl
-0.022193	Preheat Temperature
-0.134966	Fuel Composition
-0.053337	Flame Temperature
-0.000028	Preheat Temperature * Fuel Composition
+0.000098	Fuel Composition * Flame Temperature
+0.000017	Preheat Temperature ²
-0.000482	Fuel Composition ²
+0.000014	Flame Temperature ²

Figure 23. CO Model

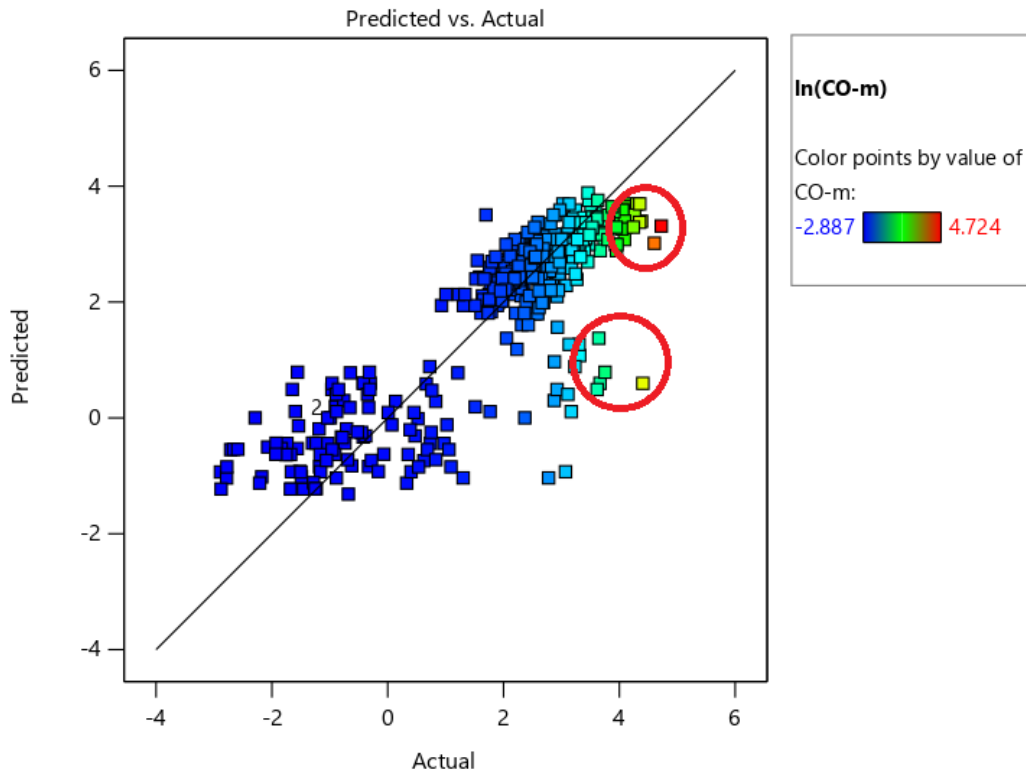


Figure 24. Predicted vs. Actual for CO Model

The “outliers” (indicated by the red circles in Figure 24) in the model corresponded to hydrogen cases where CO emissions were high (i.e., ~20-30 ng/J). When operating on hydrogen, one should expect low CO levels due to no carbon in the composition. These levels of high CO are most likely caused by residual methane in the combustion chamber which have not been

burned completely or unburned hydrocarbons. The Brooks mass flow controller value fluctuates from +/- 0.05% to +/-0.1%, or 0.00706 SCFM to 0.00782 SCFM.

Other models of CO were studied to assess the sensitivity of the natural log model. The flame temperature as a factor was ignored since high levels of CO indicate that the calculated vs. actual flame temperature are different. This model showed that the plot of residuals best fitted the normal distribution, however the predicted vs. actual plot was poorly represented. The power model with a lambda of 0.2 was also investigated which was similar to the natural log model. Regardless, the main interactions of factors A, C, E, F, G, FG, E², F², and G² were present in the natural log and power model. With the exclusion of the flame temperatures, all factors with the exception of G (flame temperature) were present. Thus, the best model, natural log, was selected based on overall fit and normally and randomly distributed residuals.

From Figure 22, the factor with the highest F value is the fuel composition at 631.11. The injector fuel swirl and pressure drop do not significantly impact CO emissions. Fuel composition having the greatest influence on CO is plausible because with Hydrogen fuel, absolute or near zero CO emissions are achieved. With mixtures and pure methane, the level of CO is affected by other factors such as flame and preheat temperature. This is noted by factor interaction FG (fuel composition and flame temperature). To elaborate, at a flame temperature of 1500K, with pure methane, incomplete combustion is likely to take place since the fuel mixture is approaching the lean limit of stability. CO emissions at 1500K for methane can be as high as 5000 ppm. On the contrary, CO emissions are lower (~less than 100 ppm) at flame temperatures of 1850K. Higher temperature helps stabilize and complete the reaction. The tradeoff of stable combustion temperatures can be increased NO and NO_x emissions. The relationship between fuel composition and flame temperature is shown in Figure 25 where the red dots represent the design

points in the matrix at which data was obtained experimentally. The test matrix with all of the design points is shown in Table A- 6.

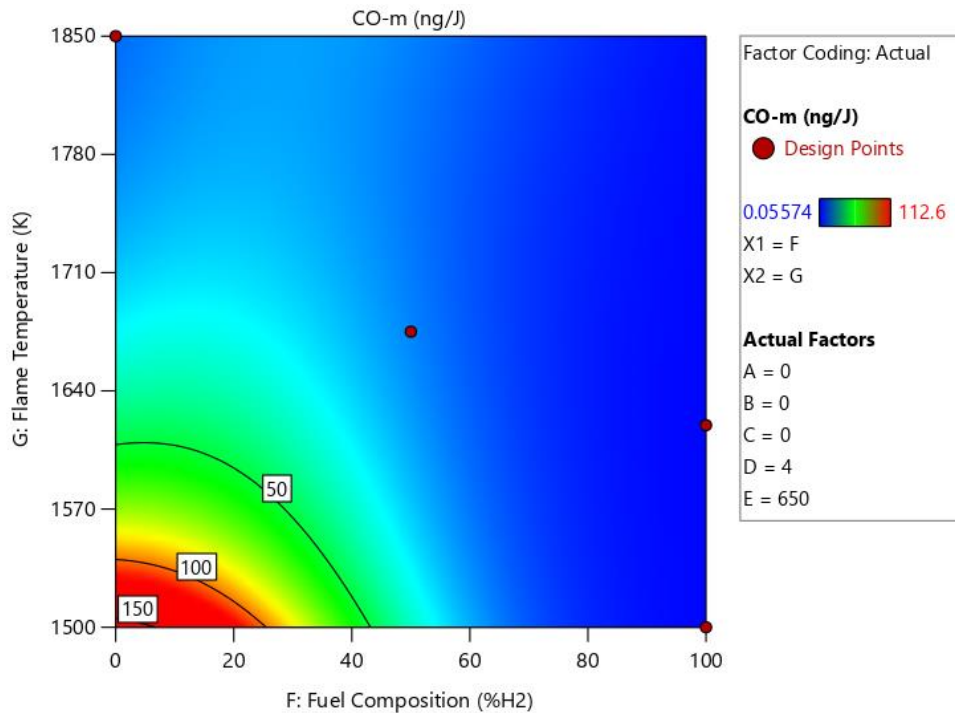


Figure 25. Flame Temperature vs. Fuel Composition for CO Model

For similar reasons, the other factor interaction, EF (preheat temperature and fuel composition) is best explained with the fact that hydrogen fuel has no carbon in its composition. As a result, even when preheat is increased, the level of CO emitted is still near zero for hydrogen. As opposed to methane, in which when preheat is increased, CO emissions also slightly decrease. It should be emphasized that preheat and adiabatic flame temperature are separate factors. While preheat has effects on the flame temperature, flame temperature was held constant while the equivalence ratio changed to reach the desired conditions of preheat and adiabatic flame temperature. Preheat temperature also reduces ignition time which can increase emissions if there is not enough time for the fuel and air to thoroughly mix.

The effect of single factors: A, C, E, F, and G can be more easily comprehended (see Figure 26-Figure 30). The warnings in the figures indicate that these factors have interactions with other factors. Factor interactions are discussed after the discussion of single factors. The first factor, A or the plate split, investigates the flow through the injector vs. through the injector plate. More air through the injector is signified by the upper portion of the design matrix. Having more air pass through the injector lowers CO emissions due to more interaction with the fuel. The more interaction between the air and the fuel inside the injector, the more likely complete combustion can take. Next, factor C describes the air swirl where the steepest swirl angle is the upper portion of the design matrix. With a greater swirl angle, mixing is enhanced, thus leading to more complete combustion and lower CO emissions. This increase in mixing between the air and fuel ultimately leads to greater stability. Factor E (preheat temperature) is more complex than other factors as it comes with interaction as discussed previously. Overall, factor E has a slight parabolic relationship where lower and higher preheats lead to more CO emissions. This is most likely due to the model's fit since there are squared terms in the model. If the squared terms were removed, increasing preheat decreases CO emissions. For factor F (fuel composition) the reasoning is straightforward as higher compositions of hydrogen leads to lower CO emissions as carbon is eliminated. Lastly, for factor G or flame temperature, as the flame temperature increases, the overall CO emissions are lowered likely due to complete combustion taking place at higher temperatures rather than lower temperatures.

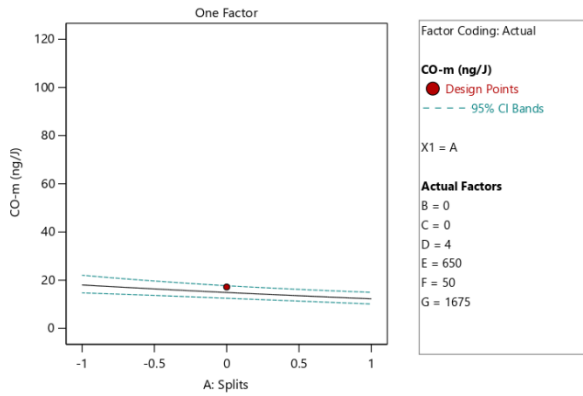


Figure 26. CO Emissions vs. Air Splits

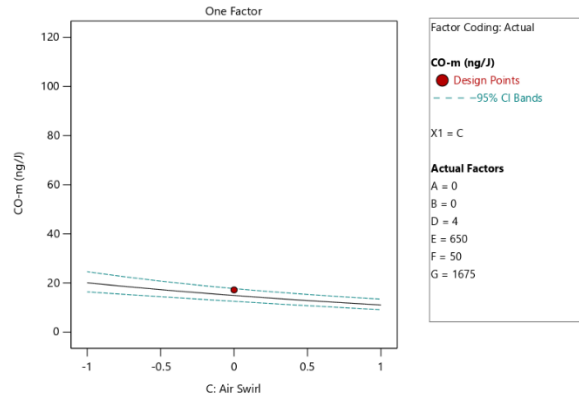


Figure 27. CO Emissions vs. Air Swirl

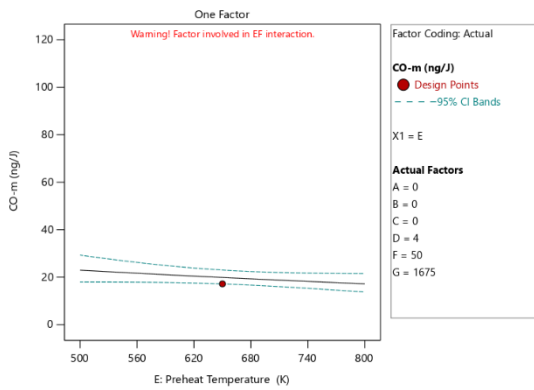


Figure 28. CO Emissions vs. Preheat Temperature. (No Squared Terms)

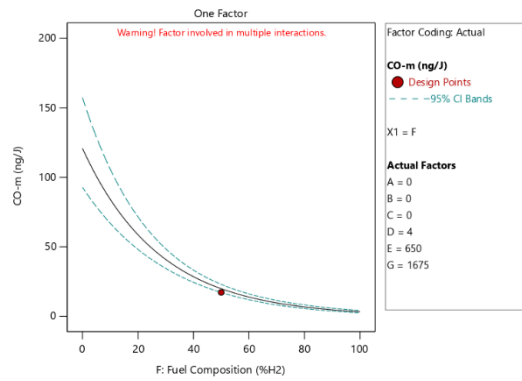


Figure 29. CO Emissions vs. Fuel Composition. (No Squared Terms)

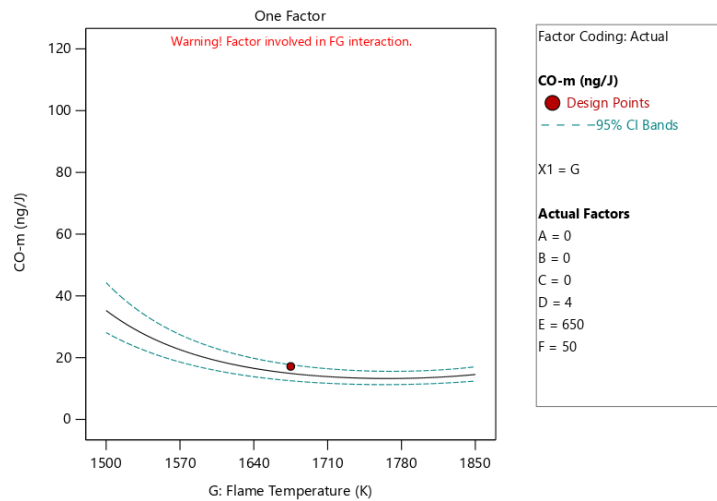


Figure 30. CO Emissions vs. Flame Temperature

Other high level terms E^2 , F^2 , and G^2 's effect were much more complex and not thoroughly understood. Removing these terms from the model will wash out the effect of the

preheat factor and flame temperature factor. To elaborate, when removing these terms, an increase in preheat temperature does not increase CO emissions for a particular fuel composition which is the opposite conclusion of what was previously discussed. The same can be said about the flame temperature. The best explanation for these squared terms are most probably due to the pronounced effect of preheat temperature, fuel composition, and flame temperature. Thus these terms are simply to add “weight” to the model to pronounce these terms more.

5.1.2 NO Model

The experimental data obtained from each injector are plotted in Figure 31 and are sorted by the corresponding run number. As observed, the injector that gives rise to the largest NO emissions is Injector 2 and the injector that yields the lowest emissions are Injector 7 and 14. Injector 2 has a negative air split, neutral (in the middle of the design space) fuel split, and a positive air split. Injector 7 and 14 both share a positive air split and air swirl angle, but Injector 7 has a neutral air split whereas Injector 14 has a positive fuel split. From this chart alone, it can be inferred that higher air splits and air swirl angle are preferred for lower emissions. The effect of each factor on emissions will be explained in more detail in the paragraphs that follow. Notice that there is also a gap of data between run numbers 34-39. These gaps represent missing data where the flame was unsustainable at the specified conditions. These mainly pertained to lower adiabatic flame temperatures between 1100K-1300K for 50% CH₄/50% H₂ and for pure methane cases. At these lower temperatures, methane is unable to sustain a flame as it is below its LBO limits.

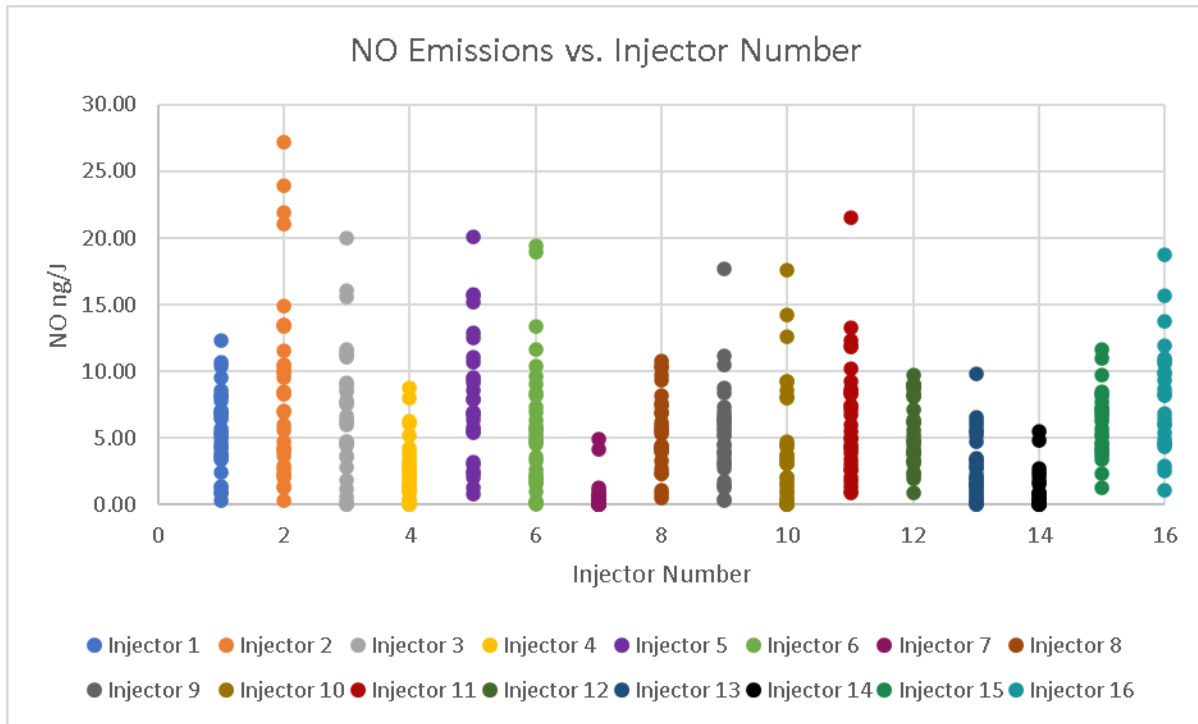


Figure 31. NO Emissions vs. Run Number, Sorted by Injector Number

Figure 32 shows the ANOVA results for NO model and Figure 33 shows the NO model as an equation with its corresponding factor values. From Figure 34 and Figure A- 12 and Figure A- 14 (within the Appendix) show a normally distributed model as well as randomized residuals on a square root model. Thus, normal statistics are confirmed, and ANOVA can be used. All factors were determined as significant based on a p value of $p < 0.05$ or 95% confidence with a square root model. Compared to the previous model, there are more factor interactions reported.

There were several points in the ANOVA results that are indicated as outliers. As mentioned in the discussion of the CO model, these are not actually outliers as they correspond to cases of highest NO emissions. Thus, these points should not be removed simply to better fit the model as they are valuable data points to assess which factors work best to decrease emissions. Moreover, all outlier points corresponded to cases of high hydrogen content

suggesting that methane and hydrogen should not be represented on the same model. This fact is verified in literature, but due to the nature of the Box-Behnken approach, separating these points into a purely hydrogen model vs. a purely methane model is not feasible. If these points were to be removed, the conclusions for the top five factors remain the same, but the order of ranking is different. Other transforms such as the power model with a lambda of 0.3, were also investigated. The same main factors were also present in this model. The square root was ultimately chosen because it was more normally distributed, and majority of residuals fall within the limits.

Source	Sum of Squares	df	Mean Square	F-value	p-value	
Model	424.17	25	16.97	66.74	< 0.0001	significant
A-Splits	0.4514	1	0.4514	1.78	0.1833	
B-Fuel Swirl	2.02	1	2.02	7.93	0.0051	
C-Air Swirl	12.87	1	12.87	50.61	< 0.0001	
D-Pressure Drop	0.3747	1	0.3747	1.47	0.2253	
E-Preheat Temperature	58.64	1	58.64	230.67	< 0.0001	
F-Fuel Composition	73.32	1	73.32	288.44	< 0.0001	
G-Flame Temperature	39.97	1	39.97	157.24	< 0.0001	
AB	12.23	1	12.23	48.12	< 0.0001	
AC	58.66	1	58.66	230.78	< 0.0001	
AD	3.97	1	3.97	15.63	< 0.0001	
AE	3.95	1	3.95	15.52	< 0.0001	
AF	3.30	1	3.30	13.00	0.0003	
AG	1.06	1	1.06	4.16	0.0420	
BC	1.03	1	1.03	4.07	0.0442	
BD	4.40	1	4.40	17.31	< 0.0001	
BG	0.8063	1	0.8063	3.17	0.0756	
CD	1.61	1	1.61	6.33	0.0122	
CE	1.66	1	1.66	6.52	0.0110	
DG	2.20	1	2.20	8.66	0.0034	
EG	1.11	1	1.11	4.35	0.0375	
B ²	1.37	1	1.37	5.39	0.0207	
C ²	14.23	1	14.23	55.98	< 0.0001	
E ²	1.13	1	1.13	4.44	0.0356	
F ²	1.94	1	1.94	7.64	0.0059	
G ²	10.73	1	10.73	42.20	< 0.0001	
Residual	118.46	466	0.2542			
Lack of Fit	106.26	407	0.2611	1.26	0.1357	not significant
Pure Error	12.20	59	0.2067			
Cor Total	542.63	491				

Figure 32. ANOVA Results for the NO Model

Sqrt(NO-m)	=
-8.88846	
-0.207886	Splits
-0.521351	Fuel Swirl
+0.308817	Air Swirl
-0.251714	Pressure Drop
+0.006201	Preheat Temperature
+0.007757	Fuel Composition
+0.007354	Flame Temperature
+0.402706	Splits * Fuel Swirl
-0.712869	Splits * Air Swirl
+0.114800	Splits * Pressure Drop
-0.001084	Splits * Preheat Temperature
-0.003558	Splits * Fuel Composition
+0.000300	Splits * Flame Temperature
+0.079523	Fuel Swirl * Air Swirl
+0.068154	Fuel Swirl * Pressure Drop
+0.000221	Fuel Swirl * Flame Temperature
-0.037256	Air Swirl * Pressure Drop
-0.000697	Air Swirl * Preheat Temperature
+0.000140	Pressure Drop * Flame Temperature
+2.08407E-06	Preheat Temperature * Flame Temperature
-0.130629	Fuel Swirl ²
-0.399612	Air Swirl ²
-4.50690E-06	Preheat Temperature ²
+0.000062	Fuel Composition ²
-2.05991E-06	Flame Temperature ²

Figure 33. NO Model

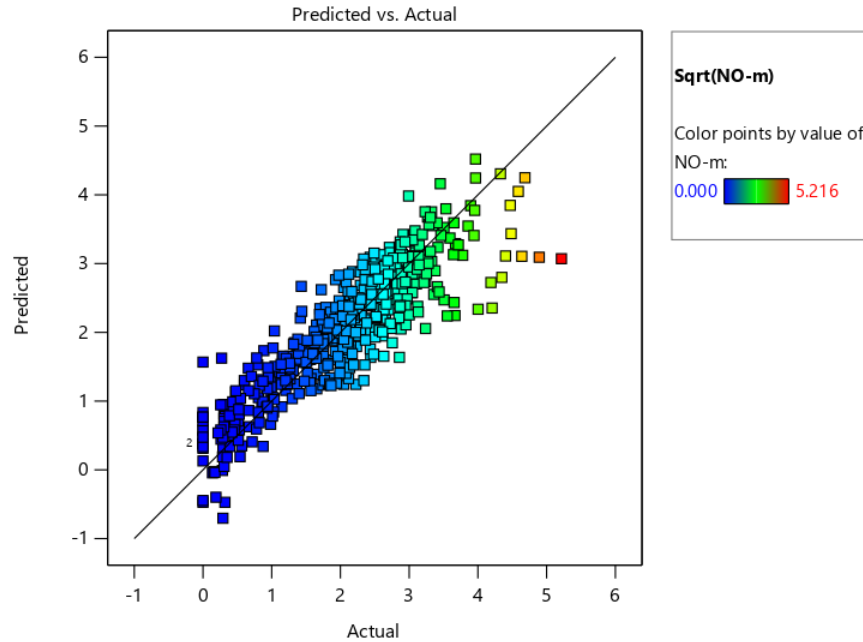


Figure 34. Predicted vs. Actual for NO Model

It is observed again that the fuel composition has the highest F factor at 288.44 followed by preheat and flame temperature. In general, as hydrogen content increases, so does NO emissions. There are several reasons why this may be caused. For instance, due to the unmixed nature of the experiment, hydrogen, with higher flame speeds, is more affected by the unmixedness. The time that it takes to ignite is shorter than the mixing time which can cause spikes in NO emissions. Another reason can be explained by the NNH route for hydrogen vs. the N₂O route for methane. More details regarding this will be discussed in section 5.2.3. This conclusion should be taken with precaution, however. As discussed briefly in section 2.2, hydrogen has wider flammability limits. Therefore, it can burn leaner and at lower adiabatic flame temperatures which has the potential to lower NO_x emissions overall. The wider flammability limits also lead to enhanced stability which is particularly useful for a non premixed system. In non premixed systems, there exists pockets of fuel that leads to a wide range

of equivalence ratios. With increased flammability limits, these pockets of fuel can still react and hold a flame even at lower equivalence ratios.

Similarly, increases in preheat and flame temperature yields higher emissions. This can be attributed to pathways that are thermally dominated such as the Zeldovich mechanism. Pathway analysis to NO formation will be later discussed. A plausible explanation for why preheat temperature has a separate effect from flame temperature is because increasing preheat raises the internal temperature of the system. When the internal temperature of the system is initially hotter, then it is easier to form NO emissions through the thermal mechanisms. This is similar to the concept of the pilot flame where the pilot flame will be more fuel rich than the actual flame.

Increasing the preheat and flame temperatures increases emissions by activating thermally sensitive mechanisms which is best explained via certain thermal mechanisms such as the Zeldovich mechanism. Thermal mechanisms for NO will be discussed in section 5.2.3. From a high-level view, above temperatures of $\sim 1900\text{K}$, NO emissions increase exponentially as the nitrogen bonds dissociate at a rapid pace to combine with oxygen and OH radicals. It was also noticed that increased preheat helped with the stability of the flame. With no preheat, LBO occurred at a higher rate compared to when preheat was added. Preheat reduces the ignition times which allows the equivalence ratio range of a particular fuel to be extended.

Other single factors in the model deal with the plate and injector geometry. Increases in the air splits (more air through the injector) lowers the NO emissions. When there is more air passing through the injector, less emissions are likely to occur due to the air having a more direct interaction with the fuel which promotes homogeneity and thus lowers peak temperatures. As for swirl angles, it is found that a steeper angle for air results in lower emissions but for fuel, results

in higher emissions. Figure 35 displays the injectors that have a higher air split and Injector 3, which is in the middle of the design space, is added for reference. Figure 36 organizes the data by the injector number which allows easy comparison of average NO emissions. With the exception of Injector 6, higher air splits yield lower emissions for all run numbers. Injector 6 a higher fuel swirl angle which negates the benefit of having a higher air split. This factor interaction (AB-air split and fuel swirl) will be explained later in the paragraphs to follow. Similarly, Figure 37 and Figure 38 displays all the injectors with higher air swirl angles Injector 3 as the reference point. With the exception of Injectors 2 and 16, having air swirl angle lowers NO emissions. Upon further inspection, both Injectors 2 and 16 have the lowest air split which is not favorable as observed in Figure 35. The interaction between the air split and air swirl (AC) is explained later.

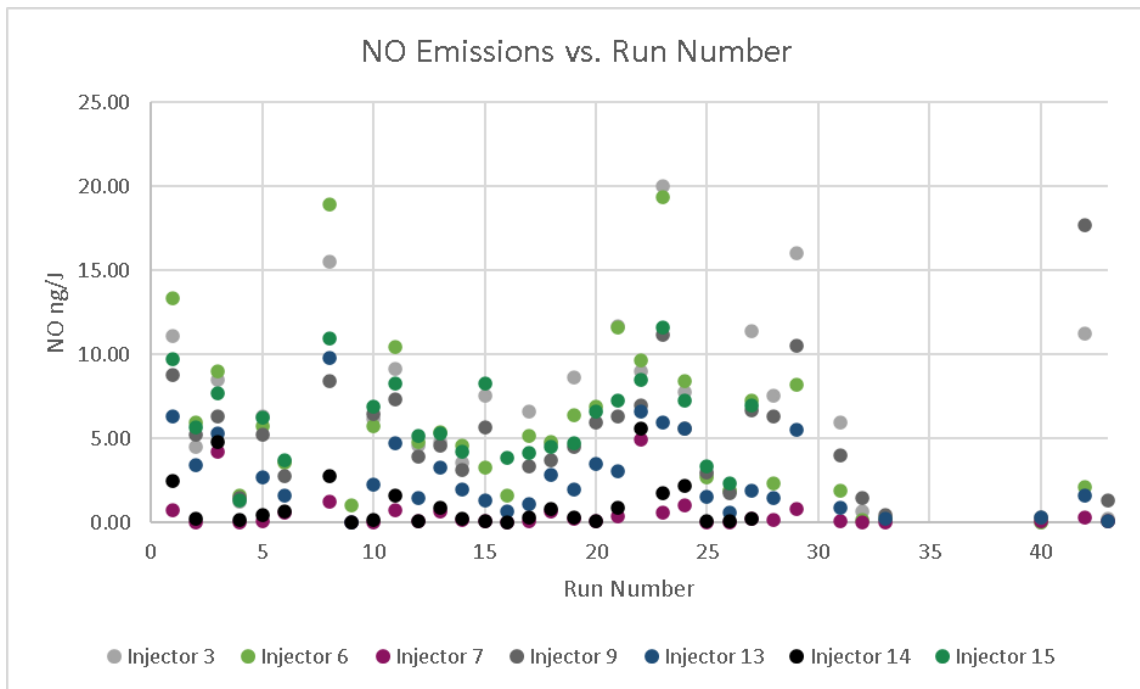


Figure 35. Higher Air Split Injectors by Run Number

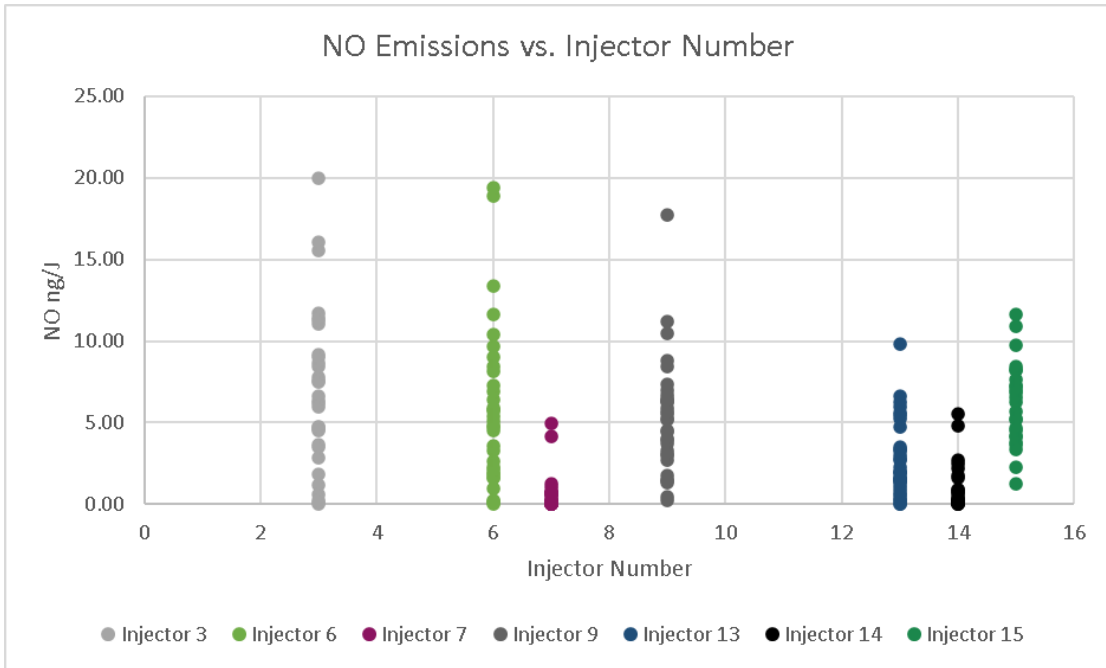


Figure 36. Higher Air Split Injectors by Injector Number

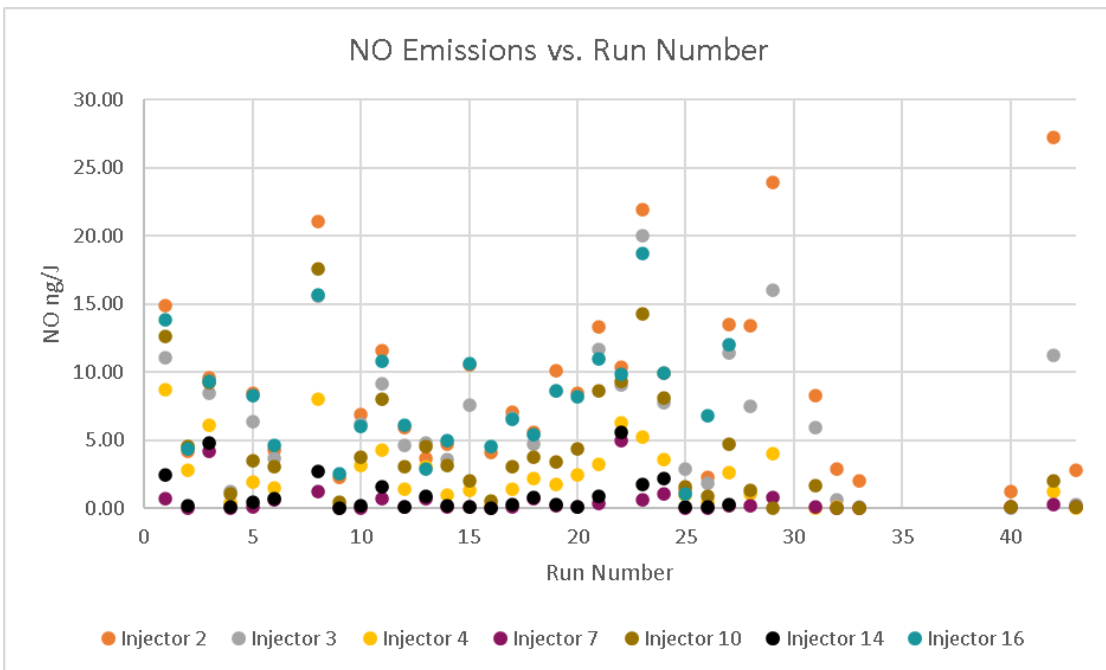


Figure 37. Higher Air Swirl Angle Injectors by Run Number

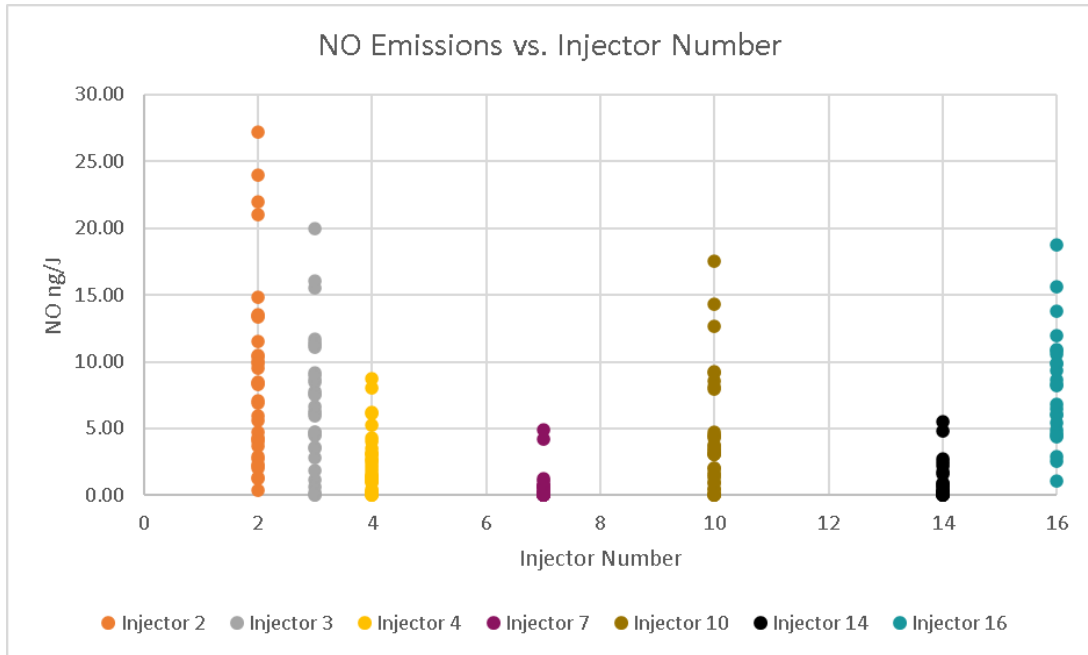


Figure 38. Higher Air Swirl Angle Injectors by Injector Number

A plausible explanation for why lower fuel swirl is favored might be due to the higher flow rate that air is expelled at from the injector, compared to fuel (i.e., 10 SCFM vs. 0.3 SCFM). As the swirl angle for fuel is increased, the axial component of the flow rate (perpendicular to the injector face) is significantly decreased, resulting in a lower velocity. Increasing the air swirl angle for the air, decreases the air velocity and decreasing the fuel swirl angle increases the fuel velocity. As the two circuits approach the same velocity, better mixing can be achieved.

Lastly, the higher the pressure drop, the lower the emissions, although not much different. To elaborate, a pressure drop of 6% and 2% will record 6 ng/J and 8 ng/J of NO emissions, respectively. As seen from Equation 24, lower pressure drops lead to lower velocities which should not promote mixing. As a result, higher pressure drops are more favorable. However, due to the small differences, the model indicates that air and fuel swirl angles impact mixing more than the pressure drop. The summary of the effect of the single factors are shown in

Figure 39-Figure 45. It is also important to note that many of these factors also have factor interactions where combinations of such factors may or may not increase emissions. Factor interactions are discussed in the following paragraphs.

$$\Delta P = \frac{1}{2}\rho(V_2^2 - V_1^2) \quad \text{Eqn. (24)}$$

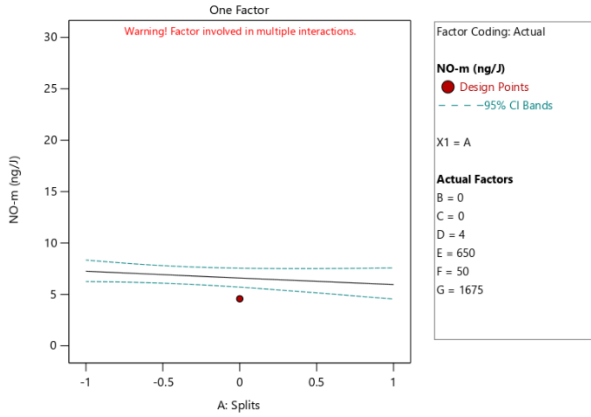


Figure 39. NO Emissions vs. Air Splits

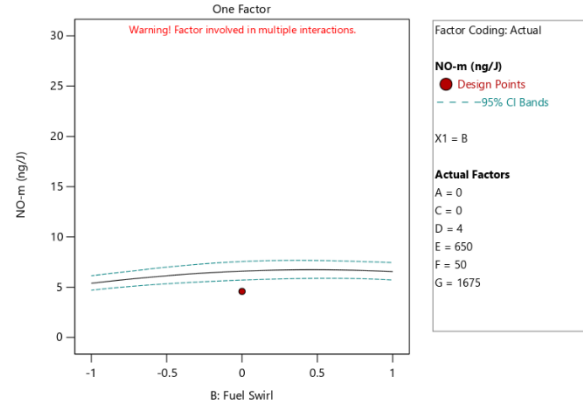


Figure 40. NO Emissions vs. Fuel Swirl

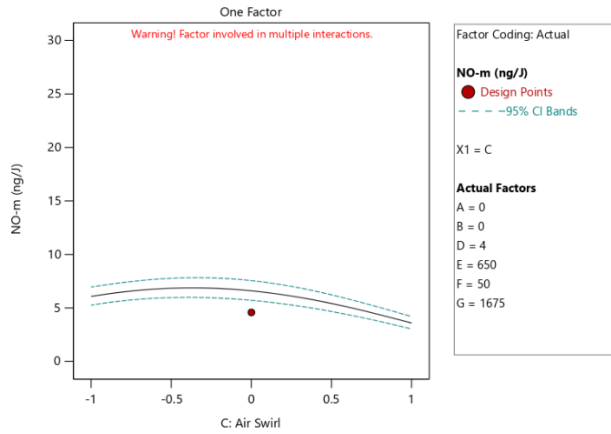


Figure 41. NO Emissions vs. Air Swirl

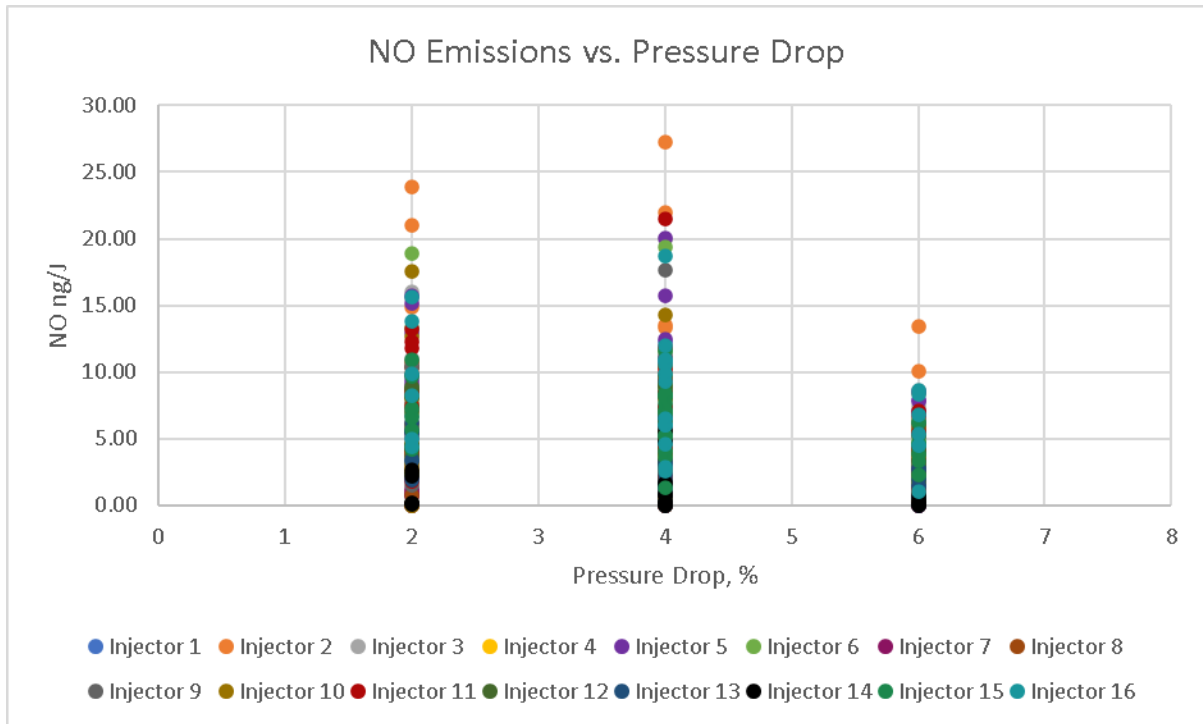


Figure 42. NO Emissions vs. Pressure Drop

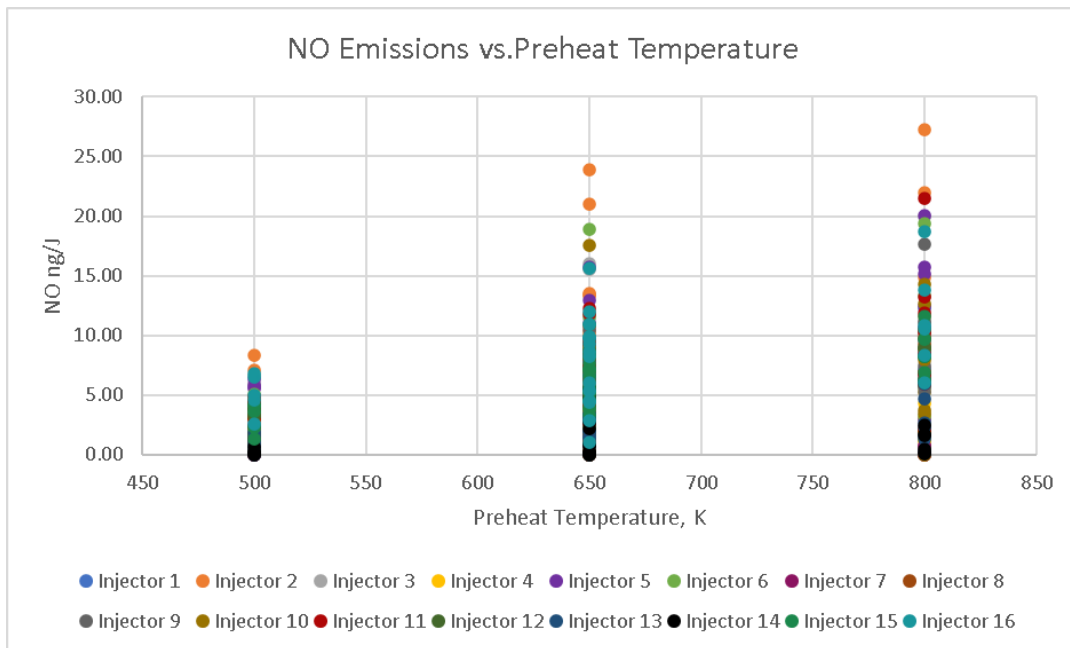


Figure 43. NO Emissions vs. Preheat Temperature

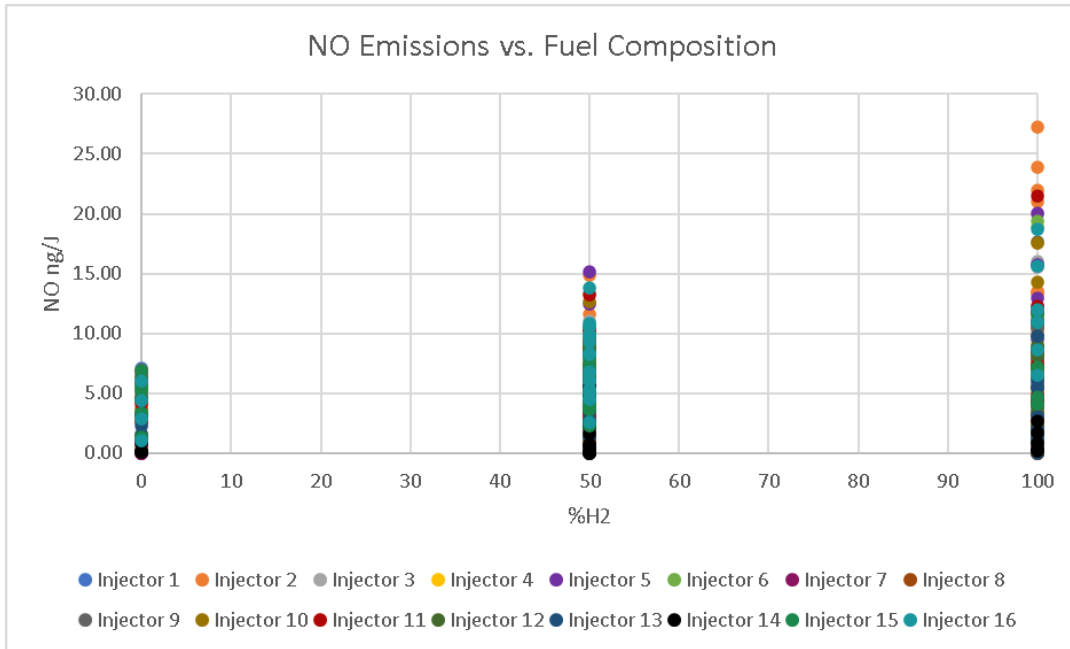


Figure 44. NO Emissions vs. Fuel Composition

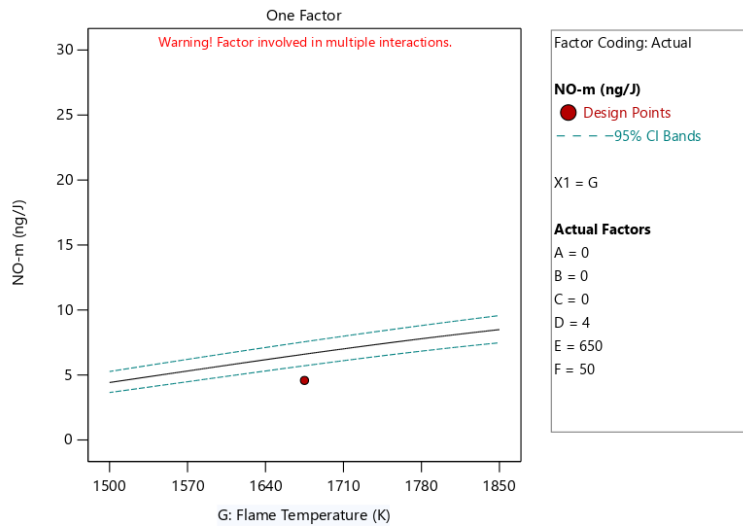


Figure 45. NO Emissions vs. Flame Temperature

The relationship with fuel swirl and air splits (AB) is dependent on how much air passes through the injector. When more air is passed through the injector, having a smaller fuel swirl angle (denoted as the black line in Figure 46) decreases emissions. If less air is passed through the injector, having a larger swirl angle (denoted as the red line in Figure 46) is better for lowering emissions. When air is passed through the injector, the air circuit also has a swirl angle.

So, when coupled with a fuel swirl angle, a less steep swirl angle is better. The interaction between the air and fuel swirl was discussed previously.

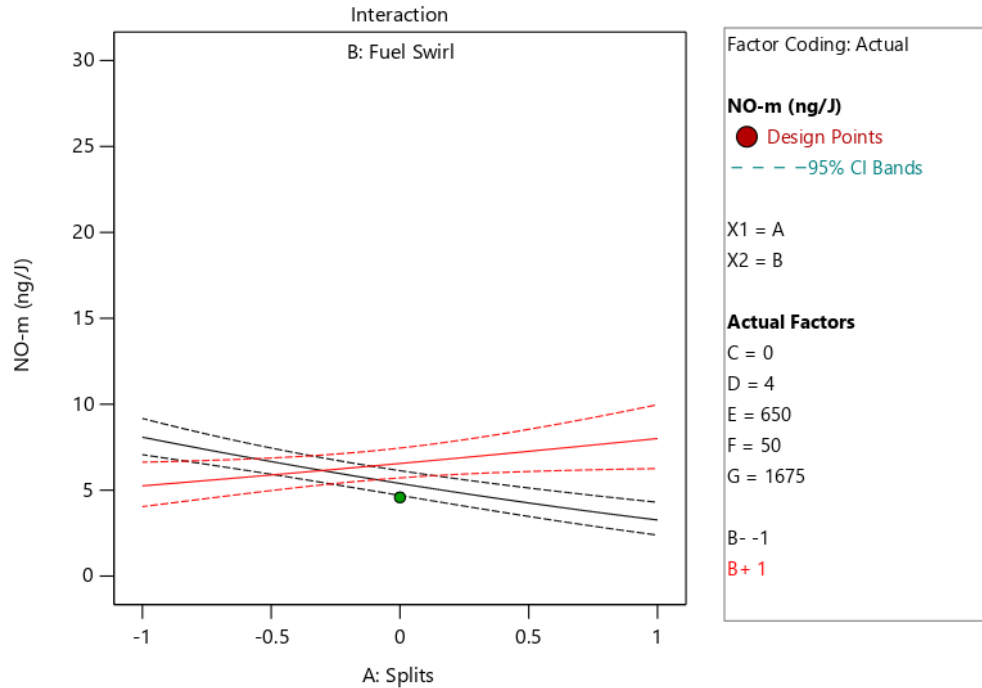


Figure 46. NO Emissions for Air Split and Fuel Swirl Interaction. (Red-Higher Fuel Swirl, Black-Lower Fuel Swirl)

The factor interaction between the air swirl and air splits (AC) follows a similar trend. If there is more air through the injector, then having a higher swirl angle decreases NO emissions. The opposite is true when you have less air through the injector. This indicates that air swirl angle is only beneficial when you have more air flow through the injector. If the flow rates are too small, steep angles will not facilitate mixing. This can be tied back to the same reason why for the fuel swirl, lower angles are preferred due to lower flow rates.

The factor interaction between pressure drops and the air splits is more difficult to discern. Besides the lower limit of the design matrix, a change in pressure drop does not increase or decrease emissions with the air splits. This is probably related with the mixedness of the fuel.

Although pressure drop also plays a role in mixing via velocities, the effect of swirling from the air and fuel are more prominent.

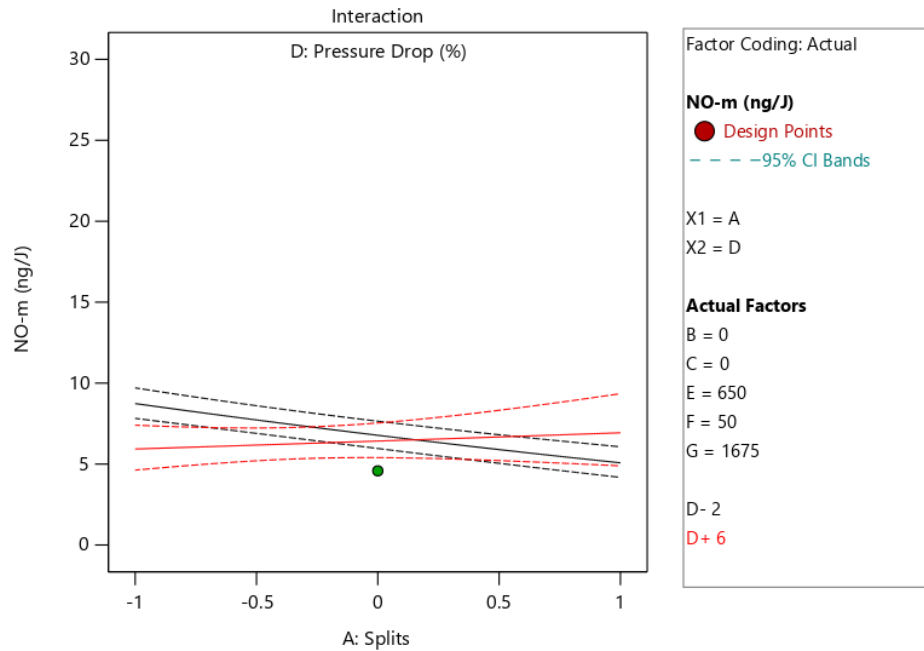


Figure 47. NO Emissions for Air Split and Pressure Drop Interaction. (Red-Higher Pressure Drop, Black-Lower Pressure Drop)

The factor interaction between preheat temperature and the air splits (AE) show that at the effect of higher preheat can be offset by having more air through the injector. More air through the injector increases the interaction between the air and fuel which leads to a more homogeneous mixture. It is reported in literature that perfectly premixed models produce lower local temperatures than those that are non-premixed which decrease emissions [75]. However, this factor interaction is very complex. Depending on other factors such as air and fuel swirl, this relationship changes as well. For instance, when steeper fuel swirls are present, to offset the effect of increasing preheat temperature, less air through the injector is preferred. This slows down the air velocity in the injector which helps with better mixing with the slower velocities of the fuel. Again, the relationship is altered depending on the air swirl as well. It becomes clear

that depending on preferred performance or desired factors, multiple combinations of factors can achieve the same effect rather than a singular solution.

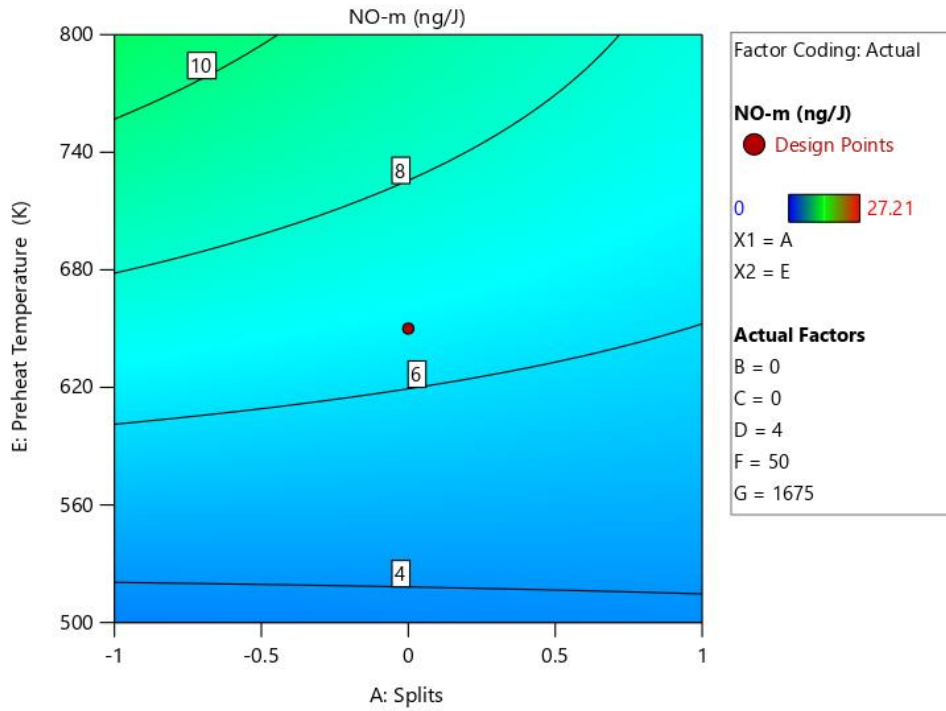


Figure 48. NO Emissions for Preheat Temperature vs. Air Split Interaction (Middle Fuel Swirl)

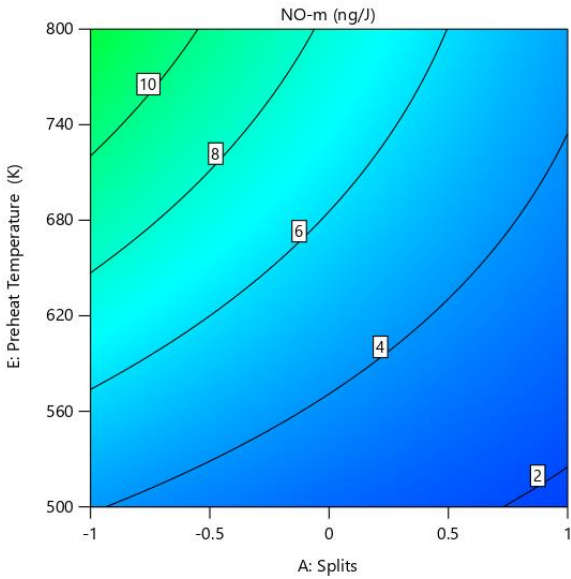


Figure 49. NO Emissions for Preheat vs. Air Split Interaction (Lower Fuel Swirl)

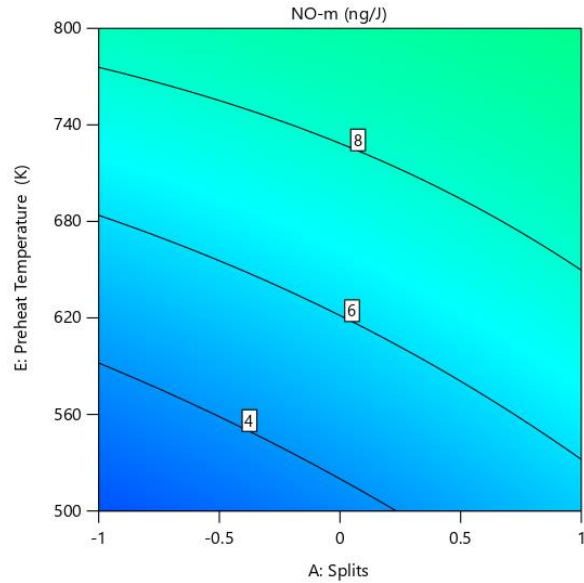


Figure 50. NO Emissions for Preheat vs. Air Split Interaction (Higher Fuel Swirl)

The factor interaction between the air split and fuel composition (AF) also shows that the effect of adding hydrogen content can be compensated by modifying the air splits (see Figure 51). For example, when increasing hydrogen content which increases NO emissions, increasing the air through the injector will keep emissions the same. When there is increased air through the injector, more air interacts with the fuel which can lead to a more homogenous mixture. Thus, lower temperatures are achieved. The same effect is not observed on methane fuel which is most probably due to the differences in weight of the fuel. Since hydrogen is lighter, it is more easily affected by the small changes in the flow rates through the injector. Hydrogen's flame speeds are also much faster which means that by adding in more air, it could mix fast and lowers the temperature. Just like the previous factor interaction, AE, the factor interaction is complex and depends on many other factors. Particularly modifying the flow or air swirl will shift the graphs in opposite directions indicating there are more than one way to achieve a desired performance.

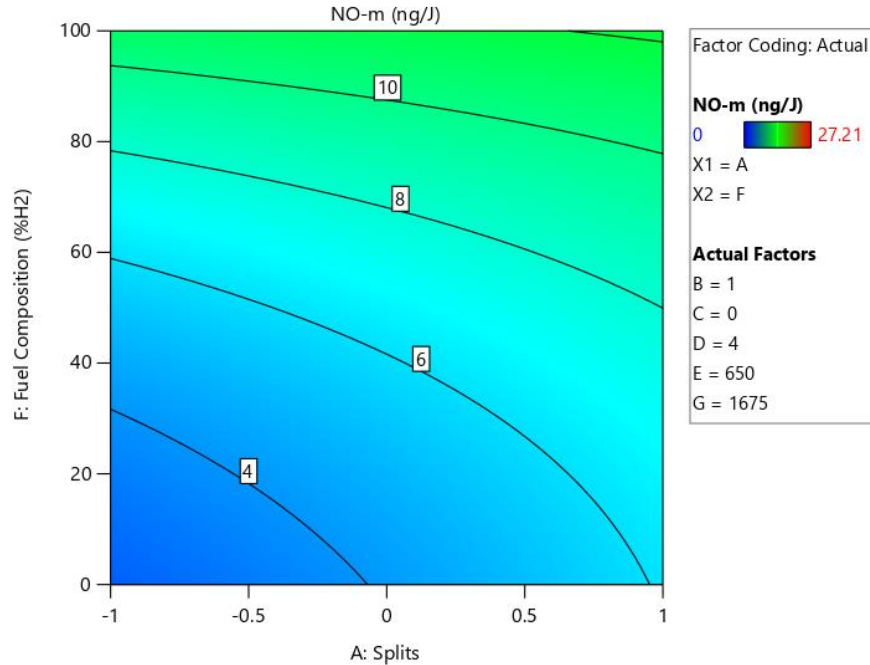


Figure 51. NO Emissions for Fuel Composition vs. Air Splits Interaction

The factor interaction between the flame temperature and the air splits (AG) are similar to the previous two interactions (see Figure 52). The effect of increasing flame temperature can be offset by increasing the air flow to the injector. By having more air through the injector, interaction between the fuel and air is increased which promotes mixing. Thereby, lowering peak temperatures and emissions. It should be noted again that depending on the presence of low or high air swirl the interpretation of the interaction becomes different. If both fuel and air swirl are at the lowest levels in the design space, to offset the effect of increasing flame temperature, less air should pass through the injector. That is because without sufficient swirling, the fuel and air do not mix as well and leads to greater unmixedness. Although unmixedness is currently unclassified, it would be a good next step to design another experiment to be able to measure unmixedness to confirm these solutions. Nevertheless, if air and swirl angles are at the highest levels, then the effect of increasing flame temperature can be offset by increasing the air passing through the injector. There are many more combinations such as high air swirl and low air swirl,

but the takeaway is that there are multiple combinations of factors that can increase or decrease emissions depending on desired geometric preferences.

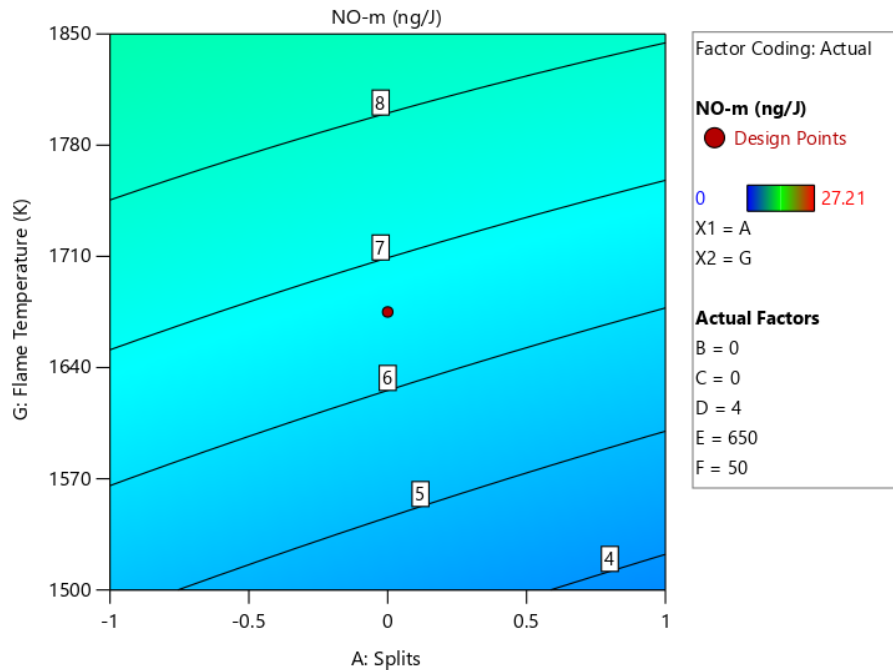


Figure 52. NO Emissions for Flame Temperature vs. Air Splits Interaction

The interaction between air and fuel swirl (BC) shows that to minimize emissions, air swirl should be maximized while fuel swirl should be minimized (see Figure 53). This was briefly touched upon in previous interactions. To get the two velocities of the air and fuel to match, the air should slow down, and the fuel should speed up. To do this, angles are involved where higher angles decrease the velocity perpendicular to the injector face. Thus, for air which has much higher flow rates, the angle should be maximized, and the opposite is true for fuel swirl. Perhaps counter swirl angles for the injector would be better. Figure 53 also reveals high NO emissions concentrated at the bottom center. This suggests there are four ways to approach to highest levels of NO emissions. The first two methods involve decreasing the air swirl, but the fuel swirl can either decrease or increase to reach the midpoint. The last two methods involve

increasing the air swirl, but the fuel swirl can also either decrease or increase to reach the midpoint. One thing does remain clear. The highest air swirl and lowest fuel swirl results in the least NO emissions.

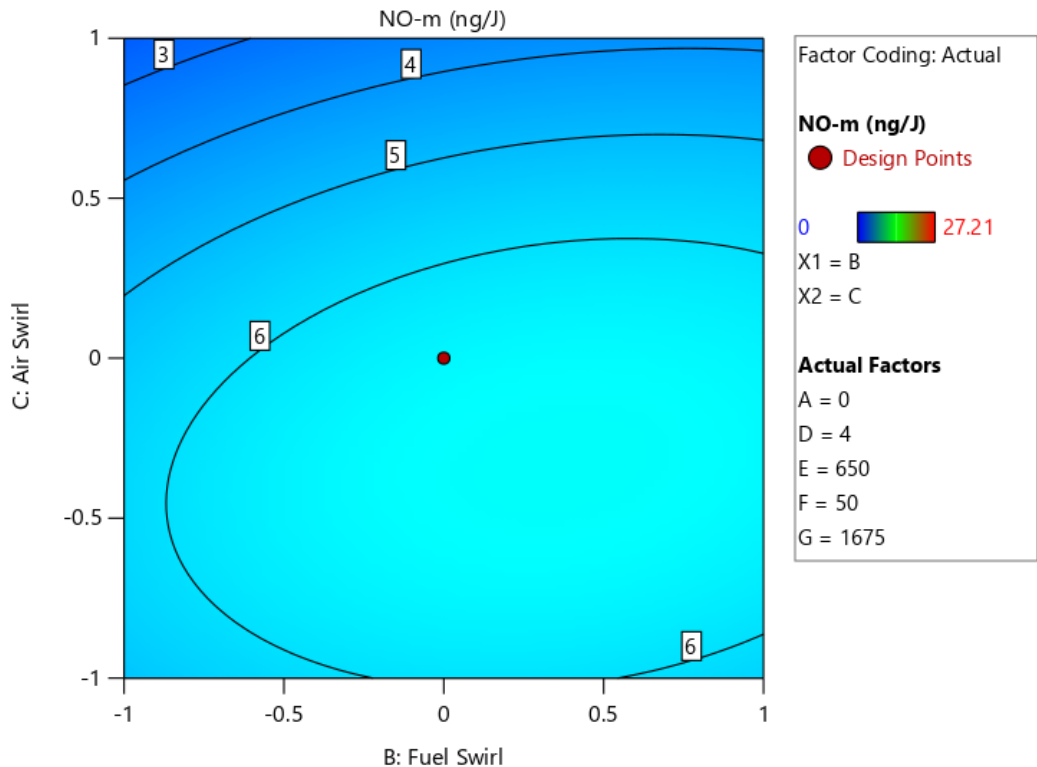


Figure 53. NO Emissions for Air Swirl vs. Fuel Swirl Interaction

The interaction between pressure drop and fuel swirl (BD) show that in the presence of fuel swirl, the effect of pressure drop does not matter (see Figure 54). The red line indicates higher pressure drops and the black line indicates lower pressure drops. This is most probably due to the fact that air and fuel swirl play a larger role than pressure drop in facilitating mixing. Pressure drop is tied to the velocities but since the changes are minor, the effect is not significant. Perhaps even higher pressure drops are worth exploring. The same conclusion can be drawn for the factor interaction between the pressure drop and air swirl (CD).

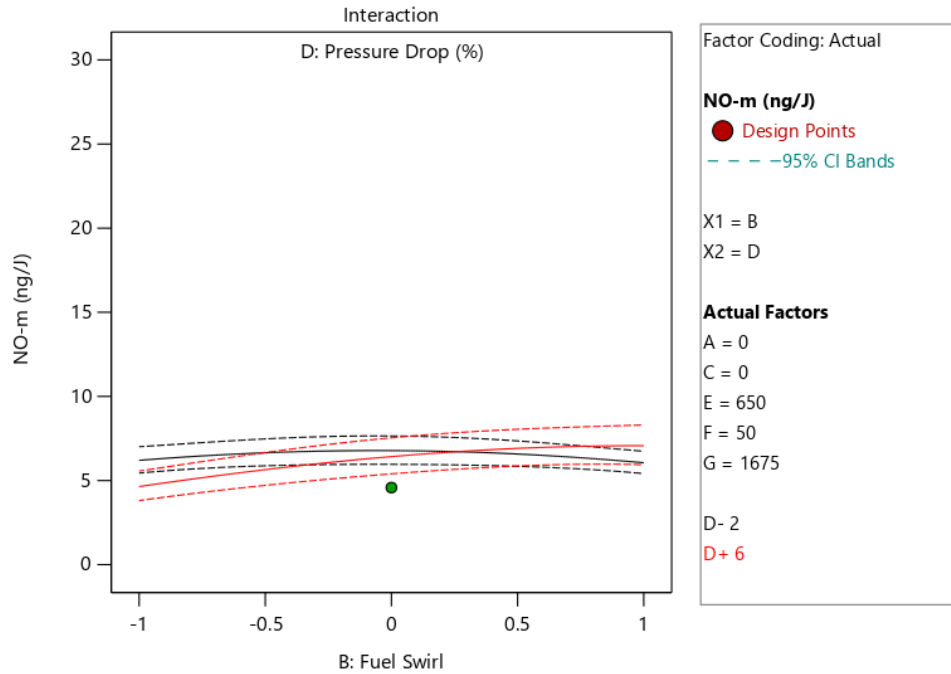


Figure 54. NO Emissions for Fuel Swirl vs. Pressure Drop Interaction. (Red-Higher Pressure Drop, Black-Lower Pressure Drop)

The interaction between the preheat temperature and air swirl (CE) show that both lower and higher swirl angles can be altered to keep emissions from increasing as preheat temperature is increased. This is best explained via other interactions discussed previously. The air swirl is also affected by the amount of air that enters the injector and the level of fuel swirl. As a result, simple conclusions cannot be drawn. Take a look at Figure 55 for example. The figure displays NO emissions at the middle of the design space for air splits, fuel swirl, pressure drop, fuel composition, and flame temperatures. By shifting the air split to the lower (Figure 56) or upper portion (Figure 57) of the design matrix, there are clear differences. When there is less air through the injector, increasing the preheat is mostly affected if there is no air swirl. This is most likely because the higher temperature air is not sufficiently mixed with the fuel causing more local peak temperatures. When more air passes the injector with fuel swirl, then the opposite effect takes place. In sum, factors can be adjusted to achieve a desired performance.

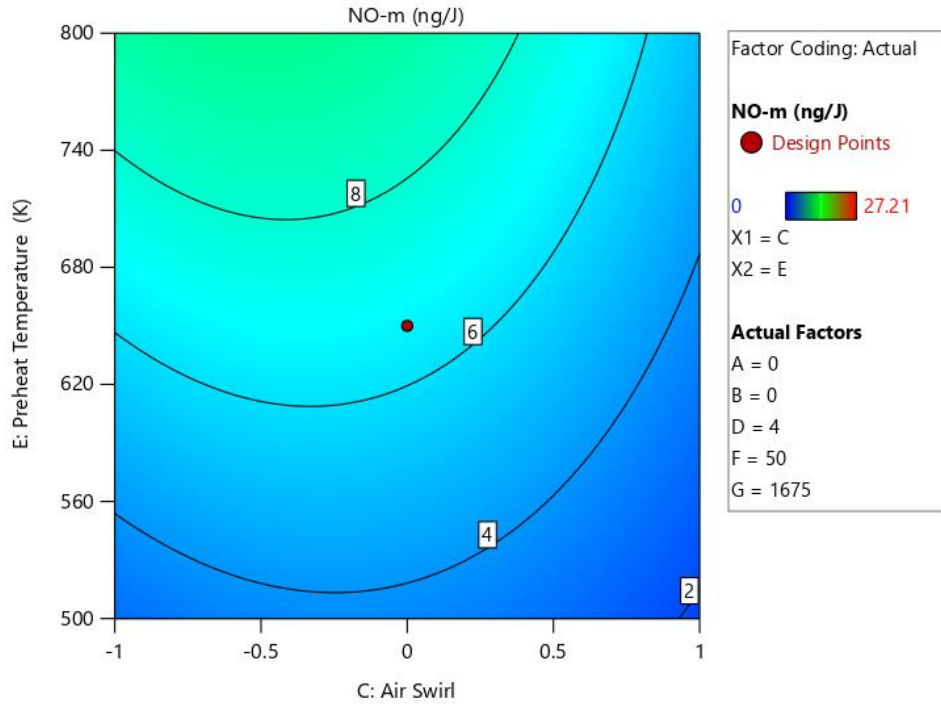


Figure 55. NO Emissions for Preheat Temperature vs. Air Swirl Interaction (Middle Air Split))

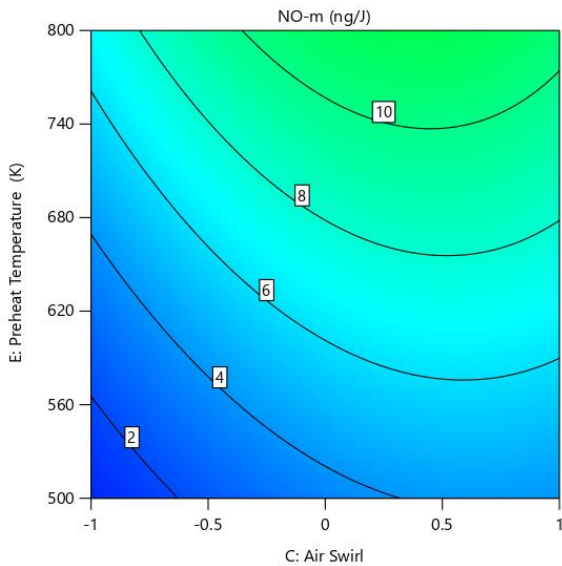


Figure 56. NO Emissions for Preheat Temperature vs. Air Swirl Interaction (Lower Air Split)

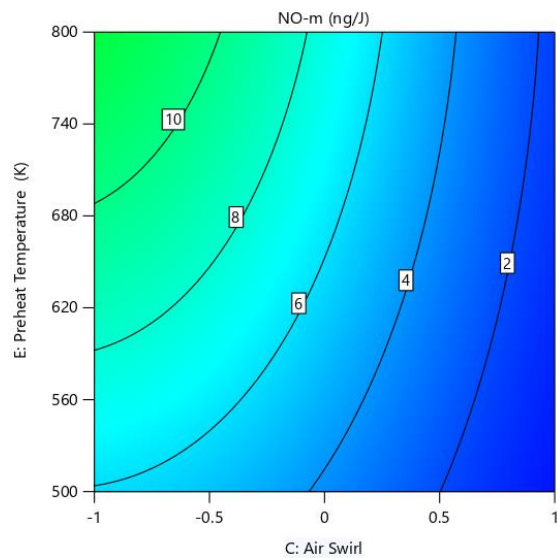


Figure 57. NO Emissions for Preheat Temperature vs. Air Swirl Interaction (Higher Air Split)

The interaction between the pressure drop and flame temperature (DG) show that flame temperatures increase emissions more than the effect of the pressure drop. No matter the pressure drop, a higher flame temperature increases NO emissions. The effects of thermal mechanisms are

stronger than the effects of pressure drop. Moreover, air swirl and fuel swirl affect the emissions profile over the pressure drop as noted by the small F factor of 1.47.

The last significant interaction is between the preheat and flame temperature (EG). No matter which combination of factors are adjusted, the highest levels of preheat and flame temperature yields the highest NO emissions. Increased adiabatic flame temperatures increases emissions as the thermal NO_x mechanism begins to dominate after 1675K. This will be discussed in section 5.2.3. It was expected that preheat should be insignificant when the adiabatic flame temperature is used since preheats are already factored into the calculations to determine the adiabatic flame temperatures. The air and fuel were varied as a result. The model suggests otherwise indicating there is more to decipher. A possible reason as to why preheat has an independent effect is due to reductions in ignition times and mixing times which are especially important in non-premixed systems. The fact that preheat is a significant factor signifies the system is not perfectly premixed. The factor interaction is best summarized in Figure 58 where all factors are held at the middle of the design matrix.

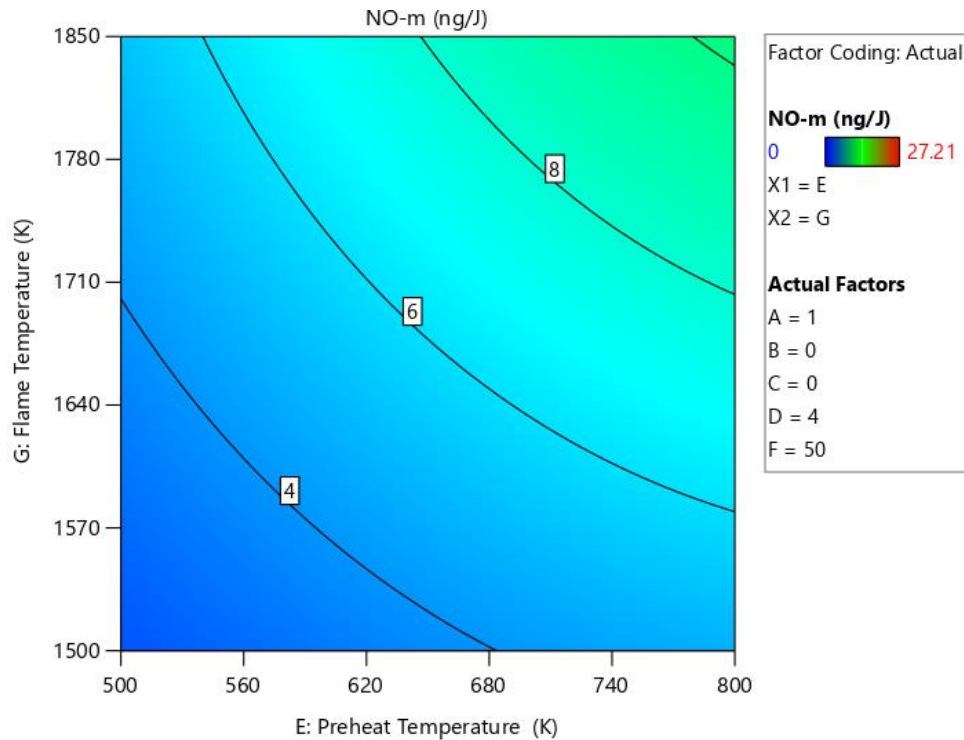


Figure 58. NO Emissions for Flame Temperature vs. Preheat Temperature Interaction

For second order terms B^2 , C^2 , E^2 , F^2 , and G^2 , when these terms were eliminated, they had no effect on the conclusions drawn previously. However, without these terms, the effect of factors is weakened. For instance, in the case of preheat temperature, when removed the squared terms, at certain points the effect of preheat temperature can no longer be tuned by adding different swirl angles. The best guess as to why these terms were added to simply were added weight to the model especially since E, F and G were the highest ranked factors. Having a squared term, can better predict the model by capturing curvature effects.

While FG (flame temperature and fuel composition) is not a significant factor, increasing the hydrogen content also increases emissions (see Figure 59). For the given estimated adiabatic flame temperature, increasing hydrogen content increases NO emissions. There are multiple reasons as to why NO emissions increases. First, the system is not perfectly premixed so the actual adiabatic flame temperature could be different. Also, hydrogen has higher flame speeds

which can mean that insufficient mixing leads rise to higher NO emissions. Another reason could be due to the NNH pathway that opens up when operating on hydrogen fuel. This is discussed in section 5.2.3. At a high level, hydrogen produces more emissions due to the activation of the NNH mechanism compared to methane. Figure 108-Figure 112 show more views in the model where one can compare increasing hydrogen content with increasing flame temperatures. Despite this conclusion, recall that hydrogen has wider flammability limits which allow hydrogen to combust at lower adiabatic flame temperatures that allow for a reduction in NO_x emissions. These will be discussed in detail in section 5.1.5. Moreover, the increased flammability ranges lead to more stability which is ideal for non premixed systems. In non premixed systems, there is a wide range of equivalence ratios so with increased flammability ranges, the system is still able to combust with little to no difficulty without worries of lean blowout.

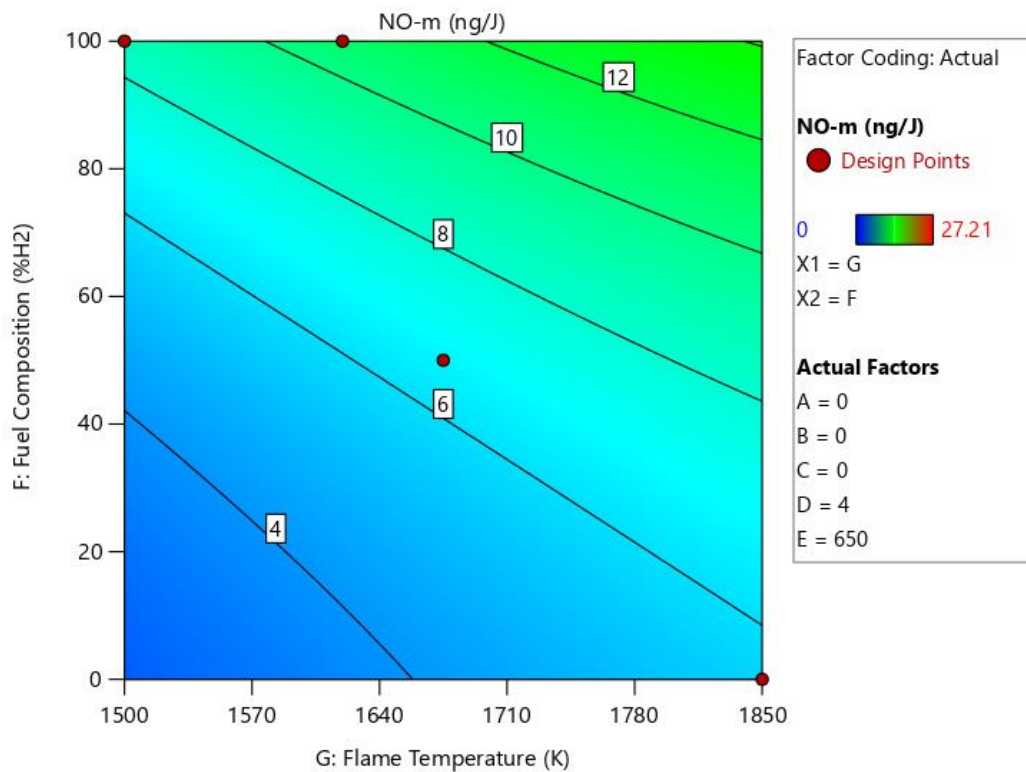


Figure 59. NO Emissions for Fuel Composition vs. Flame Temperature Interaction

In sum, the most important factors are the fuel composition followed by preheat temperature and flame temperature in order of highest F values. The most important interactions were between the air splits and the air swirl where when there is more air passing through the injector, more air swirl is beneficial. Air swirl and fuel swirl were also more important than the pressure drop in terms of curbing emissions. This is also reflected in a low F value of 1.47 for pressure drop. The relationship between air and fuel swirl were contradictory towards one another. A steeper air swirl is more beneficial to lower emissions due to high flow rates and the opposite can be said about the fuel swirl. When the velocities of the two flows are similar, better mixing is promoted.

5.1.3 NO_x Model

The experimental data obtained from each injector are plotted in Figure 60 and are sorted by the corresponding run number. The plot reveals that the NO_x model is very similar to the NO model. Comparing Figure 31 and Figure 60, it is estimated that up to 60-80% of NO_x is comprised of NO emissions. As a result, similar conclusions can be drawn for both the NO and NO_x model. This is also seen in the ANOVA results which will be discussed later in the following paragraphs. In the NO_x model, Injector 2 also gives rise to the largest NO emissions while Injectors 7 and 14 yields the lowest emissions. Recall that Injector 2 has a negative air split, neutral (in the middle of the design space) fuel split, and a positive air split. Injector 7 and 14 both share a positive air split and air swirl angle, but Injector 7 has a neutral air split whereas Injector 14 has a positive fuel split. This chart further corroborates the conclusions found in the NO model. Higher air splits and air swirl angle are preferred for lower emissions. The gap of data between run numbers 34-39 also exist since the flame was unsustainable at the specified conditions. These points corresponded to lower adiabatic flame temperatures between 1100K-

1300K for 50% CH₄/50% H₂ and for pure methane cases. At these lower temperatures, methane is unable to sustain a flame as it is below its LBO limits.

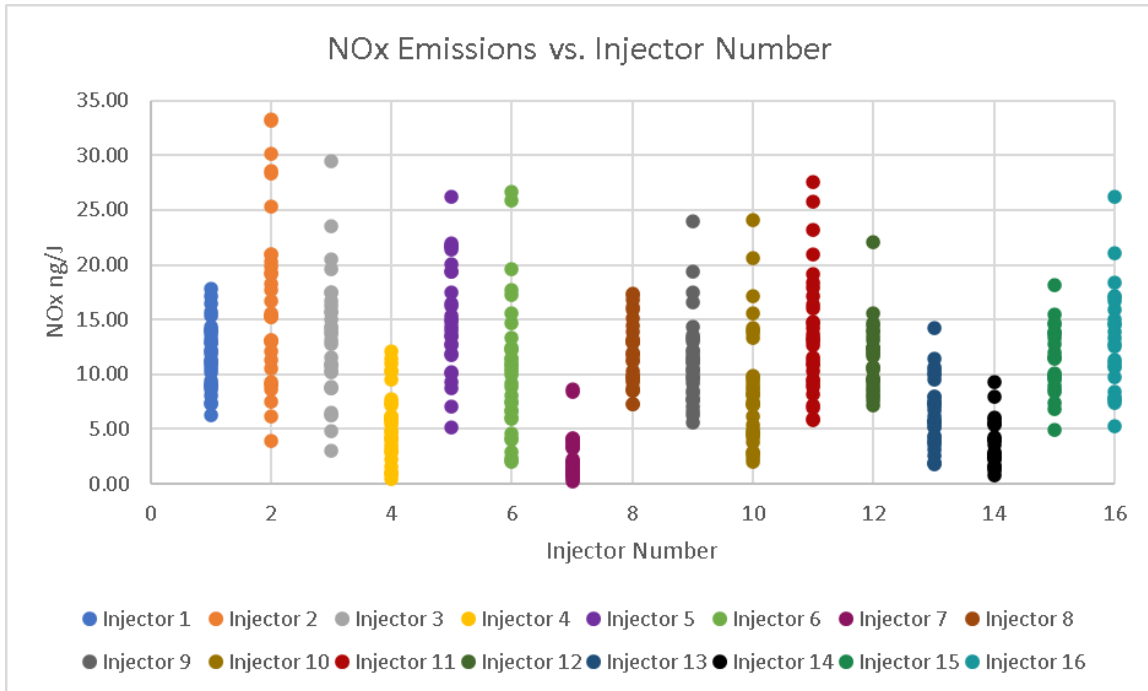


Figure 60. NOx Emissions vs. Run Number, Sorted by Injector Number

Since NOx versus fuel composition is of particular interest in literature, Figure 61-Figure 76 are plotted (NOx emissions versus the fuel composition) for each injector. As observed, with an increase in hydrogen content, there is an increase in NOx emissions. This trend is shared among all injectors except for Injector 4, 7 and 14. Injector 4, 7, and 14 have NOx emissions that range from 0-10 ng/J compared to other injectors who had NOx emissions range from 0-25 ng/J. Injector 7 and 14 as discussed hold a favorable trait amongst the other injectors in that there is more air fed through the injector and the plate. With more air through the injector, there is more interaction with the fuel which leads to an increase in mixing. More mixing leads to lower local temperatures and lower emissions as a result. Injector 4 also possess favorable characteristics. In fact, it favors two desirable traits: lower fuel swirl and higher air swirl. Injector 4 does not possess the desirable trait to have more air through the injector, however. Still, since produces

low emissions with increased hydrogen content just like Injector 7 and 14, this suggests that have desirable air and fuel swirl can compensate for having less air through the injector. The more favorable traits an injector possesses, the more potential it has to be insensitive to fuel composition. More discussions on favorable factors are made in the following paragraphs.

Other key things to note is that Injectors 3, 4, 6, 7, 10, and 13 all had some points where low NO_x emissions were obtained even at 100% H₂. Majority of them corresponded to cases with lower adiabatic flame temperatures (1100-1300K). For other injectors, the same trend is not observed. Sometimes lower adiabatic flame temperatures yield higher emissions or that increasing hydrogen content will increase NO_x emissions. The best explanation for why Injectors 3, 4, 6, 7, 10, and 13 are different from other injectors is that they all possess higher air swirl or air split (more air through the injector). As observed from the NO model, these traits help lower emissions by giving it more interaction with the fuel and that higher air swirl helps with the mixedness of the system. Some injectors like Injectors 6 and 10 have some traits where it is in the middle of the design matrix (zero), but still showed that lower NO_x emissions were possible at lower adiabatic flame temperatures. This is most likely because of different combinations at play. For example, if higher fuel swirl is present and higher air swirl are present then the air split can be in the middle of the design matrix. Air split does not necessarily have to be at the highest level. The conclusion is that as long as the air swirl and air split (more air through the injector) is present, then lower emissions at 100% H₂ with lower adiabatic flame temperatures can be achieved. The fuel swirl was not as important as there are a mix of injectors that had higher, lower, or were in the middle of the design matrix.

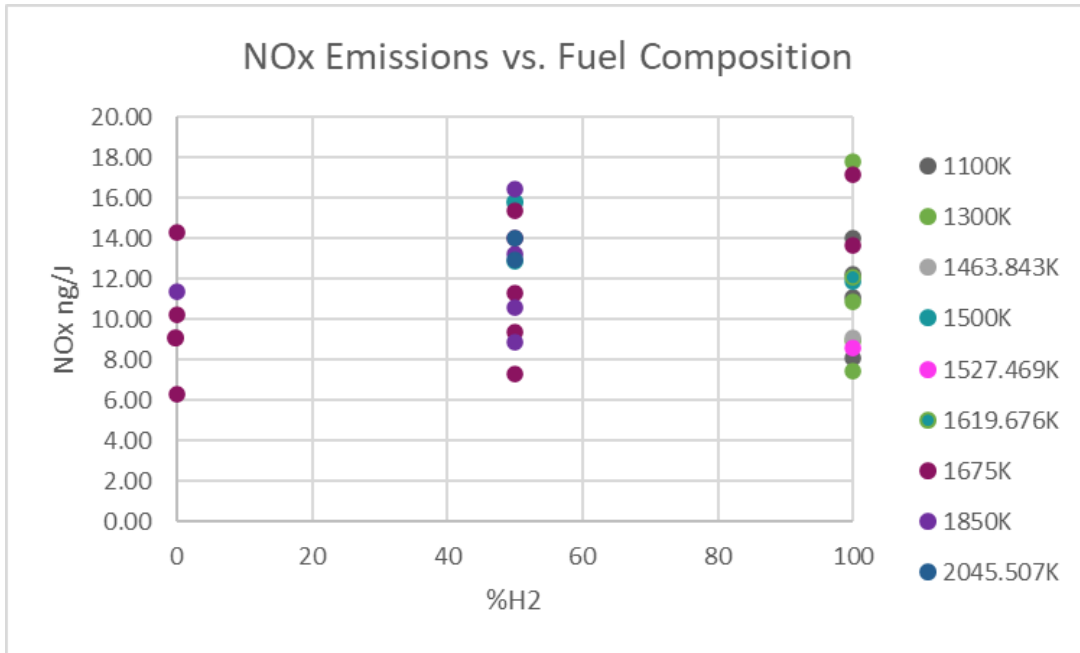


Figure 61. NOx Emissions vs. %H2 for Injector 1

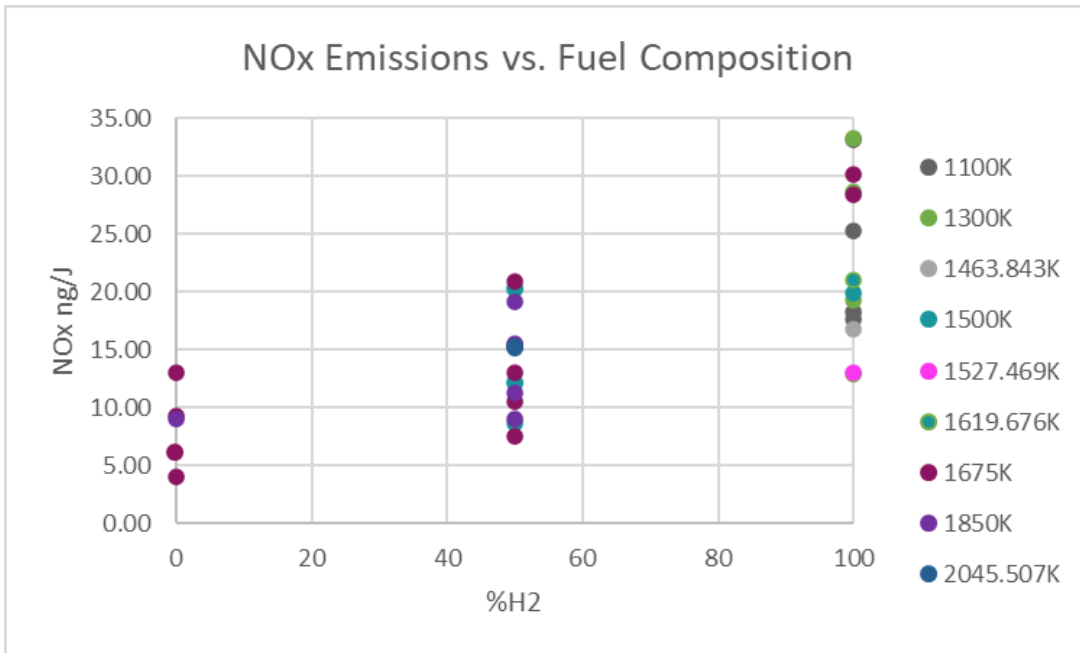


Figure 62. NOx Emissions vs. %H2 for Injector 2

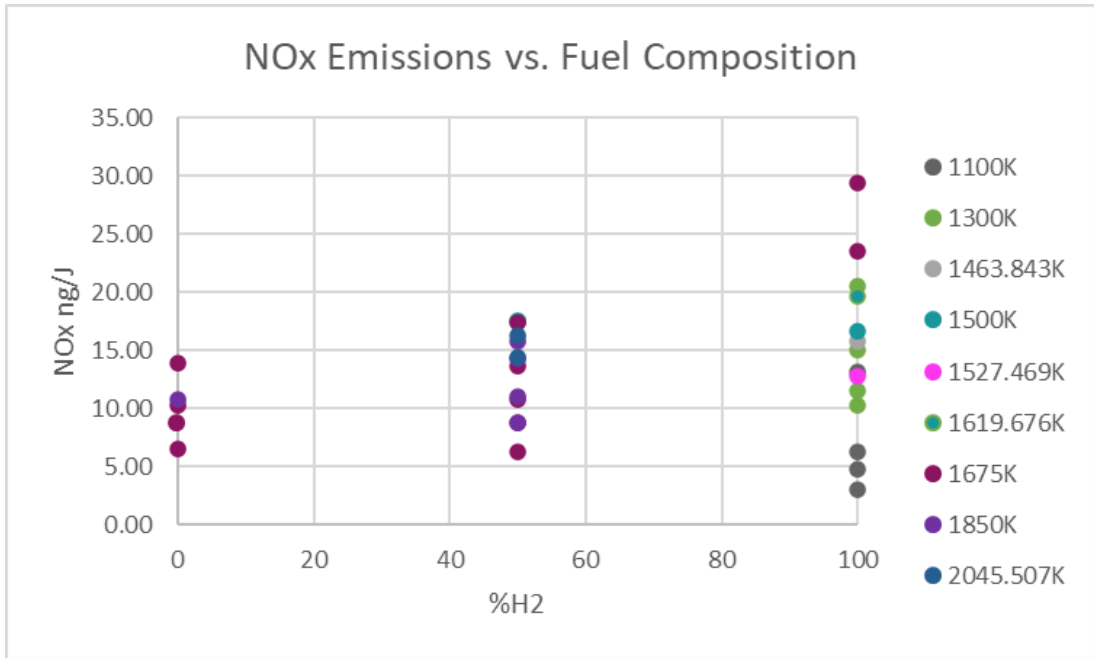


Figure 63. NOx Emissions vs. %H2 for Injector 3

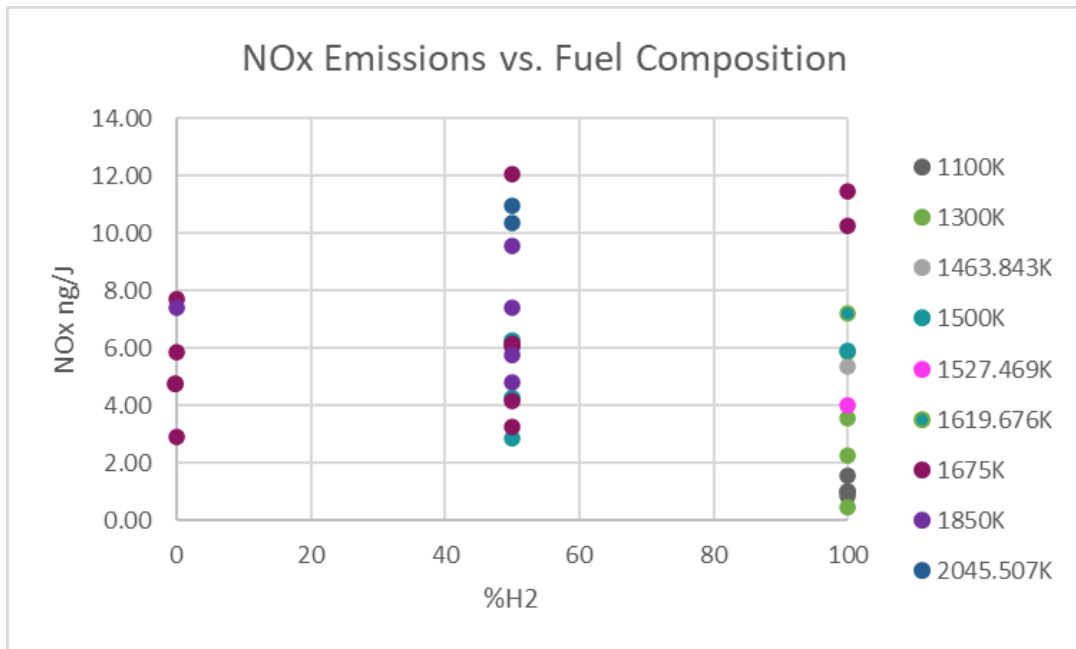


Figure 64. NOx Emissions vs. %H2 for Injector 4

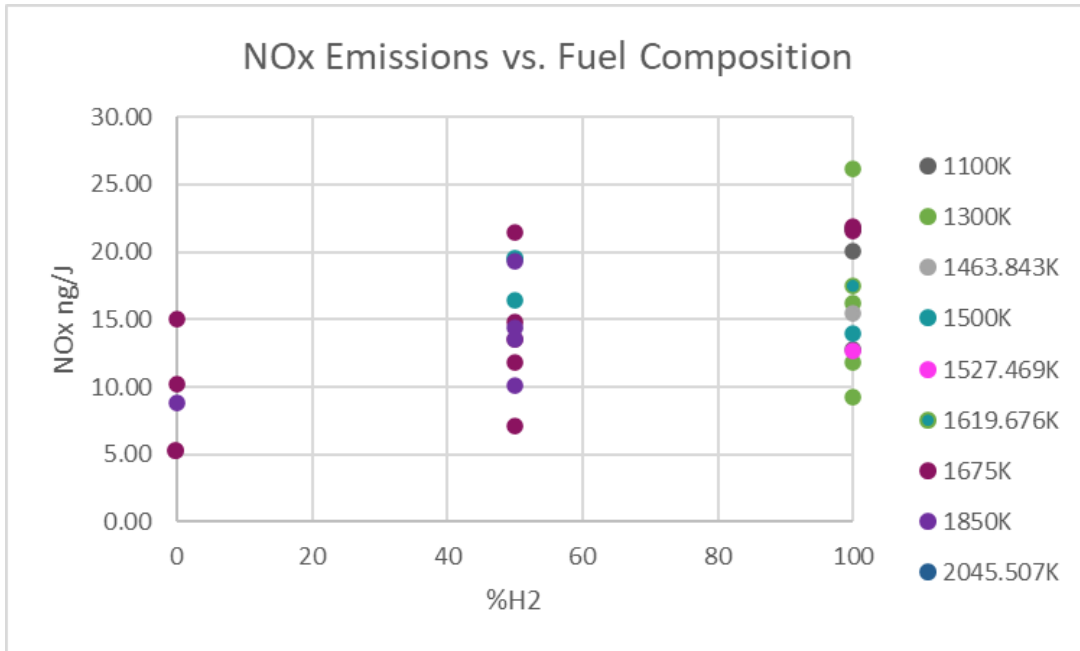


Figure 65. NOx Emissions vs. %H2 for Injector 5

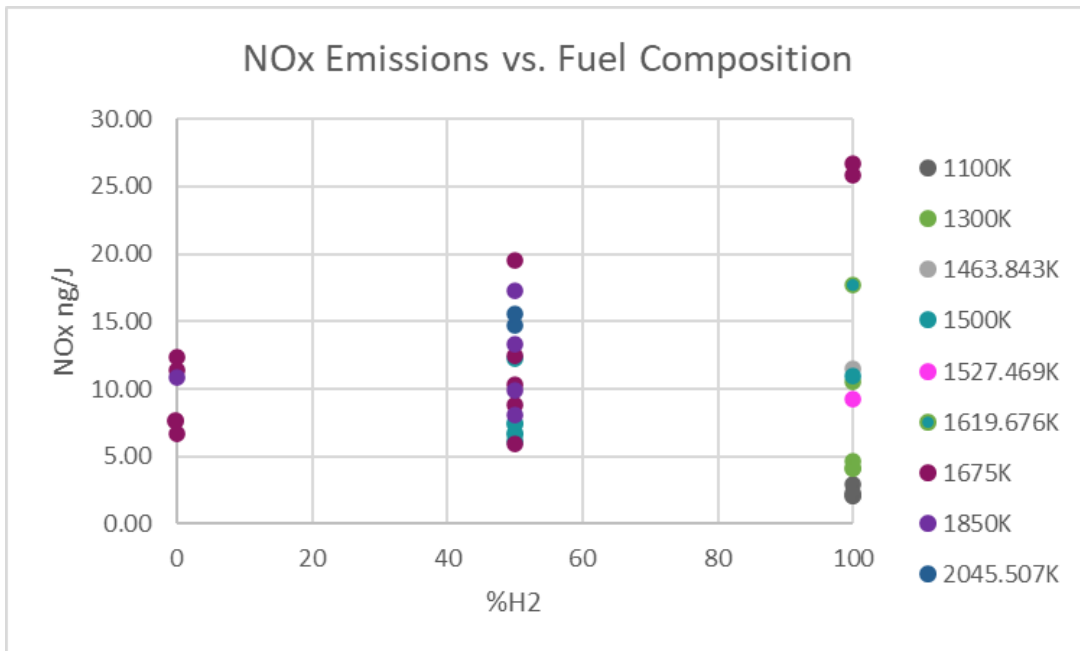


Figure 66. NOx Emissions vs. %H2 for Injector 6

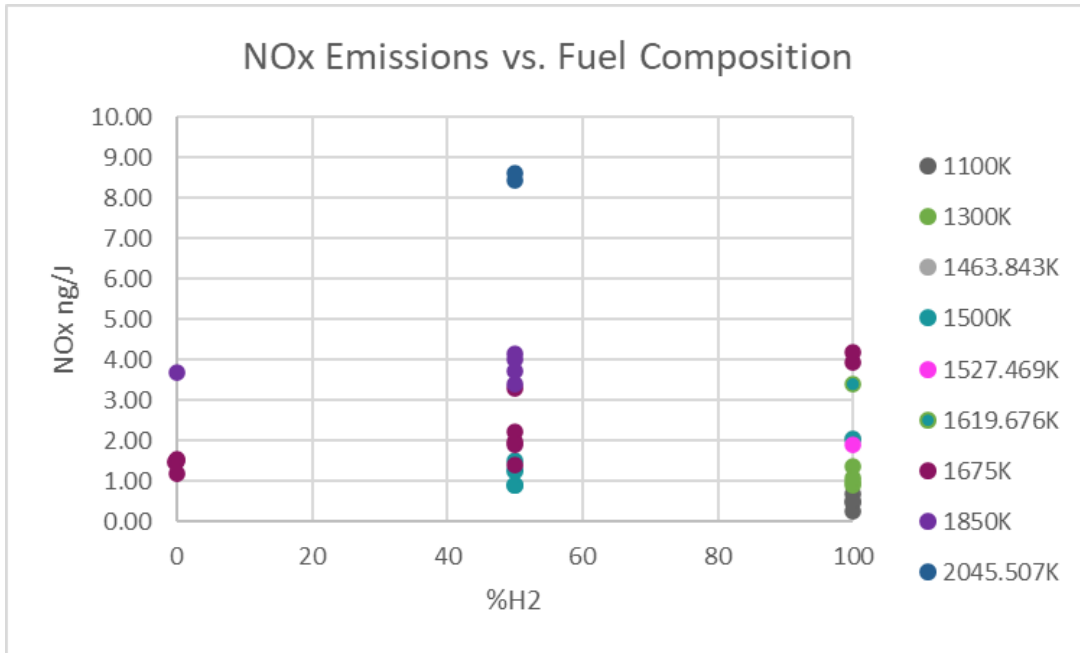


Figure 67. NOx Emissions vs. %H2 for Injector 7

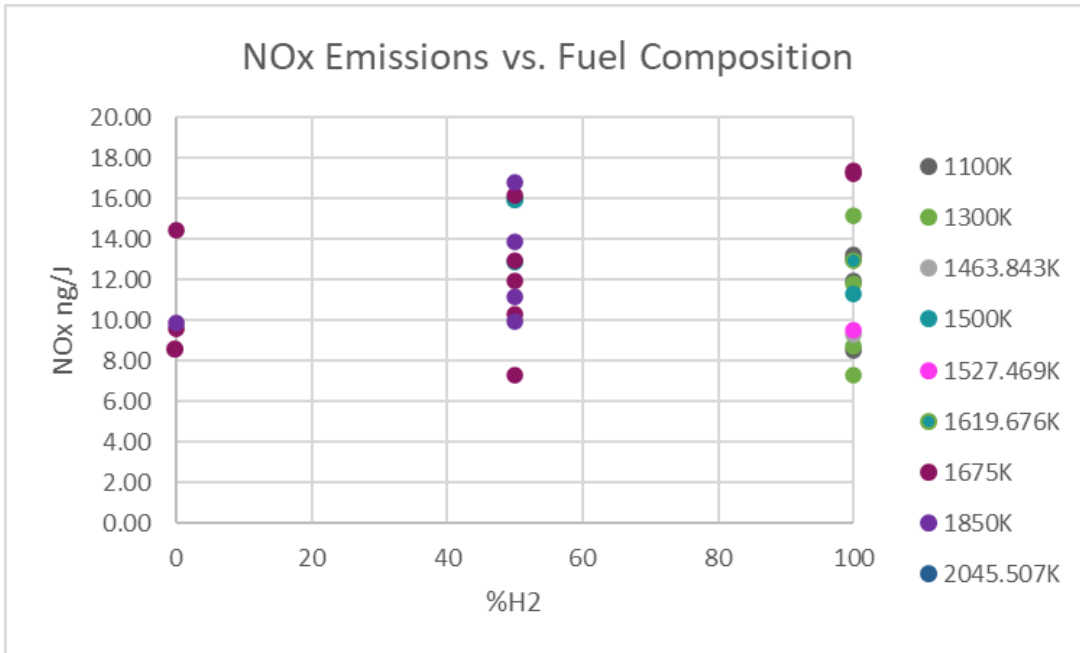


Figure 68. NOx Emissions vs. %H2 for Injector 8

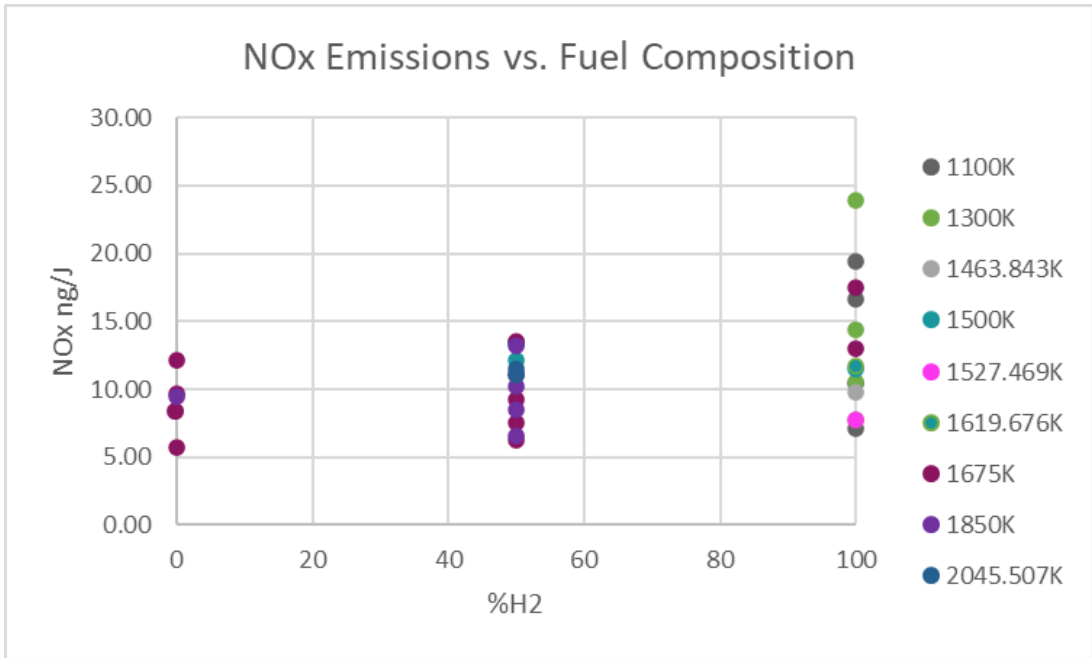


Figure 69. NOx Emissions vs. %H2 for Injector 9

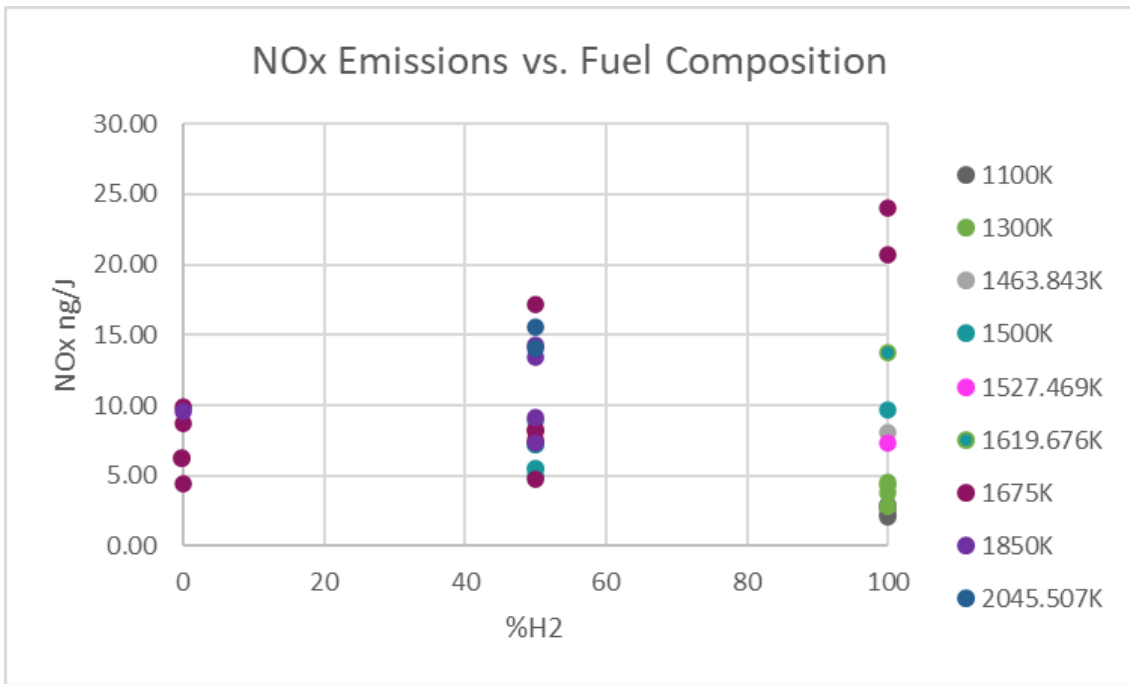


Figure 70. NOx Emissions vs. %H2 for Injector 10

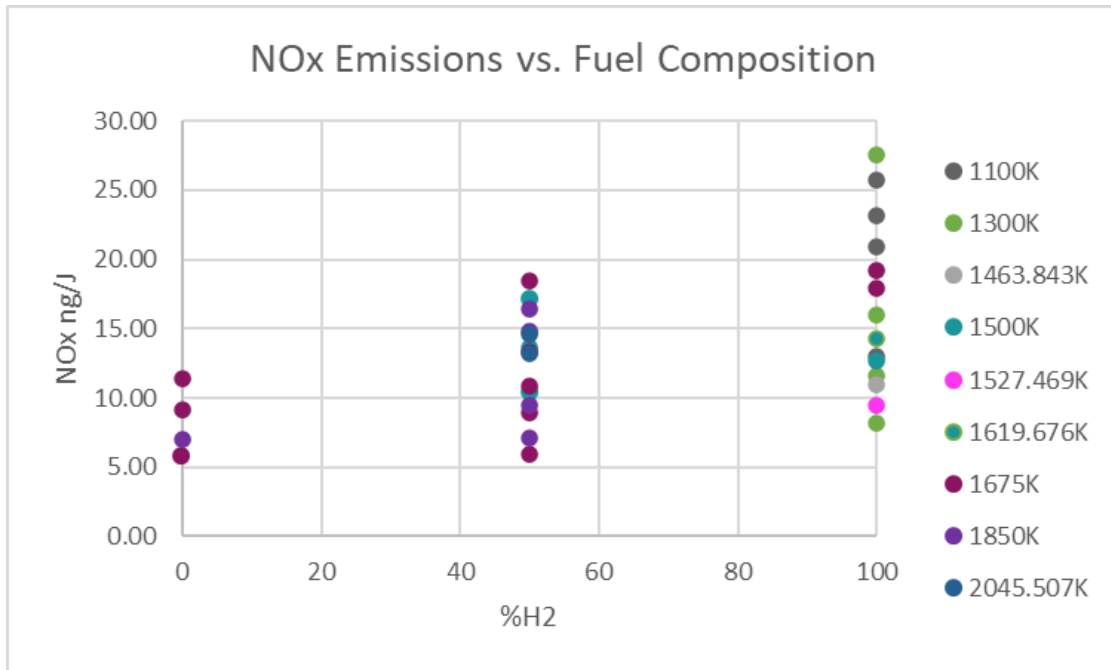


Figure 71. NOx Emissions vs. %H2 for Injector 11

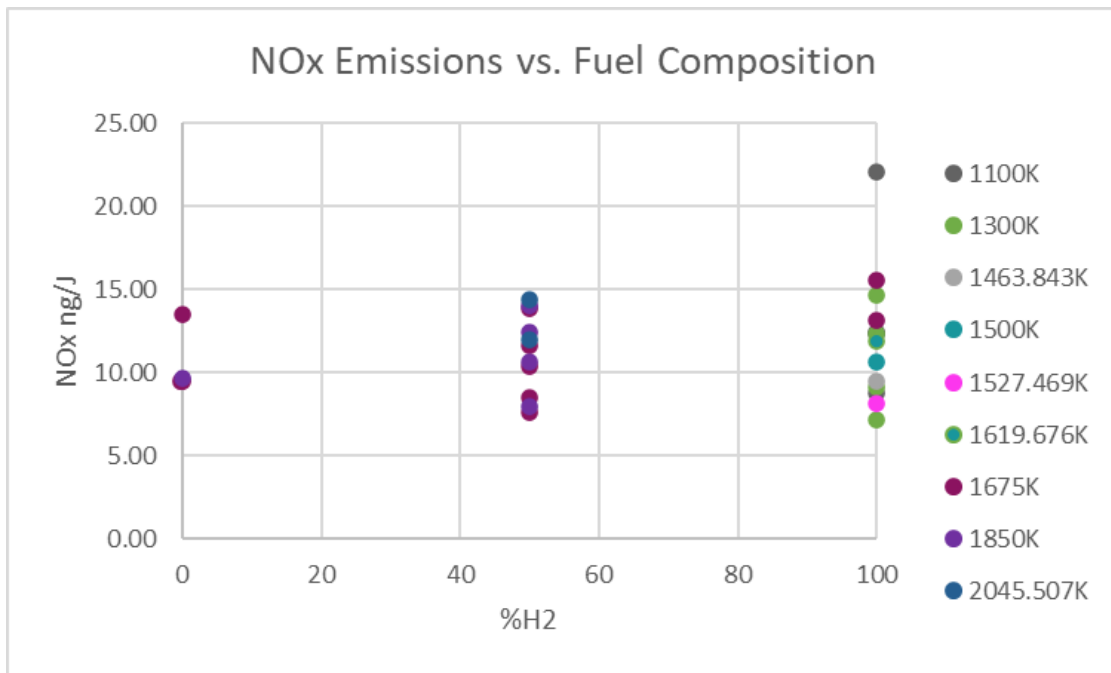


Figure 72. NOx Emissions vs. %H2 for Injector 12

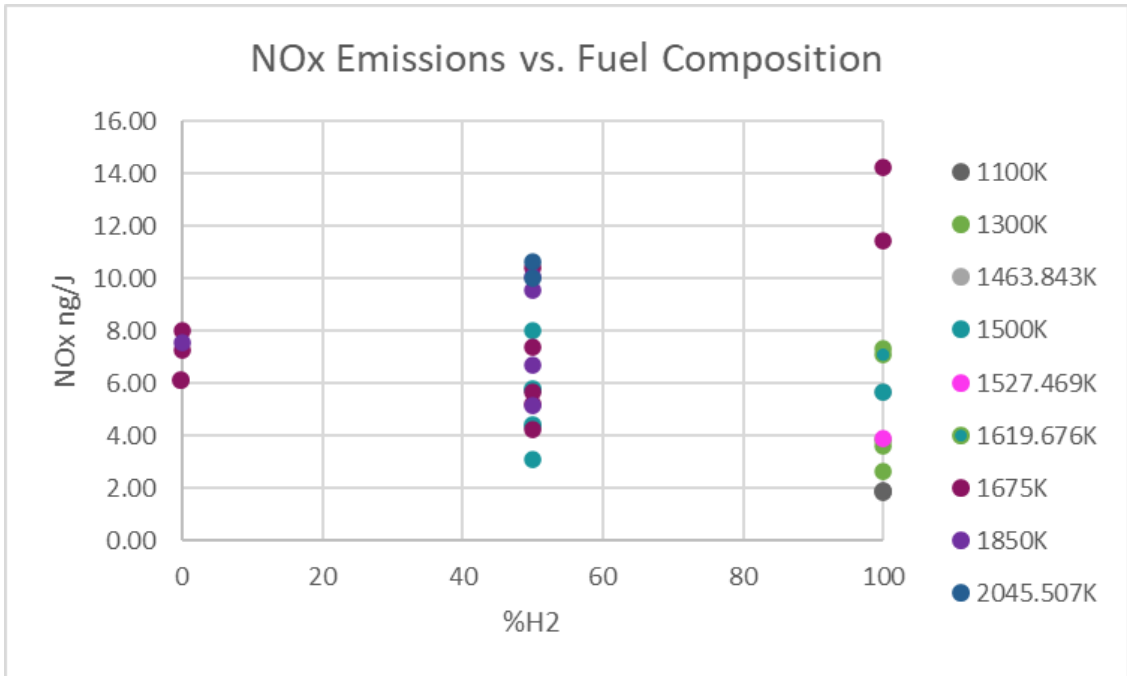


Figure 73. NOx Emissions vs. %H2 for Injector 13

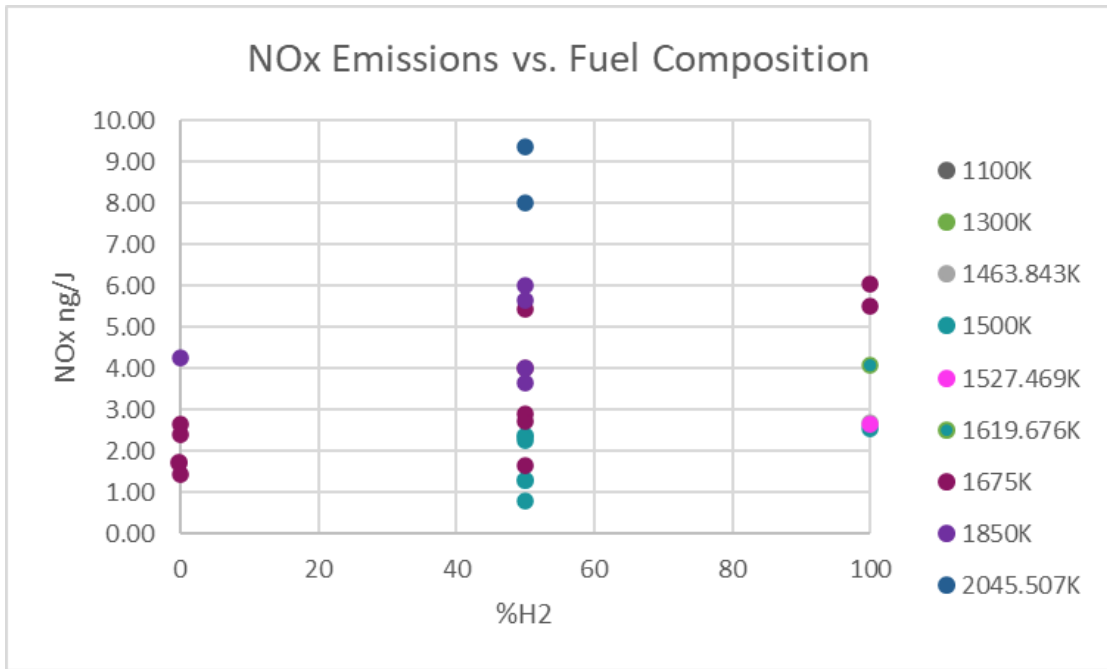


Figure 74. NOx Emissions vs. %H2 for Injector 14

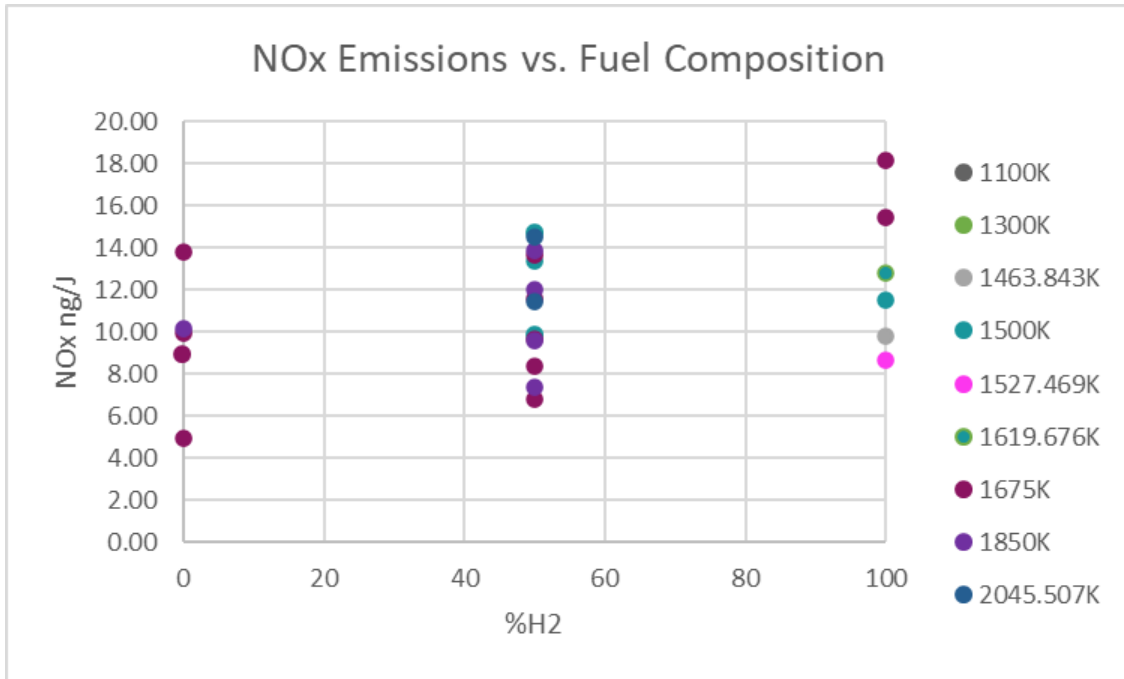


Figure 75. NOx Emissions vs. %H2 for Injector 15

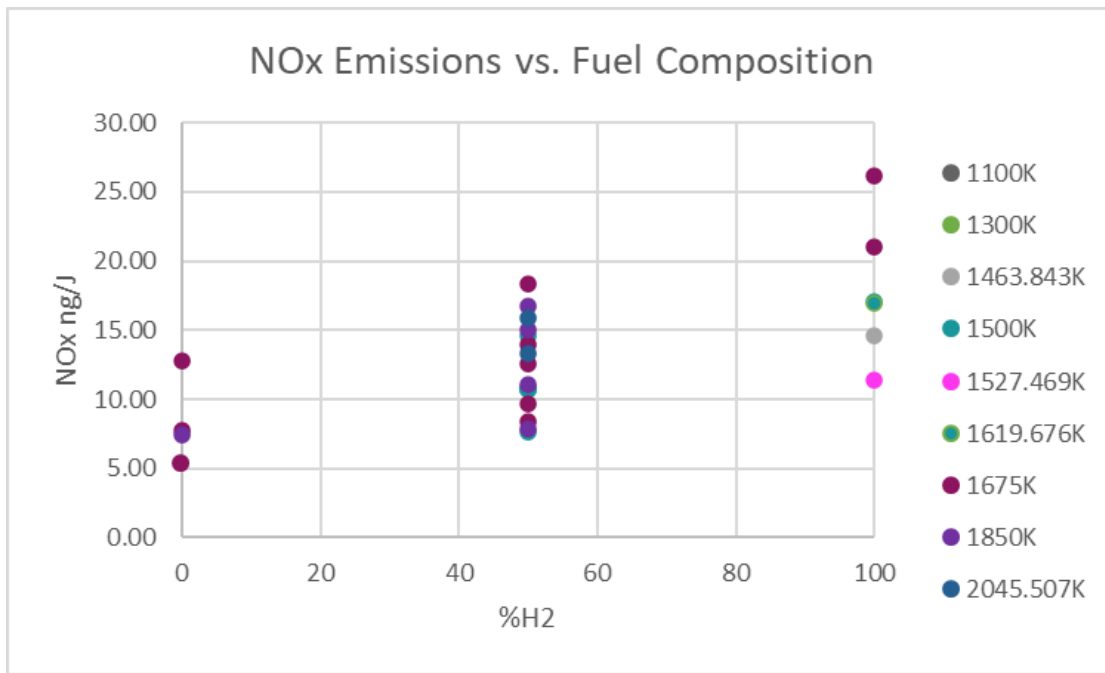


Figure 76. NOx Emissions vs. %H2 for Injector 16

The results of the ANOVA for the NOx model are shown in Figure 77 and its corresponding NOx model equation is shown in Figure 78. Figure 77 is based on a square root model where the criteria of significance was set for a p value of less than 0.5 to ensure at least

95% confidence. Figure 79 and Figure A- 15-Figure A- 17 in the Appendix confirms a normally distributed plot for residuals and randomized residuals for the most part. The “outliers” in the model correlated to cases with highest levels of NO_x emissions and were mainly as the result of pure hydrogen cases. Similar to the previous two models, these points were left in the model since their spikes in NO_x emissions signal a key difference rather than being considered as “outliers”.

To corroborate the model, other models were investigated such as removing higher order terms, using a power model of 0.2, and removing the “outliers”. Changes to the model did not affect the interpretation of the model. For instance, the main four factors with the highest F values are the preheat temperature, fuel composition, air splits and air swirl remained the same. Moreover, the majority of the interactions did not change from model to model. As a result, the square root model was ultimately selected as it was the best for the predicted vs. experimental values and its normally distributed residuals.

Source	Sum of Squares	df	Mean Square	F-value	p-value	
Model	384.14	24	16.01	89.11	< 0.0001	significant
A-Splits	24.94	1	24.94	138.82	< 0.0001	
B-Fuel Swirl	3.41	1	3.41	18.97	< 0.0001	
C-Air Swirl	25.63	1	25.63	142.70	< 0.0001	
D-Pressure Drop	3.99	1	3.99	22.19	< 0.0001	
E-Preheat Temperature	50.13	1	50.13	279.06	< 0.0001	
F-Fuel Composition	28.16	1	28.16	156.79	< 0.0001	
G-Flame Temperature	5.70	1	5.70	31.72	< 0.0001	
AB	2.58	1	2.58	14.38	0.0002	
AC	55.20	1	55.20	307.32	< 0.0001	
AE	2.90	1	2.90	16.13	< 0.0001	
AF	1.29	1	1.29	7.18	0.0076	
AG	11.81	1	11.81	65.74	< 0.0001	
BC	3.32	1	3.32	18.47	< 0.0001	
BD	0.1126	1	0.1126	0.6268	0.4289	
CE	1.27	1	1.27	7.05	0.0082	
CF	2.19	1	2.19	12.19	0.0005	
CG	9.57	1	9.57	53.28	< 0.0001	
DG	0.8722	1	0.8722	4.86	0.0280	
EG	2.26	1	2.26	12.60	0.0004	
FG	1.23	1	1.23	6.84	0.0092	
B ²	3.25	1	3.25	18.08	< 0.0001	
C ²	16.27	1	16.27	90.57	< 0.0001	
D ²	7.39	1	7.39	41.13	< 0.0001	
E ²	2.28	1	2.28	12.72	0.0004	
Residual	83.89	467	0.1796			
Lack of Fit	78.04	408	0.1913	1.93	0.0013	significant
Pure Error	5.85	59	0.0991			
Cor Total	468.03	491				

Figure 77. ANOVA Results for NOx Model

Sqrt(NOx-m)	=
+0.980787	
-1.35016	Splits
+0.101699	Fuel Swirl
-1.53258	Air Swirl
+0.103918	Pressure Drop
+0.006797	Preheat Temperature
-0.008520	Fuel Composition
-0.001764	Flame Temperature
+0.151280	Splits * Fuel Swirl
-0.568954	Splits * Air Swirl
-0.000929	Splits * Preheat Temperature
-0.002238	Splits * Fuel Composition
+0.001002	Splits * Flame Temperature
+0.137387	Fuel Swirl * Air Swirl
+0.011209	Fuel Swirl * Pressure Drop
-0.000610	Air Swirl * Preheat Temperature
+0.002878	Air Swirl * Fuel Composition
+0.000872	Air Swirl * Flame Temperature
+0.000086	Pressure Drop * Flame Temperature
+2.97371E-06	Preheat Temperature * Flame Temperature
+0.000010	Fuel Composition * Flame Temperature
-0.195132	Fuel Swirl ²
-0.413887	Air Swirl ²
-0.042692	Pressure Drop ²
-6.33032E-06	Preheat Temperature ²

Figure 78. NOx Model

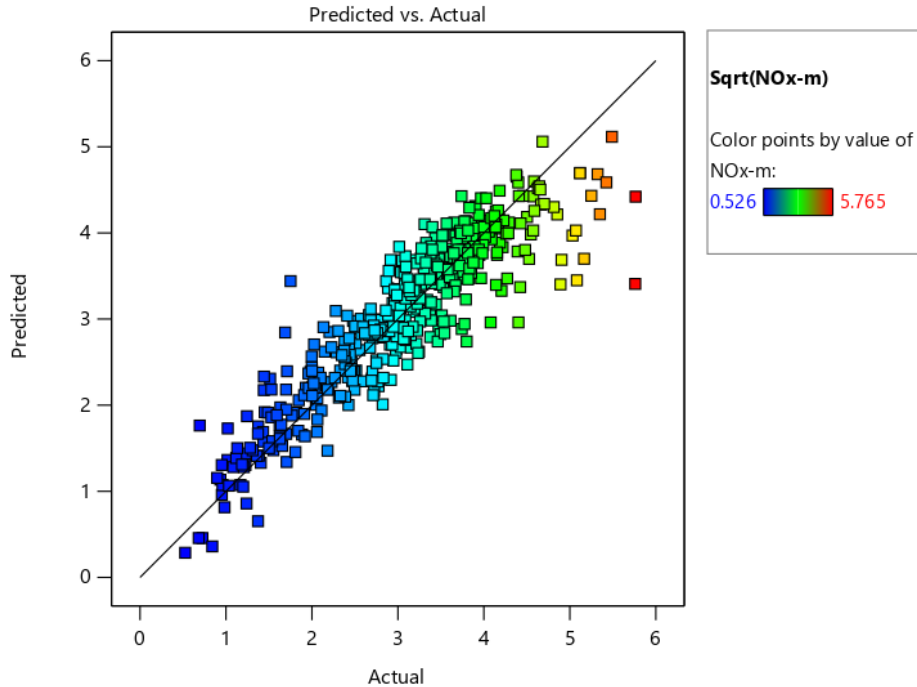


Figure 79. Predicted vs. Actual for NOx Model

The factor with the highest F factor is the preheat temperature at 279.06 followed by the fuel composition, air swirl, air splits. The significance of these factors is self-explanatory and were discussed in the previous NO emissions model. The same conclusions apply to the NOx model. The highest factor interaction, AC (air split and air swirl) had an even higher F factor at 307.32. This is best explained that when more air passes through the injector, then an increased swirling is favored to bring down the velocity of the air to be closer to that of the fuel for better mixing. The flame temperature was not as significant in the NOx model compared to the NO model with an F factor of 5.70, which is most probably due to NO's direct interaction with the thermal NO mechanism.

Since the ANOVA results for the NO and NOx model are very similar, the focus will be on interactions and factors that were not present in the NO model or if there is a discrepancy between the two models. As shown in Table 6, the factors highlighted in green are shared

between the two models. The factors highlighted in yellow are only present in the NO model and the ones in blue are only in the NOx model. Overall, the two models only differ in five interactions.

Table 6. Comparison Between the NO and NOx Model

Factors in the NO Model	Factors in the NOx Model
A	A
B	B
C	C
D	D
E	E
F	F
G	G
AB	AB
AC	AC
AD	AE
AE	AF
AF	AG
AG	BC
BC	BD
BD	CE
BG	CF
CD	CG
CE	DG
DG	EG
EG	FG
B ²	B ²
C ²	C ²
E ²	D ²
F ²	E ²
G ²	

Although the pressure drop factor is in both models, pressure drop is more prominent in the NOx model. As shown in Figure 80, an increase in pressure drop leads to decrease in NOx emissions which can be traced back to an increase in velocity in Equation 24. Higher velocities can be associated with more mixedness and thus lower temperatures. All other single factors had the same conclusion as in the NO model.

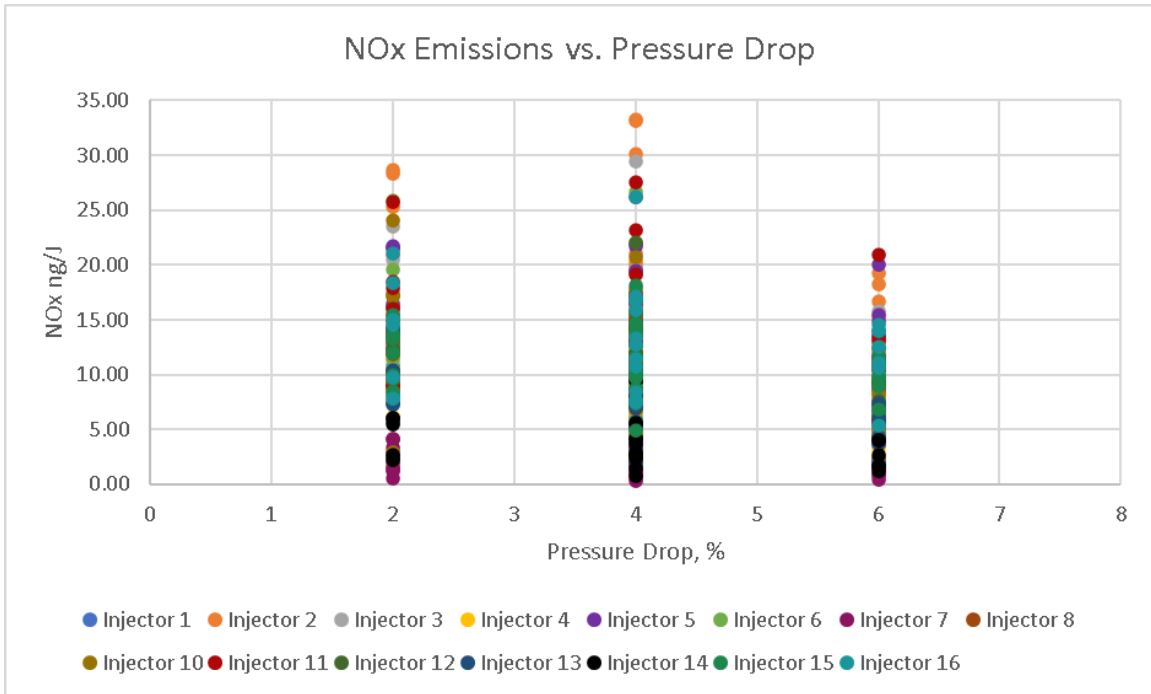


Figure 80. NOx Emissions vs. Pressure Drop

From Figure 81, it is found that when less air is passed through the injector, both low and high fuel swirl will achieve identical emissions. When the volumetric flow rate of air that passes through the injector is increased, then a lower fuel swirl is favored. The steeper swirl decreases the velocity of the fuel which makes it more difficult to mix with the faster velocity of air. The key difference between the AB interaction between the NO and NOx model is that there is no crisscross pathway where at one condition, lowered swirl angle is preferred over the other. With the NOx model, a steeper fuel angle mostly produces more emissions with the exception of the lower end of the design matrix where it does not matter.

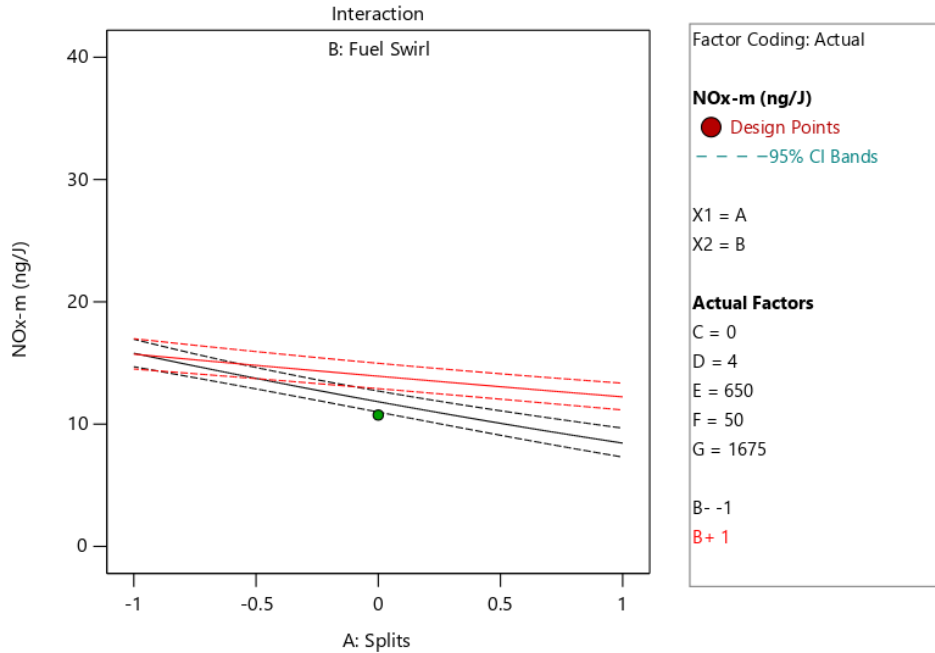


Figure 81. NOx Emissions for Air Splits vs. Fuel Swirl Interaction. (Red-Higher Fuel Swirl, Black-Lower Fuel Swirl)

The factor interaction between the air split and flame temperature (AG) behaves slightly different in the NOx model. In general, both models show that to achieve the lowest emissions, more air should flow through injector as flame temperature increases. However, when adding in fuel swirl, the differences between the two models begin to emerge. In the NOx model, when fuel swirl is the steepest, to maintain the lowest emissions, low flame temperatures and a greater flow rate through the injector should be maintained (Figure 83). In the NO model, to maintain the lowest emissions, less air should be going through the injector. A plausible reason for this is because NO cannot be directly compared to NOx since NO₂ is also a factor in NOx. In most instances NO is the dominating factor so NO and NOx share the same conclusions. When NO₂ dominates, conclusions begin to differ. As a result, it can be inferred that NO₂ is formed when there is more air through the injector. More interaction with the fuel and more air helps decrease the local temperatures which promote NO₂ production.

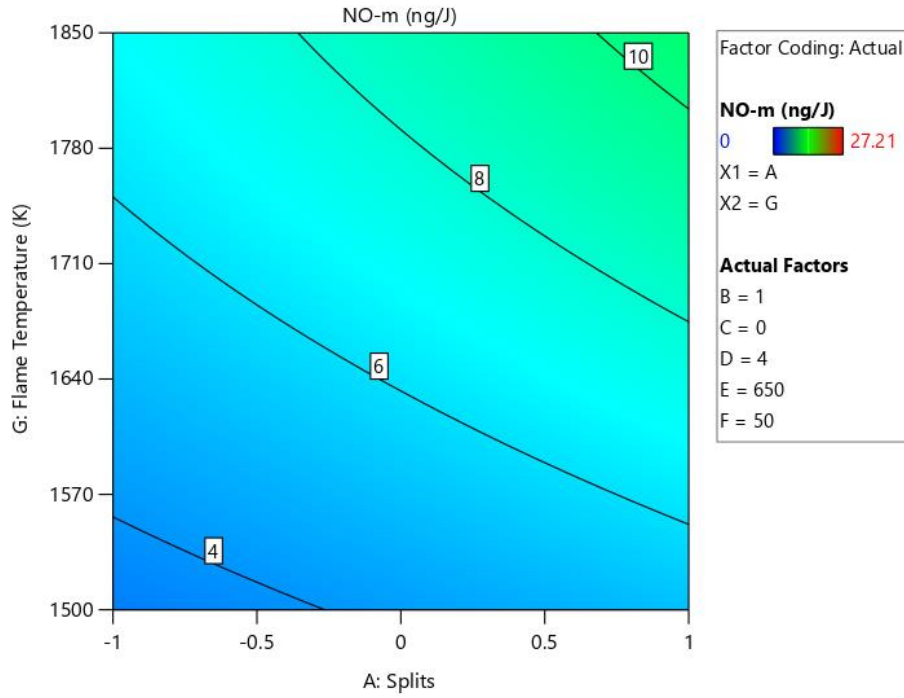


Figure 82. NO Emissions for Flame Temperature vs. Air Splits Interaction (Higher Fuel Swirl)

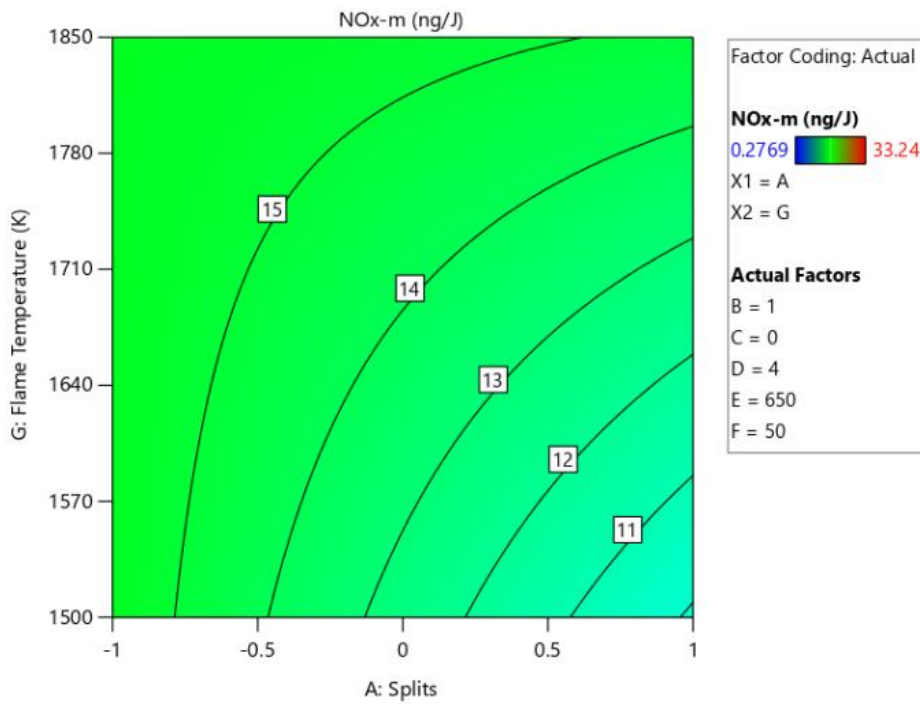


Figure 83. NOx Emissions for Flame Temperature vs. Air Splits Interaction (Higher Fuel Swirl)

The factor interaction between the fuel swirl and pressure drop (BD) for the NOx model shows that there is a difference between pressure drop, but the differences due to the fuel swirl are not as significant. A higher pressure drop, identified as the red line in Figure 84, records lower emissions which indicates that higher velocities are favored. Higher velocities promote mixing and decreases the temperatures.

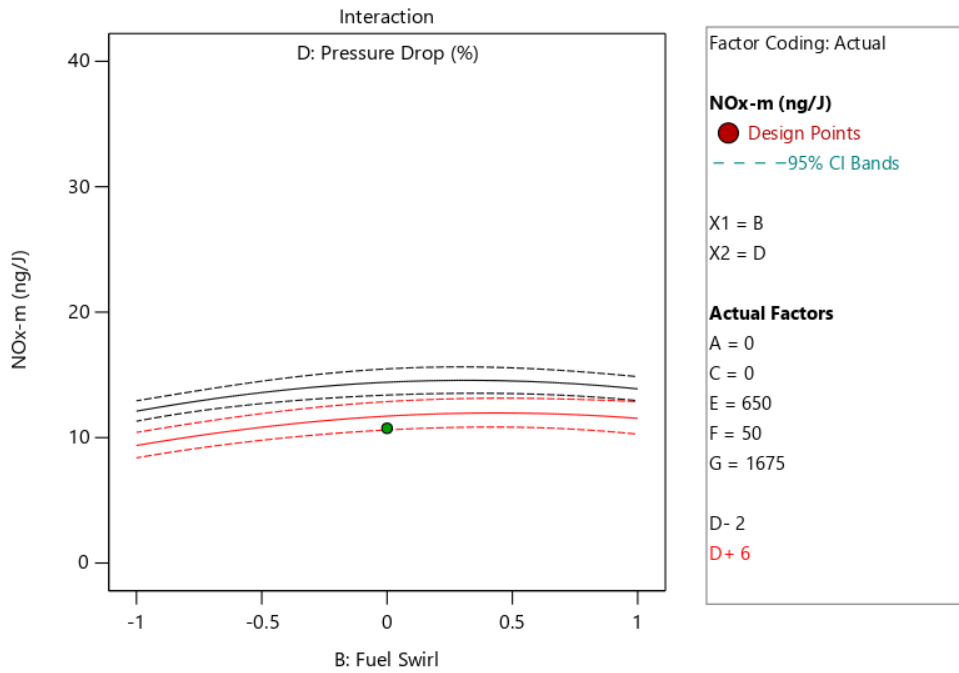


Figure 84. NOx Model for Fuel Swirl vs. Pressure Drop Interaction. (Red-Higher Pressure Drop, Black-Lower Pressure Drop)

The interaction between air swirl and fuel composition (CF) is new in the NOx model as shown in Figure 85. As more hydrogen content is added, NOx emissions are increased. But with the added benefit of air swirl, emissions can remain at the same levels as hydrogen content increases. This can be achieved because more air swirl facilitates mixing with the fuel and from previous discussions, homogeneity decreases peak temperatures. This conclusion does not change with the added effects of fuel or air swirl. However, notice that the graph is not linear and

is more parabolic symbolizing multiple solutions. Thus, based upon the desired factor or performance, multiple combinations of factors can achieve the same effect.

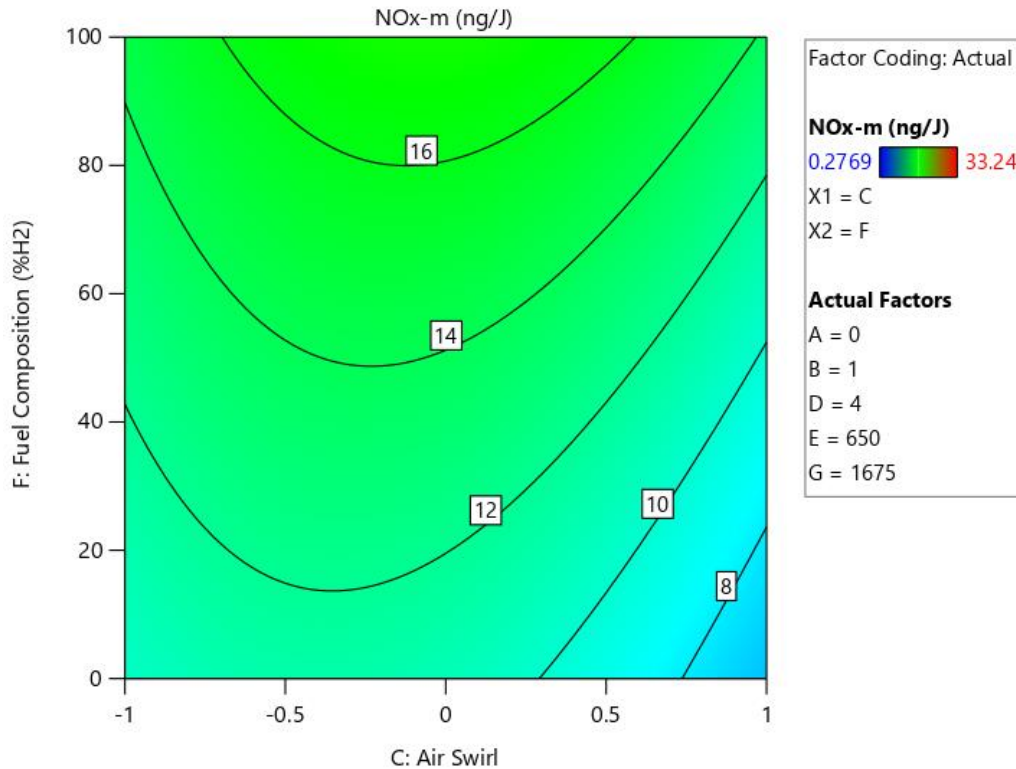


Figure 85. NOx Emissions for Fuel Composition vs. Air Swirl Interaction

Another new factor that emerges from the NOx model is the air swirl and the flame temperature (CG) as shown in Figure 86. As the air swirl angle increases, the differences between emissions for various flame temperature grow more pronounced. At lower swirl angle, the flame temperature does not matter because there is not sufficient mixing. So even when flame temperatures are lower, since it is unmixed, it has the same effect as if the system were operating at higher flame temperatures. Unmixedness leads rise to hot spots due to little pockets of fuel and air at different equivalence ratios.

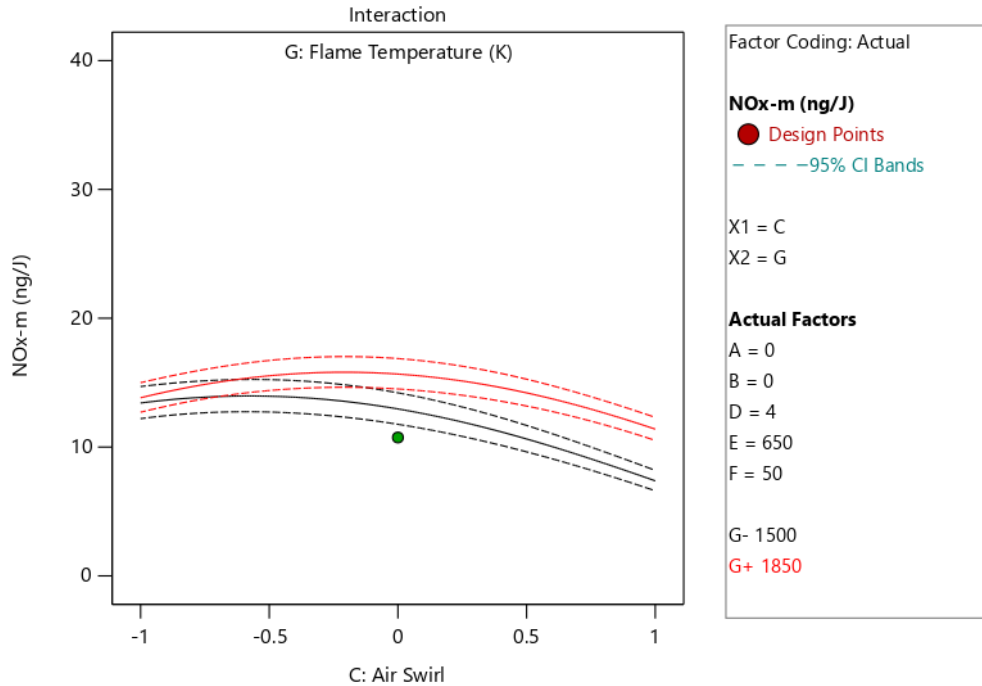


Figure 86. NOx Emissions for Air Swirl vs. Flame Temperature Interaction. (Red-Higher Flame Temperature, Black-Lower Flame Temperature)

The factor interaction between the flame temperature and pressure drop (DG) in the NOx model is different than in the NO model primarily because the effect of pressure drop is different. In the NOx model, the effect of increasing flame temperature can be offset by increasing or decreasing pressure drop. Increases in pressure drop can lower temperatures due to increases in velocities for better mixing. Decreases in pressure drop can also lower emissions when other factors like fuel and air swirl dominate to facilitate the mixing. This factor interaction continues to be more complex than Figure 87 portrays. When the effect of air split is added, it seems that an increase in flame temperature does not affect NOx emissions (see Figure 88). Instead, the pressure drop is the main driving factor for increased emissions. When majority of the flow goes through the plate rather than the injector, the surrounding air most likely cools the flame down. So even if the flame temperature is increased, it is quickly cooled down by the

surrounding air that the local temperature is cooled to a point where emissions levels are the same if the system was operating at lower flame temperatures.

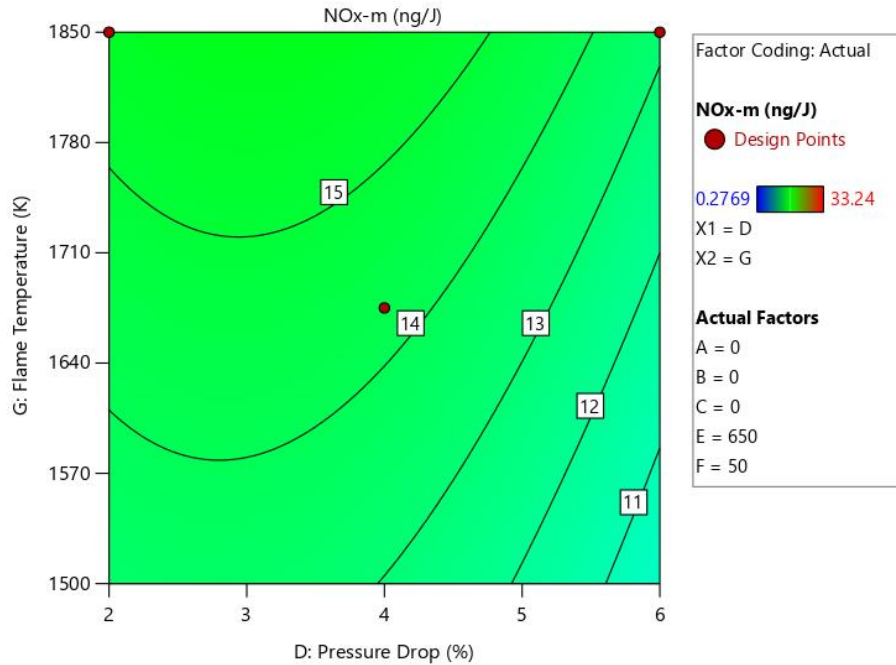


Figure 87. NOx Emissions for Flame Temperature vs. Pressure Drop Interaction (Middle Air Swirl)

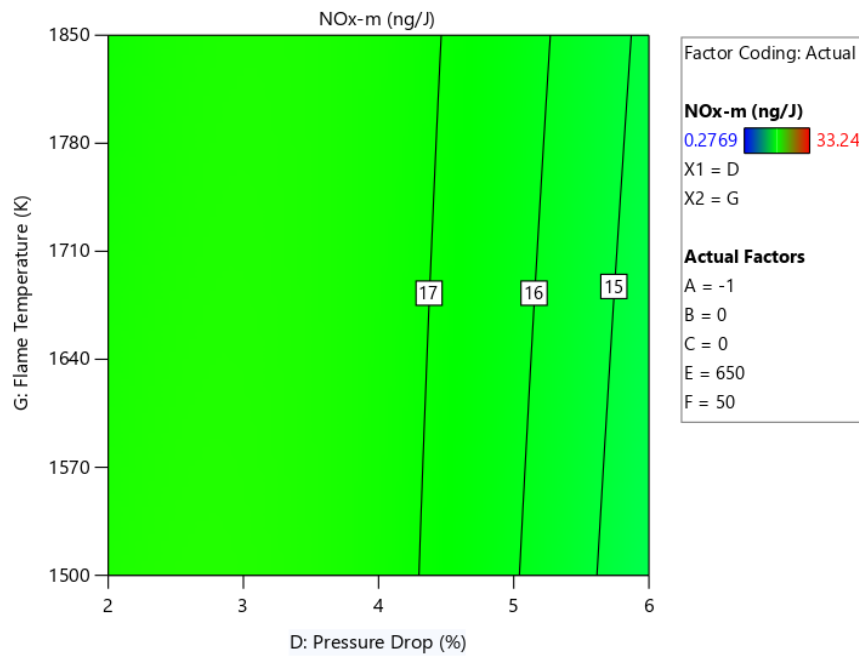


Figure 88. NOx Emissions for Flame Temperature vs. Pressure Drop Interaction (Lower Air Split)

The fuel interaction between flame temperature and preheat temperature (EG) follows the NO model for the most part where higher preheat and flame temperatures lead increase emissions (Figure 89). This is due to increased mechanisms that are activated at higher temperatures. These mechanisms will be discussed in section 5.2.3. However, when there is less air through the injector (Figure 90) or there is less air swirl (Figure 91), then increasing the flame temperature has no effect on emissions. When there is less air through the injector, the surrounding air acts as a coolant. This cools down the high flame temperature such that emissions are on the same levels of lower flame temperatures. When smaller air swirl angles are present, velocities increase which lead to more mixing. This mixedness can offset the effect of flame temperature. At well mixed conditions, at higher flame temperatures, the level of emissions can be identical to those produced at low flame temperatures.

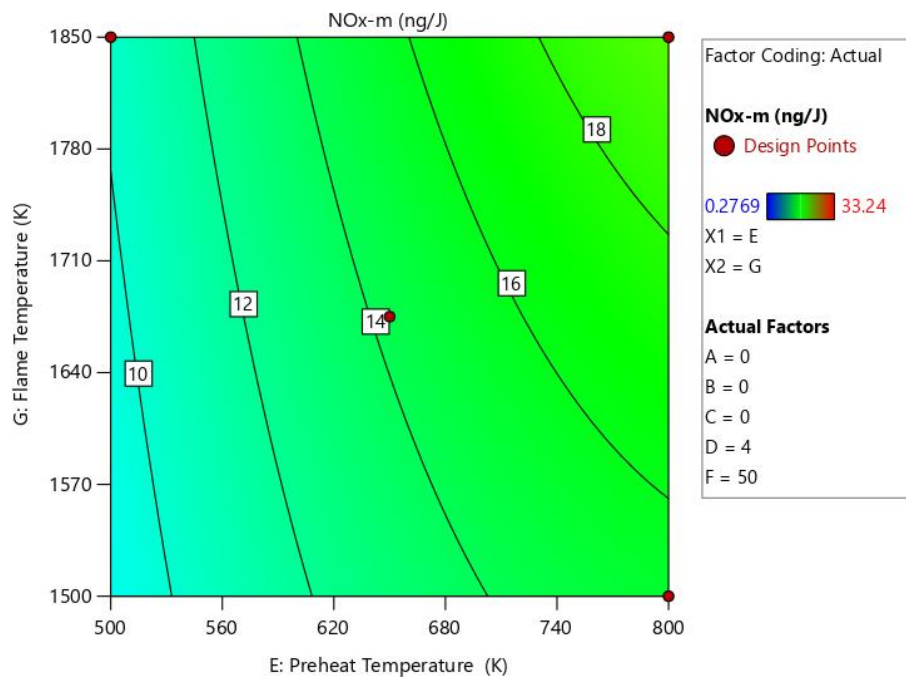


Figure 89. NOx Emissions for Flame Temperature vs. Preheat Temperature Interaction (Middle Air Split)

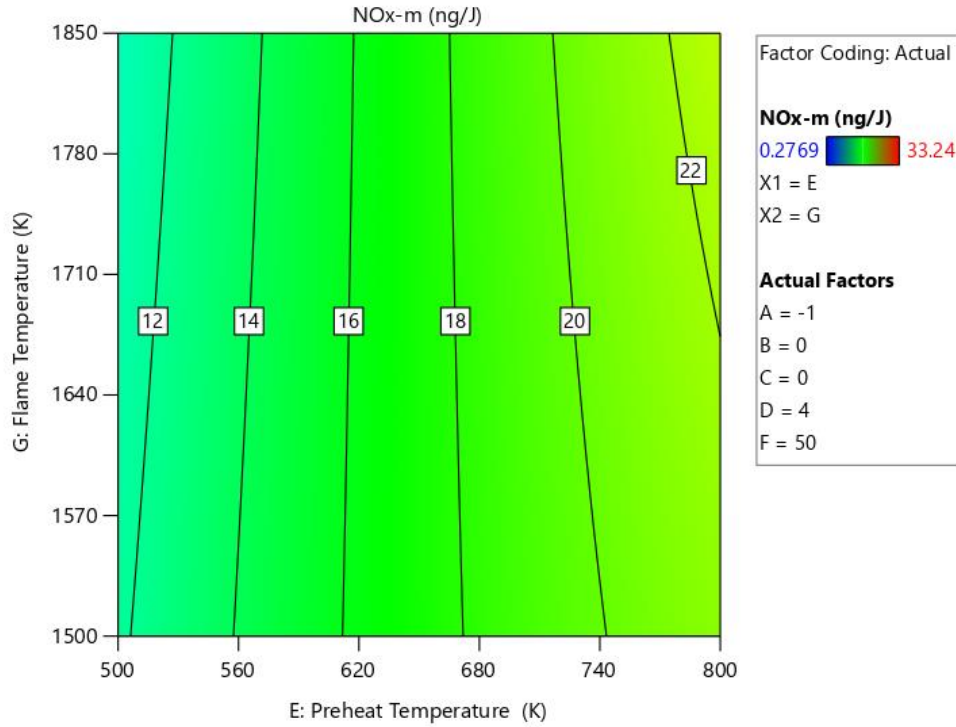


Figure 90. NOx Emissions for Flame Temperature vs. Preheat Temperature Interaction (Lower Air Split)

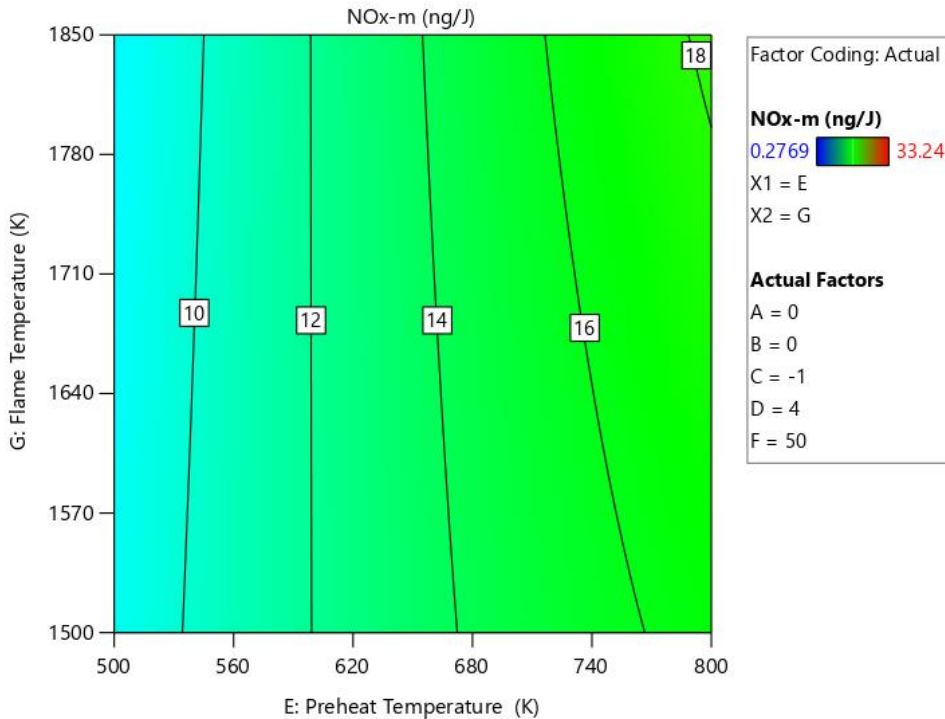


Figure 91. NOx Emissions for Flame Temperature vs. Preheat Temperature Interaction (Lower Air Swirl)

The last interaction is between the flame temperature and the fuel composition. Figure 92 shows that as hydrogen content increases, more NOx emissions are formed. Again, there are

several potential explanations for this cause. Due to higher flame speeds, and a non-perfect premixed system, hydrogen is more affected by imperfect mixing than methane. Another reason is due to the NNH pathway. Increasing hydrogen content in the fuel increases the magnitude at which the NNH pathway is activated. Details regarding this phenomenon are also explained in section 5.2.3. Figure 113-Figure 117 show more views in the model where one can compare increasing hydrogen content with increasing flame temperatures. These will be discussed in detail in section 5.1.5. Despite this conclusion, recall that hydrogen has wider flammability limits which allow hydrogen to combust at lower adiabatic flame temperatures that allow for a reduction in NO_x emissions. Moreover, since this is a non premixed system, the enhanced stability is favorable. With increased flammability limits, pockets of fuel caused by imperfect mixing, are still able to react and hold a flame.

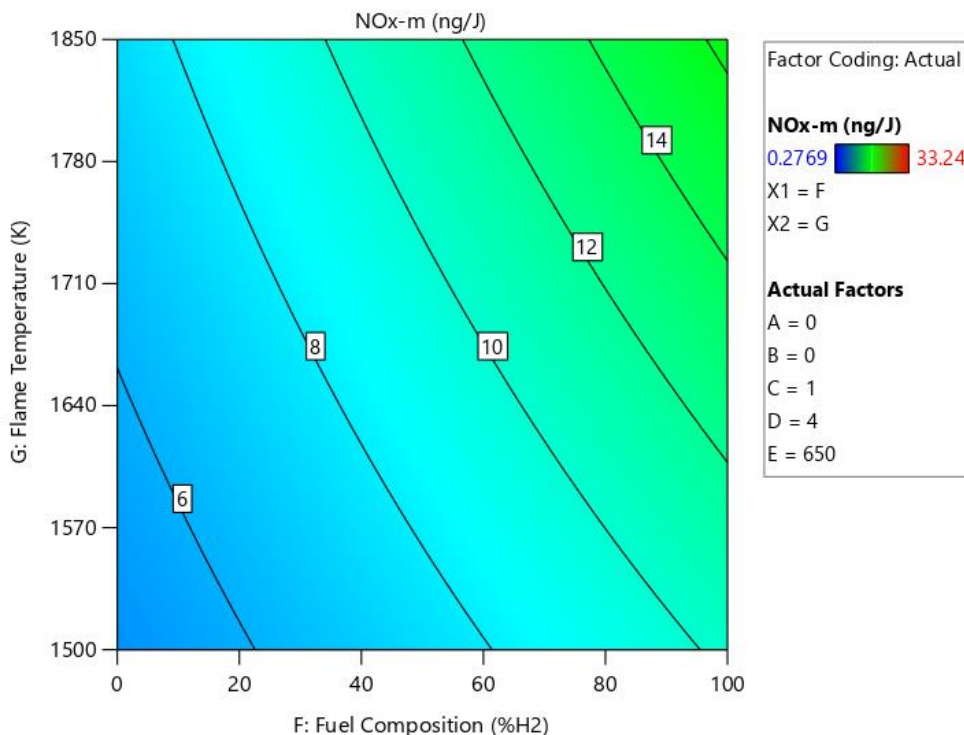


Figure 92. NO_x Emissions for Flame Temperature vs. Fuel Composition Interaction (Higher Air Swirl)

Lastly, the significance of factor interactions for B^2 , C^2 , D^2 , and E^2 is most likely to add weight to the model. Even though removing these terms from the model would not affect the major conclusions of the study, it would weaken some interactions and wash out some effects. For instance, some interactions and factors had parabolic profiles which were due to the squared terms. Thus, these factors were left in the model to better capture the experimental data.

In sum, the most important factors are the preheat temperature, fuel composition, air swirl, and air splits were the highest ranked F factors in order of greatest to least. The highest factor interaction was between the air split and the air swirl which reported an F factor of 307.32. This is higher than the F factor of preheat which is only 279.06. As more air enters the injector, the air swirl angle should decrease to lower the velocity to promote mixing with the fuel. Air swirl and fuel swirl can also be adjusted depending on desired performance and factors to achieve the absolute minimum emissions.

5.1.4 NO/NO_x Model

To study the relationship between NO vs. NO₂ production, the normalized NO/NO_x was studied using a square root model. The results of the ANOVA analysis show that all factors are significant. Like previous models, flame temperature, fuel composition and the interaction between the air swirl and air split (AC) are the highest ranked F factors. Observing the coded equation, preheat temperatures, flame temperatures, and the fuel composition are the dominant factors. Plots verifying the model's normal distribution and randomized residuals are shown in Figure 94 and Figure A- 18-Figure A- 20 in the Appendix.

Source	Sum of Squares	df	Mean Square	F-value	p-value	
Model	15.89	17	0.9348	60.66	< 0.0001	significant
A-Splits	0.0685	1	0.0685	4.44	0.0356	
B-Fuel Swirl	0.0077	1	0.0077	0.5015	0.4792	
C-Air Swirl	0.4876	1	0.4876	31.64	< 0.0001	
D-Pressure Drop	0.2002	1	0.2002	12.99	0.0003	
E-Preheat Temperature	1.22	1	1.22	79.07	< 0.0001	
F-Fuel Composition	2.22	1	2.22	144.17	< 0.0001	
G-Flame Temperature	2.49	1	2.49	161.68	< 0.0001	
AB	0.2530	1	0.2530	16.42	< 0.0001	
AC	2.03	1	2.03	131.90	< 0.0001	
AD	0.0060	1	0.0060	0.3887	0.5333	
BD	0.1168	1	0.1168	7.58	0.0061	
EF	0.0662	1	0.0662	4.29	0.0388	
FG	0.4974	1	0.4974	32.27	< 0.0001	
A ²	0.1166	1	0.1166	7.56	0.0062	
C ²	0.4651	1	0.4651	30.18	< 0.0001	
E ²	0.0828	1	0.0828	5.37	0.0209	
G ²	1.36	1	1.36	88.29	< 0.0001	
Residual	7.30	474	0.0154			
Lack of Fit	6.59	415	0.0159	1.31	0.0982	not significant
Pure Error	0.7129	59	0.0121			
Cor Total	23.20	491				

Figure 93. ANOVA Results for NO/NOx Model

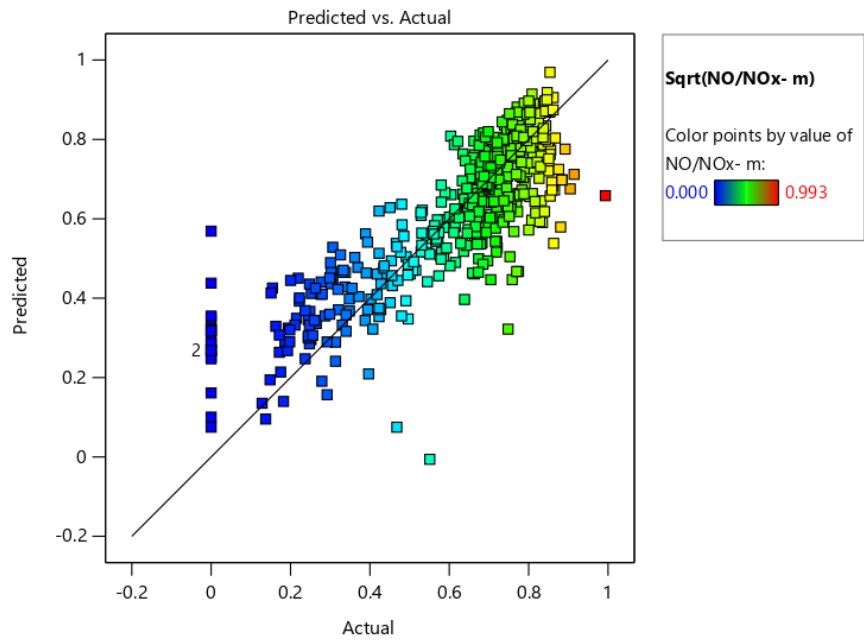


Figure 94. Predicted vs. Actual for NO/NOx Model

As more air enters the injector, the ratio between NO/NO_x is decreased which means that there is more NO₂ formation. This makes sense because more air entering through the injector would lower the overall temperature as it interacts with the fuel. Lower temperatures promote NO₂ formation. As for fuel swirl, it does not seem to affect the NO/NO_x ratio. This is justified as the factor has a p value of 0.47. For the air swirl, lower NO/NO_x ratios exist at the lower and upper portion of the design matrix. This suggests multiple solutions exist for achieve the same level of emissions. This gives the system flexibility depending on desired performance or specific factors. Air swirl is also shared with other interactions which can explain the parabolic graph. Moreover, as the pressure drop increases, the NO/NO_x ratio is decreased, or more NO₂ formation. As previously stated, the pressure drop is tied to velocities. Thus, increases in pressure drop mean higher velocities (or better mixing) thus temperatures are lower.

For the last three single factor interactions: preheat and flame temperature, and fuel composition, NO₂ production is decreased as the upper portion of the design matrix is approached. This makes sense because the upper portion of the design matrix all correspond to higher temperatures which is more dominated by NO production due to the thermal NO mechanism. The summary of the one factor interactions is illustrated in Figure 95-Figure 101.

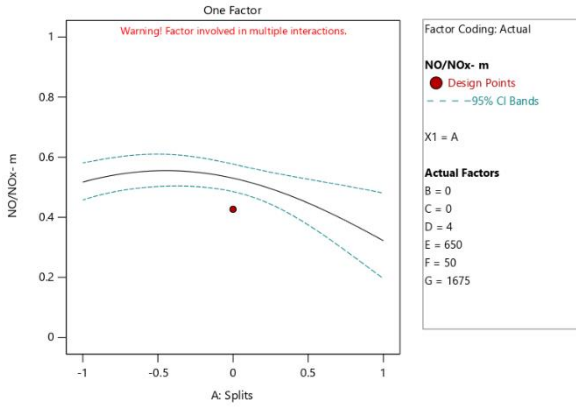


Figure 95. NO/NOx vs. Air Splits

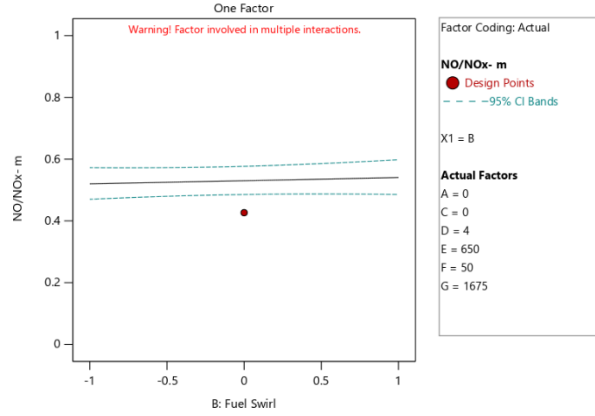


Figure 96. NO/NOx vs. Fuel Swirl

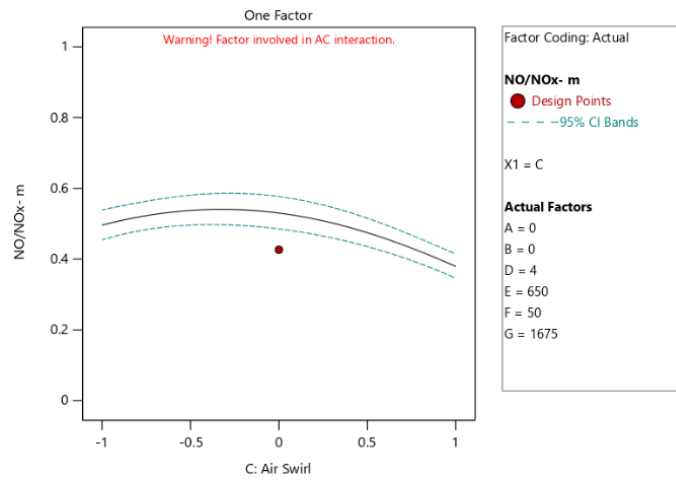


Figure 97. NO/NOx vs. Air Swirl

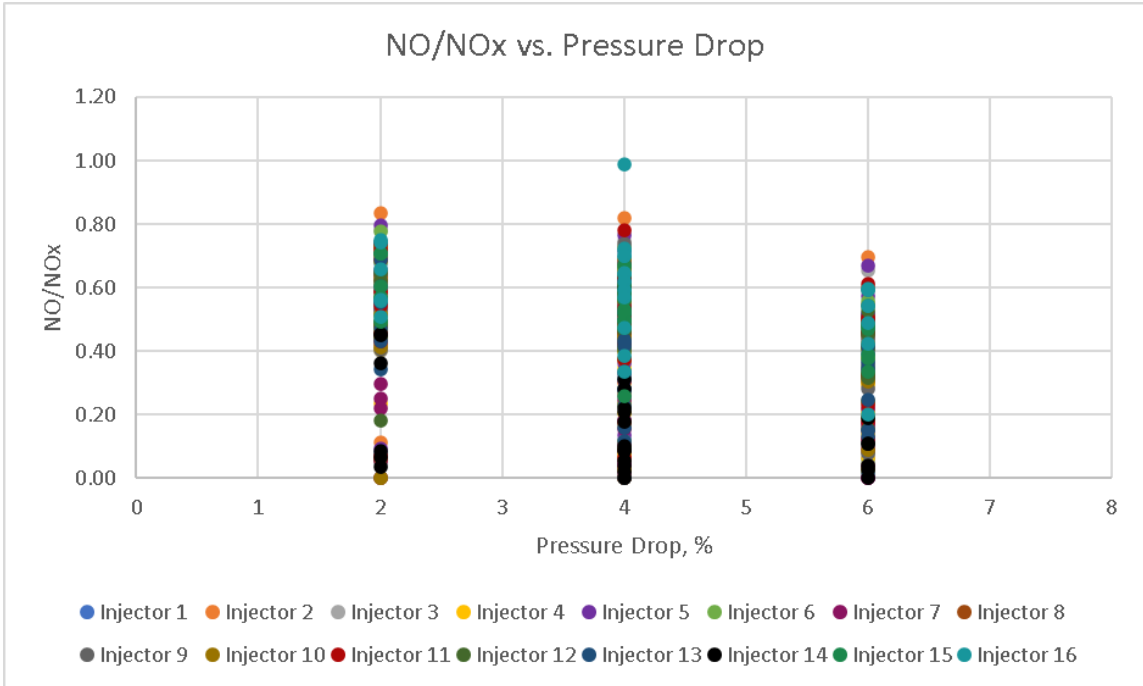


Figure 98. NO/NO_x vs. Pressure Drop

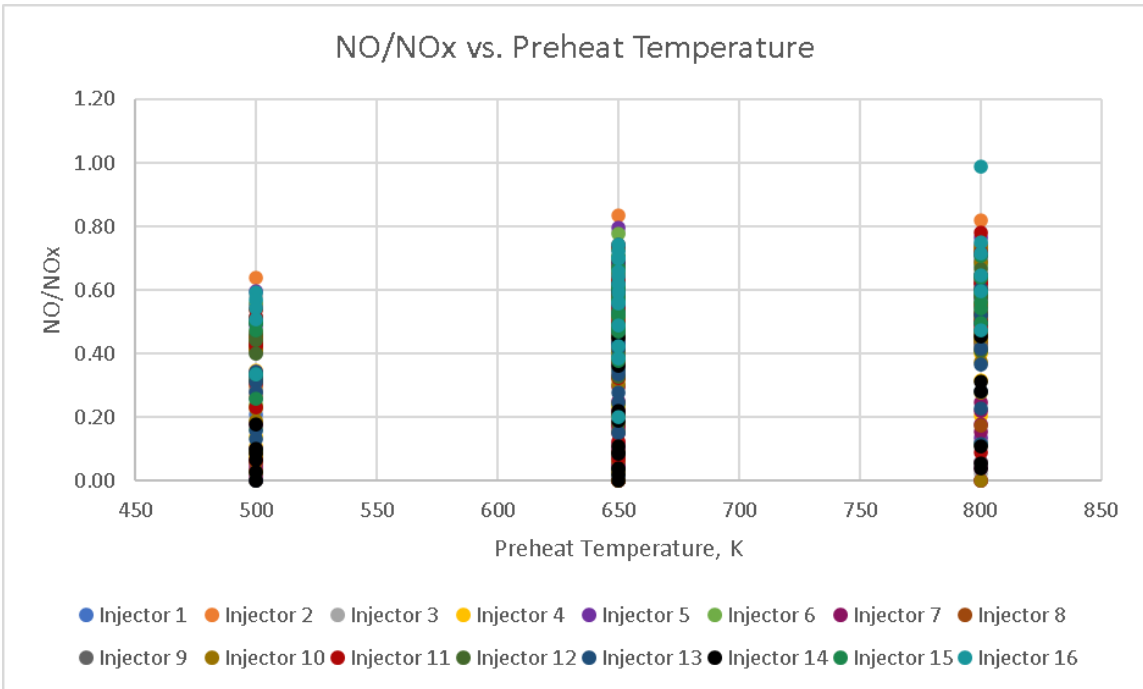


Figure 99. NO/NO_x vs. Preheat Temperature

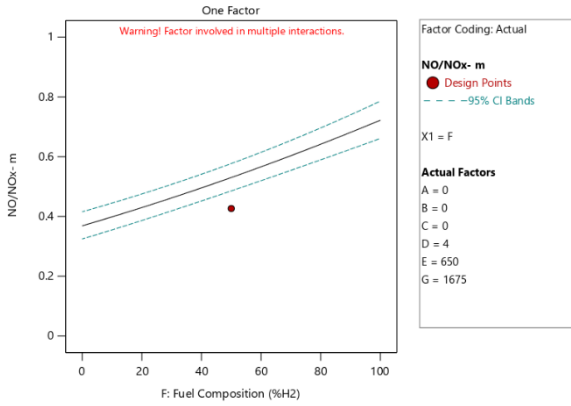


Figure 100. NO/NOx vs. Fuel Composition

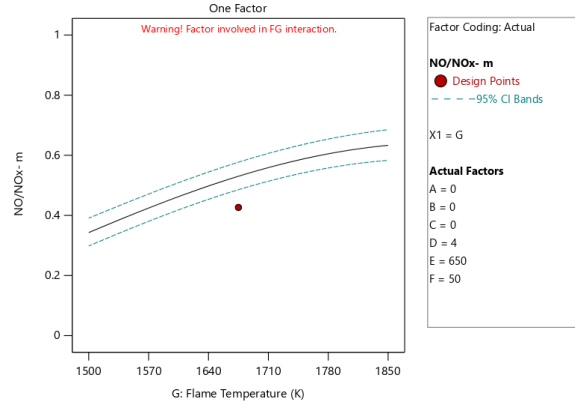


Figure 101. NO/NOx vs. Flame Temperature

The factor interaction between the fuel swirl and air splits (AB) shows that increasing the air through the injector decreases the ratio. This matches with previously drawn conclusions where more air decreases the overall temperature. However, increasing the fuel swirl angle only slightly increases the NO/NOx ratio as shown in Figure 102. A possible reason for why increasing swirl angle leads to decreases in NO₂ production is because higher fuel swirls are not optimum due to the fuel's lower relative velocity. The lower velocity promotes mixing as it approaches the air's velocity and lower peak temperatures result. This was determined multiple times in previous models-lower air swirls gave lower emissions.

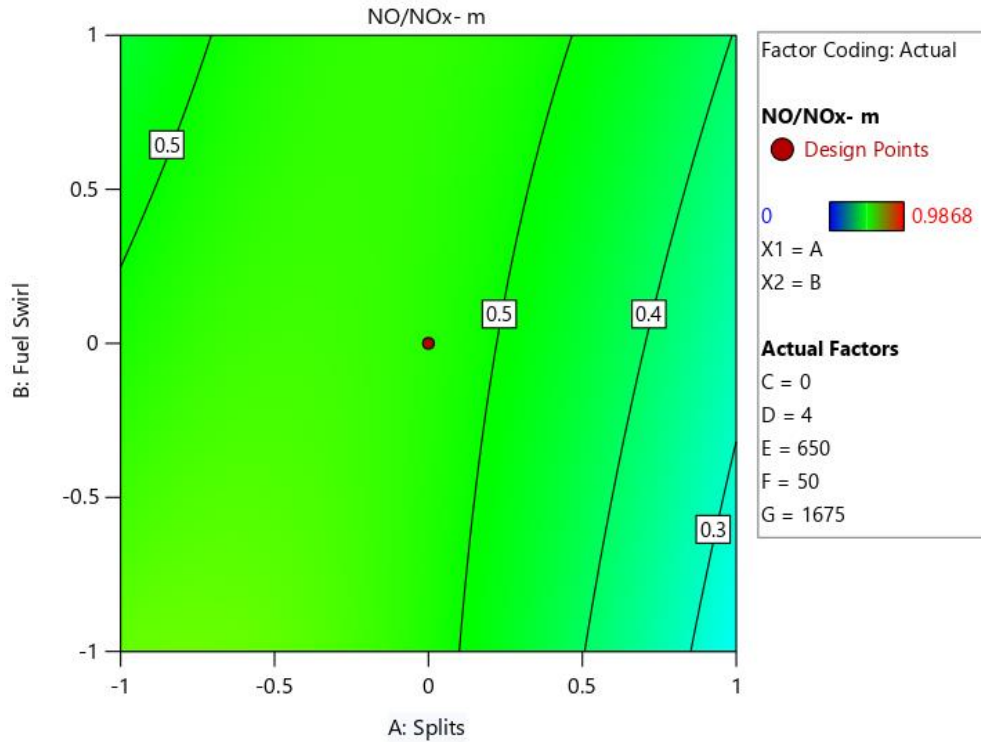


Figure 102. NO/NO_x Ratio for Fuel Swirl vs. Splits Interaction

The interaction between air splits and air swirl (AC) are shown in Figure 103. This relationship is very similar to the NO model. As more air enters through the injector, having more a higher air swirl is better to facilitate mixing and decreases the air velocity to better interact with the fuel flow. This increased mixing is reflected in the NO/NO_x ratio. From Figure 103, following the red line (steeper air swirl), with more air swirl the NO/NO_x ratio decreases. This indicates more NO₂ as a result of increased mixedness and lower overall temperatures. However, as less air enters the injector, less swirl is favored since the velocity is lowered. Thus, a smaller swirl angle is used to compensate and aid for higher velocities.

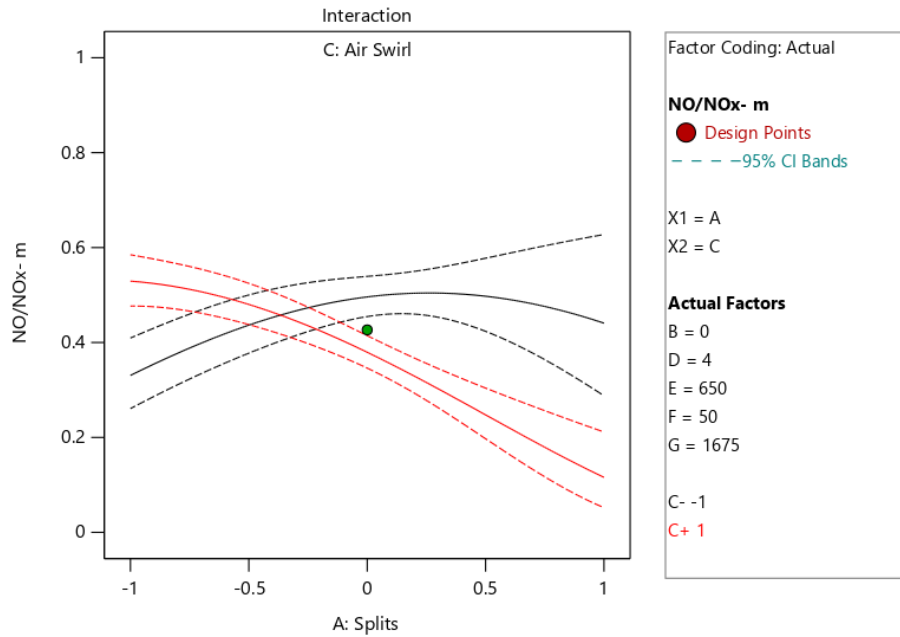


Figure 103. NO/NO_x for Air Splits vs. Air Swirl Interaction. (Red-Higher Air Swirl, Black-Lower Air Swirl)

The next significant interaction is between the fuel swirl and the pressure drop (BD). Increasing the pressure drop decreases the NO/NO_x ratio indicating that NO₂ production increases. Increased pressure drop lowers the ratio is because the higher velocities give rise to more homogenous flow fields. The lowered temperatures allow NO₂ to dominate. The trend also shows that at steeper air swirl negates the effect of pressure drop. A steeper angle increases velocity. Since pressure drop and fuel and air swirl both involve velocity, this indicates air and fuel swirl have more significance over pressure drop.

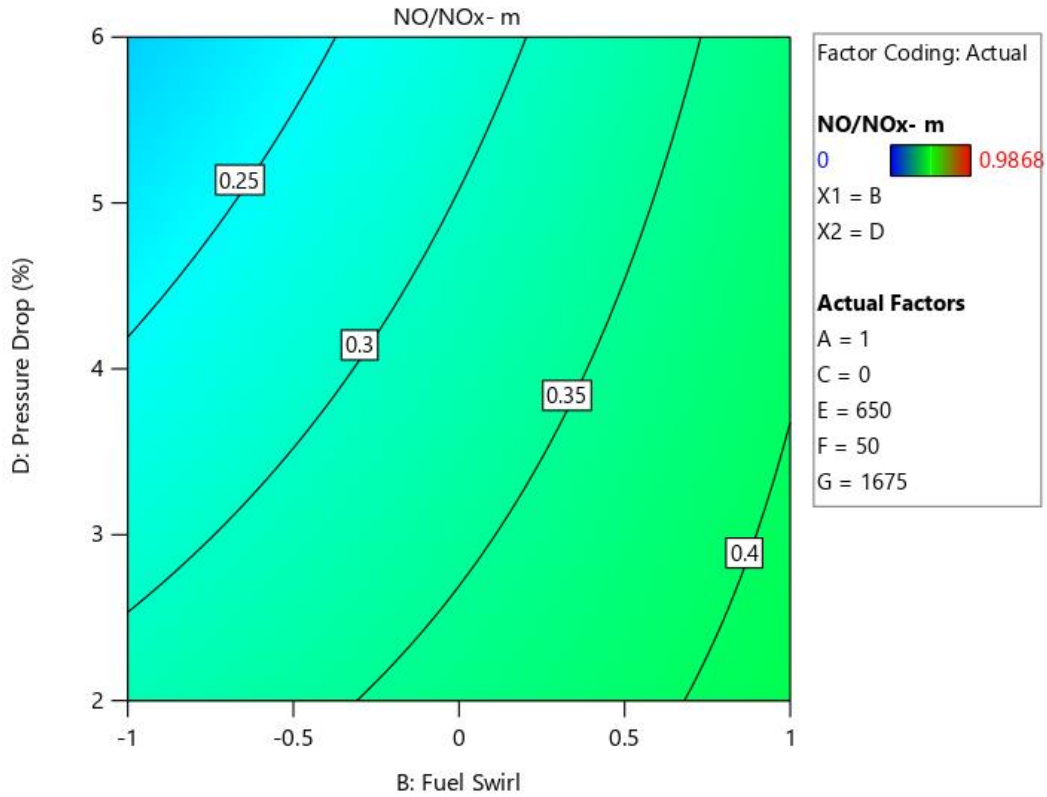


Figure 104. NO/NO_x for Fuel Swirl vs. Pressure Drop (Higher Air Split)

The relationship with increasing hydrogen and the NO/NO_x ratio reveals that NO's formation rate is more prominent in hydrogen compared to methane (Figure 105). This is best explained by the fact that hydrogen has more direct pathways to NO formation. The exact discussions and details of this pathway is discussed in section 5.2.3. Lowering preheat can also offset the effects of increased hydrogen content. The effect of flame temperatures also affects the interaction between the two fuels.

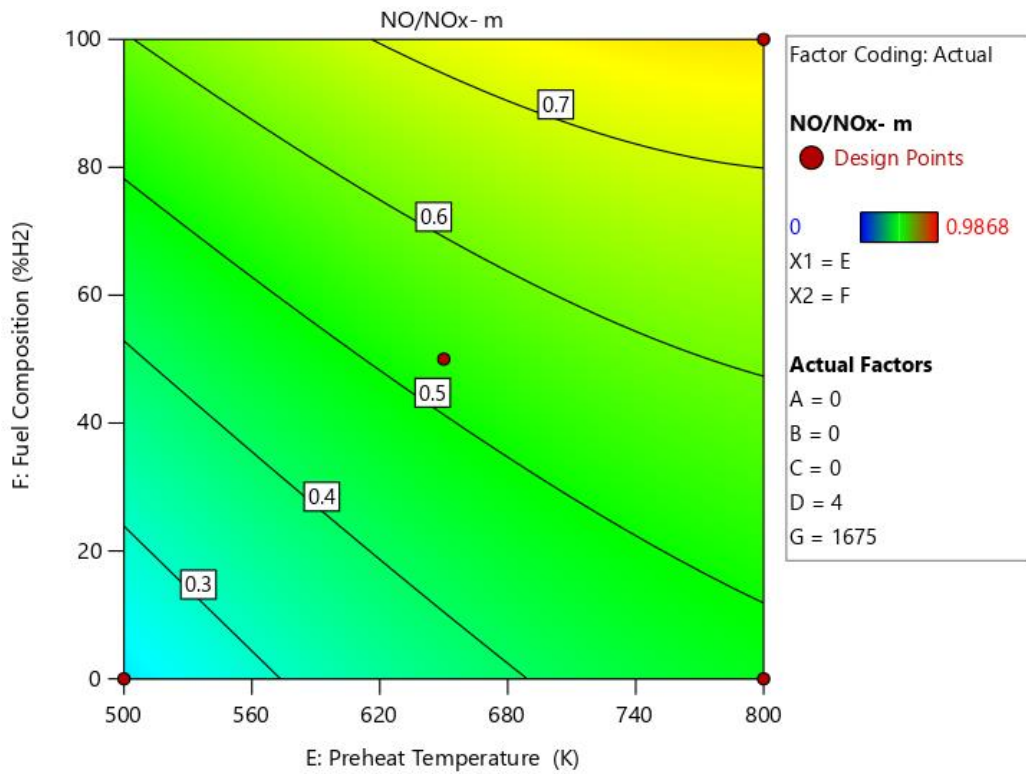


Figure 105. NO/NO_x for Fuel Composition vs. Preheat Temperature Interaction

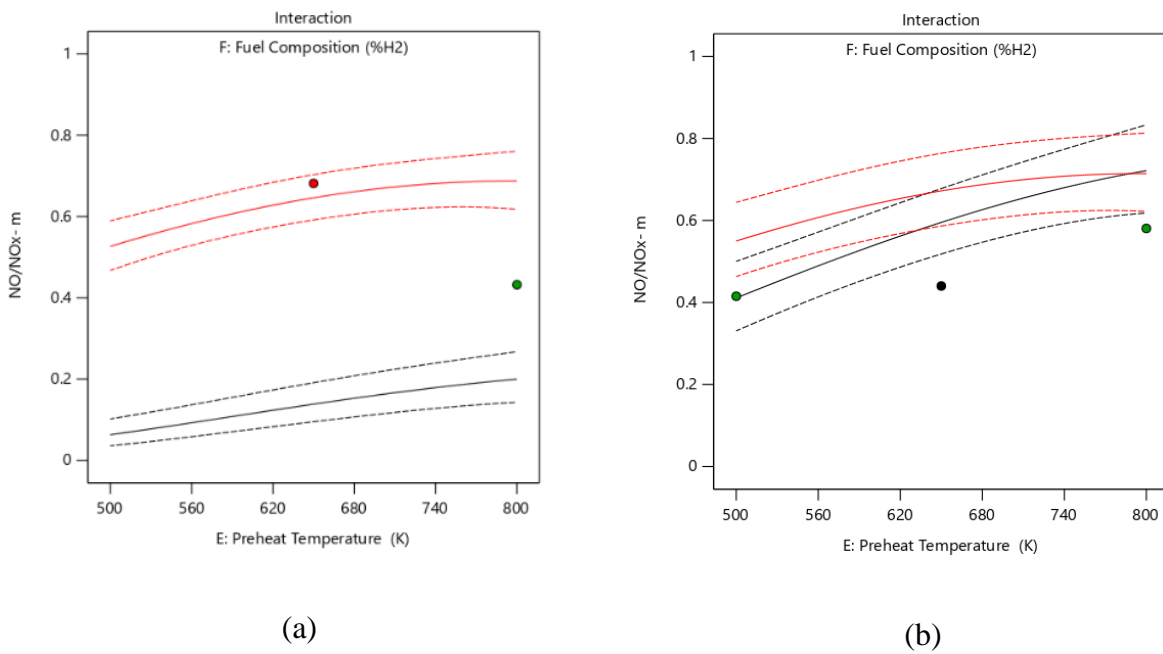


Figure 106. NO/NO_x for Preheat Temperature vs. Fuel Composition Interaction. (Red-100% H₂, Black-100% CH₄) (a) Flame Temperature of 1500K (b) Flame Temperature of 1850K. All other factors are at the middle of the design space.

At low flame temperatures, hydrogen (marked in red in Figure 106.a) distinctively produces more NO than methane (marked in black). This is especially true for higher preheat temperatures. One explanation for this is hydrogen's pathway to NO formation. At both low and high flame temperatures, hydrogen forms NO through the NNH pathway. This is why you see similar trends in both Figure 106.a and Figure 106.b with the red line (100% H₂). But with methane, there is a clear difference between adiabatic flame temperatures of 1500K and 1850K which can be traced back to the thermal mechanism that gets activated above temperatures of 1685K. More information on this is discussed in section 5.2.3.

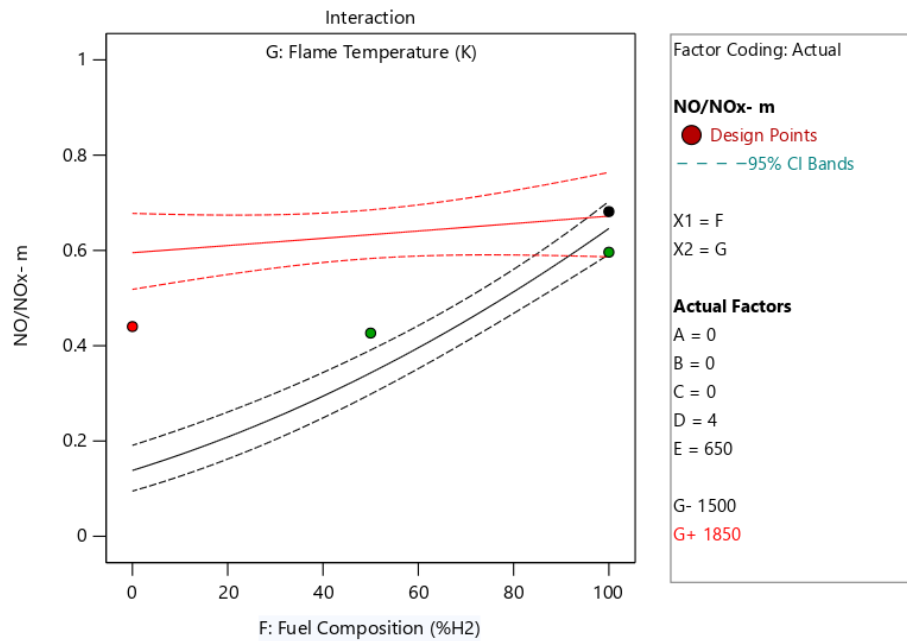


Figure 107. NO/NO_x for Fuel Composition vs. Flame Temperature Interaction. (Red-High Flame Temperature, Black-Low Flame Temperature)

When studying the fuel composition and flame temperature interaction, Figure 107, it seems that only when the fuel is comprised of 100% hydrogen then NO/NO_x ratios are roughly the same. At high flame temperatures (marked in red) and low flame temperatures (marked in black) the model yields similar NO/NO_x ratios which means the same ratio of NO to NO_x are

emitted. This indicates that Hydrogen pathways to NO and NO_x are similar, if not the same for low and high flame temperature. Comparing this to methane, there is a stark contrast. At high flame temperature, methane produces a higher NO/NO_x ratio which can be traced back to thermal NO_x mechanism that is activated at ~1900K. This is later discussed in section 5.2.3.

5.1.5 Lower Temperature (1100-1300K) Matrix

The results presented above encompassed flame temperatures ranging from 1500-1850K; however, it is known that hydrogen can burn leaner and thus produce lower emissions. Since the presented results show that hydrogen fuel yields higher NO/NO_x emissions, it is of interest to see if decreasing the flame temperature for hydrogen can result in lower NO/NO_x emissions compared to methane at 1500K. A 16-point matrix was added in addition the 27-point matrix to study hydrogen at lower temperatures of between 1100-1300K. The following studies are conducted with an air split, air swirl, fuel swirl, and a preheat temperature of 0 in the design space. While %H₂ can be plotted against flame temperatures, Design Expert was unable to plot the lower temperature ranges since they are not part of the original 27-point design matrix. Thus, 1100K and 1300K are plotted manually but in an effort to keep graphs consistent for comparison, all graphs used %H₂ vs. pressure drop.

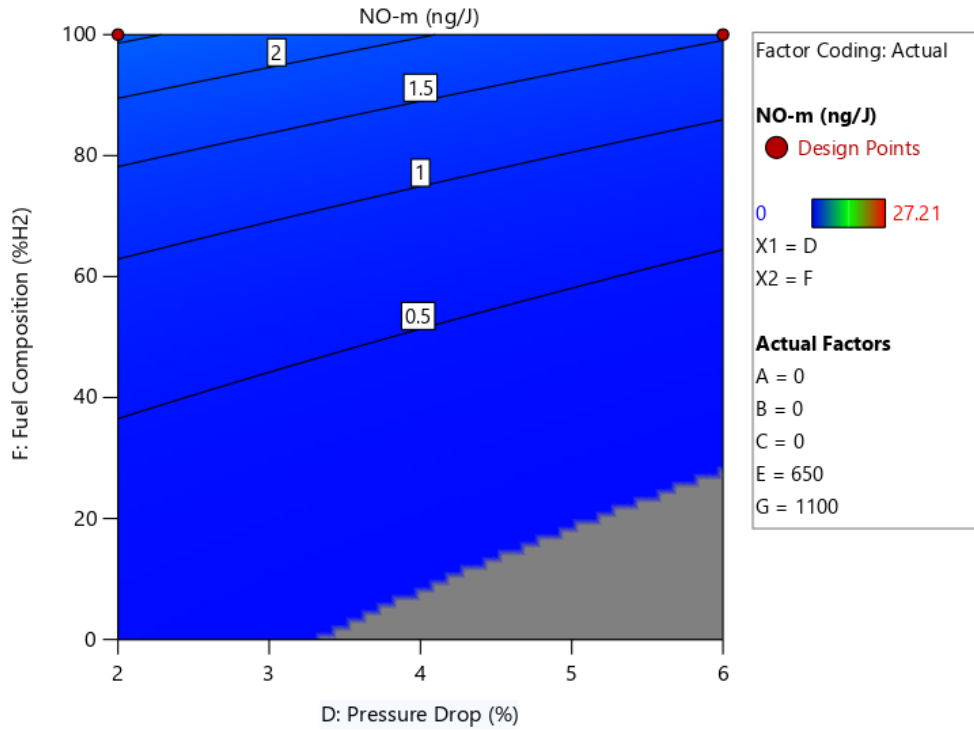


Figure 108. NO Model, 1100K Flame Temperature

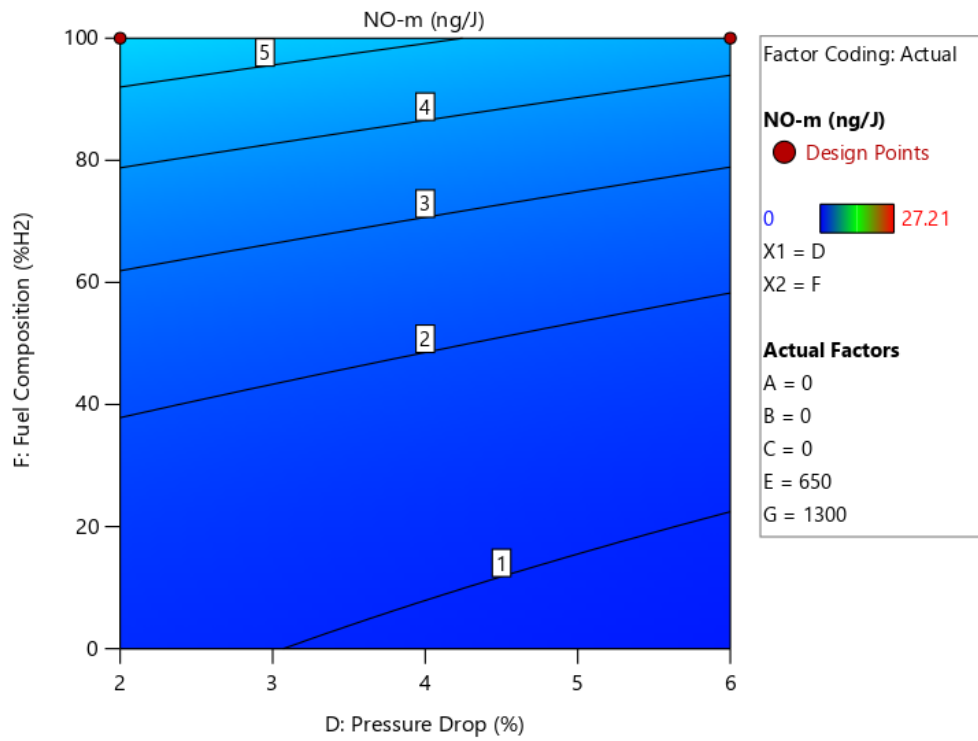


Figure 109. NO Model, 1300K Flame Temperature

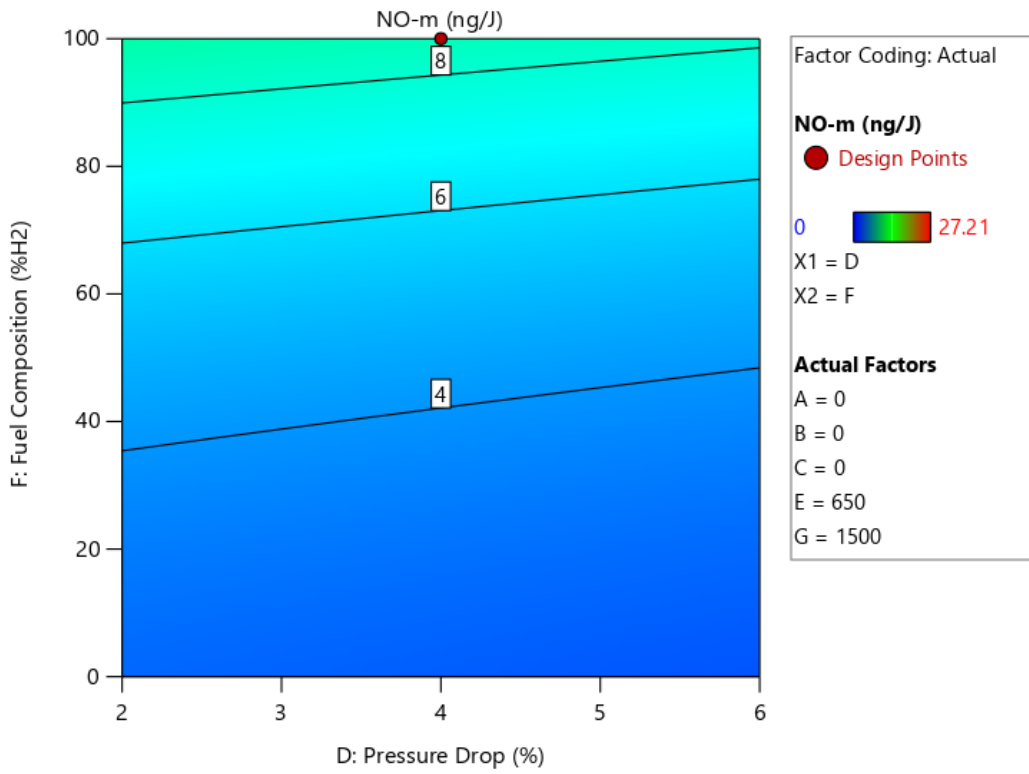


Figure 110. NO Model, 1500K Flame Temperature

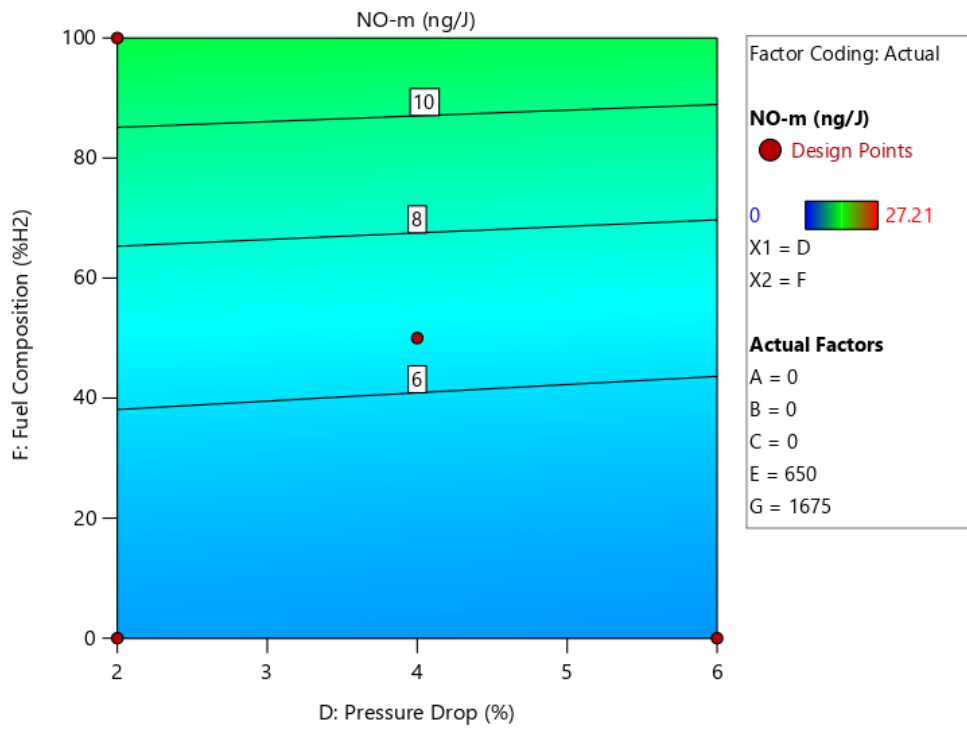


Figure 111. NO Model, 1675K Flame Temperature

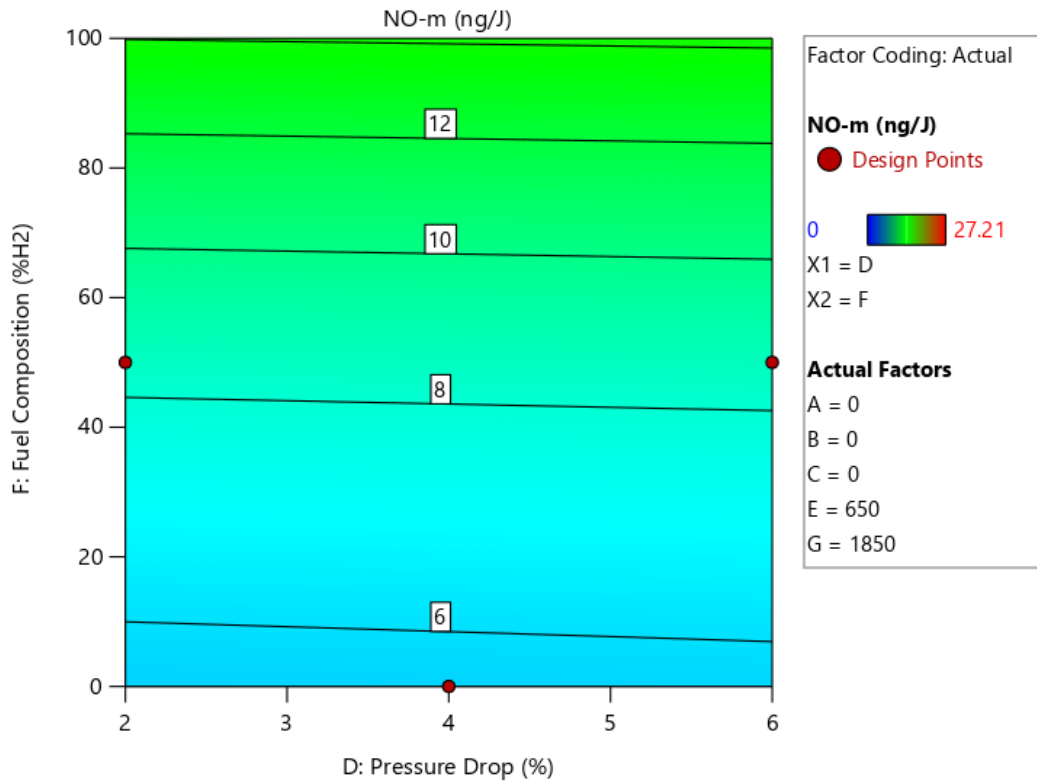


Figure 112. NO Model, 1850K Flame Temperature

Figure 108 - Figure 112, in order of increasing flame temperature show that at lower temperatures, hydrogen does produce lower emissions than pure methane. Comparing Figure 108 to Figure 112, hydrogen produces ~ 1.5 ng/J of NO emissions at 6% pressure drop compared to methane which produces ~ 5.74 ng/J at 6% pressure drop. If the flame temperature is lowered to 1500K (Figure 110), methane still produces higher NO emissions at ~2.3 ng/J.

Now, to validate the claim that hydrogen produces lower emissions at lower flame temperatures, it will be compared to methane's best-case scenario. As seen previously in other models, a pressure drop of 6% gives the lowest emissions thus a methane case at 1500K at 6% is the best-case scenario for methane. Comparing this point to hydrogen at 2% pressure drop at 1100K (hydrogen's worse case at 1100K), concludes that hydrogen produces more emissions but not by a far amount. At 2% pressure drop with a flame temperature of 1100K, hydrogen

produces ~2.6 ng/J of NO emissions but the methane case only produces ~2.3 ng/J of NO emissions. In this case, hydrogen does not produce lower emissions. The extremes do not necessarily justify switching over to hydrogen fuel due to all the challenges associated with the inherent fuel characteristics for a 1 ng/J reduction in NO.

It should be noted that the lower temperature figures should be interpreted with precaution because there exists no data for pure methane at 1100 or 1300K or even mixtures. Methane cannot sustain flames at temperatures below 1500K due to its LBO limit. The model is compensating for methane based on surrounding data points. Moving forward, only hydrogen data points are considered are lower flame temperatures.

Next, the NO_x model will be studied. To keep things consistent, the same conditions from the NO study was applied to the NO_x study. Air split, fuel swirl, air swirl and preheat temperature were set at 0 in the design matrix. Figure 113- Figure 117 are in order of increasing flame temperature.

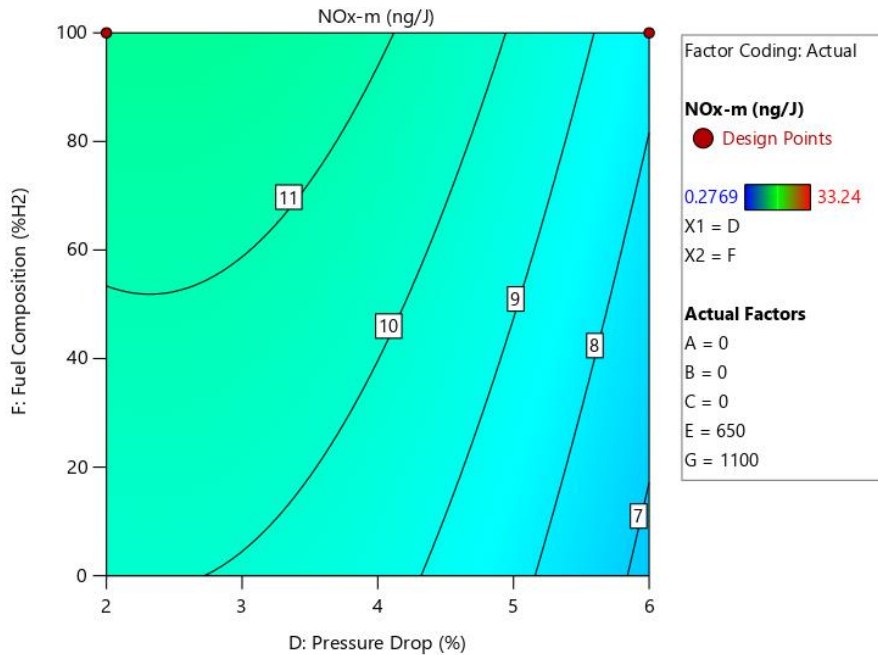


Figure 113. NOx Model, 1100K Flame Temperature

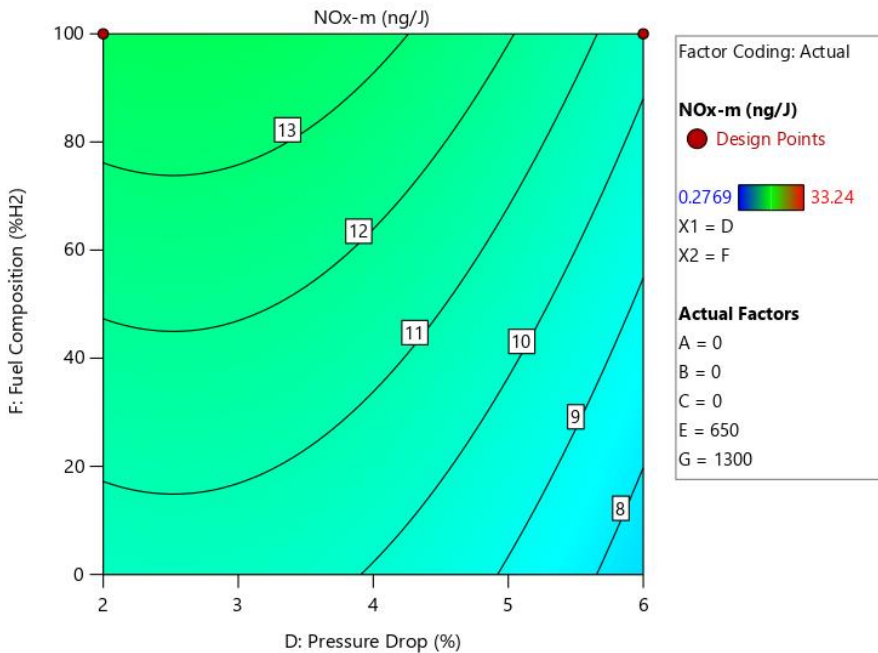


Figure 114. NOx Model, 1300K Flame Temperature

Just like the NO model, there exists no real data for methane at lower flame temperatures of 1100-1300K. Even 50-50 mixtures were not included in the model due to high levels of CO emissions. These figures are distorted as the model compensates for methane based on nearby

data points. As a result, only hydrogen points are analyzed in the lower flame temperature figures.

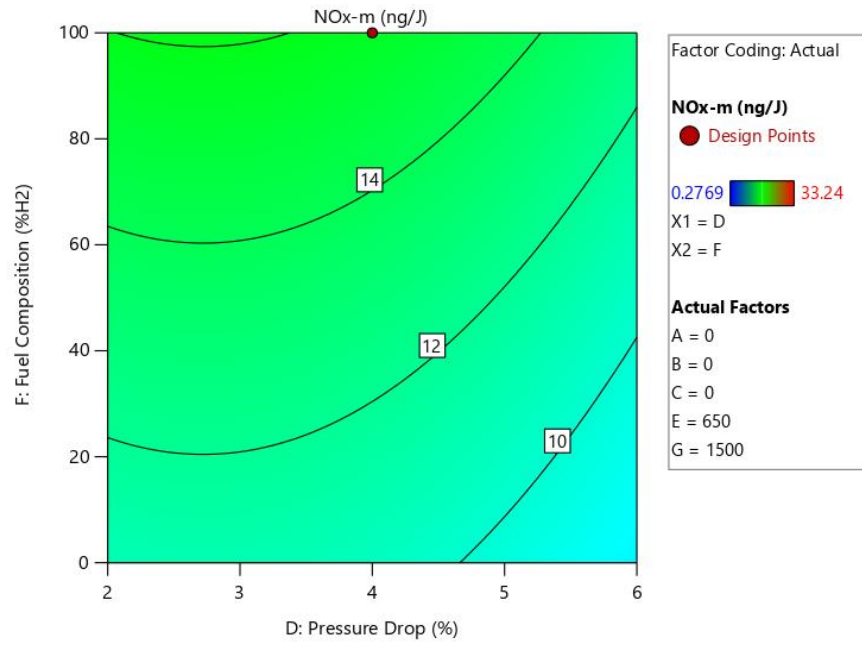


Figure 115. NOx Model, 1500K Flame Temperature

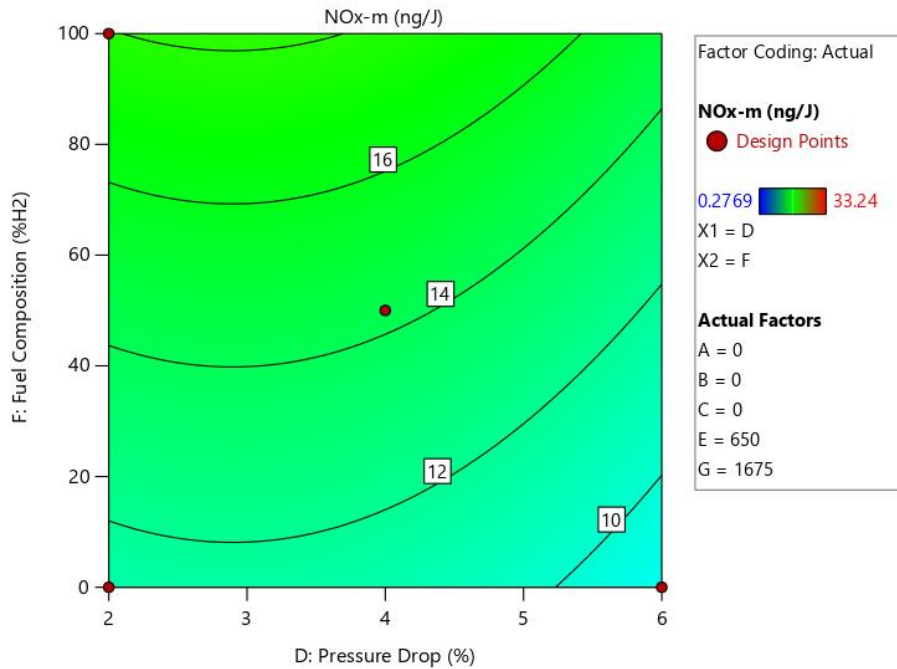


Figure 116. NOx Model, 1675K Flame Temperature

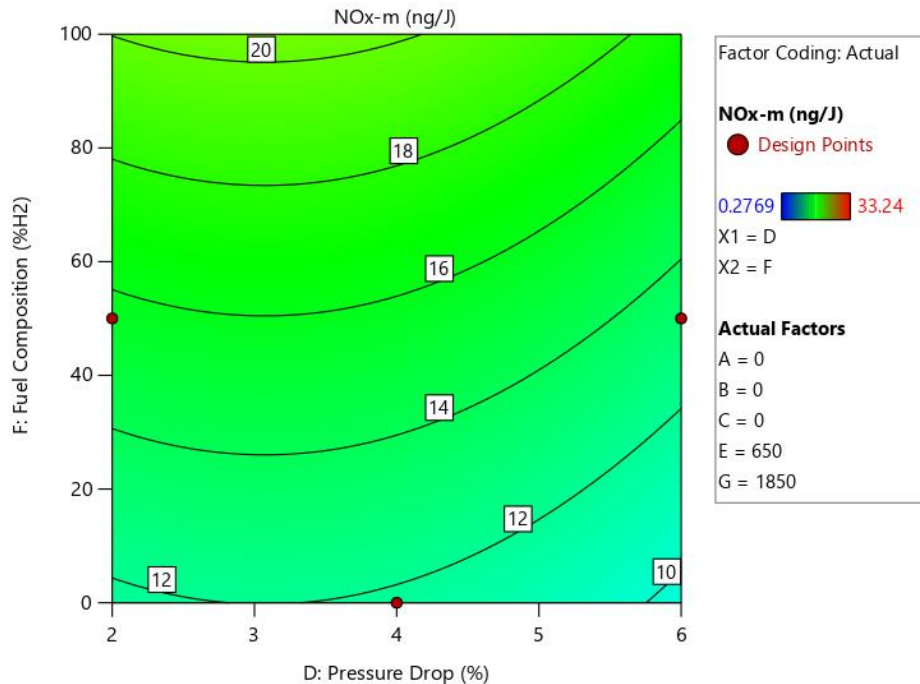


Figure 117. NOx Model, 1850K Flame Temperature

As flame temperature increases, NOx emissions increases. At the lowest temperature of 1100K, at 100% H₂, on 6% pressure drop, NOx emissions are reported to be ~8.3 ng/J. Then when comparing that to the highest temperature at 1850K on 100% CH₄, on 6% pressure drop, emissions is ~9.7 ng/J which is only slightly higher than hydrogen. Nevertheless, hydrogen produces less emissions than methane. Now assuming the worst-case scenario for hydrogen, at a pressure drop of 2% at 1100K, NOx emissions are ~11.9 g/J. Comparing that to the best-case scenario for methane at 1500K and 6% pressure drop, ~8.3 ng/J is also obtained. While hydrogen does have the ability to produce less emissions at lower temperatures, it is not by a far margin compared to methane. Additionally, any little tweaks such as a decrease in pressure drop as presented here, can change the result. It cannot be stated for certain that hydrogen produces lower emissions compared to methane just because flame temperatures are lower. Moreover, a decrease in ~1 ng/J is not enough to justify an entire hydrogen economy especially when it

comes with more challenges than the current existing natural gas ecosystem. More investigations should be made to study more factors and interactions.

5.1.6 Optimization

To determine the best combination of factors and conditions, Design Expert's optimization was utilized. For the optimization, all factors were set to minimize emissions for the responses (CO, NO, NO_x). As for the factors in question such as air split, air swirl, fuel swirl, pressure drop, preheat temperature, fuel composition and flame temperature were set to be within range. The specific ranges can be found Table 3. Based on the results of the previous models, the preheat and flame temperature, and fuel swirl angle were minimized whereas the pressure drop, air swirl and air split were maximized. The fuel angle was minimized to give rise to a higher relative velocity such that it can mix better with a higher air velocity. Preheat and flame temperature were also minimized to limit the production of NO and NO₂ due to thermal effects. Next, the air swirl was maximized as the higher angle helps decrease the air velocity to better match the fuel velocity. A higher degree for air swirl was paired with more air through the injector (air split) which decreases emissions. Then, higher pressure drops yield lower emissions due to more homogenous mixtures. Lastly, for the responses, it is known that the lower the emissions, the more desirable. As such, for each response, the maximum weight was given to lower emissions.

A total of 100 solutions were found. The first solution proposes, an air split ratio, fuel swirl angle, and an air swirl angle of 1, -1, and 1, respectively. A pressure drop of 5.97% should be maintained for maximum mixedness due to higher velocities that aid in mixing. The preheat and flame temperatures should be kept at the lowest at 522K and 1500 K, respectively. Lastly,

the fuel composition should be comprised of 98.995% H₂. The predicted emissions are shown in Table 7.

Table 7. Predicted Emissions for Optimization Study with Flame Temperature Range 1500-1850K

Ng/J		
CO	NO	NO _x
0.597	0.004	0.363

Previously it was discussed that hydrogen similar if not more emissions compared to methane when comparing to best vs. worse case scenarios. However, the optimization study seems to suggest higher contents of hydrogen produces the lowest emissions. This is because when Design Expert calculates the optimal configuration, it searches through an iterative process to increasingly get to the desired solution. Thus, once a point on the space is detected as the lowest or optimal point, the software will keep encroaching that solution. So, in the instances where emissions can drop down to as much as 0.1 ng/J for NO and 1 ng/J for NO_x, these solutions were seen desirable. These points also corresponded to high levels of hydrogen content. As a result, the optimization reveals that higher levels of hydrogen content can decrease emissions.

There are also factor interactions and injector geometry to consider. This phenomenon was also noted and discussed previously in section 5.1.3. Recall Figure 61-Figure 76 where some injectors (3, 4, 6, 7, 10, and 13) had some points where at 100% hydrogen, it had less NO_x emissions than the methane cases. Most of these were due to lower adiabatic flame temperature conditions (1100K-1300K), but it was found that the injector geometry was at play as well. Injectors (3, 4, 6, 7, 10, and 13) all had higher air splits (more air in the injector) and higher air swirl which are favorable traits in both the NO and NO_x model. More air through the injector

helps with the increased interaction with the fuel and higher air swirl lowers the air velocity for better mixing with the lower fuel velocity. Perhaps developing an injector with these parameters is the next step. The closest match to this configuration that has been tested is Injector 4, but the plate will need to be swapped from Plate 2 to 1.

When including the lower temperature matrix as part of the optimization, the optimization solution hovers the flame temperature over 1400 K vs. 1500K. Even though 1100K was included, in many instances due to injector and plate geometries at 1100K, incomplete combustion took place leading to higher emissions. As a result, a higher flame temperature of 1440K was proposed. A split ratio, air swirl, and fuel swirl angle of 1, -1, and 1 were designated to achieve the lowest emissions. The pressure drop of 5.692% and a preheat temperature of 573K should be maintained. Lastly, the fuel composition should be comprised of 100% H₂. The predicted emissions are shown in Table 8.

Table 8. Predicted Emissions for Optimization Study with Flame Temperature Range 1500-1850K

Ng/J		
CO	NO	NO _x
0.484	0.000	0.393

From the results of the optimization study, Injector 4 best matches the criteria in terms of injector geometry. The air swirl and fuel swirl are at the upper and lower portion of the test matrix, respectively. However, the plate should be swapped to Plate 1 which is designed to have a 60/40 split where 60% of the air flow enters the injector. Currently Injector 4 is paired with Plate 2 which does not have any air splits. Then when operating at low flame and preheat temperatures at 6% pressure drop, the results of the optimization test can be replicated.

From the previous studies, it was determined that flame temperatures play a big role in NO/NO_x emissions. Thus, the optimization model will be fixed at different flame temperatures: 1500K, 1675K, and 1850K for both methane and hydrogen and 1100K and 1300K for only hydrogen. This is to see if there are different optimal configurations for different flame temperatures or for different fuels. The results of the optimization study are shown in Table 9- Table 10.

Table 9. Optimization Model for Hydrogen for Various Flame Temperatures

Flame Temperature, K	Air Split	Fuel Swirl	Air Swirl	Pressure Drop, %	Preheat Temperature, K	CO, ng/J	NO, ng/J	NO _x , ng/J
1100	0.675	-0.766	0.564	4.075	679.124	7.942	0.026	2.223
1300	0.992	-0.897	0.565	4.512	531.779	1.632	0.077	1.463
1500	1.000	-0.999	1.000	6.000	573.078	0.398	0.046	0.550
1675	1.000	-1.000	1.000	6.000	544.928	0.466	0.415	1.538
1850	1.000	-1.000	1.000	6.000	544.310	1.077	1.035	3.283

Table 10. Optimization Model for Methane for Various Flame Temperature

Flame Temperature, K	Air Split	Fuel Swirl	Air Swirl	Pressure Drop, %	Preheat Temperature, K	CO, ng/J	NO, ng/J	NO _x , ng/J
1500	0.984	-0.432	0.645	6.000	500.000	106.976	0.006	0.716
1675	0.999	-0.647	1.000	6.000	614.504	12.203	0.016	0.595
1850	1.000	-1.000	1.000	6.000	553.726	5.729	0.000	0.519

From Table 9 and Table 10, the optimal injector geometry and injector configurations do not differ drastically for methane or hydrogen at different flame temperatures. The optimal air split, fuel swirl, air swirl, and pressure drop are conserved at 1, -1, 1, and 6%, respectively. Preheat temperature is also maintained at the lowest levels. These are the same conclusions drawn for the previous optimization models. A few exceptions are noted. At lower flame temperatures for hydrogen, these factors are modified to 0.7, -0.7, 0.5, and 4% for air split, fuel swirl, air swirl, and pressure drop, respectively. At 1500K, for methane, the fuel and air swirl should be adjusted to -0.4 and 0.6, respectively. A possible explanation for why lower pressure drops is preferred for lower temperature hydrogen cases is because lower velocities help stabilize the flames before the LBO limit is reached. For lower temperatures, for both hydrogen and methane, the preferred angle for the fuel swirl is increased and decreased for the air swirl. This means the fuel velocity is decreased and the air velocity is increased. A lower fuel velocity is better at lower temperatures to keep the flame anchored near LBO limits and a higher fuel velocity is better at lower temperatures to aid in mixing as the fuel velocity is decreased. Overall, Injector 4 is still best suited for the lowest emissions. However, Injector 4's current plate paring should be changed from 2 to 1 to modify its air split from 0 to 1. It still should be noted that hydrogen still produces more emissions compared to methane for the same flame temperature.

Comparing these results to current existing systems, the injector in question has the ability to achieve emissions as low as 1.5 ng/J for NO and 8.3 ng/J for NO_x while operating on hydrogen. When operating on methane, emissions as low as 2.3 ng/J for NO and 8.3 ng/J for NO_x can be achieved. Furthermore, from optimization, even lower, near zero emissions can be obtained as a result of combining all favorable factors. These emissions can compete with the results in the Parker Hannifin, Honeywell, General Electric, and Mitsubishi study (recall Table

2). Collins Aerospace's injectors are capable of operating on either 100% methane and 100% hydrogen all while still obtaining less than 10 ng/J (~5 ppmvd 15% O₂) of NO and NO_x emissions. When comparing atmospheric tests, Parker Hannifin's design was able to achieve under 5 ppmvd 15% O₂, however their experiment ran on syngas fuels. Honeywell's injector was able to achieve 1.3 ppmvd @15% O₂ of NO_x emissions with equivalence ratio of 0.4, but this was also with 90% H₂/10% CO. Likewise, General Electric reported lower than 5ppmvd @15% O₂ of NO_x emissions up to pressures of 17 atm, but this was with only 65% hydrogen content. Mitsubishi tested up to 40-84% H₂, NO_x emissions were lower than 10 ppmvd 15% O₂ of NO_x emissions for all fuels at atmospheric conditions.

5.2 CHEMKIN

In this section, chemical kinetics will be discussed to understand the key differences between hydrogen and methane. Before diving into the reaction pathways, the model and approach used for the study is explained. Depending on the certain conditions, the model was adjusted to obtain a better fit of the experimental data. Various steps were taken to try to validate the model including a fully premixed vs. a non premixed study and a heat loss study. Lastly, the comparison between specific cases were selected to study the effects of hydrogen vs. methane and low vs. high temperatures.

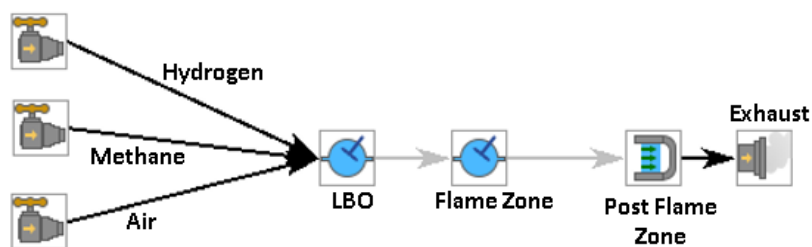


Figure 118. CHEMKIN Model

The CHEMKIN model used in this study is shown in Figure 118. It is comprised of three inlets to mimic air and fuel entering the injector separately. The model is then followed by two perfectly stirred reactors (PSR 1 and PSR 2) and a plug flow reactor (PFR). This model takes inspiration from the Bragg cell and many similar studies whom have successfully modeled emissions [71], [70], [72], [73], [74]. It should be noted the experimental setup is non premixed. However, the model being applied is a perfectly premixed reactor. To resolve this issue, uncertainty analysis and parametric studies were conducted.

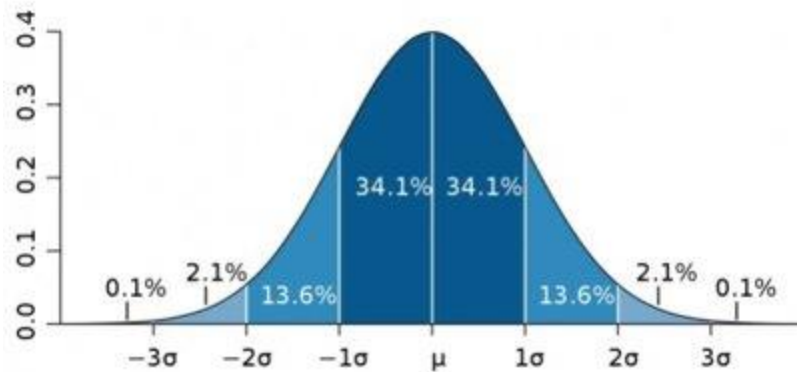


Figure 119. Normal Distribution Curve

When fuel and air are not perfectly premix, there exists “patches” of different equivalence ratios per cross sectional area even if it mixes rapidly. Fortunately, due to micromixing technology, air and fuel can rapidly mix before entering the combustion chamber, but it is still not perfect. Thus, since this unmixedness is unknown, assuming a normal distribution and tweaking the standard deviation, the unmixedness can be determined by comparing it to experimental data. For example, if the test matrix calls for an equivalence ratio of 0.5, for a given cross sectional area, 34% of the cells will have an equivalence ratio of 0.4 vs. 0.5. After taking the emissions data for each equivalence ratio, the average emissions can be calculated, and the true emissions data is tabulated.

The following assumptions were made for the model:

- At 4% and 6% pressure drop:
 - At 1850K, it was fully premixed
 - For 100% H₂ cases for the upper matrix (STD 1-27), 0.15 mixedness was used and PSR 2 was adjusted to be 1/9 of the total volume
 - For the lower matrix (STD28-43), 0.15 mixedness was used and PSR 2 was adjusted to be 1/3 of the total volume
 - For all other cases, a 0.001 mixedness was used and PSR 2 was 1/3 of the total volume
- At 2% pressure drop:
 - For the lower matrix (STD28-43), 0.20 mixedness was used and PSR 2 was adjusted to be 1/3 of the total volume
 - For all other cases, a 0.05 mixedness was used and PSR 2 was 1/3 of the total volume
- In all cases, a standard 114 cal/s heat loss was incorporated into PSR 2 and 13.04 cal/cms heat loss was incorporated into the PFR

As mentioned previously, the higher the pressure drop, the more mixed a case is leading to lower emissions. Thus, at 2% pressure drops, the model was modified to have a higher standard deviation compared to 4% and 6%. Moreover, it is known that the reaction volume of Hydrogen is smaller than that of methane, Hydrogen's cases were adjusted to be 1/3 of the methane volume or 1/9 of the total volume [28]. As the equivalence ratio is decreased, Hydrogen's reaction volume is roughly equal to methane's volume [28]. As a result, at the lower matrix where

equivalence ratios and flame temperatures are low, the reaction volume was 1/3 of the total volume regardless of fuel mixture.

Other checks were made using photos accompanied during testing to verify and validate the model.

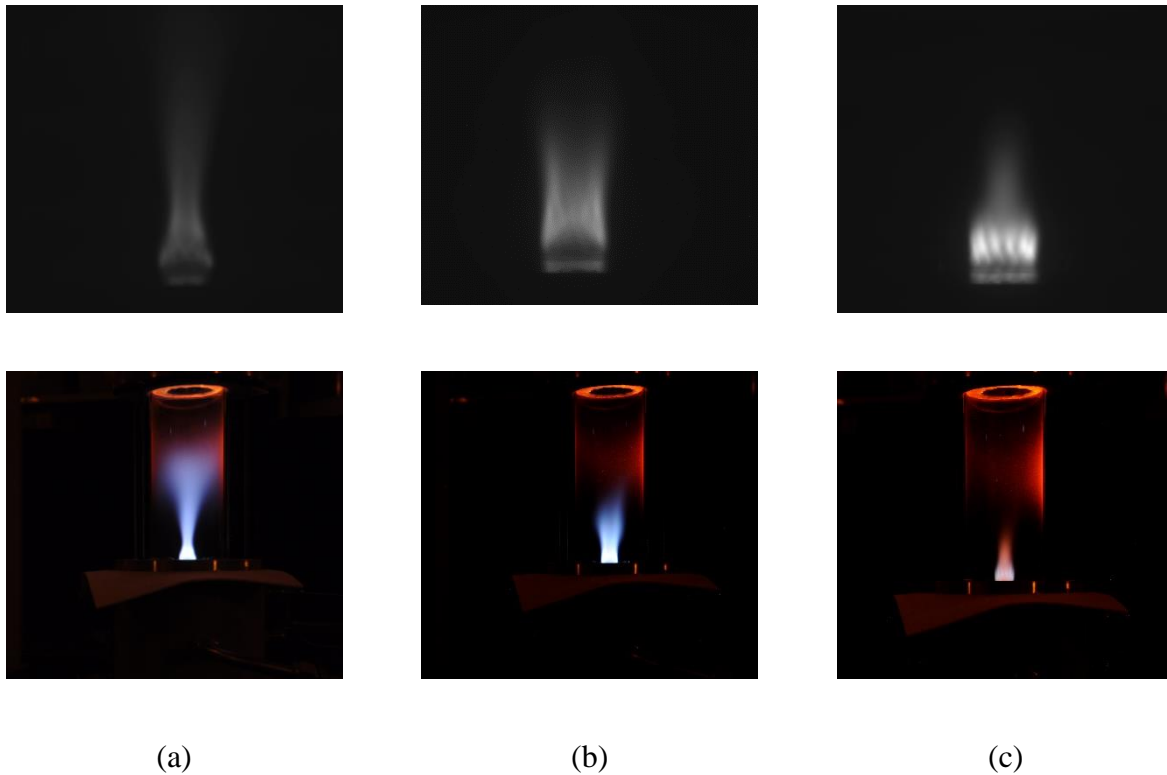


Figure 120. (a) STD 13 0% H₂, (b) STD 25 50% H₂, (c) STD16 100% H₂. Black and white images were captured with a Dynacolor camera and colored images with a Nikon camera.

CHEMKIN reactors' input are measured by volume which can be compared to the volume obtained from the photos (see Figure 120). In the photos, the height of the quartz tube height can be used as a reference as it is fixed to determine the actual height from proportions. With height known, the volume can be determined since the exit area of the injector plate is known. The

radius is approximated to be 20mm compared to the injector exit plate diameter of 22.86mm.

The procedure is explained through Equations in 25-27.

$$V = \pi r^2 h \quad \text{Eqn. (25)}$$

$$V_{CHEMKIN,guess} = \pi r^2 h_{CHEMKIN,guess} \quad \text{Eqn. (26)}$$

$$h_{CHEMKIN,guess} \sim h_{measured} \quad \text{Eqn. (27)}$$

Table 11. CHEMKIN Volume vs. Measured Volume

Region	CHEMKIN Volume m ³	Measured Volume m ³
PSR 1	0.000335	0.00037
PSR 2	0.0001	0.000125

From Table 11, the predicted CHEMKIN volume is very similar to the measured volume. Therefore, the validity of the model is further corroborated. Next, the predicted CHEMKIN emissions can be compared directly to the experimental data. This study was only conducted on Injector 3 and results are tabulated in Table A- 31-Table A- 36. Injector 3 was selected to study as it is in the middle of the design matrix.

The CO model has the highest average deviation of 76% for the 15% O2 ppmvd model and 64% for ng/J model. The high deviations could be the result of the combination of nuanced factors. CO is essentially a measure of incomplete combustion and many factor including the plate or injector geometry. Extra remaining fuel from the previous case during result in higher CO emissions for example. Obtaining exact values for CO is not practical. Rather a range of CO emissions is better for analyzing and comparing results. Nevertheless, CO is not as crucial as the NO and NOx models.

For the NO model, the average deviation is 26% and 55% for the 15% O₂ ppmvd and ng/J models, respectively. The reason for the higher deviations for the mass model is due to compounding uncertainties and deviations from the 15% O₂ ppmvd models. To obtain the mass models, Equations 18-22 are utilized. A deviation of 26%, while is not the best, it can still be utilized to analyze trends. A deviation of 5% is already accepted for the experimental values due to uncertainties in the PG 350 analyzer, Brooks mass flow controller sonic orifice, and pressure transducer (affects effective area and thus flow rates). Moreover, the GRI Mech 3.0 mechanism itself comes with uncertainties.

For the NO_x model, the average deviation is 11% and 25% for the 15% O₂ ppmvd and ng/J models, respectively. As stated previously, a 5% deviation for the experimental values have been accepted due to uncertainties of the PG 350 analyzer and flow metering instruments. Larger deviations also corresponded to experimental cases of high CO emissions. Lastly, the mass model has higher deviations due to the compounding uncertainty effect.

A future action to take to increase the fidelity of the model and to better compare differences between the analytical and experimental results is to observe the average differences between the two. Comparing average differences allows one to see how far off the model are from the true experimental values. Percent deviations can only assess the relative error within the model. Additionally, percent differences can reveal if there is a constant deviation from the actual values for certain cases. If found, this constant can be used to fit the model, similar to how ANOVA models are created.

5.2.1 Fully Premixed vs. Non Premixed

In this study some unmixedness was incorporated into the model. However, if the system was perfectly premixed, the emissions would decrease dramatically. The results for fully

premixed are shown in Figure 121 and Figure 122. Figure A- 3 and Figure A- 4 in the appendix show the experimental results for emissions vs. flame temperature. Simply comparing the y axis, in perfectly premixed conditions, up to a factor of two, emissions can be reduced. Comparing current experimental data, most emissions range from 5-15 ng/J vs. in fully premixed, emissions range from 3-10 ng/J.

From viewing in Figure 121 and Figure 122, an exponential trend in NO and NOx can be observed for temperatures $\sim 1900\text{K}$ as expected. At 1500K , the NO and NOx models begin to curve before rapidly increasing up to $\sim 38\text{-}39$ 15% O₂ ppmvd and ng/J. This point is at an adiabatic flame temperature of 2045K which is at the point where NO and NOx rapidly increases. This trend is supported in literature which indicates the CHEMKIN has some level of fidelity of the assumptions made to obtain the model [71].

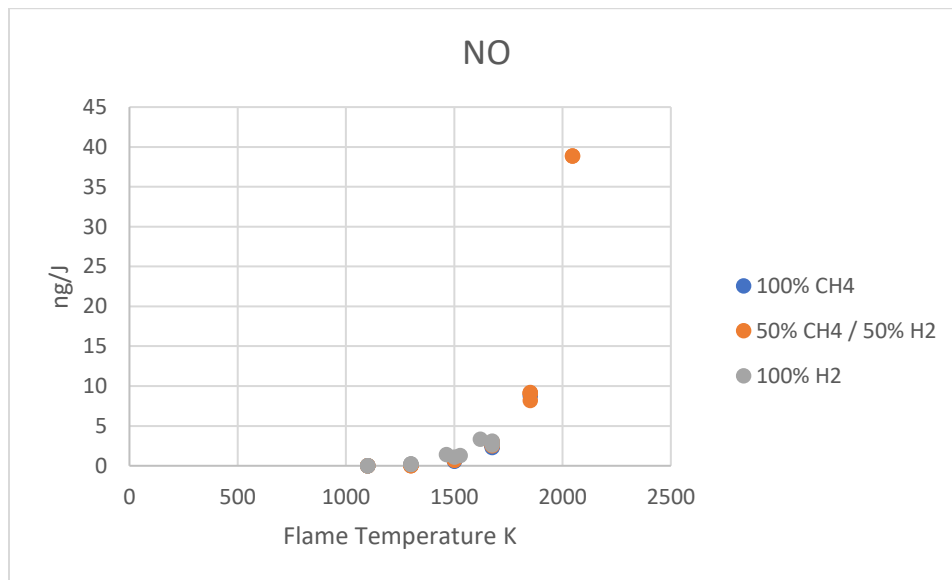


Figure 121. NO ng/J vs. Flame Temperature (CHEMKIN Fully Mixed)

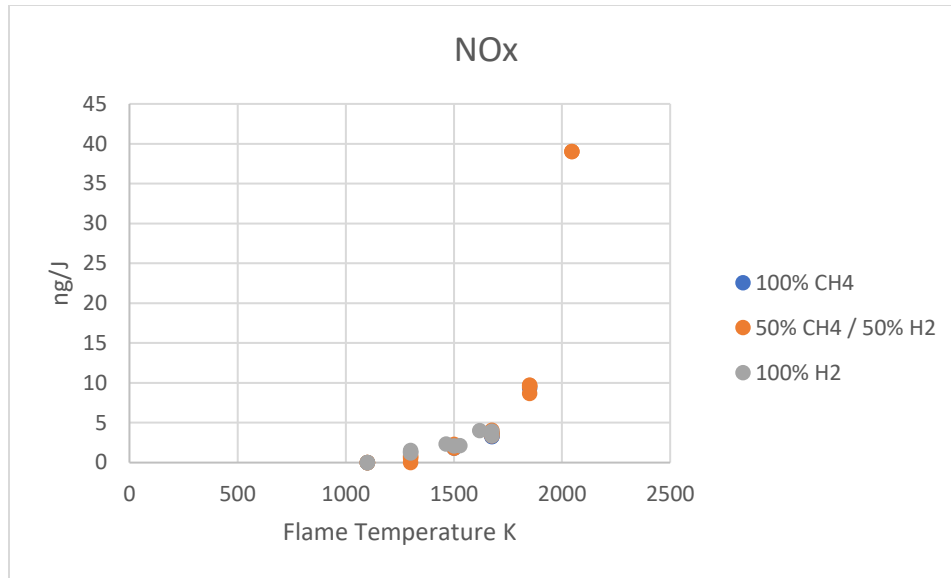


Figure 122. NO ng/J vs. Flame Temperature (CHEMKIN Fully Mixed)

5.2.2 Heat Loss Study

Since heat losses were estimated, a heat loss study was conducted to see how different assumptions of heat loss impacts on the model. The study was conducted on STD 13 on Injector 3 where CO, NO, and NOx were 39.23 ng/J, 1.20 ng/J, and 6.52 ng/J, respectively. As heat losses are increased, NO and NOx emissions decreased. It is estimated that the heat loss should be no more than 6 kW since the current heater input is maximum at 6kW. There are also known losses across the airbox which were accounted for in the model via air temperatures. These temperatures were obtained using thermocouples placed in the airbox. Besides this, there are additional heat losses through the quartz tube during combustion. In the current study, a heat loss of 1.43kW was best suited to match experimental results which is roughly 20% of the heater's input. Results of the heat loss study are shown in Table 12. From Table 12, 2kW seems like a better fit than 1.43kW, but it should be reminded that these numbers were converted from 15% O₂ ppmvd as the default in CHEMKIN. The results differ a little for the 15% O₂ ppmvd. Regardless, 1.43 kW better matched the broader range of experimental data than 2kW.

Table 12. Varying Heat Loss Assumptions with Accompanying Emissions Data

Case	Heater	PSR 2 Heat Loss (cal/s)	PFR 2 Heat Loss (cal/cms)	CO (ng/J)	NO (ng/J)	NOx (ng/J)
1	0.5 kW	30	3.41	72.56	6.44	7.96
2	1.43 kW	114	13.04	73.01	4.95	6.62
3	2 kW	119	13.66	73.38	4.86	6.55
4	4 kW	239	27.31	96.02	3.30	5.05
5	6 kW	358	40.97	161.74	2.14	3.88

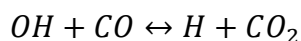
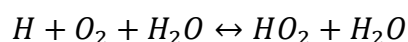
5.2.3 Chemical Kinetics Analysis

Chemical kinetic will be used to explain the key differences between hydrogen and methane in terms of emissions production. From previous analysis, it was observed that at the same estimated adiabatic flame temperature, hydrogen produces more emissions than methane. To investigate the factors that directly affect hydrogen vs. methane, STD 13 and 16 for Injector 3 is compared. Studying the same Injector configuration eliminates differences between fuel, and air swirl or air splits. STD 13 and STD 16 have the same pressure drop at 4% and a flame temperature of 1675K. The only difference is that STD 13 is pure methane and STD 16 is pure hydrogen.

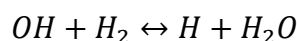
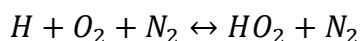
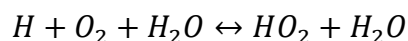
First, in PSR 1 or LBO region, practically no emissions are formed because the region is non reacting. The region is a purely mixing zone for the air and fuel as the reactor's temperature is equivalent to the temperature of the air and fuel when mixed together. Thus, moving forward only PSR 2, or the flame zone, and PFR, or the post flame zone will be discussed. It is then observed that most of the NO and NOx emissions is formed in PSR 2. Approximately 88-95% of

emissions are formed here in this region. More detailed focus and explanations will be conducted on PSR 2 rather than the PFR as a result.

When looking at temperature sensitivities only two reactions were found to have a thermal effect which makes sense considering this case study was conducted at a flame temperature of 1675K. The two thermal sensitive equations for STD 13 are shown below. This is true for both PSR 2 and the PFR regions.



Meanwhile, for STD 16, there is an additional thermally sensitive chemical reaction. The three thermal sensitive equations are shown below. All three equations exist in PSR 2 but only the first equation ($H + O_2 + H_2O = HO_2 + H_2O$) is true for the PFR region.



These chemical reactions work to increase the combustion temperature of the system. If more of these reactions take place, the temperature of the combustion chamber increases which leads to an increase in emissions. With more thermally sensitive equations, Hydrogen has the potential chance for more pathways to increase the combustion temperature over methane.

Now, when comparing the normalized sensitivities between the two cases, it becomes apparent that the N2O mechanism is dominant in methane cases and NNH is dominant in hydrogen cases.

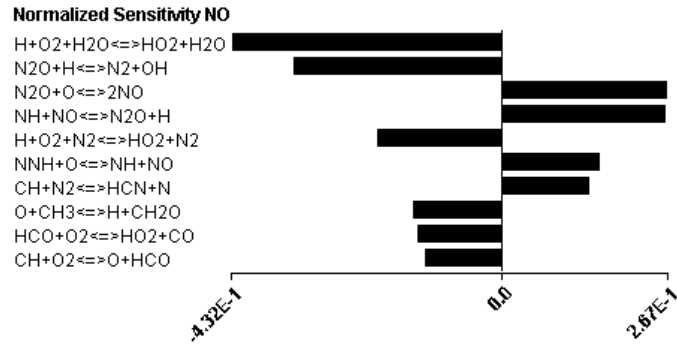


Figure 123. NO Normalized Sensitivity for STD 13 (100% CH4) for PSR 2

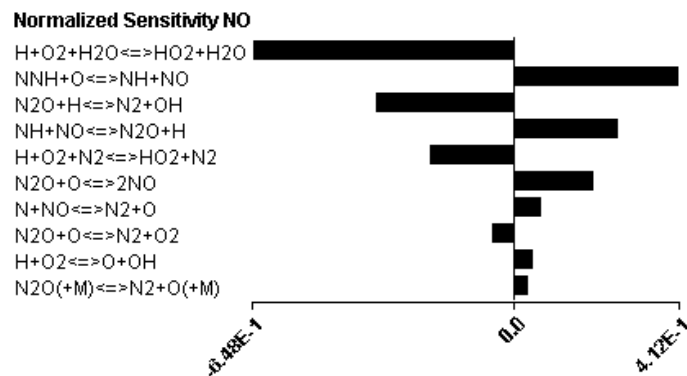
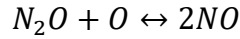
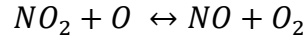
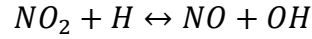


Figure 124. NO Normalized Sensitivity for STD 16 (100% H2) for PSR 2

In STD 13, the top two mechanisms are traced to the N2O mechanism (see Figure 123) followed by the NNH mechanism and prompt NO. In contrast, for STD 16, the top mechanism is the NNH mechanism followed by N2O and thermal NO (see Figure 124). While the normalized sensitivities only reveal that increasing a certain reaction leads to more NO formation, conclusions can still be drawn. For instance, the top producing NO mechanisms mainly involve O radicals. In some cases, H radicals also form NO emissions, but some H radicals also destroy NO at a higher rate. Thus, at a high level, if there were more O radicals present, then more NO will form.

Next, the absolute rate of production of NO is analyzed. The top three mechanisms producing NO in PSR 2 and PFR are listed below and holds true for both methane and hydrogen. It seems that NO and NO₂ cycle one another to form emissions. To understand, how NO and

NO₂ are first formed, chemical pathways traced back to the fuel composition. This study is conducted later.



Next, the normalized sensitivity analysis is conducted on NO₂ in Figure 125 and Figure 126 show that NO₂ as a byproduct to NO. To form, NO₂, NO needs to be formed first. This makes intuitive sense as NO_x is typically 1.2 to 2 times higher than NO. It is also observed that for STD 68, or pure hydrogen, the NNH pathway dominates again.

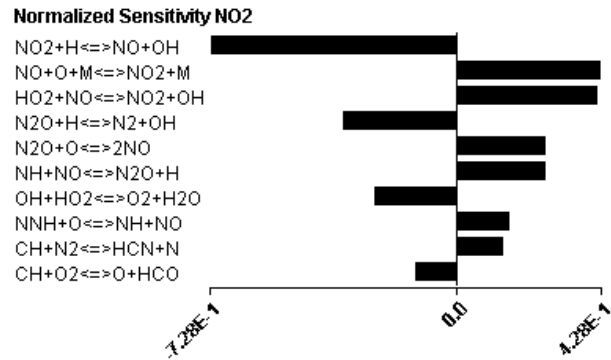


Figure 125. NO₂ Normalized Sensitivity for STD 13 (100% CH₄) in PSR 2

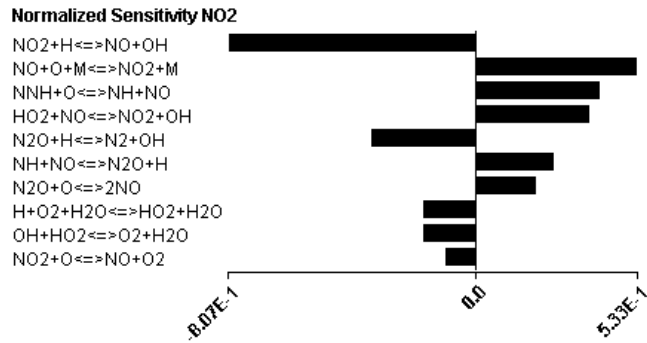
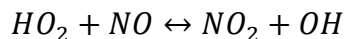
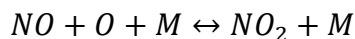
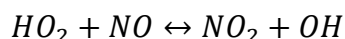
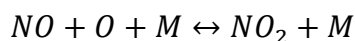


Figure 126. NO₂ Normalized Sensitivity for STD 16 (100% H₂) in PSR 2

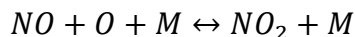
The top two mechanisms producing NO₂ in PSR 2 are listed below. These are the most important mechanisms for both methane and hydrogen fuel.



As explained, for the PFR methane and Hydrogen differ a little. For methane, the top sensitive mechanisms are listed below:



For hydrogen,



When tracing these mechanisms back to the originally fuel component (CH₄ or H₂), it is observed that the fuel is first attached by H, OH or O radicals to break down into smaller species such as CH₃ and CH₂ for methane. More details will be explained in the following sections.

Now, the normalized sensitivities of NO and NO₂ for the PFR region are discussed. For STD 13, or pure methane, the top two mechanisms in the PSR and PFR are the same. However, in the PFR region, there is less of “attacks” for the destruction of the NO. A probable explanation for this is that in the post flame zone, there is not as many reaction kinetics taking place in comparison to the PSR 2 zone. Moreover, since the PFR represents the post flame, it is considerably cooler compared to the reaction zone. Auxiliary emissions are formed through other pathways such as N₂O for hydrogen rather than the primary NNH mechanisms in the PFR. Still

88-95% of emissions are formed in the flame zone (PSR 2), so the PFR is not as significant contributor to emissions.

The normalized sensitivities for NO_2 emissions in the PFR are very similar to PSR 2. In both cases, $\text{NO} + \text{O} + \text{M} \leftrightarrow \text{NO}_2 + \text{M}$ are the dominant sensitive reactions for both hydrogen and methane. In the PSR 2, the second ranked dominant sensitive reaction is their respective primary mechanisms. In other words, for methane in the PSR when it comes NO_2 sensitivities, the N_2O mechanism is dominant whereas for hydrogen, the NNH is dominant. On the contrary, in the PFR region, for both hydrogen and methane, the second ranked sensitive reaction is $\text{H} + \text{O}_2 + \text{H}_2\text{O} \leftrightarrow \text{HO}_2 + \text{H}_2\text{O}$. Results for NO and NO_2 sensitivities are shown in the Appendix in Figure A- 21-Figure A- 24. Overall, this shows that NO plays a role in emissions more than NO_2 and that PSR 2 is more significant than the PFR for producing emissions.

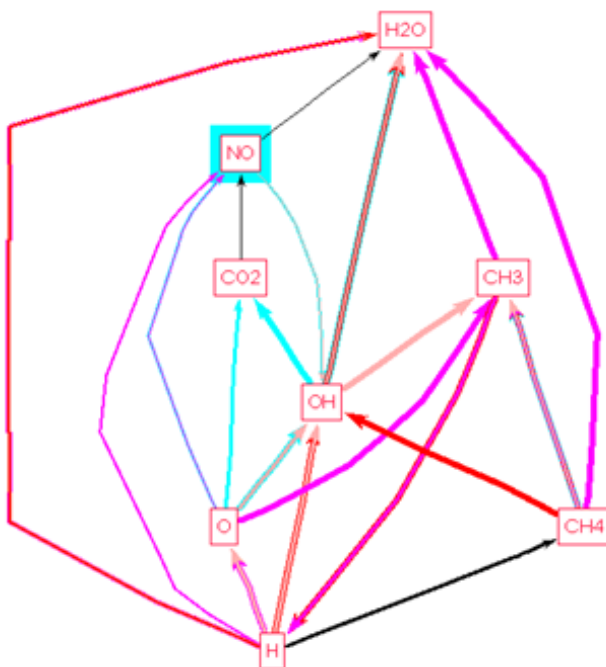


Figure 127. Main CH_4 Pathways to NO in PSR 2, STD 13. The colors represent different side species that are involved in a reaction line that connect two species in the diagram.

For these reaction pathways analysis, the thicker the lines, the more relative importance the pathway is compared to those shown on the diagram. The colors represent the different side species that are involved in a reaction line that connects two species in the diagram. From Figure 127, methane is first attacked is attacked by OH and O radicals to break down to CH₃ and water. CH₃ then proceeds to H radicals to further break down. The most compelling evidence as to why hydrogen produces more emissions than methane is revealed when comparing Figure 127 and Figure 128. On the way to NO formation, a significant amount of OH radicals go on to form CO₂ (and also water) which lower the available OH radicals to form NO in methane's case.

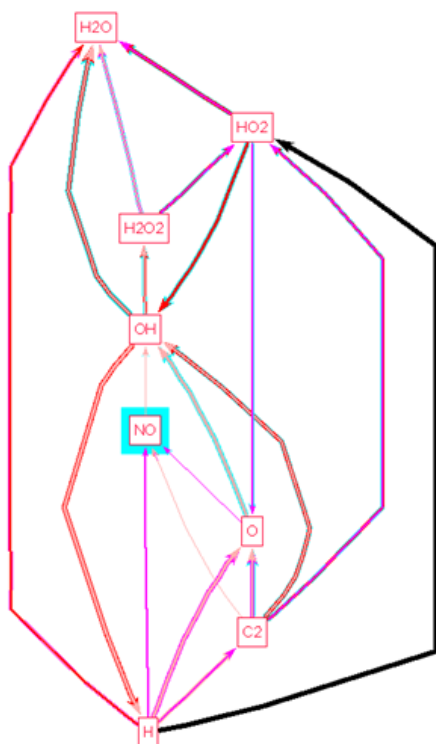


Figure 128. Main H₂ Pathways to NO in PSR 2, STD 16. The colors represent different side species that are involved in a reaction line that connect two species in the diagram.

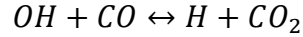
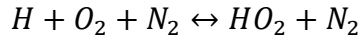
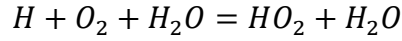
From Figure 128, hydrogen breaks down to H radicals which then has a direct path to NO. Just like methane, a significant amount of radicals go on to form water. However, since this exists in both cases, it can be excluded during our investigation as to why hydrogen produces more emissions than methane. Ignoring water formation, the next largest pathway would be to

the O radical. The O radical then has a direct path to NO, or it can form OH to then break down to H radicals again. As mentioned previously, H radicals have a direct path to NO when operating on hydrogen fuel as opposed to methane.

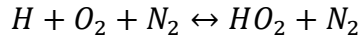
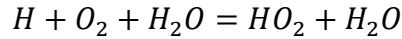
Ignoring the water route on the methane case, the next largest pathway from CH₄ fuel would be the OH radicals. From there, OH radicals go on to form CO₂ and only a small amount goes to form NO. Besides the main difference of OH radicals going to CO₂ in methane, smaller pathways to NO exist in both hydrogen and methane. For methane, it is the both the O and H radical and for hydrogen it is the H and O radical so equally 2 pathways. Thus, the reason for higher emissions for hydrogen is due to the direct route to NO and that there is no CO₂ to reduce the magnitude to NO emissions.

The previous case was studied at a flame temperature of 1675K and thus the thermal mechanism was not present. Studying another case at 1850K will reveal other mechanisms present at higher temperature. As such, STD 7 and 8 were selected. STD 7 and 8 share the same pressure drop and injector. The only difference now is the flame temperature and fuel composition. STD 7 is on pure methane and STD 8 is on pure hydrogen. It should be noted that STD 8 does not exist during experimental data so there is no data point to compare against to determine the accuracy of the model. That is because the current Brooks mass flow controller is limited to 40 SLPM which is not enough to reach a flame temperature of 1850K. The closest point on the matrix at a fixed pressure drop of 4% is at a flame temperature of 1619.68K produces ~20 ng/J. The NO_x model from Design Expert can also be used to estimate this case. As such, 20.03 ng/J was predicted and not far off from the original estimate.

The thermal sensitivities for STD 7 are the obtained below for the PSR. For the PFR, only the first equation remains.



The thermal sensitivities for STD 8 are obtained below. For the PSR, only the first two equations apply. For the PFR, only the first equation and third equation are applied.



In comparison to the previous case of 1675K, there are more thermal sensitive mechanisms for methane when the temperature is increased. The opposite is true for hydrogen. Hydrogen had more thermal sensitive equations at lower temperatures. While the thermal sensitivities cannot report how temperatures affect emissions. It does allow conclusions to be drawn that if more of a certain reaction takes place, it increases the overall combustion temperature increases. Equally at higher temperatures, methane and hydrogen have the same number of thermally sensitive mechanisms. Thus, it cannot be used to explain as a factor as to why hydrogen produces more emissions.

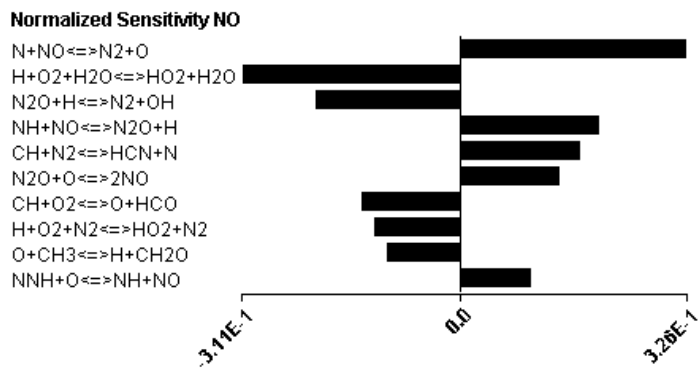


Figure 129. NO Normalized Sensitivity for STD 7 (100% CH4) for PSR 2

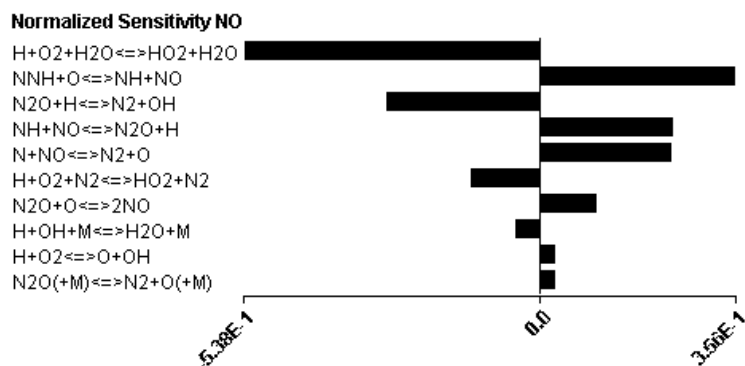


Figure 130. NO Sensitivity for STD 8 (100% H2) in PSR 2

Again, for STD 8 (Figure 130), the NNH pathway is dominant followed by the thermal and N_2O mechanism when it comes to NO formation. The thermal and N_2O mechanisms are about equal in magnitude and are the second and third prospective mechanisms. For methane (see Figure 129), the significance of the thermal NOx and prompt mechanisms start to emerge. The two mechanisms completely overtake the N_2O mechanism previously seen at lower temperature of 1675K. As these fuel approach the critical thermal NOx temperature of 1900K, these mechanisms are expected to be the large factor to emissions. The normalized sensitivities only can show which mechanism, when increased, leads to higher formation rates of NO. It cannot explain how to increase certain mechanisms. Still, conclusions can be inferred.

The top absolute production of NO comes from the mechanism presented below. This is true for both hydrogen and methane.



Next, the normalized sensitivities of NO₂ are discussed. Comparing differences between methane and hydrogen (see Figure 131 and Figure 132), the first ranked normalized sensitivity mechanism, $NO + O + M \leftrightarrow NO_2 + M$ is present in both cases. However, looking at the second ranked sensitivity, the key difference is that hydrogen is forming emissions through the NNH pathway compared to methane which forms it through the thermal NO_x route. Notice the difference when compared to STD 13 where methane's top ranked normalized sensitivity for NO₂ was through the N₂O mechanism.

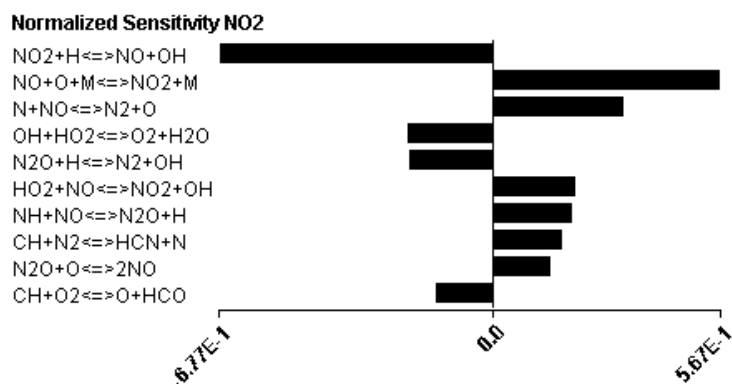


Figure 131. NO₂ Sensitivities for STD 7 (100% CH₄) in PSR 2

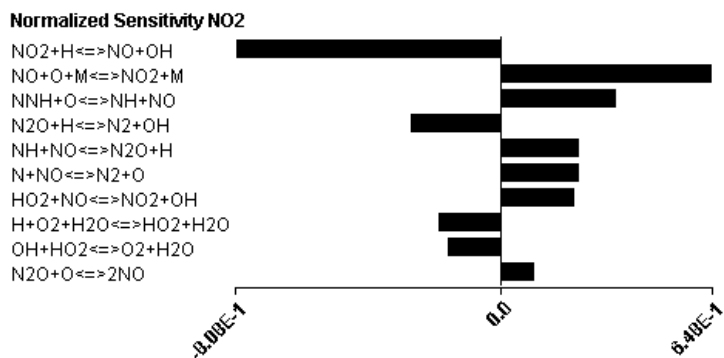
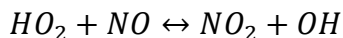
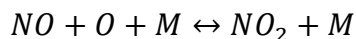


Figure 132. NO₂ Sensitivities for STD 8 (100% H₂) in PSR 2

The top absolute rates of production of NO₂ for hydrogen and methane is



The same conclusions can be drawn for the PFR (see Figure A- 25-Figure A- 28 in the Appendix). First for both methane and hydrogen, the first ranked normalized sensitivity is $NO + O + M \leftrightarrow NO_2 + M$ but when looking at the second ranked, they are both the same as opposed to previous results in the PSR where the second ranked mechanism was the thermal NO_x pathway for methane vs. the NNH pathway for hydrogen. Instead, they share the same second ranked normalized sensitivity reaction which is $H + O_2 + H_2O \leftrightarrow HO_2 + H_2O$.

For the normalized sensitivity for NO in the PSR vs. the PFR, they are practically the same for methane. However, for hydrogen there is a shift from the primary NNH in the PSR to the N₂O mechanism in the PFR. This can be explained due to the fact in the PFR, temperatures are much lower, and it is no longer part of the flame zone where the majority of the chemical kinetics take place. Thus, NO is formed via auxiliary pathways in the PFR rather than the primary pathway, NNH, during combustion.

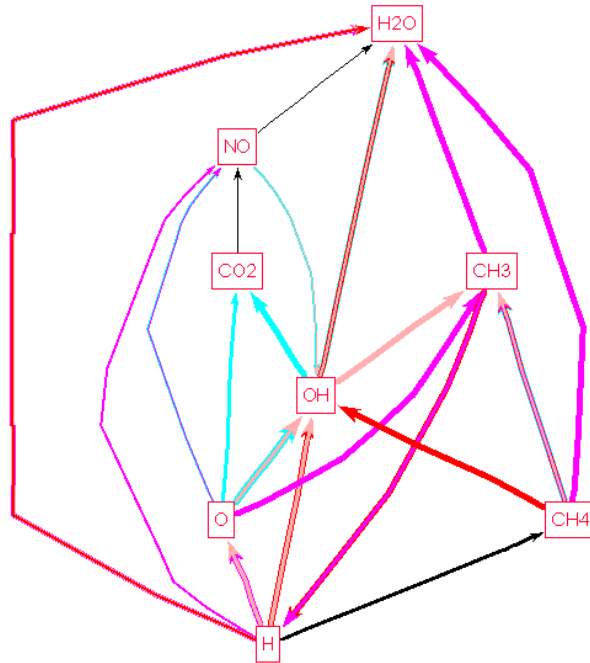


Figure 133. Main CH₄ Pathways to NO in PSR 2, STD 7. The colors represent different side species that are involved in a reaction line that connect two species in the diagram.

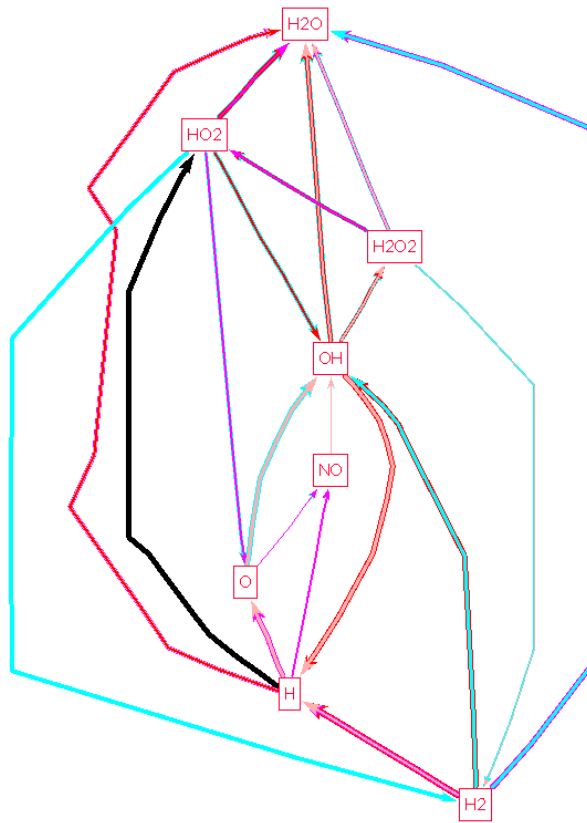


Figure 134. Main H₂ Pathways to NO in PSR 2, STD 7. The colors represent different side species that are involved in a reaction line that connect two species in the diagram.

Just like the case for 1675 K flame temperature, the OH radicals in methane go toward forming CO₂ rather than NO. Unlike methane, hydrogen also has a direct path to NO from O and H radicals. In both cases, a significant amount of radicals go towards forming water. Thus, to study the key difference between hydrogen and methane, one must look at the smaller and other potential pathways. From Figure 133 and Figure 134, NO is formed via O and H radicals for both methane and hydrogen. Thus, the only main difference is again attributed to the formation of CO₂ reducing methane's pathway to NO formation. The OH radicals in Figure 134 cycle with the H radicals which have a direct path to NO formation. Since NO_x is typically ~1.2 to 2 times higher than NO emissions, it can be concluded majority of emissions are formed from NO. Moreover, when analyzing NO₂ pathways, majority of NO₂ formation comes from requiring the NO species. Thus, pathways to NO₂ were not analyzed as a potential factor to why hydrogen produces more emissions than methane.

6. Summary, Conclusions, and Recommendations

6.1 Summary

The following research questions were presented to assess the current set of injectors and remaining research questions that will shed light on the ongoing debate on hydrogen fuel. To organize the conclusions, the answers and conclusions to each presented question will be presented in the following order:

1. Assess emissions for all 16 injectors and create a predictive model for the factors in question.
 - a. What factors and factor interactions are significant to the injector performance?

All seven factors (air splits, air swirl, fuel swirl, pressure drop, preheat temperature, fuel composition, and the flame temperature) had some significance in the emissions model. The most significant factor interactions were with the air split with air swirl (AC), air split with flame temperature (AG), and air swirl with flame temperature (CG).

- i. Which combination of factors minimizes pollutant emissions?

Increasing the air swirl angle, pressure drop, and air split (more air through the injector) decreases NO and NO_x emissions. Meanwhile, decreasing the fuel swirl angle, preheat temperature, estimated adiabatic flame temperature, and hydrogen content decreases NO and NO_x emissions. The following bullet points give a brief an explanation as to why increasing or decreasing such factors can decrease emissions.

- Increasing the air swirl lowers the air velocity to better match the fuel's velocity for mixing.

- Increasing pressure drop increases the velocity which can promote mixing. As the system approaches a fully premixed system, peak temperatures are lower, and emissions can be lowered by a factor of two.
- Increasing the air split, or the amount of air that enters the injector, increases the interaction between the fuel and air which helps with mixing. A more homogenous flow field will yield lower NO and NO_x emissions.
- The fuel swirl showed that lower swirl angles was preferred to increase the fuel axial velocity for mixing.
- Decreasing the preheat temperatures and flame temperature decreases emissions by hindering thermally sensitive mechanisms that break the nitrogen bonds
- Lastly, an increase in hydrogen content, leads to more NO and NO_x emissions because of the NNH pathway and that there is no CO₂ to redirect the OH radicals from forming NO.

ii. From 1ai, does the desired combination of factors change with the different fuels?

No, a higher air split (more air through the injector), air swirl angle, pressure drop and lower fuel swirl angle, preheat temperature and flame temperature is preferred for both hydrogen and methane fuel mixtures.

b. What modifications to the current injector design can be suggested to further improve performance?

Out of the 16 injectors, Injector 4 best matches the criteria for low emissions because it has the highest air split (more air through the injector) and air swirl angle, but the lowest fuel

swirl angle. Injector 4 currently is paired with Plate 2 which has an air split of 0. To further decrease emissions, Injector 4 should be paired with Plate 1 instead which has an air split of 1 (highest air split).

2. How does Collins Aerospace's LDI design perform compared to current micromixing designs?

The current injector design can rival those of Parker Hannifin, Honeywell, General Electric and Mitsubishi's design by producing less than ~10 ng/J (~5 ppmvd 15% O₂) in emissions and can operate both with pure methane and hydrogen. When comparing atmospheric tests, Parker Hannifin's design was able achieve under 5 ppmvd 15% O₂, however their experiment ran on syngas fuels. Honeywell's injector was able to achieve 1.3 ppmvd @15% O₂ of NO_x emissions with equivalence ratio of 0.4, but this was also with 90% H₂/10% CO. Likewise, General Electric reported lower than 5ppmvd @15% O₂ of NO_x emissions up to pressures of 17 atm, but this was with only 65% hydrogen content. Mitsubishi tested up to 40-84% H₂, NO_x emissions were lower than 10 ppmvd 15% O₂ of NO_x emissions for all fuels at atmospheric conditions.

Moreover, the injectors manufactured by Collins Aerospace are nearly repeatable. The effective area of the air and fuel circuit were measured experimentally to be 0.15 in² and 0.007 in² (see Table A- 1 for details) with standard deviations of 0.003 and 0.0007, respectively. These results indicate a high-fidelity manufacturing process.

3. Does the current design of injectors produce higher or lower NO_x emissions when operating on hydrogen fuel compared to natural gas?

The current injector design produces higher NO and NO_x emissions when hydrogen content is increased. However, this conclusion should be taken with precaution because the system is not fully premixed. Thus, with increased flame speeds, hydrogen is affected more by unmixedness which is a potential reason as to why increased hydrogen content give rise to more NO and NO_x emissions. Another potential reason is due to the NNH pathway that is enabled as a result of adding hydrogen due to more H radicals being present. It should also be noted that hydrogen has higher flammability limits compared to methane which allows it to have more stability. The enhanced stability is particularly ideal for non premixed systems since there is a wide range of equivalence ratios present within the flame itself due to imperfect mixing. With increased flammability limits, the pockets of lower and higher equivalence ratios are still allowed to burn and hold a flame.

- a. Can the current design operate on mixtures of hydrogen and natural gas up to 100%?

Yes, the current set of injectors can operate on pure methane and hydrogen while achieving emissions below 10 ng/J of NO and NO_x.

- b. Which blend of fuel achieves the lowest emissions?

Methane produces more CO emissions than hydrogen fuel since hydrogen does not have carbon in its fuel composition. When focusing on NO and NO_x emissions, both fuels have the potential to achieve low emissions. However, on the current set of injectors, methane produces less NO and NO_x emissions on average compared to hydrogen. But it is important to note that the difference in emissions for the two fuels are not that significant. At methane's best-case scenario, at 1500K at 6% pressure drop, methane produces ~2.3 ng/J of NO emissions.

Comparing this to hydrogen's worst-case scenario at 2% pressure drop at 1100K (hydrogen's worse case at 1100K), hydrogen produces ~2.6 ng/J of NO emissions. If the adiabatic flame temperature for methane were to increase to 1850K, methane would produce ~5.74 ng/J of NO emissions. Thus, the emissions results are highly dependent on the combination of factors. It is inconclusive which fuel is "better" than the other.

The same conclusion is drawn for the NO_x model. At hydrogen's worst-case scenario at a pressure drop of 2% at 1100K, NO_x emissions are ~11.9 g/J. Comparing that to the best-case scenario for methane at 1500K and 6% pressure drop, ~8.3 ng/J of NO_x emissions obtained. If the pressure drop for the hydrogen case were to increase to 6%, NO_x emissions are reported to also be ~8.3 ng/J. This corroborates the fact that the current set of injectors should be restudied with new factors or change the current range of the factors as the emissions results are sensitive to the selection of factors. It is inconclusive which fuel is "better" than the other. Both have the potential to produce low NO and NO_x emissions.

- i. How does the NO_x formation mechanism change, if at all, as a function of fuel composition?

At higher estimated adiabatic flame temperatures (1850K) the thermal NO_x pathway begins to dominate for methane. For hydrogen, the NNH pathway is still dominate, but the thermal NO_x mechanism begins to emerge. However, at lower estimated adiabatic flame temperatures (below 1675K), the N₂O pathway is dominant for methane while the NNH pathway is dominant for hydrogen. These conclusions were drawn based on the GRI Mech 3.0 chemical mechanism.

4. How do the ANOVA and CHEMKIN models compare to the experimental results? How can the ANOVA and CHEMKIN models be modified to better fit experimental data?

The predictive models from the ANOVA results did not perfectly match the experimental results. The CO, NO, NO_x, and NO/NO_x models had a coefficient of variance of 44%, 25%, 13%, and 20%, respectively. These predictive models were still able to capture the emissions trends, however. The high deviations were mainly caused by a few select cases that were left in the model. For example, hydrogen cases with high NO and NO_x emissions could be considered outliers from a purely statistical basis, but these were not removed from the model since the study is interested in studying factors and factor interactions that affect emissions. Thus, these outlier points were valuable to understand which factors were desirable for methane compared to hydrogen. Moreover, the predictive model for CO had the highest deviations which can be traced back to the gas analyzer itself. CO emissions on the analyzer can fluctuate +/-10ppmvd. Additionally, if combustion time were to be increased, CO emissions would decrease slowly over time. Thus, CO emissions should be viewed more as an indicator of complete combustion. Lastly, the large deviations can also be traced to the experimental setup itself. The flow metering systems each have their own deviations and uncertainties as described in section 4. Recommendations to increase the fidelity of the ANOVA model are discussed in section 6.2.

For the chemical kinetics model on CHEMKIN, the average deviation for the CO, NO, and NO_x emissions model were 64%, 55% and 25%, respectively. Although these deviations are high, trends can still be studied to understand the differences between operating on hydrogen vs. methane fuel. High deviations can be contributed to compounded effects of equipment uncertainty and data collection (especially for the CO emissions model). The conversion from ppmvd 15% O₂ to ng/J also has its own uncertainties since it relies on the measured oxygen

values from the experiment. The NO and NO_x deviations for the ppmvd model were lower than the ng/J model. The average deviation for the CO, NO, and NO_x ppmvd 15% O₂ emissions model were 76%, 24%, and 11%, respectively. Recommendations to increase the fidelity of the CHEMKIN model are discussed in section 6.2.

6.2 Conclusions

1. Assess emissions for all 16 injectors and create a predictive model for the factors in question.
 - a. What factors and factor interactions are significant to the injector performance?
 - i. Which combination of factors minimizes pollutant emissions?
 - ii. From 1ai, does the desired combination of factors change with the different fuels?
 - b. What modifications to the current injector design can be suggested to further improve performance?

Takeaway of Question 1: A higher air split (more air through the injector), air swirl angle, pressure drop and lower fuel swirl angle and preheat temperatures is preferred for both hydrogen and methane fuel mixtures. This shows that the current injector design is robust and insensitive to fuel mixture or estimated adiabatic flame temperatures. As a result, the current injector design can rival those of Parker Hannifin, Honeywell, General Electric and Mitsubishi's design by producing less than ~10 ng/J in emissions and can operate both with pure methane and hydrogen.

2. How does Collins Aerospace's LDI design perform compared to current micromixing designs?

Takeaway of Question 2: The Collins Aerospace injector design is one that is unique as it can operate on 100% methane and hydrogen fuel with mixtures in between across a wide range of adiabatic flame temperatures while obtaining low emissions. Most current injector designs must rely on dilution strategies or use high mixtures of hydrogen (not 100%) to obtain lower emissions. The manufacturing process is also of high fidelity with standard deviations of 0.003 and 0.0007 for the air and fuel circuits, respectively. With impressive achievements, the injector can be adapted to higher pressure test facilities to further advance a gas turbine design and contribute to the transition to a hydrogen economy. This can go on to become Collins Aerospace's first aeroengine that has been adapted to a ground-based gas turbine for power generation.

3. Does the current design of injectors produce higher or lower NO_x emissions when operating on hydrogen fuel compared to natural gas?
 - a. Can the current design operate on mixtures of hydrogen and natural gas up to 100%?
 - b. Which blend of fuel achieves the lowest emissions?
 - i. How does the NO_x formation mechanism change, if at all, as a function of fuel composition?

Takeaway for Question 3: It is clear that more experiments should be curated for ones that involve fully premixed systems. A fully premixed experiment will eliminate any questions pertaining to unmixedness and adiabatic flame temperatures that will present hydrogen in a fairer light considering its increased flame speeds. Nevertheless, hydrogen has the potential to achieve the lowest NO and NO_x emissions at lower estimated flame temperatures.

Additionally, only one chemical mechanism was investigated, GRI Mech 3.0. However, there are known issues with GRI Mech 3.0's chemical mechanism especially when it comes to modeling chemical kinetics of non-hydrocarbons. Nevertheless, GRI Mech 3.0 was used in this study because it was well established and used ubiquitously throughout the field. Much of the discussed literature presented in section 2 is based on this mechanism. However, for a more accurate model (and/or to establish sensitivity to mechanism), other mechanisms such as UCSD and Galway should be investigated.

4. How do the ANOVA and CHEMKIN models compare to the experimental results? How can the ANOVA and CHEMKIN models be modified to better fit experimental data?

Takeaway for Question 4: While the deviations were high, these are compared to experimental values which are more real and have real world effects such as unmixedness, heat losses, and temperature fluctuations. Moreover, the calculated adiabatic flame temperatures are different from the actual adiabatic flame temperatures which could not be measured during testing. Thus, more experiments and simulations should be conducted to help address and quantify the sensitivities in the models. To prepare for the transition to phase two of the project, for higher pressure testing, experiments such as fully premixed, adjusted factor ranges, and different factors selection like level of mixedness or arrays should be addressed. Perhaps an entire test matrix should be design for pure methane and another separate one for pure hydrogen so that the hydrogen "outliers" can be better fitted to a model could also work. More recommendations will be elaborated in the next succeeding section.

6.3 Recommendations

The following recommendations and next steps are summarized below and can be taken to improve the project:

- Verify the mixedness of the experiment by studying the mixing effect in CFD simulations
- Range and test the level of mixedness in the experiment to assess how mixedness affects hydrogen compared to methane
- Experimentally run cases with fully premixed air and fuel and compare to the numerically obtained numbers from the CHEMKIN model
- Conduct CHEMKIN analysis to compare the effect of plate configurations. The current CHEMKIN study is conducted on Injector 3 with Plate 2. Other mechanisms like Galway and UCSD should also be studied.
- Increase the fuel flow capability to analyze Hydrogen at higher flame temperatures
- Perform experimental tests with a pure hydrogen and pure methane matrix
- Compare the percent differences rather than percent deviations between the experimental model vs. CHEMKIN model
- Investigate other factors like counterflow swirl or increase/decrease current ranges for air split, air swirl, fuel swirl, pressure drop, and preheat temperature.

7. Appendices

7.1 Appendix A: Effective Area Tests

The results of the effective area test for the air and fuel circuits are shown in Table A- 1. These numbers are within the ballpark range given the expected values of 0.144 in² for the air circuit and 0.006 in² for the fuel circuit, provided by Collins Aerospace. The necessary calibration curves for the pressure lines and sonic orifice are summarized in Table A- 2. Considering the large number of calibrations, second checks were performed to ensure the effective area tests were valid.

Table A- 1. Effective Areas for Air and Fuel Circuits

Configuration	Effective Area in ² , AIR	Effective Area in ² , FUEL
Injector 1, Plate 2	0.1512	0.0070
Injector 2, Plate 3	0.1485	0.0062
Injector 3, Plate 2	0.1458	0.0061
Injector 4, Plate 2	0.1497	0.0062
Injector 5, Plate 3	0.1474	0.0067
Injector 6, Plate 1	0.1465	0.0049
Injector 7, Plate 1	0.1538	0.0062
Injector 8, Plate 2	0.1550	0.0050
Injector 9, Plate 1	0.1525	0.0062
Injector 10, Plate 2	0.1494	0.0052
Injector 11, Plate 3	0.1429	0.0050
Injector 12, Plate 3	0.1485	0.0061
Injector 13, Plate 1	0.1489	0.0071
Injector 14, Plate 1	0.1524	0.0051
Injector 15, Plate 1	0.1484	0.0052

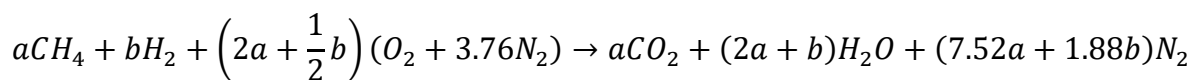
Injector 16, Plate 3	0.1456	0.0052
----------------------	--------	--------

Table A- 2. Calibration Curves Used in Effective Area Tests

Category	Calibration Curve
Pressure Transmitter to Dial Readings	Y=0.7985xBluePSI-2.0076
Methane Brooks Mass Flow % to SCFM	Y=0.0152x%+0.0063
Hydrogen Ch 2 Brooks Mass Flow % to SCFM	Y=0.0142x%+0.0058
Hydrogen Ch 3 Brooks Mass Flow % to SCFM	Y=0.0070x%+0.0000

Emission results were performed as a second check to these calibrations. By comparing the expected oxygen to the actual oxygen level measured (via PG 350 emissions machine), it can be checked if the air and fuel flow rates entering the system is what the pressure transmitter is reading. Equation 14 can be used to calculate the expected oxygen levels. If the emissions match, then the air and fuel being fed into the system is properly displayed and recorded. Essentially, emissions are a good check because both the air and fuel flows must match as opposed to just matching one gas circuit. The results from the emissions test are shown in Table A- 3. It is also important to note that calibration curves have been applied to the air and fuel flows before the expected oxygen levels are calculated.

The general equation for methane and hydrogen combustion is shown below in Equation A-1:



where a is the number of moles of methane and b is the number of moles of hydrogen fuel.

Table A- 3. Expected vs. Actual % O2 from Emissions Test

Air SCFM	CH ₄ SCFM	H ₂ SCFM	O ₂ Measured, %	O ₂ Expected, %	CO, ppmvd
7.317	0.274	0.274	12.46	12.47	27.8
7.971	0.424	0.000	11.09	11.12	38.2
11.434	0.682	0.682	6.92	6.94	75.4
12.685	0.732	0.000	10.19	10.22	69.2
12.839	0.483	0.483	12.34	12.43	26.2

The deviation between the expected and measured oxygen levels are within 0-5%, indicating that the calibration curves are correct. The actual flow rate entering the system is then properly correlated. Deviations of 0-5% can be attributed to losses along the line, the emissions analyzer’s repeatability, and the mass flow controller’s precision. Although carbon monoxide levels were low, in some instances deviations can go above 5% due to incomplete combustion.

Finally, as a third check, as mentioned previously Collins Aerospace was able to measure the effective area of the fuel circuit and determined it to be 0.006 in². They were not able to directly measure the effective area of the air, however, an estimate of 0.144 in² was given. From Table A- 1, the effective area of the fuel circuit ranges from 0.005 to 0.007 in². This not only matches Collins Aerospace’s number but also verifies the method for calculating the effective area for the air circuit and the calibrations curves.

7.2 Appendix B: Emissions on a Volume vs. a Mass Basis

Emissions results for the test matrix for injectors 1, 2, 3, 4, 5, 8 and 10, are reported in Table A- 15-Table A- 19, Table A- 22, and Table A- 24 in the Appendix. Excess oxygen was measured and compared to expected oxygen levels as a check against the analyzer and air and

fuel lines. For all emissions results, oxygen deviation was less than 5% which corroborates the accuracy of the fuel and air lines. The air and fuel flows are reported in Table A- 14. It should be noted that when reporting emissions on a volume dry basis, hydrogen is not accurately represented [67]. Hydrogen is smaller in mass so comparing simply by volume would not be a fair comparison. Additionally, the drying process favors hydrocarbons since hydrogen produces more water in the exhaust. During the drying process, the removal of water concentrates the pollutant in hydrogen gas streams more [67]. Hydrogen exhaust also requires less dilution to reach an oxygen concentration due to lower oxygen consumption. This gives it a smaller correction factor when reporting on a volume basis. When calculating ppmvd, a correction factor is used to account for consumed oxygen which dilutes the emissions sample.

This phenomenon can be seen when comparing Figure A- 1 (15% O₂ ppmvd) and Figure A- 3 (ng/J). For ease of comparison, the y axis is set to the same scale and can be used to directly compare emissions. On average, hydrogen fuel produces 2.97 times more NO emissions when reporting on a volume basis than when reporting on a mass basis which is only 2.07 higher. For NO_x, when reporting on a volume basis hydrogen produces 2.15 times more emissions compared to 1.37 times on a mass basis. Plots of NO_x emissions on volume vs. mass basis are shown in Figure A- 2 and Figure A- 4. It should be emphasized that even on a mass basis, hydrogen still produces more emissions compared to methane but when looking at a mass basis, the percent increase in emissions for hydrogen vs. methane fuel is lower. Thus, all emissions results are reported both on a volume and mass basis.

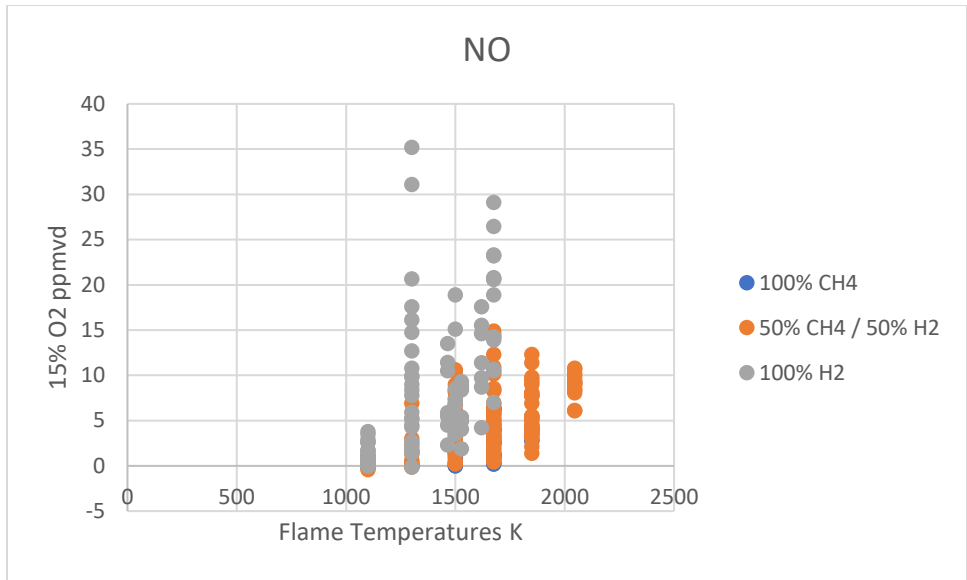


Figure A- 1. NO 15% O2 ppmvd. vs. Flame Temperature

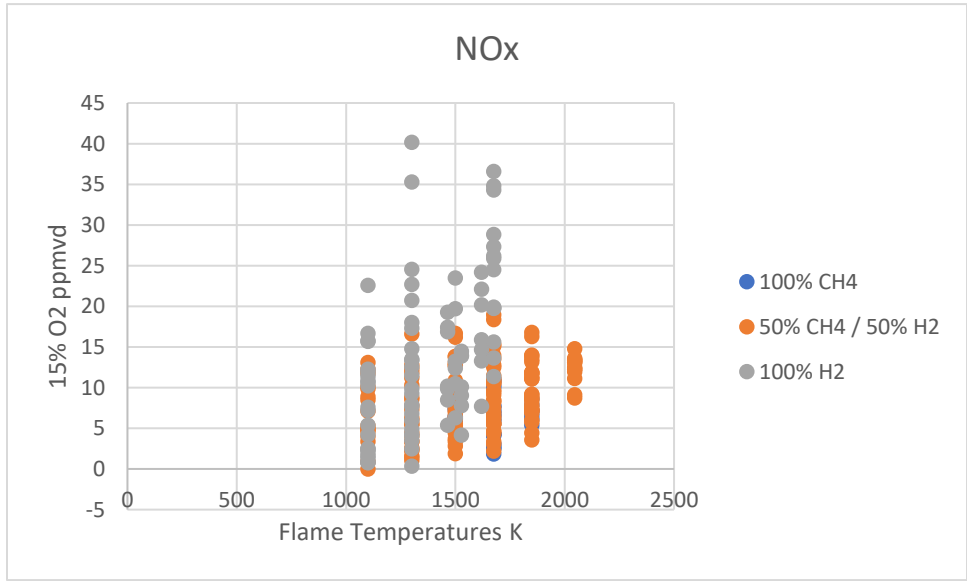


Figure A- 2. NOx 15% O2 ppmvd. vs. Flame Temperature

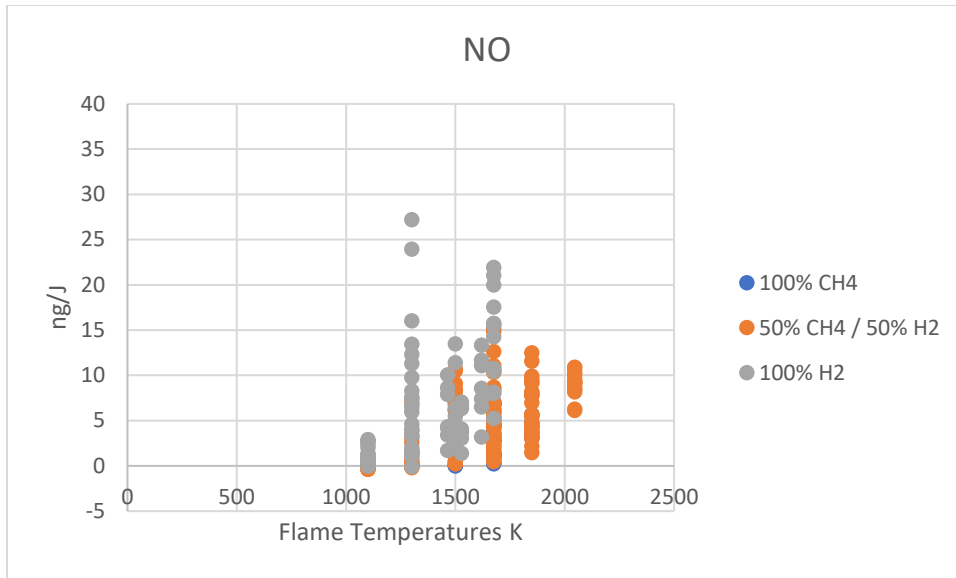


Figure A- 3. NO ng/J vs. Flame Temperature

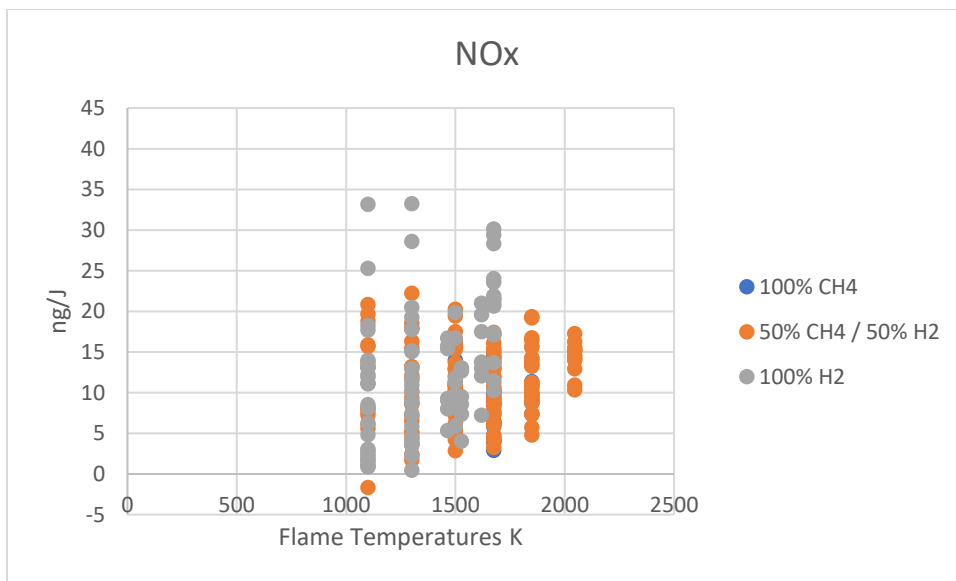


Figure A- 4. NOx ng/J vs. Flame Temperature

7.3 Appendix C: Volume/Confinement Study

A volume analysis was conducted on STD 8, 17, 20, 21, 24, and 25 for Injector 3. The cylinder properties are shown in Table A- 4 with different volumes. Emissions results are shown in Table A- 5. The differences in recorded emissions were too small to equate it to a statistical difference. Thus, the volume of the cylinder and confinement does not affect emissions.

However, the stability and flame impingement were affected. Sample images are shown in

Figure A- 5 and Figure A- 6 where the smaller cylinder had the flame structure curved back into an M shape. Flame structures will not be discussed in the context of the thesis.

Table A- 4. Cylinder Characteristics

Cylinder #	ID/OD (mm)	Height (mm)
1	80/85	200
2	Rectangle	200
3	47/50	200

Configuration 1 is shown in Figure 14 and Configuration 2 and 3 are shown in Figure A- 5 and Figure A- 6.

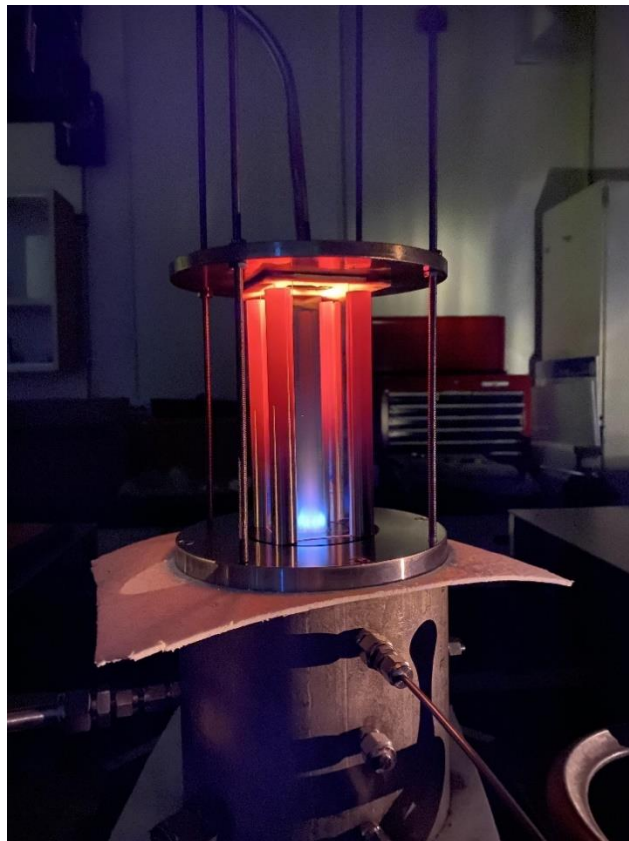


Figure A- 5. Rectangular Configuration, Case 2

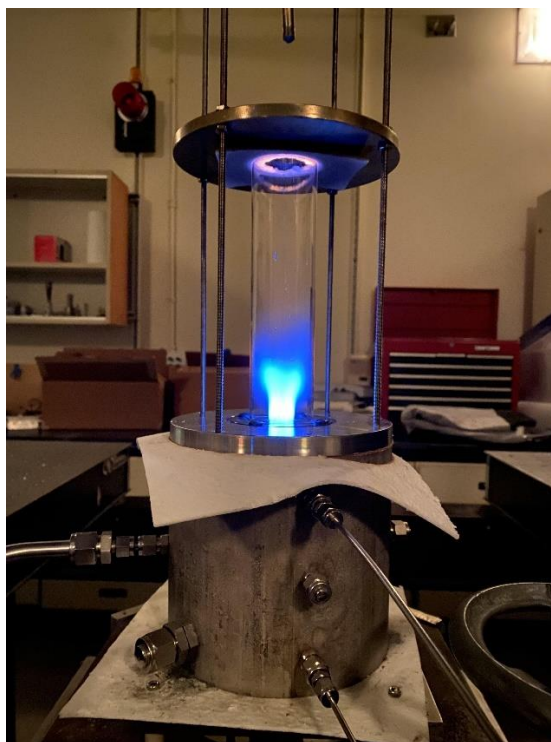


Figure A- 6. Tall Cylinder Configuration, Case 3

Table A- 5. Emissions Data for Volume/ Confinement Study

Std order	CO		NO		NOx		%O2 Measured	% O2 Expected	% O2 Deviation
	[ppm]	[ng/J]	[ppm]	[ng/J]	[ppm]	[ng/J]			
8-1	1.00	0.54	15.53	11.69	22.13	19.60	13.12	13.07	0.00
8-2	30.80	59.89	0.11	0.08	2.30	2.70	18.75	18.49	0.01
8-2.2	25.10	45.04	1.08	0.87	4.75	5.19	18.57	18.49	0.00
8-3	8.20	15.37	0.30	0.20	2.50	2.97	18.67	18.49	0.01
8-3.2	6.60	12.10	0.80	0.59	6.60	7.51	18.62	18.49	0.01
17-1	38.20	23.64	4.14	4.49	7.57	10.34	11.09	11.12	0.00
17-2	47.80	30.48	3.81	4.17	7.00	9.49	11.38	11.12	0.02
17-3	19.20	12.22	4.45	4.91	8.40	11.49	11.36	11.12	0.02
20-1	1.40	0.93	11.42	8.63	17.44	15.74	14.64	14.64	0.00
20-2	-0.20	-0.14	9.50	7.26	14.29	12.76	14.91	14.64	0.02
20-2.2	0.90	0.63	9.90	7.56	15.12	13.56	14.92	14.64	0.02
20-3	0.60	0.41	10.63	8.11	16.80	15.35	14.83	14.64	0.01

20-3.2	0.10	0.07	11.80	8.96	18.00	16.18	14.87	14.64	0.02
21-1	194.00	131.32	1.41	1.39	5.57	7.97	12.61	12.62	0.00
21-2	93.60	64.92	1.34	1.35	4.35	6.04	12.81	12.62	0.02
21-2.2	81.90	57.09	1.47	1.49	4.92	6.86	12.85	12.62	0.02
21-3	65.60	45.33	1.60	1.63	5.40	7.52	12.78	12.62	0.01
24-1	19.90	10.82	9.00	9.13	13.19	15.73	10.58	10.45	0.01
24-2	43.80	24.34	9.16	9.25	13.83	16.52	10.80	10.45	0.03
24-3	30.90	16.85	10.00	10.17	15.40	18.49	10.61	10.45	0.02
25-1	28.50	17.16	4.56	4.58	8.52	10.74	11.58	11.60	0.00
25-2	41.80	26.09	3.86	3.91	7.53	9.58	11.91	11.60	0.03
25-3	15.80	9.69	4.50	4.54	8.65	11.01	11.75	11.60	0.01

Configuration dashes 1, 2, and 3 represent the different confinement conditions in Table A- 4.

For example, 20-2.2 represent STD 20 with the rectangle configuration and the X.2 represents a repeated point. Flow rates for the standard runs are in Table A- 14.

7.4 Appendix D: Supplementary Tables and Figures

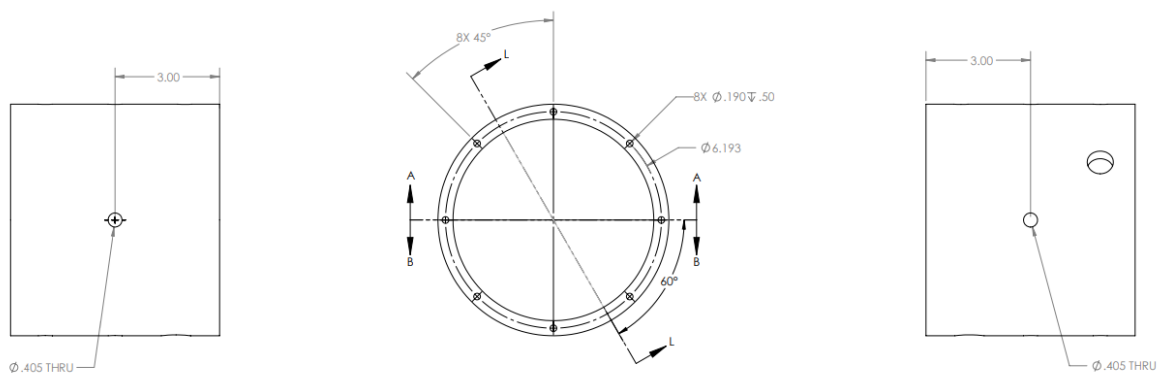


Figure A- 7. Solidworks Drawing of Airbox with Heater Plate Interface

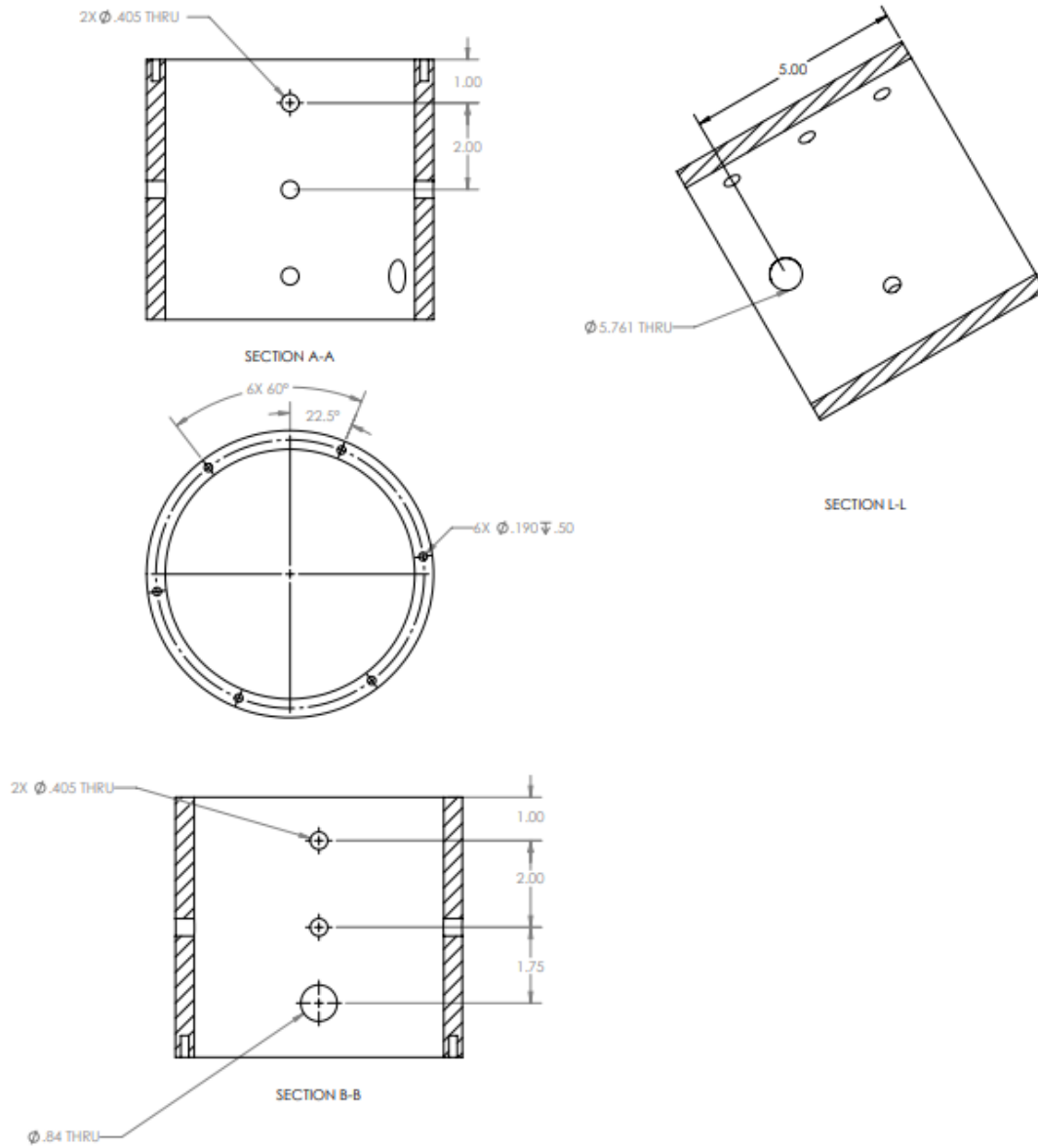


Figure A- 8. Solidworks Drawing of Airbox with Injector Plate Interface and Side Profiles

Table A- 6. Standard Order for Test Matrix

STD Order	Run Order	Pressure Drop %	Preheat Temperature K	Fuel Composition % H2	Flame Temperature K
1	14	2	500	50	1675
2	26	6	500	50	1675
3	1	2	800	50	1675

4	5	6	800	50	1675
5	7	4	650	0	1500
6	27	4	650	100	1500
7	13	4	650	0	1850
8	21	4	650	100	1619.676
9	20	2	650	50	1500
10	16	6	650	50	1500
11	24	2	650	50	1850
12	18	6	650	50	1850
13	4	4	500	0	1675
14	10	4	800	0	1675
15	17	4	500	100	1527.469
16	23	4	800	100	1675
17	2	2	650	0	1675
18	25	6	650	0	1675
19	8	2	650	100	1675
20	19	6	650	100	1463.843
21	9	4	500	50	1500
22	15	4	800	50	1500
23	6	4	500	50	1850
24	11	4	800	50	1850
25	12	4	650	50	1675
26	22	4	650	50	2045.507
27	3	4	650	50	2045.507
28	14	6	650	100	1300
29	9	2	650	100	1300
30	5	4	500	50	1100
31	16	4	500	100	1300
32	3	2	650	100	1100

33	7	4	800	100	1100
34	13	4	800	50	1100
35	6	2	650	50	1300
36	8	6	650	50	1100
37	11	4	500	50	1300
38	2	6	650	50	1300
39	1	4	800	50	1300
40	10	4	500	100	1100
41	12	2	650	50	1100
42	4	4	800	100	1300
43	15	6	650	100	1100

Table A- 7. Corresponding Air Flow Rates in SCFM at Specified Preheat Temperatures and Pressure Drops for Injector 3

	Pressure Drops		
Preheat Temperature K	2%	4%	6%
500	8.971	12.685	15.571
650	7.971	11.434	13.993
800	7.317	10.491	12.839

Table A- 8. Actual Pressure Drops for Injector 1 with Respect to Injector 3

	Pressure Drops		
Preheat Temperature K	2% (Injector 3)	4% (Injector 3)	6% (Injector 3)
500	2.03	3.97	6.02
650	2.00	4.03	6.02
800	1.88	3.89	6.12

Table A- 9. Actual Pressure Drops for Injector 2 with Respect to Injector 3

	Pressure Drops

Preheat Temperature K	2% (Injector 3)	4% (Injector 3)	6% (Injector 3)
500	1.96	3.86	5.83
650	1.94	3.92	5.76
800	1.96	3.90	5.80

Table A- 10. Actual Pressure Drops for Injector 4 with Respect to Injector 3

	Pressure Drops		
Preheat Temperature K	2% (Injector 3)	4% (Injector 3)	6% (Injector 3)
500	2.18	4.25	6.40
650	2.15	4.31	6.34
800	2.00	4.26	6.44

Table A- 11. Actual Pressure Drops for Injector 5 with Respect to Injector 3

	Pressure Drops		
Preheat Temperature K	2% (Injector 3)	4% (Injector 3)	6% (Injector 3)
500	1.87	3.78	5.74
650	1.93	3.85	5.71
800	1.97	3.73	5.93

Table A- 12. Actual Pressure Drops for Injector 8 with Respect to Injector 3

	Pressure Drops		
Preheat Temperature K	2% (Injector 3)	4% (Injector 3)	6% (Injector 3)
500	2.03	3.93	5.95
650	2.00	3.31	5.91
800	1.96	3.97	6.16

Table A- 13. Actual Pressure Drops for Injector 10 with Respect to Injector 3

	Pressure Drops		
--	----------------	--	--

Preheat Temperature K	2% (Injector 3)	4% (Injector 3)	6% (Injector 3)
500	2.04	3.99	6.02
650	2.02	4.06	6.02
800	1.97	4.07	6.09

Table A- 14. Flow Rates for Test Matrix

Std order	Air SCFM	CH4 SCFM	H2 SCFM
1	8.971	0.400	0.400
2	15.571	0.694	0.694
3	7.317	0.274	0.274
4	12.839	0.483	0.483
5	11.434	0.493	0.000
6	11.434	0.000	1.677
7	11.434	0.729	0.000
8	11.434	0.000	2.126
9	7.971	0.266	0.266
10	13.993	0.466	0.466
11	7.971	0.393	0.393
12	13.993	0.690	0.690
13	12.685	0.732	0.000
14	10.491	0.510	0.000
15	12.685	0.000	2.126
16	10.491	0.000	1.745
17	7.971	0.424	0.000
18	13.993	0.743	0.000
19	7.971	0.000	1.446
20	13.993	0.000	2.126

21	12.685	0.468	0.468
22	10.491	0.316	0.316
23	12.685	0.673	0.673
24	10.491	0.480	0.480
25	11.434	0.470	0.470
26	11.434	0.682	0.682
27	11.434	0.682	0.682
28	7.971	0.140	0.140
29	13.993	0.246	0.246
30	7.971	0.000	0.612
31	13.993	0.000	1.075
32	12.685	0.265	0.265
33	10.491	0.150	0.150
34	12.685	0.000	1.161
35	10.491	0.000	0.657
36	7.971	0.201	0.201
37	13.993	0.352	0.352
38	7.971	0.000	0.880
39	13.993	0.000	1.547
40	12.685	0.363	0.363
41	10.491	0.230	0.230
42	12.685	0.000	1.592
43	10.491	0.000	1.007

Table A- 15. Emissions Results for Injector 1

Std order	CO		NO		NOx		%O2 Measured	% O2 Expected	% O2 Deviation
	[ppm]	[ng/J]	[ppm]	[ng/J]	[ppm]	[ng/J]			

1	23.00	12.41	4.20	4.25	7.56	9.38	10.50	10.73	-2.16%
2	43.40	23.81	2.44	2.43	5.54	7.28	10.67	10.74	-0.66%
3	21.80	14.18	10.17	10.39	13.54	15.37	12.27	12.47	-1.61%
4	22.60	14.70	6.92	7.08	11.50	14.01	12.27	12.43	-1.28%
5	409.00	306.57	2.30	2.48	7.46	11.10	12.80	13.07	-2.05%
6	0.40	0.27	8.50	6.44	13.28	11.87	14.78	14.87	-0.62%
7	39.00	19.46	5.18	5.69	8.63	11.38	8.73	9.02	-3.19%
8	0.40	0.21	8.70	6.52	13.32	12.09	12.93	13.07	-1.06%
9	95.80	70.64	6.80	6.85	10.63	12.86	13.29	13.46	-1.23%
10	121.60	89.67	3.48	3.51	8.19	10.77	13.29	13.46	-1.29%
11	15.70	7.65	7.73	7.80	11.09	13.26	9.38	9.58	-2.08%
12	34.10	16.60	5.30	5.43	8.69	10.57	9.37	9.57	-2.12%
13	92.70	51.35	1.24	1.32	4.27	6.32	9.94	10.22	-2.72%
14	31.20	20.61	6.45	7.05	10.78	14.31	11.71	12.00	-2.44%
15	3.90	2.29	4.92	3.70	9.07	8.59	13.79	13.92	-0.94%
16	0.30	0.18	14.25	10.68	19.74	17.14	13.76	13.98	-1.57%
17	45.60	27.63	4.57	5.00	7.73	10.24	10.88	11.12	-2.13%
18	44.40	26.80	3.12	3.45	6.50	9.09	10.84	11.12	-2.51%
19	3.90	2.09	10.67	8.13	15.64	13.68	13.11	13.28	-1.30%
20	0.70	0.45	5.87	4.34	9.87	9.10	14.39	14.64	-1.68%
21	178.70	117.97	2.03	2.06	6.17	8.56	12.40	12.62	-1.72%
22	76.30	61.69	8.14	8.23	13.07	15.74	13.96	14.23	-1.90%
23	34.00	15.44	3.84	3.90	7.16	8.88	8.54	8.63	-1.07%
24	19.60	10.31	9.52	9.54	13.92	16.45	10.23	10.45	-2.11%
25	22.80	13.48	5.22	5.34	9.13	11.27	11.41	11.60	-1.64%
26	90.60	35.98	8.42	8.55	11.96	14.05	6.77	6.94	-2.45%
27	84.40	33.45	8.06	8.17	11.15	12.94	6.74	6.94	-2.88%
28	3260.00	5882.21	0.50	0.48	11.80	18.80	17.79	17.12	3.90%

29	3068.00	7651.66	-0.05	-0.05	4.92	8.05	18.65	17.12	8.91%
30	4.90	6.72	1.10	0.94	10.79	12.25	17.85	17.91	-0.31%
31	11.60	16.00	1.20	0.89	12.29	14.01	17.87	17.91	-0.20%
32	3641.00	7323.18	0.12	0.09	7.11	11.17	18.11	16.36	10.71%
33	2715.00	7617.68	0.17	0.18	4.02	6.07	18.90	17.85	5.87%
34	4.80	5.45	0.38	0.28	7.20	8.11	17.22	17.28	-0.37%
35	5.40	9.03	1.75	1.34	10.25	11.08	18.40	18.49	-0.51%
36	2601.30	2688.27	1.59	1.63	11.22	16.32	15.47	15.37	0.62%
37	5880.00	6444.52	0.02	0.02	7.34	11.72	15.78	15.38	2.61%
38	0.70	0.65	8.99	6.82	12.55	10.90	16.43	16.47	-0.26%
39	0.80	0.74	5.93	4.62	9.90	8.93	16.38	16.47	-0.54%
40	6222.00	6371.36	0.16	0.16	5.51	8.56	15.42	14.58	5.78%
41	3079.00	3652.85	2.49	2.56	12.33	17.91	16.17	16.14	0.19%
42	9.50	7.79	4.50	3.43	7.92	7.43	15.80	15.81	-0.09%
43	36.10	39.10	16.15	12.31	20.75	17.80	17.04	17.09	-0.31%

Table A- 16. Emissions Results for Injector 2

Std order	CO		NO		NOx		%O2 Measured	% O2 Expected	% O2 Deviation
	[ppm]	[ng/J]	[ppm]	[ng/J]	[ppm]	[ng/J]			
1	14.90	8.28	4.70	4.71	8.40	10.54	10.80	10.73	0.64%
2	29.40	16.61	2.20	2.24	5.60	7.52	10.97	10.74	2.13%
3	14.90	10.18	14.50	14.87	18.40	20.93	12.69	12.47	1.76%
4	18.80	12.63	8.30	8.43	12.80	15.37	12.55	12.43	0.97%
5	412.00	321.52	1.40	1.51	6.10	9.31	13.12	13.07	0.40%
6	1.00	0.72	18.90	13.50	23.50	19.87	15.09	14.87	1.46%
7	28.90	14.74	3.40	3.66	6.60	9.10	9.00	9.02	-0.19%
8	0.10	0.06	17.60	13.33	24.20	21.00	13.40	13.07	2.53%
9	54.20	42.01	8.40	8.47	12.80	15.34	13.66	13.46	1.52%

10	76.90	59.69	4.02	4.08	9.20	12.10	13.67	13.46	1.53%
11	15.00	7.53	9.80	9.90	13.50	15.58	9.72	9.58	1.47%
12	29.70	14.91	5.50	5.60	9.20	11.28	9.72	9.57	1.54%
13	73.40	41.57	0.30	0.36	2.50	3.99	10.18	10.22	-0.37%
14	23.40	16.04	6.30	6.91	10.04	13.09	12.04	12.00	0.31%
15	4.40	2.78	9.30	7.05	14.50	13.07	14.29	13.92	2.65%
16	0.50	0.31	29.10	21.95	36.60	30.14	14.12	13.98	1.00%
17	22.20	14.00	3.80	4.19	6.80	9.26	11.27	11.12	1.38%
18	33.60	20.94	1.20	1.34	4.10	6.14	11.16	11.12	0.37%
19	5.30	2.98	23.20	21.05	34.30	28.34	13.47	13.28	1.41%
20	0.50	0.34	13.50	10.06	19.30	16.73	14.84	14.64	1.39%
21	90.40	62.40	2.20	2.29	6.30	8.63	12.77	12.62	1.21%
22	50.50	43.00	10.40	10.50	16.70	20.27	14.31	14.23	0.56%
23	32.80	15.25	4.20	4.29	7.30	9.09	8.83	8.63	2.29%
24	17.00	9.21	11.40	11.56	16.30	19.19	10.54	10.45	0.86%
25	15.60	9.52	5.90	5.95	10.50	13.05	11.70	11.60	0.86%
26	82.90	33.73	10.20	10.38	13.40	15.25	7.11	6.94	2.45%
27	84.00	33.91	9.50	9.56	13.10	15.19	7.00	6.94	0.86%
28	3440.00	7599.90	0.40	0.47	12.30	19.68	18.36	17.12	7.23%
29	3488.00	9365.12	0.20	0.29	9.90	15.70	18.81	17.12	9.84%
30	9.00	14.31	3.80	2.90	22.60	25.32	18.27	17.91	2.03%
31	4.00	6.41	3.50	2.75	16.70	18.25	18.29	17.91	2.14%
32	3726.00	8534.14	0.50	0.49	10.10	15.89	18.45	16.36	12.79%
33	3246.00	9536.70	0.20	0.31	8.90	13.81	18.99	17.85	6.37%
34	20.30	26.36	1.70	1.25	15.80	33.19	17.68	17.28	2.29%
35	5.10	10.61	2.60	2.01	15.70	17.70	18.89	18.49	2.14%
36	2461.00	2734.66	3.00	3.10	12.80	18.59	15.85	15.37	3.09%
37	3870.00	4352.05	0.60	0.60	8.60	13.14	15.91	15.38	3.46%

38	0.40	0.41	31.10	23.94	35.30	28.62	16.80	16.47	1.99%
39	0.40	0.41	17.60	13.44	22.70	19.30	16.80	16.47	2.01%
40	6741.00	7565.49	0.07	0.07	6.30	10.08	15.90	14.58	9.07%
41	990.00	1254.05	6.90	7.06	16.60	22.23	16.47	16.14	2.05%
42	20.00	17.79	10.80	8.30	14.80	12.96	16.20	15.81	2.44%
43	3.70	4.54	35.20	27.21	40.20	33.24	17.49	17.09	2.32%

Table A- 17. Emissions Results for Injector 3

Std order	CO		NO		NOx		%O2 Measured	% O2 Expected	% O2 Deviation
	[ppm]	[ng/J]	[ppm]	[ng/J]	[ppm]	[ng/J]			
1	21.30	11.65	3.52	3.54	6.97	8.82	10.64	10.73	-0.85%
2	31.90	17.64	1.79	1.86	4.66	6.30	10.75	10.74	0.09%
3	27.80	18.48	10.93	11.07	15.13	17.45	12.46	12.47	-0.08%
4	26.20	17.18	6.28	6.34	10.96	13.65	12.34	12.43	-0.72%
5	775.00	593.36	0.92	1.03	6.40	10.19	12.97	13.07	-0.75%
6	1.10	0.76	15.10	11.40	19.71	16.72	14.81	14.87	-0.42%
7	36.70	18.63	4.36	4.77	7.89	10.83	8.94	9.02	-0.86%
8	1.00	0.54	15.53	11.69	22.13	19.60	13.12	13.07	0.39%
9	102.00	76.11	6.05	6.17	10.92	13.68	13.38	13.46	-0.56%
10	133.10	99.32	2.68	2.72	7.60	10.41	13.38	13.46	-0.63%
11	16.00	7.96	7.74	7.79	11.86	14.26	9.62	9.58	0.42%
12	33.00	16.36	4.72	4.73	8.74	10.98	9.58	9.57	0.07%
13	69.20	39.23	1.20	1.20	4.31	6.52	10.19	10.22	-0.27%
14	36.20	24.45	5.65	6.16	10.26	13.90	11.91	12.00	-0.78%
15	2.80	1.69	8.78	6.63	13.97	12.79	13.96	13.92	0.28%
16	-0.04	-0.02	26.47	19.99	34.81	29.43	13.93	13.98	-0.36%
17	38.20	23.64	4.14	4.49	7.57	10.34	11.09	11.12	-0.24%
18	42.30	25.84	2.59	2.85	6.10	8.72	10.96	11.12	-1.43%

19	3.40	1.87	20.58	15.55	27.37	23.56	13.29	13.28	0.06%
20	1.40	0.93	11.42	8.63	17.44	15.74	14.64	14.64	0.03%
21	194.00	131.32	1.41	1.39	5.57	7.97	12.61	12.62	-0.06%
22	96.40	80.14	7.44	7.58	13.85	17.53	14.15	14.23	-0.56%
23	32.10	14.67	3.60	3.63	6.90	8.75	8.62	8.63	-0.14%
24	19.90	10.82	9.00	9.13	13.19	15.73	10.58	10.45	1.24%
25	28.50	17.16	4.56	4.58	8.52	10.74	11.58	11.60	-0.18%
26	83.00	33.53	8.93	9.02	13.50	16.29	7.01	6.94	1.01%
27	75.40	30.27	8.40	8.45	12.29	14.36	6.92	6.94	-0.29%
28	2947.00	6833.57	-0.14	-0.25	5.30	8.23	18.48	17.12	7.93%
29	2234.00	6563.46	2.64	2.74	-0.24	-1.64	18.99	17.12	10.89%
30	3.60	4.95	0.79	0.63	11.34	13.17	17.86	17.91	-0.26%
31	3.50	4.89	0.30	0.22	4.22	4.86	17.91	17.91	0.02%
32	2397.50	6033.05	-0.20	-0.38	3.38	5.57	18.67	16.36	14.14%
33	1711.00	6358.52	-0.43	-0.40	0.91	1.73	19.39	17.85	8.61%
34	36.20	42.63	-0.03	-0.03	5.41	6.27	17.35	17.28	0.38%
35	3.50	5.97	0.09	0.07	2.58	3.07	18.45	18.49	-0.24%
36	3553.00	3625.06	0.43	0.36	8.80	13.21	15.40	15.37	0.17%
37	6640.00	7844.36	0.00	0.00	4.46	6.99	16.15	15.38	5.02%
38	0.00	0.00	20.67	16.03	24.55	20.49	16.49	16.47	0.10%
39	0.50	0.47	9.85	7.51	13.40	11.50	16.44	16.47	-0.18%
40	6264.00	7247.58	0.00	0.00	4.07	6.51	16.05	14.58	10.10%
41	3551.40	4313.61	-0.15	-0.20	5.50	8.73	16.28	16.14	0.87%
42	33.20	27.54	7.80	5.96	11.55	10.24	15.86	15.81	0.29%
43	16.20	17.73	14.76	11.27	18.02	15.06	17.08	17.09	-0.08%

Table A- 18. Emissions Results for Injector 4

	CO	NO	NOx			
--	-----------	-----------	------------	--	--	--

Std order	[ppm]	[ng/J]	[ppm]	[ng/J]	[ppm]	[ng/J]	%O2 Measured	% O2 Expected	% O2 Deviation
1	10.70	5.80	1.01	0.99	3.08	4.19	10.54	10.73	-1.79%
2	16.40	9.00	0.45	0.45	2.20	3.27	10.67	10.74	-0.66%
3	9.00	5.88	8.56	8.72	10.73	12.06	12.31	12.47	-1.29%
4	10.00	6.47	1.90	1.94	4.66	6.15	12.23	12.43	-1.60%
5	700.00	3148.13	0.00	0.00	4.65	14.01	19.55	13.07	49.61%
6	-0.50	-0.34	3.50	2.65	6.30	5.91	14.81	14.87	-0.42%
7	25.10	12.68	2.77	3.04	5.40	7.42	8.88	9.02	-1.52%
8	2.60	1.39	4.23	3.21	7.70	7.23	13.07	13.07	0.01%
9	30.00	22.36	2.43	2.47	4.79	6.10	13.37	13.46	-0.64%
10	52.90	39.27	0.26	0.26	2.83	4.24	13.34	13.46	-0.92%
11	12.90	6.33	3.52	3.55	6.01	7.42	9.47	9.58	-1.14%
12	24.20	11.92	2.12	2.17	4.46	5.74	9.51	9.57	-0.66%
13	19.50	10.70	0.28	0.32	1.85	2.91	9.84	10.22	-3.70%
14	16.20	10.86	2.80	3.09	5.60	7.70	11.84	12.00	-1.36%
15	2.70	1.61	1.89	1.40	4.17	4.04	13.87	13.92	-0.37%
16	0.70	0.41	7.00	5.25	11.37	10.27	13.81	13.98	-1.22%
17	11.80	7.15	2.51	2.74	4.34	5.88	10.88	11.12	-2.13%
18	22.60	13.71	0.88	0.97	3.14	4.76	10.89	11.12	-2.06%
19	6.80	3.68	10.50	8.01	13.65	11.46	13.18	13.28	-0.77%
20	1.30	0.85	2.30	1.72	5.41	5.35	14.52	14.64	-0.79%
21	38.00	24.82	0.21	0.20	1.90	2.89	12.31	12.62	-2.43%
22	37.00	30.09	1.25	1.28	4.46	6.22	14.00	14.23	-1.62%
23	22.00	9.91	1.40	1.45	3.60	4.81	8.44	8.63	-2.22%
24	14.90	7.92	4.24	4.28	7.57	9.57	10.34	10.45	-1.06%
25	11.70	6.94	1.40	1.40	4.35	6.05	11.44	11.60	-1.38%
26	67.50	26.98	6.11	6.26	9.13	10.94	6.86	6.94	-1.15%

27	62.90	24.73	6.10	6.12	8.75	10.34	6.63	6.94	-4.47%
28	N/A	N/A	N/A	N/A	N/A	N/A	N/A	N/A	N/A
29	N/A	N/A	N/A	N/A	N/A	N/A	N/A	N/A	N/A
30	6.40	6.93	0.12	0.09	1.40	1.55	17.04	17.91	-4.84%
31	6.40	5.75	0.02	0.02	0.80	0.87	16.25	17.91	-9.25%
32	N/A	N/A	N/A	N/A	N/A	N/A	N/A	N/A	N/A
33	N/A	N/A	N/A	N/A	N/A	N/A	N/A	N/A	N/A
34	26.90	25.27	0.10	0.08	0.90	1.04	16.45	17.28	-4.83%
35	6.50	8.26	0.00	0.00	0.80	1.04	17.61	18.49	-4.78%
36	7000.00	6927.84	0.00	0.00	1.60	2.43	15.23	15.37	-0.94%
37	3077.00	5034.04	0.00	0.00	1.44	2.28	17.47	15.38	13.60%
38	-0.20	-0.19	5.20	4.01	6.80	5.85	16.43	16.47	-0.26%
39	0.40	0.37	1.40	1.06	3.50	3.55	16.40	16.47	-0.42%
40	3222.00	4913.16	0.06	0.07	2.40	3.72	17.22	14.58	18.12%
41	5348.00	7145.38	0.03	0.03	1.06	1.74	16.70	16.14	3.48%
42	4.70	3.36	-0.12	-0.09	0.37	0.48	15.05	15.81	-4.83%
43	12.00	10.67	1.55	1.18	2.50	2.29	16.20	17.09	-5.23%

Table A- 19. Emissions Results for Injector 5

Std order	CO		NO		NOx		%O2 Measured	% O2 Expected	% O2 Deviation
	[ppm]	[ng/J]	[ppm]	[ng/J]	[ppm]	[ng/J]			
1	20.60	11.80	5.70	5.80	9.70	11.86	11.10	10.73	3.43%
2	32.30	17.96	2.40	2.44	5.40	7.10	10.81	10.74	0.64%
3	17.00	11.62	14.90	15.17	18.98	21.44	12.69	12.47	1.76%
4	22.80	15.66	8.40	8.54	12.50	14.85	12.73	12.43	2.42%
5	369.00	298.31	1.98	2.17	6.50	9.86	13.39	13.07	2.47%
6	0.10	0.07	12.50	9.52	16.20	13.99	14.92	14.87	0.32%
7	41.80	21.88	2.90	3.20	6.20	8.78	9.30	9.02	3.14%

8	-0.80	-0.46	14.60	11.06	20.20	17.50	13.65	13.07	4.45%
9	64.50	51.71	9.00	9.11	13.80	16.47	13.90	13.46	3.30%
10	109.00	87.76	4.50	4.49	9.90	13.07	13.93	13.46	3.46%
11	24.40	11.95	9.30	9.40	12.50	14.37	9.44	9.58	-1.46%
12	37.70	19.34	6.90	6.98	11.10	13.54	9.96	9.57	4.04%
13	120.00	69.39	0.63	0.74	2.70	4.06	10.40	10.22	1.78%
14	36.00	25.62	6.13	6.71	11.10	15.00	12.37	12.00	3.06%
15	1.10	0.72	8.40	6.32	13.90	12.66	14.52	13.92	4.30%
16	0.10	0.07	20.70	15.72	26.20	21.92	14.60	13.98	4.43%
17	31.20	19.96	4.96	5.42	7.81	10.24	11.41	11.12	2.64%
18	66.00	40.27	0.70	0.78	3.40	5.19	10.95	11.12	-1.52%
19	3.40	1.99	20.80	15.73	25.90	21.58	13.75	13.28	3.52%
20	0.40	0.29	10.50	7.89	16.90	15.41	15.16	14.64	3.58%
21	150.00	107.64	2.70	2.77	6.93	9.27	13.08	12.62	3.67%
22	68.00	60.47	10.60	10.68	16.20	19.43	14.59	14.23	2.53%
23	44.00	20.78	5.50	5.62	8.40	10.11	9.02	8.63	4.50%
24	21.60	12.05	12.30	12.50	16.80	19.36	10.84	10.45	3.73%
25	21.80	13.71	6.80	6.88	11.10	13.48	11.98	11.60	3.27%
26	101.00	40.80	9.40	9.57	11.80	13.02	7.01	6.94	1.01%
27	100.00	40.90	10.70	10.83	13.60	15.26	7.18	6.94	3.46%
28	3500.00	6703.22	0.60	0.62	13.00	20.40	17.97	17.12	4.95%
29	3962.00	8753.14	0.50	0.47	10.30	16.05	18.36	17.12	7.21%
30	6.40	9.39	2.60	2.04	19.30	21.77	18.05	17.91	0.80%
31	6.40	9.69	3.20	2.44	18.20	20.07	18.14	17.91	1.31%
32	4000.00	7634.77	0.60	0.61	8.20	12.51	17.96	16.36	9.79%
33	3200.00	8016.50	0.50	0.54	10.30	16.15	18.66	17.85	4.52%
34	21.60	26.48	1.60	1.31	11.50	12.77	17.49	17.28	1.19%
35	4.00	7.37	3.90	2.96	19.40	21.69	18.63	18.49	0.73%

36	2600.00	2805.78	2.40	2.43	11.80	17.12	15.70	15.37	2.12%
37	5400.00	6012.38	0.00	0.00	8.00	12.78	15.86	15.38	3.13%
38	0.20	0.19	16.90	12.91	19.70	16.23	16.56	16.47	0.53%
39	0.40	0.38	10.10	7.88	13.60	11.79	16.52	16.47	0.31%
40	6300.00	6534.71	0.09	0.09	6.30	9.82	15.49	14.58	6.26%
41	1180.00	1452.11	7.20	7.39	15.80	21.11	16.34	16.14	1.25%
42	32.10	27.22	7.30	5.55	10.50	9.30	15.97	15.81	0.98%
43	16.00	18.63	26.30	20.10	31.50	26.21	17.31	17.09	1.27%

Table A- 20. Emissions Results for Injector 6

Std order	CO		NO		NOx		%O2 Measured	% O2 Expected	% O2 Deviation
	[ppm]	[ng/J]	[ppm]	[ng/J]	[ppm]	[ng/J]			
1	10.70	6.13	4.48	4.54	7.30	8.86	11.10	10.73	3.43%
2	20.00	11.50	1.90	1.91	4.50	5.97	11.14	10.74	3.72%
3	14.50	10.15	13.20	13.35	17.20	19.56	12.88	12.47	3.28%
4	12.00	8.22	5.70	5.73	10.00	12.47	12.71	12.43	2.26%
5	4000.00	8149.52	0.17	0.17	5.70	9.60	17.92	13.07	37.13%
6	0.30	0.22	9.60	7.29	12.90	11.00	15.18	14.87	2.07%
7	22.00	11.49	4.90	5.37	8.20	10.89	9.27	9.02	2.80%
8	0.20	0.11	15.30	11.63	20.50	17.69	13.54	13.07	3.60%
9	41.00	32.27	6.90	6.92	10.20	12.21	13.77	13.46	2.33%
10	65.00	51.16	1.60	1.60	4.80	6.64	13.77	13.46	2.27%
11	10.00	5.14	8.40	8.43	11.50	13.32	9.98	9.58	4.18%
12	19.50	10.02	4.77	4.79	8.00	9.93	9.98	9.57	4.25%
13	27.00	15.63	1.45	1.62	4.54	6.73	10.41	10.22	1.88%
14	17.60	12.40	5.20	5.74	9.12	12.32	12.28	12.00	2.31%
15	0.00	0.00	6.80	5.12	10.20	9.20	14.34	13.92	3.01%
16	0.50	0.31	25.70	19.38	32.05	26.69	14.24	13.98	1.86%

17	19.60	12.59	5.40	5.92	8.70	11.40	11.45	11.12	3.00%
18	21.30	13.56	2.50	2.66	5.40	7.57	11.36	11.12	2.17%
19	37.30	21.57	25.00	18.91	31.00	25.83	13.67	13.28	2.92%
20	0.00	0.00	8.50	6.40	12.80	11.47	14.95	14.64	2.14%
21	83.00	58.73	1.00	0.99	4.30	6.09	12.97	12.62	2.80%
22	37.40	32.59	3.20	3.27	5.90	7.41	14.46	14.23	1.62%
23	20.00	9.46	3.50	3.55	6.50	8.12	9.03	8.63	4.61%
24	13.00	7.22	10.30	10.42	14.70	17.26	10.80	10.45	3.35%
25	11.00	6.86	4.70	4.75	8.30	10.37	11.90	11.60	2.58%
26	52.00	21.66	9.50	9.65	13.30	15.59	7.43	6.94	7.06%
27	47.00	19.48	8.94	9.02	12.60	14.69	7.36	6.94	6.05%
28	N/A	N/A	N/A	N/A	N/A	N/A	N/A	N/A	N/A
29	N/A	N/A	N/A	N/A	N/A	N/A	N/A	N/A	N/A
30	6.00	9.91	0.10	0.18	2.50	2.89	18.37	17.91	2.59%
31	4.80	7.78	0.14	0.10	2.10	2.34	18.32	17.91	2.31%
32	N/A	N/A	N/A	N/A	N/A	N/A	N/A	N/A	N/A
33	N/A	N/A	N/A	N/A	N/A	N/A	N/A	N/A	N/A
34	72.40	99.89	0.00	0.00	1.70	2.10	17.87	17.28	3.39%
35	2.80	6.26	0.20	0.24	1.60	2.07	19.03	18.49	2.89%
36	5555.00	8805.70	0.32	0.31	3.28	4.99	17.36	15.37	12.91%
37	3260.00	8629.09	0.15	0.17	2.40	3.82	18.78	15.38	22.12%
38	0.00	0.00	10.60	8.17	12.70	10.53	16.84	16.47	2.23%
39	0.20	0.20	3.00	2.28	5.00	4.61	16.78	16.47	1.89%
40	3600.00	7509.88	0.31	0.31	2.70	3.94	18.21	14.58	24.91%
41	3846.00	9507.50	0.10	0.11	2.10	3.59	18.63	16.14	15.44%
42	28.50	25.35	2.50	1.87	4.30	4.12	16.20	15.81	2.44%
43	19.50	23.84	2.60	2.10	4.40	4.10	17.48	17.09	2.26%

Table A- 21. Emissions Results for Injector 7

Std order	CO		NO		NOx		%O2 Measured	% O2 Expected	% O2 Deviation
	[ppm]	[ng/J]	[ppm]	[ng/J]	[ppm]	[ng/J]			
1	8.10	4.58	0.10	0.12	1.30	1.97	10.97	10.73	2.22%
2	11.80	6.76	0.00	0.00	0.90	1.41	11.10	10.74	3.34%
3	7.40	5.22	0.80	0.73	2.40	3.31	12.94	12.47	3.77%
4	9.40	6.48	0.09	0.09	1.40	2.21	12.76	12.43	2.66%
5	N/A	N/A	N/A	N/A	N/A	N/A	N/A	N/A	N/A
6	0.40	0.29	0.25	0.19	1.90	2.05	15.16	14.87	1.94%
7	19.30	10.10	0.60	0.67	2.40	3.68	9.30	9.02	3.14%
8	0.90	0.51	0.45	0.36	3.10	3.41	13.48	13.07	3.14%
9	16.70	13.16	0.08	0.08	0.99	1.51	13.78	13.46	2.41%
10	26.40	20.81	0.00	0.00	0.60	0.90	13.78	13.46	2.34%
11	9.80	5.01	1.03	1.04	3.02	4.15	9.93	9.58	3.66%
12	18.00	9.10	0.60	0.65	2.60	3.72	9.80	9.57	2.37%
13	21.60	12.76	0.02	0.03	0.90	1.54	10.62	10.22	3.94%
14	14.40	10.21	0.00	0.00	0.90	1.51	12.34	12.00	2.81%
15	0.20	0.13	0.13	0.09	1.70	1.91	14.26	13.92	2.44%
16	0.30	0.19	0.80	0.61	3.70	3.94	14.30	13.98	2.29%
17	16.20	10.55	0.00	0.00	0.70	1.18	11.58	11.12	4.16%
18	17.00	10.82	0.00	0.00	0.90	1.46	11.36	11.12	2.17%
19	0.40	0.23	1.70	1.24	4.10	4.18	13.67	13.28	2.92%
20	0.40	0.28	0.26	0.19	1.90	2.06	14.88	14.64	1.67%
21	41.80	29.39	0.03	0.03	0.60	0.91	12.92	12.62	2.40%
22	20.90	18.30	0.08	0.08	0.80	1.25	14.49	14.23	1.83%
23	17.00	8.01	0.60	0.61	2.40	3.39	8.99	8.63	4.15%
24	11.80	6.56	0.70	0.71	2.80	3.99	10.80	10.45	3.35%

25	8.60	5.36	0.09	0.09	1.30	1.89	11.89	11.60	2.49%
26	51.10	21.07	4.90	4.95	7.30	8.60	7.29	6.94	5.04%
27	45.90	18.91	4.15	4.20	6.90	8.45	7.28	6.94	4.90%
28	N/A	N/A	N/A	N/A	N/A	N/A	N/A	N/A	N/A
29	N/A	N/A	N/A	N/A	N/A	N/A	N/A	N/A	N/A
30	2.30	3.70	0.00	0.00	0.50	0.53	18.30	17.91	2.20%
31	1.60	2.53	0.14	0.10	0.40	0.47	18.26	17.91	1.98%
32	N/A	N/A	N/A	N/A	N/A	N/A	N/A	N/A	N/A
33	N/A	N/A	N/A	N/A	N/A	N/A	N/A	N/A	N/A
34	3.60	4.70	0.12	0.08	0.30	0.28	17.70	17.28	2.40%
35	2.10	4.53	0.00	0.00	0.40	0.71	18.96	18.49	2.51%
36	550.00	3547.53	0.00	0.00	0.63	1.16	20.03	15.37	30.28%
37	N/A	N/A	N/A	N/A	N/A	N/A	N/A	N/A	N/A
38	0.00	0.00	1.07	0.77	1.55	1.37	16.80	16.47	1.99%
39	0.30	0.31	0.20	0.15	0.90	0.92	16.80	16.47	2.01%
40	N/A	N/A	N/A	N/A	N/A	N/A	N/A	N/A	N/A
41	N/A	N/A	N/A	N/A	N/A	N/A	N/A	N/A	N/A
42	2.20	1.95	0.14	0.09	0.80	0.97	16.18	15.81	2.31%
43	0.40	0.49	0.40	0.26	1.00	1.07	17.50	17.09	2.38%

Table A- 22. Emissions Results for Injector 8

Std order	CO		NO		NOx		%O2 Measured	% O2 Expected	% O2 Deviation
	[ppm]	[ng/J]	[ppm]	[ng/J]	[ppm]	[ng/J]			
1	22.40	12.06	4.40	4.33	8.20	10.34	10.48	10.73	-2.35%
2	41.00	22.45	2.30	2.29	5.50	7.32	10.65	10.74	-0.85%
3	20.10	13.18	10.40	10.33	13.96	16.13	12.34	12.47	-1.05%
4	27.80	18.06	5.90	5.92	10.50	12.95	12.26	12.43	-1.36%
5	385.00	291.46	2.34	2.52	7.30	10.83	12.88	13.07	-1.43%

6	0.70	0.48	7.30	5.49	12.40	11.32	14.78	14.87	-0.62%
7	52.20	26.19	3.90	4.30	7.20	9.90	8.80	9.02	-2.41%
8	0.30	0.16	9.75	7.41	14.70	12.98	13.03	13.07	-0.30%
9	83.10	62.09	6.10	6.17	10.40	12.91	13.39	13.46	-0.49%
10	117.00	87.66	3.20	3.29	8.20	11.03	13.41	13.46	-0.40%
11	21.20	10.40	8.10	8.15	11.80	13.86	9.46	9.58	-1.25%
12	39.80	19.47	5.50	5.66	9.15	11.16	9.43	9.57	-1.49%
13	463.00	256.95	0.20	0.24	2.60	4.24	9.96	10.22	-2.52%
14	34.50	23.02	6.30	6.87	10.80	14.42	11.80	12.00	-1.69%
15	1.90	1.15	5.40	4.08	10.10	9.53	13.98	13.92	0.42%
16	0.60	0.36	13.90	10.44	19.90	17.35	13.86	13.98	-0.86%
17	37.70	23.07	4.00	4.40	7.14	9.61	10.98	11.12	-1.23%
18	56.70	34.29	2.54	2.76	6.00	8.55	10.86	11.12	-2.33%
19	4.80	2.64	14.20	10.75	19.80	17.25	13.31	13.28	0.21%
20	1.00	0.66	5.50	4.19	10.20	9.28	14.52	14.64	-0.79%
21	143.00	95.99	2.30	2.30	6.50	8.91	12.54	12.62	-0.61%
22	90.00	73.73	6.90	6.94	12.70	15.94	14.05	14.23	-1.27%
23	45.50	20.67	4.40	4.47	7.90	9.93	8.55	8.63	-0.95%
24	23.50	12.44	9.20	9.31	14.00	16.77	10.30	10.45	-1.44%
25	22.10	13.15	5.20	5.29	9.50	11.97	11.47	11.60	-1.13%
26	122.00	48.49	9.90	10.10	13.30	15.21	6.78	6.94	-2.31%
27	112.00	44.35	9.09	9.20	12.50	14.55	6.73	6.94	-3.03%
28	3470.00	6761.14	0.40	0.42	13.10	20.87	18.02	17.12	5.24%
29	2530.00	7887.35	0.07	0.07	4.90	7.63	19.10	17.12	11.54%
30	6.80	9.64	1.02	0.76	10.70	11.92	17.95	17.91	0.25%
31	10.80	15.46	1.45	1.07	11.70	13.05	17.98	17.91	0.41%
32	3680.00	7792.65	-0.14	-0.14	8.50	13.27	18.25	16.36	11.57%
33	2482.00	8597.45	0.29	0.30	4.60	7.23	19.28	17.85	8.00%

34	50.30	60.08	0.70	0.51	7.60	8.54	17.40	17.28	0.67%
35	5.10	9.15	2.90	2.31	12.10	13.20	18.57	18.49	0.41%
36	3000.00	3194.43	1.30	1.37	10.30	15.51	15.63	15.37	1.66%
37	6214.00	6850.72	0.00	0.00	7.80	12.11	15.81	15.38	2.81%
38	0.40	0.38	9.90	7.59	13.50	11.83	16.53	16.47	0.35%
39	0.70	0.66	5.20	3.93	9.30	8.77	16.45	16.47	-0.12%
40	6212.00	6235.95	0.07	0.06	6.02	9.35	15.31	14.58	5.02%
41	3000.00	3651.77	1.60	1.57	11.90	17.94	16.29	16.14	0.94%
42	45.80	38.29	4.30	3.32	7.70	7.29	15.90	15.81	0.54%
43	72.90	81.93	12.70	9.76	17.30	15.14	17.18	17.09	0.51%

Table A- 23. Emissions Results for Injector 9

Std order	CO		NO		NOx		%O2 Measured	% O2 Expected	% O2 Deviation
	[ppm]	[ng/J]	[ppm]	[ng/J]	[ppm]	[ng/J]			
1	15.00	8.52	3.05	3.08	5.90	7.59	11.02	10.73	2.69%
2	25.30	14.41	1.70	1.77	4.70	6.26	11.05	10.74	2.88%
3	17.40	12.01	8.70	8.81	11.77	13.58	12.77	12.47	2.40%
4	18.90	12.89	5.15	5.25	9.00	11.09	12.67	12.43	1.94%
5	700.00	554.83	1.10	1.19	5.40	8.34	13.24	13.07	1.32%
6	0.20	0.15	8.80	6.67	12.90	11.47	15.19	14.87	2.14%
7	36.50	19.07	4.10	4.54	7.11	9.51	9.28	9.02	2.91%
8	4.10	2.30	8.40	6.31	13.00	11.73	13.44	13.07	2.84%
9	77.00	60.94	5.90	5.94	9.80	12.17	13.81	13.46	2.63%
10	100.00	78.48	2.44	2.48	6.40	8.60	13.75	13.46	2.12%
11	14.20	7.29	5.50	5.56	8.50	10.19	9.97	9.58	4.08%
12	29.00	14.81	3.70	3.72	6.80	8.50	9.91	9.57	3.52%
13	45.00	24.55	1.40	1.46	4.10	5.67	9.77	10.22	-4.38%
14	26.00	18.23	5.90	6.46	9.20	12.10	12.24	12.00	1.97%

15	2.50	1.57	4.40	3.31	8.20	7.75	14.26	13.92	2.44%
16	0.30	0.19	14.80	11.17	20.30	17.52	14.20	13.98	1.57%
17	33.90	21.64	4.80	5.20	7.50	9.70	11.39	11.12	2.46%
18	36.60	23.29	2.70	3.00	5.90	8.32	11.36	11.12	2.17%
19	0.70	0.40	11.20	8.42	15.20	13.03	13.61	13.28	2.47%
20	0.00	0.00	5.90	4.46	10.40	9.78	14.97	14.64	2.28%
21	131.00	93.29	1.50	1.53	4.80	6.67	13.02	12.62	3.19%
22	81.80	70.95	5.50	5.67	10.60	13.35	14.43	14.23	1.40%
23	30.30	14.29	2.70	2.73	5.20	6.60	9.00	8.63	4.26%
24	17.60	9.82	7.24	7.36	10.90	13.21	10.84	10.45	3.73%
25	16.50	10.24	3.90	3.93	7.40	9.22	11.86	11.60	2.24%
26	76.80	31.83	6.90	6.98	9.80	11.46	7.36	6.94	6.05%
27	72.00	29.93	6.23	6.33	9.30	11.10	7.40	6.94	6.63%
28	3000.00	7287.73	0.30	0.31	8.90	14.18	18.59	17.12	8.57%
29	N/A	N/A	N/A	N/A	N/A	N/A	N/A	N/A	N/A
30	5.60	8.61	1.90	1.48	17.60	19.38	18.18	17.91	1.53%
31	10.40	16.41	1.68	1.30	14.40	16.64	18.25	17.91	1.92%
32	2000.00	6235.06	0.50	0.47	4.60	6.91	19.10	16.36	16.76%
33	N/A	N/A	N/A	N/A	N/A	N/A	N/A	N/A	N/A
34	87.00	112.60	0.40	0.28	9.30	10.47	17.67	17.28	2.23%
35	5.30	10.76	0.50	0.44	5.85	7.09	18.84	18.49	1.87%
36	3580.00	4050.27	0.90	0.97	10.40	15.63	15.94	15.37	3.68%
37	5900.00	8948.15	0.29	0.29	4.20	6.81	17.20	15.38	11.85%
38	0.40	0.41	13.60	10.49	16.90	14.37	16.84	16.47	2.23%
39	0.70	0.71	8.20	6.28	11.90	10.58	16.76	16.47	1.77%
40	6000.00	7566.14	0.30	0.27	4.70	7.30	16.45	14.58	12.84%
41	5400.00	7390.83	0.00	0.00	4.50	7.18	16.80	16.14	4.10%
42	10.50	9.32	5.30	4.00	8.40	7.78	16.19	15.81	2.37%

43	18.90	22.45	23.15	17.70	28.50	23.93	17.38	17.09	1.68%
----	-------	-------	-------	-------	-------	-------	-------	-------	-------

Table A- 24. Emissions Results for Injector 10

Std order	CO		NO		NOx		%O2 Measured	% O2 Expected	% O2 Deviation
	[ppm]	[ng/J]	[ppm]	[ng/J]	[ppm]	[ng/J]			
1	10.60	5.84	3.10	3.13	5.96	7.56	10.72	10.73	-0.11%
2	18.50	10.37	0.90	0.90	3.40	4.76	10.89	10.74	1.39%
3	10.60	7.26	12.30	12.63	15.30	17.15	12.71	12.47	1.92%
4	12.20	8.17	3.40	3.45	6.54	8.33	12.52	12.43	0.73%
5	3696.00	9121.90	0.00	0.00	6.20	11.33	18.44	13.07	41.11%
6	0.00	0.00	6.80	4.69	10.50	9.72	15.17	14.87	2.00%
7	26.30	13.33	4.11	4.50	7.14	9.55	8.92	9.02	-1.08%
8	0.20	0.11	11.40	8.58	15.90	13.79	13.27	13.07	1.54%
9	38.50	29.88	4.30	4.33	7.20	8.91	13.67	13.46	1.59%
10	67.40	51.95	0.50	0.50	3.70	5.43	13.62	13.46	1.16%
11	13.60	6.83	8.00	8.12	11.40	13.39	9.72	9.58	1.47%
12	22.00	10.93	3.70	3.74	7.20	9.18	9.60	9.57	0.28%
13	27.60	15.53	0.96	1.03	3.01	4.46	10.11	10.22	-1.05%
14	17.70	12.10	3.43	3.71	7.10	9.92	12.02	12.00	0.14%
15	1.10	0.68	4.04	3.06	7.81	7.34	14.17	13.92	1.79%
16	0.10	0.06	18.90	14.27	24.50	20.67	14.15	13.98	1.21%
17	16.50	10.31	4.00	4.49	6.60	8.69	11.18	11.12	0.57%
18	23.40	14.51	1.40	1.53	4.24	6.23	11.11	11.12	-0.08%
19	28.40	16.09	23.30	17.55	28.86	24.05	13.52	13.28	1.79%
20	0.00	0.00	4.50	3.40	8.50	8.03	14.83	14.64	1.32%
21	81.70	56.32	0.40	0.44	3.40	4.97	12.76	12.62	1.13%
22	35.90	30.71	1.90	2.02	5.30	7.21	14.34	14.23	0.77%
23	24.20	11.09	3.04	3.06	5.80	7.32	8.65	8.63	0.21%

24	15.20	8.24	7.80	7.96	11.90	14.28	10.55	10.45	0.95%
25	11.90	7.27	3.00	3.08	6.30	8.18	11.71	11.60	0.94%
26	67.50	27.33	9.20	9.29	13.10	15.53	7.04	6.94	1.44%
27	64.40	25.70	9.15	9.20	12.30	14.04	6.84	6.94	-1.44%
28	N/A	N/A	N/A	N/A	N/A	N/A	N/A	N/A	N/A
29	N/A	N/A	N/A	N/A	N/A	N/A	N/A	N/A	N/A
30	2.10	3.40	0.00	0.00	2.40	2.92	18.32	17.91	2.31%
31	1.70	2.73	0.09	0.07	1.99	2.34	18.30	17.91	2.20%
32	N/A	N/A	N/A	N/A	N/A	N/A	N/A	N/A	N/A
33	N/A	N/A	N/A	N/A	N/A	N/A	N/A	N/A	N/A
34	14.10	17.92	0.11	0.08	2.40	2.67	17.61	17.28	1.88%
35	1.80	3.80	0.00	0.00	1.60	2.08	18.92	18.49	2.30%
36	3000.00	3313.91	0.00	0.00	3.40	5.25	15.82	15.37	2.90%
37	2600.00	7972.70	0.12	0.13	2.60	4.46	19.07	15.38	24.01%
38	0.00	0.00	8.40	6.46	6.00	3.62	16.81	16.47	2.05%
39	0.10	0.10	1.80	1.31	4.30	4.30	16.78	16.47	1.89%
40	3180.00	7529.42	0.00	0.00	3.40	5.05	18.53	14.58	27.11%
41	4300.00	10869.22	0.00	0.00	2.26	3.94	18.68	16.14	15.75%
42	0.60	0.52	2.20	1.69	4.10	3.84	16.12	15.81	1.93%
43	0.30	0.36	2.70	2.03	4.90	4.56	17.37	17.09	1.62%

Table A- 25. Emissions Results for Injector 11

Std order	CO		NO		NOx		%O2 Measured	% O2 Expected	% O2 Deviation
	[ppm]	[ng/J]	[ppm]	[ng/J]	[ppm]	[ng/J]			
1	15.50	8.99	3.80	3.86	7.10	8.90	11.23	10.73	4.64%
2	27.70	16.04	1.40	1.37	4.30	5.92	11.21	10.74	4.37%
3	19.20	13.67	13.40	13.28	16.50	18.42	13.02	12.47	4.41%
4	20.00	14.15	6.60	6.75	10.80	13.37	12.97	12.43	4.35%

5	600.00	490.29	1.20	1.31	5.80	8.95	13.47	13.07	3.08%
6	0.10	0.08	9.80	7.42	14.40	12.72	15.34	14.87	3.15%
7	30.90	16.40	2.40	2.62	5.00	6.97	9.46	9.02	4.91%
8	0.30	0.17	11.20	8.47	16.10	14.24	13.65	13.07	4.45%
9	64.80	52.17	7.30	7.42	11.30	13.63	13.93	13.46	3.52%
10	96.30	77.53	3.30	3.37	7.80	10.36	13.93	13.46	3.46%
11	14.70	7.67	8.60	8.67	12.60	14.84	10.15	9.58	5.96%
12	27.30	14.17	4.30	4.34	7.60	9.45	10.09	9.57	5.40%
13	300.00	178.05	0.15	0.17	2.38	3.91	10.67	10.22	4.43%
14	27.40	19.57	5.50	5.97	8.70	11.36	12.40	12.00	3.31%
15	0.80	0.52	6.40	4.89	10.40	9.48	14.48	13.92	4.02%
16	0.60	0.38	15.70	11.92	22.10	19.16	14.36	13.98	2.72%
17	27.40	17.98	3.80	4.15	6.70	9.10	11.65	11.12	4.79%
18	43.10	27.87	0.90	1.04	3.80	5.81	11.51	11.12	3.51%
19	4.90	2.88	16.30	12.29	21.00	17.88	13.79	13.28	3.82%
20	0.20	0.15	7.10	5.47	11.90	10.96	15.16	14.64	3.58%
21	139.00	101.30	1.60	1.64	4.90	6.78	13.20	12.62	4.62%
22	64.90	57.81	8.20	8.40	14.00	17.17	14.60	14.23	2.60%
23	27.20	13.11	3.00	3.05	5.70	7.16	9.26	8.63	7.28%
24	18.40	10.41	10.00	10.19	14.00	16.40	10.98	10.45	5.07%
25	17.60	11.21	5.00	5.05	8.70	10.90	12.09	11.60	4.22%
26	81.50	34.13	9.20	9.29	12.70	14.65	7.50	6.94	8.07%
27	70.40	29.66	8.20	8.31	11.40	13.22	7.58	6.94	9.22%
28	3600.00	7891.25	0.60	0.61	12.90	20.17	18.34	17.12	7.11%
29	3863.00	10322.58	0.00	0.00	9.70	15.78	18.80	17.12	9.78%
30	8.60	14.27	2.30	1.78	22.70	25.72	18.38	17.91	2.65%
31	10.30	16.89	3.50	2.64	19.00	20.92	18.35	17.91	2.48%
32	4100.00	9202.95	0.00	0.00	9.00	14.36	18.40	16.36	12.48%

33	3400.00	10202.82	0.31	0.32	8.40	13.12	19.03	17.85	6.60%
34	43.80	59.84	1.20	0.88	11.20	12.98	17.84	17.28	3.21%
35	6.00	12.86	2.60	2.07	20.30	23.16	18.95	18.49	2.46%
36	2600.00	3171.75	2.30	2.48	11.10	17.29	16.30	15.37	6.02%
37	4500.00	5316.21	0.15	0.15	7.90	12.32	16.15	15.38	5.02%
38	0.40	0.43	15.30	11.81	18.80	16.01	16.99	16.47	3.14%
39	0.70	0.74	9.20	7.09	13.20	11.57	16.92	16.47	2.74%
40	6400.00	7139.95	0.40	0.36	5.50	8.59	15.87	14.58	8.86%
41	1188.00	1561.25	6.20	6.34	16.70	22.72	16.63	16.14	3.04%
42	25.00	22.97	5.70	4.43	9.00	8.20	16.35	15.81	3.39%
43	29.30	37.23	28.00	21.52	32.60	27.57	17.61	17.09	3.02%

Table A- 26. Emissions Results for Injector 12

Std order	CO		NO		NOx		%O2 Measured	% O2 Expected	% O2 Deviation
	[ppm]	[ng/J]	[ppm]	[ng/J]	[ppm]	[ng/J]			
1	23.10	13.35	3.80	3.78	6.80	8.52	11.19	10.73	4.27%
2	39.70	23.04	2.40	2.43	5.80	7.66	11.23	10.74	4.55%
3	27.80	19.85	8.80	8.95	12.05	13.87	13.04	12.47	4.57%
4	39.00	27.32	6.00	6.16	9.60	11.67	12.89	12.43	3.71%
5	645.00	522.84	1.60	1.74	6.80	10.51	13.41	13.07	2.62%
6	0.80	0.59	7.30	5.57	11.70	10.69	15.27	14.87	2.67%
7	45.10	23.91	4.30	4.72	7.30	9.67	9.45	9.02	4.80%
8	0.80	0.46	8.20	6.20	13.10	11.93	13.60	13.07	4.06%
9	113.00	90.46	5.60	5.66	10.10	12.75	13.89	13.46	3.23%
10	155.00	125.15	3.50	3.55	8.00	10.70	13.95	13.46	3.61%
11	16.00	8.30	7.10	7.12	10.50	12.47	10.08	9.58	5.23%
12	34.70	18.00	5.10	5.17	5.60	10.61	10.08	9.57	5.30%
13	1900.00	1154.72	0.10	0.13	2.30	3.72	10.91	10.22	6.78%

14	44.60	31.78	5.80	6.34	10.10	13.47	12.38	12.00	3.14%
15	3.30	2.15	4.40	3.28	8.60	8.18	14.47	13.92	3.94%
16	1.00	0.64	11.80	8.95	17.30	15.53	14.34	13.98	2.57%
17	52.40	34.28	4.20	4.56	7.10	9.49	11.62	11.12	4.52%
18	58.00	37.22	2.80	3.10	6.60	9.41	11.44	11.12	2.88%
19	3.60	2.12	10.80	8.14	15.10	13.16	13.80	13.28	3.90%
20	0.30	0.21	5.20	3.91	10.00	9.53	15.05	14.64	2.83%
21	244.00	175.99	1.80	1.86	5.70	7.89	13.12	12.62	3.99%
22	101.00	90.68	7.80	7.89	13.20	16.43	14.65	14.23	2.95%
23	34.80	16.69	4.00	3.96	6.50	7.97	9.20	8.63	6.58%
24	22.20	12.47	8.10	8.25	11.90	14.05	10.91	10.45	4.40%
25	25.50	16.26	4.80	4.85	8.30	10.40	12.10	11.60	4.30%
26	90.00	37.61	8.80	8.82	12.30	14.44	7.47	6.94	7.63%
27	77.30	32.25	8.00	8.10	10.60	12.00	7.45	6.94	7.35%
28	3200.00	6345.22	0.60	0.64	13.20	20.80	18.07	17.12	5.53%
29	4000.00	10440.10	0.20	0.28	9.00	14.41	18.75	17.12	9.49%
30	9.00	14.70	2.90	2.28	11.40	12.45	18.34	17.91	2.42%
31	14.40	23.52	2.40	1.93	11.40	12.37	18.34	17.91	2.42%
32	4388.00	9543.99	0.50	0.47	10.00	15.80	18.32	16.36	12.00%
33	3500.00	10123.93	0.00	0.00	8.60	14.23	18.96	17.85	6.20%
34	58.00	77.72	1.00	0.86	7.80	8.77	17.78	17.28	2.87%
35	5.70	11.97	11.90	9.01	22.60	22.10	18.91	18.49	2.24%
36	3300.00	3833.98	1.20	1.25	11.00	16.49	16.07	15.37	4.52%
37	5000.00	6046.93	0.13	0.13	8.20	13.02	16.26	15.38	5.73%
38	0.20	0.21	11.40	8.69	14.40	12.32	16.93	16.47	2.78%
39	0.70	0.73	5.60	4.14	9.80	9.09	16.89	16.47	2.56%
40	6000.00	6512.44	0.05	0.05	6.10	9.41	15.73	14.58	7.90%
41	2200.00	2911.65	4.50	4.54	15.20	21.47	16.66	16.14	3.23%

42	20.60	18.76	4.30	3.32	7.80	7.20	16.31	15.81	3.13%
43	34.20	42.68	12.80	9.77	16.90	14.68	17.55	17.09	2.67%

Table A- 27. Emissions Results for Injector 13

Std order	CO		NO		NOx		%O2 Measured	% O2 Expected	% O2 Deviation
	[ppm]	[ng/J]	[ppm]	[ng/J]	[ppm]	[ng/J]			
1	10.60	6.05	1.90	1.96	4.30	5.70	11.07	10.73	3.15%
2	17.90	10.34	0.60	0.56	2.90	4.25	11.19	10.74	4.18%
3	9.70	6.76	6.20	6.28	8.80	10.39	12.85	12.47	3.04%
4	13.00	8.85	2.70	2.70	5.70	7.39	12.66	12.43	1.86%
5	N/A	N/A	N/A	N/A	N/A	N/A	N/A	N/A	N/A
6	N/A	N/A	N/A	N/A	N/A	N/A	N/A	N/A	N/A
7	26.20	13.65	3.00	3.30	5.60	7.57	9.25	9.02	2.58%
8	0.40	0.23	4.00	3.02	7.50	7.09	13.48	13.07	3.14%
9	31.50	24.90	3.40	3.47	6.40	8.01	13.80	13.46	2.56%
10	66.80	52.50	0.60	0.67	3.00	4.41	13.76	13.46	2.20%
11	12.10	6.24	5.50	5.58	8.40	10.07	10.02	9.58	4.60%
12	22.70	11.59	2.80	2.79	5.30	6.73	9.91	9.57	3.52%
13	160.00	92.52	0.19	0.21	2.00	3.30	10.40	10.22	1.78%
14	16.00	11.20	2.00	2.25	5.50	7.99	12.23	12.00	1.89%
15	2.30	1.47	1.50	1.10	3.90	3.93	14.37	13.92	3.23%
16	0.30	0.19	7.80	5.97	12.70	11.46	14.29	13.98	2.22%
17	17.00	10.79	3.12	3.40	5.40	7.25	11.33	11.12	1.92%
18	22.80	14.59	1.40	1.51	4.10	6.13	11.41	11.12	2.61%
19	2.60	1.50	12.90	9.82	16.70	14.25	13.64	13.28	2.69%
20	0.00	0.00	2.60	1.97	5.80	5.68	14.99	14.64	2.42%
21	70.60	49.77	0.00	0.00	2.00	3.12	12.94	12.62	2.56%
22	35.70	31.11	1.30	1.31	4.20	5.74	14.46	14.23	1.62%

23	23.80	11.15	1.60	1.61	3.90	5.14	8.92	8.63	3.34%
24	14.50	8.01	4.70	4.74	7.80	9.54	10.74	10.45	2.77%
25	11.40	7.08	1.40	1.46	3.90	5.23	11.86	11.60	2.24%
26	69.70	28.97	6.50	6.59	9.10	10.62	7.40	6.94	6.63%
27	60.40	24.90	5.20	5.26	8.20	9.99	7.29	6.94	5.04%
28	N/A	N/A	N/A	N/A	N/A	N/A	N/A	N/A	N/A
29	N/A	N/A	N/A	N/A	N/A	N/A	N/A	N/A	N/A
30	N/A	N/A	N/A	N/A	N/A	N/A	N/A	N/A	N/A
31	4.00	6.64	0.05	0.04	1.70	1.89	18.38	17.91	2.65%
32	N/A	N/A	N/A	N/A	N/A	N/A	N/A	N/A	N/A
33	N/A	N/A	N/A	N/A	N/A	N/A	N/A	N/A	N/A
34	17.30	23.48	0.40	0.29	1.70	1.85	17.82	17.28	3.10%
35	3.10	6.29	0.30	0.22	1.80	1.88	18.84	18.49	1.87%
36	6600.00	8613.08	0.20	0.14	3.20	4.85	16.60	15.37	7.97%
37	4000.00	9431.18	0.20	0.25	2.40	3.73	18.52	15.38	20.43%
38	0.00	0.00	7.20	5.48	8.80	7.36	16.89	16.47	2.53%
39	0.40	0.41	1.80	1.44	3.70	3.65	16.86	16.47	2.37%
40	3200.00	7608.88	0.34	0.36	2.30	3.32	18.54	14.58	27.18%
41	5500.00	4029.18	0.14	0.05	1.70	0.94	13.24	16.14	-17.96%
42	2.30	2.07	1.20	0.87	2.70	2.64	16.25	15.81	2.75%
43	4.70	5.87	2.10	1.61	4.00	3.86	17.55	17.09	2.67%

Table A- 28. Emissions Results for Injector 14

Std order	CO		NO		NOx		%O2 Measured	% O2 Expected	% O2 Deviation
	[ppm]	[ng/J]	[ppm]	[ng/J]	[ppm]	[ng/J]			
1	9.50	5.29	0.20	0.18	1.80	2.74	10.82	10.73	0.82%
2	12.80	7.22	0.05	0.05	1.10	1.64	10.95	10.74	1.95%
3	8.30	5.78	2.40	2.46	4.40	5.43	12.84	12.47	2.96%

4	10.60	7.23	0.40	0.44	2.80	4.02	12.67	12.43	1.94%
5	N/A	N/A	N/A	N/A	N/A	N/A	N/A	N/A	N/A
6	0.40	0.29	0.30	0.23	2.30	2.53	15.04	14.87	1.13%
7	22.00	11.33	0.80	0.88	2.80	4.26	9.11	9.02	1.03%
8	0.00	0.00	1.20	0.89	3.90	4.08	13.37	13.07	2.30%
9	25.00	19.46	0.10	0.08	1.40	2.25	13.69	13.46	1.74%
10	40.60	31.64	0.00	0.00	0.80	1.28	13.70	13.46	1.75%
11	11.20	5.67	2.15	2.17	4.60	5.99	9.82	9.58	2.51%
12	20.90	10.58	0.70	0.76	2.90	4.00	9.82	9.57	2.58%
13	20.90	12.00	0.10	0.12	0.90	1.44	10.33	10.22	1.10%
14	15.40	10.66	0.10	0.15	1.60	2.65	12.13	12.00	1.06%
15	0.00	0.00	0.30	0.27	2.40	2.65	14.27	13.92	2.51%
16	0.30	0.19	2.30	1.73	5.50	5.51	14.18	13.98	1.43%
17	40.00	25.59	0.20	0.21	1.50	2.41	11.41	11.12	2.64%
18	18.10	11.39	0.05	0.07	1.10	1.72	11.25	11.12	1.18%
19	0.10	0.06	3.60	2.72	6.50	6.04	13.48	13.28	1.49%
20	0.00	0.00	0.40	0.30	2.50	2.70	14.90	14.64	1.80%
21	81.40	57.03	0.00	0.00	0.60	0.80	12.89	12.62	2.16%
22	27.80	24.11	0.10	0.09	1.50	2.37	14.43	14.23	1.40%
23	20.90	9.79	0.70	0.65	2.60	3.65	8.92	8.63	3.34%
24	13.10	7.19	1.60	1.59	4.20	5.64	10.68	10.45	2.20%
25	9.70	5.99	0.10	0.07	1.90	2.90	11.81	11.60	1.80%
26	68.50	27.92	5.50	5.55	7.97	9.36	7.13	6.94	2.74%
27	60.20	24.51	4.70	4.80	6.90	8.01	7.12	6.94	2.59%
28	N/A	N/A	N/A	N/A	N/A	N/A	N/A	N/A	N/A
29	N/A	N/A	N/A	N/A	N/A	N/A	N/A	N/A	N/A
30	N/A	N/A	N/A	N/A	N/A	N/A	N/A	N/A	N/A
31	N/A	N/A	N/A	N/A	N/A	N/A	N/A	N/A	N/A

32	N/A	N/A	N/A	N/A	N/A	N/A	N/A	N/A	N/A
33	N/A	N/A	N/A	N/A	N/A	N/A	N/A	N/A	N/A
34	N/A	N/A	N/A	N/A	N/A	N/A	N/A	N/A	N/A
35	N/A	N/A	N/A	N/A	N/A	N/A	N/A	N/A	N/A
36	N/A	N/A	N/A	N/A	N/A	N/A	N/A	N/A	N/A
37	N/A	N/A	N/A	N/A	N/A	N/A	N/A	N/A	N/A
38	N/A	N/A	N/A	N/A	N/A	N/A	N/A	N/A	N/A
39	N/A	N/A	N/A	N/A	N/A	N/A	N/A	N/A	N/A
40	N/A	N/A	N/A	N/A	N/A	N/A	N/A	N/A	N/A
41	N/A	N/A	N/A	N/A	N/A	N/A	N/A	N/A	N/A
42	N/A	N/A	N/A	N/A	N/A	N/A	N/A	N/A	N/A
43	N/A	N/A	N/A	N/A	N/A	N/A	N/A	N/A	N/A

Table A- 29. Emissions Results for Injector 15

Std order	CO		NO		NOx		%O2 Measured	% O2 Expected	% O2 Deviation
	[ppm]	[ng/J]	[ppm]	[ng/J]	[ppm]	[ng/J]			
1	13.80	7.71	4.20	4.19	6.90	8.41	10.86	10.73	1.20%
2	23.20	13.11	2.30	2.30	5.20	6.84	10.97	10.74	2.13%
3	18.10	12.52	9.50	9.72	12.10	13.69	12.79	12.47	2.56%
4	17.80	11.96	6.20	6.27	9.60	11.56	12.55	12.43	0.97%
5	459.00	361.45	1.60	1.77	5.90	9.00	13.19	13.07	0.94%
6	0.20	0.14	9.30	6.99	13.00	11.51	15.13	14.87	1.73%
7	32.60	16.72	4.80	5.28	7.70	10.15	9.06	9.02	0.47%
8	0.90	0.50	9.60	7.23	14.40	12.81	13.40	13.07	2.53%
9	66.50	51.76	6.40	6.59	10.80	13.36	13.69	13.46	1.74%
10	89.50	69.56	3.70	3.83	7.60	9.82	13.68	13.46	1.60%
11	14.30	7.24	7.20	7.27	10.20	12.00	9.81	9.58	2.41%
12	26.50	13.41	4.50	4.50	7.70	9.56	9.81	9.57	2.48%

13	64.80	37.19	1.20	1.29	3.40	4.96	10.32	10.22	1.00%
14	25.10	17.46	6.30	6.86	10.40	13.82	12.17	12.00	1.39%
15	1.60	1.01	5.40	4.13	9.40	8.69	14.28	13.92	2.58%
16	0.50	0.31	15.40	11.60	21.00	18.13	14.18	13.98	1.43%
17	29.40	18.77	5.20	5.68	7.70	9.97	11.39	11.12	2.46%
18	32.20	20.22	3.10	3.37	6.40	8.93	11.23	11.12	1.00%
19	2.50	1.43	14.50	10.94	18.30	15.43	13.57	13.28	2.17%
20	0.00	0.00	6.20	4.68	10.70	9.80	14.87	14.64	1.60%
21	127.00	89.31	2.20	2.26	5.60	7.45	12.92	12.62	2.40%
22	53.20	45.44	8.10	8.24	12.30	14.68	14.33	14.23	0.70%
23	27.70	12.85	3.60	3.68	6.10	7.41	8.80	8.63	1.95%
24	17.60	9.59	8.10	8.23	11.80	13.86	10.60	10.45	1.43%
25	14.80	9.11	5.00	5.14	8.00	9.69	11.78	11.60	1.55%
26	75.00	30.63	8.40	8.45	12.20	14.54	7.16	6.94	3.17%
27	68.90	28.20	7.60	7.68	10.00	11.44	7.19	6.94	3.60%
28	N/A	N/A	N/A	N/A	N/A	N/A	N/A	N/A	N/A
29	N/A	N/A	N/A	N/A	N/A	N/A	N/A	N/A	N/A
30	N/A	N/A	N/A	N/A	N/A	N/A	N/A	N/A	N/A
31	N/A	N/A	N/A	N/A	N/A	N/A	N/A	N/A	N/A
32	N/A	N/A	N/A	N/A	N/A	N/A	N/A	N/A	N/A
33	N/A	N/A	N/A	N/A	N/A	N/A	N/A	N/A	N/A
34	N/A	N/A	N/A	N/A	N/A	N/A	N/A	N/A	N/A
35	N/A	N/A	N/A	N/A	N/A	N/A	N/A	N/A	N/A
36	N/A	N/A	N/A	N/A	N/A	N/A	N/A	N/A	N/A
37	N/A	N/A	N/A	N/A	N/A	N/A	N/A	N/A	N/A
38	N/A	N/A	N/A	N/A	N/A	N/A	N/A	N/A	N/A
39	N/A	N/A	N/A	N/A	N/A	N/A	N/A	N/A	N/A
40	N/A	N/A	N/A	N/A	N/A	N/A	N/A	N/A	N/A

41	N/A	N/A	N/A	N/A	N/A	N/A	N/A	N/A	N/A
42	N/A	N/A	N/A	N/A	N/A	N/A	N/A	N/A	N/A
43	N/A	N/A	N/A	N/A	N/A	N/A	N/A	N/A	N/A

Table A- 30. Emissions Results for Injector 16

Std order	CO		NO		NOx		%O2 Measured	% O2 Expected	% O2 Deviation
	[ppm]	[ng/J]	[ppm]	[ng/J]	[ppm]	[ng/J]			
1	11.50	6.46	4.90	4.94	7.90	9.73	10.91	10.73	1.66%
2	22.80	12.83	6.70	6.82	10.40	12.54	10.93	10.74	1.76%
3	18.00	12.20	13.70	13.80	16.50	18.36	12.62	12.47	1.20%
4	14.50	9.77	8.20	8.30	11.80	13.94	12.57	12.43	1.13%
5	720.00	567.71	0.80	0.85	5.30	8.47	13.20	13.07	1.01%
6	0.00	0.00	15.70	11.98	20.20	17.10	15.14	14.87	1.80%
7	27.90	14.39	2.60	2.88	5.40	7.44	9.13	9.02	1.25%
8	0.40	0.22	14.40	10.95	19.60	16.99	13.41	13.07	2.61%
9	34.10	26.39	8.10	8.21	12.20	14.56	13.65	13.46	1.44%
10	57.60	44.89	4.40	4.51	8.40	10.65	13.70	13.46	1.75%
11	13.90	7.04	9.70	9.88	13.10	15.03	9.82	9.58	2.51%
12	26.90	13.66	5.30	5.39	8.90	11.05	9.85	9.57	2.89%
13	169.00	97.07	0.50	0.55	2.10	3.19	10.33	10.22	1.10%
14	18.20	12.63	5.50	6.03	9.50	12.74	12.15	12.00	1.22%
15	1.70	1.08	8.60	6.51	12.80	11.38	14.29	13.92	2.65%
16	0.10	0.06	24.80	18.74	31.00	26.19	14.18	13.98	1.43%
17	18.40	11.70	4.00	4.36	6.00	7.80	11.35	11.12	2.10%
18	30.10	18.98	1.00	1.08	3.50	5.32	11.27	11.12	1.36%
19	3.00	1.71	20.60	15.63	25.20	21.05	13.56	13.28	2.09%
20	0.50	0.35	11.40	8.64	16.50	14.56	14.88	14.64	1.67%

21	69.00	48.40	2.50	2.56	5.80	7.62	12.90	12.62	2.24%
22	39.50	34.21	10.50	10.58	15.11	10.72	14.42	14.23	1.33%
23	27.30	12.68	4.60	4.63	6.60	7.83	8.82	8.63	2.18%
24	16.30	8.93	10.60	10.81	14.46	16.70	10.66	10.45	2.01%
25	12.50	7.67	6.00	6.06	9.40	8.37	11.76	11.60	1.37%
26	79.70	32.53	9.80	9.84	13.60	15.87	7.15	6.94	3.02%
27	72.40	29.53	9.20	9.31	11.90	13.32	7.14	6.94	2.88%
28	N/A	N/A	N/A	N/A	N/A	N/A	N/A	N/A	N/A
29	N/A	N/A	N/A	N/A	N/A	N/A	N/A	N/A	N/A
30	N/A	N/A	N/A	N/A	N/A	N/A	N/A	N/A	N/A
31	N/A	N/A	N/A	N/A	N/A	N/A	N/A	N/A	N/A
32	N/A	N/A	N/A	N/A	N/A	N/A	N/A	N/A	N/A
33	N/A	N/A	N/A	N/A	N/A	N/A	N/A	N/A	N/A
34	N/A	N/A	N/A	N/A	N/A	N/A	N/A	N/A	N/A
35	N/A	N/A	N/A	N/A	N/A	N/A	N/A	N/A	N/A
36	N/A	N/A	N/A	N/A	N/A	N/A	N/A	N/A	N/A
37	N/A	N/A	N/A	N/A	N/A	N/A	N/A	N/A	N/A
38	N/A	N/A	N/A	N/A	N/A	N/A	N/A	N/A	N/A
39	N/A	N/A	N/A	N/A	N/A	N/A	N/A	N/A	N/A
40	N/A	N/A	N/A	N/A	N/A	N/A	N/A	N/A	N/A
41	N/A	N/A	N/A	N/A	N/A	N/A	N/A	N/A	N/A
42	N/A	N/A	N/A	N/A	N/A	N/A	N/A	N/A	N/A
43	N/A	N/A	N/A	N/A	N/A	N/A	N/A	N/A	N/A

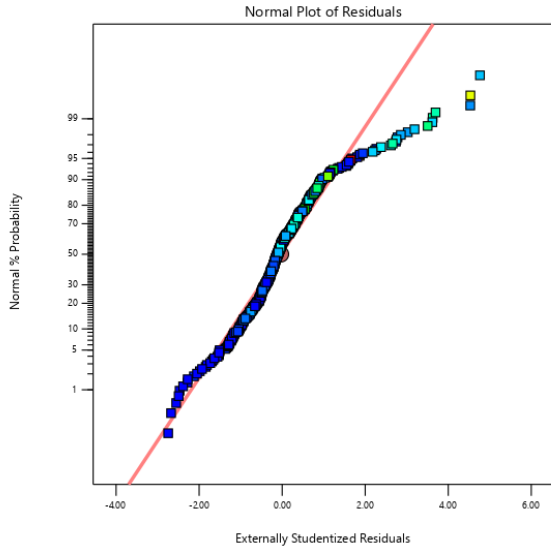


Figure A- 9. Normal Plot of Residuals for CO Model

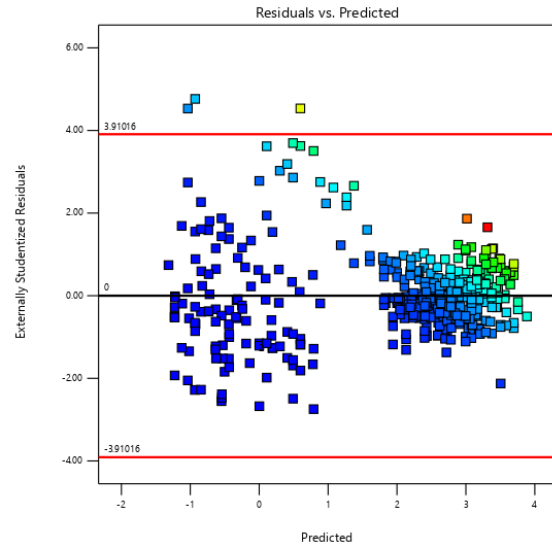


Figure A- 10. Residuals vs. Predicted for CO Model

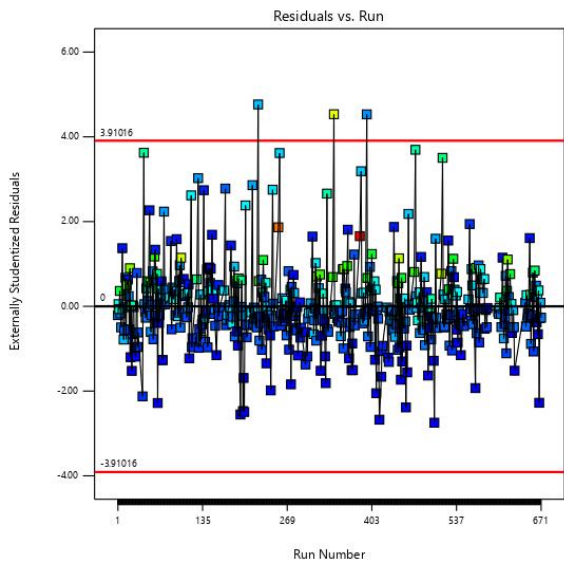


Figure A- 11. Residuals vs. Run for CO Model

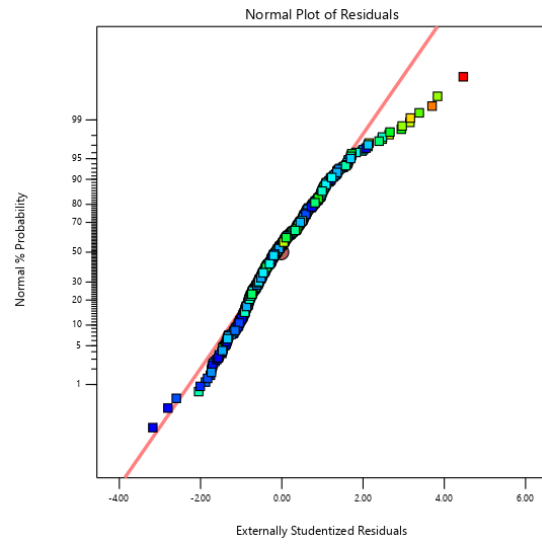


Figure A- 12. Normal Plot of Residuals for NO Model

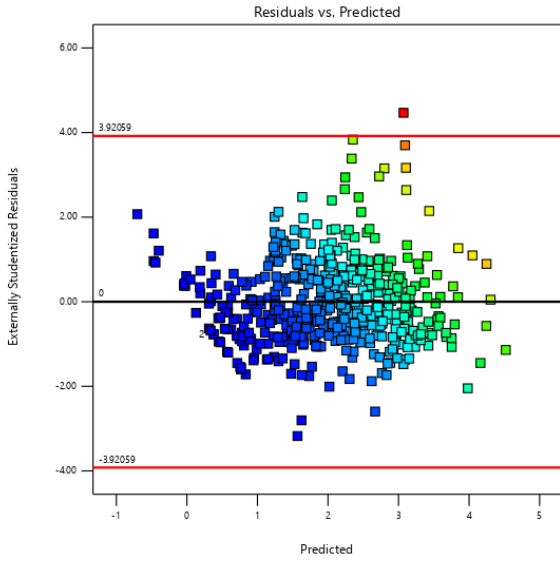


Figure A- 13. Residuals vs. Predicted for NO Model

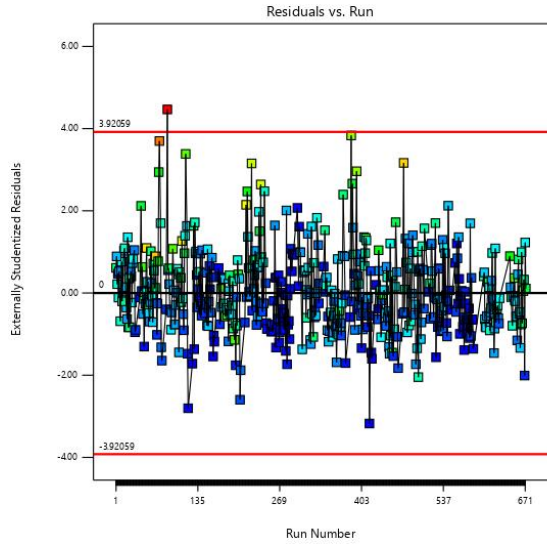


Figure A- 14. Residuals vs. Run for NO Model

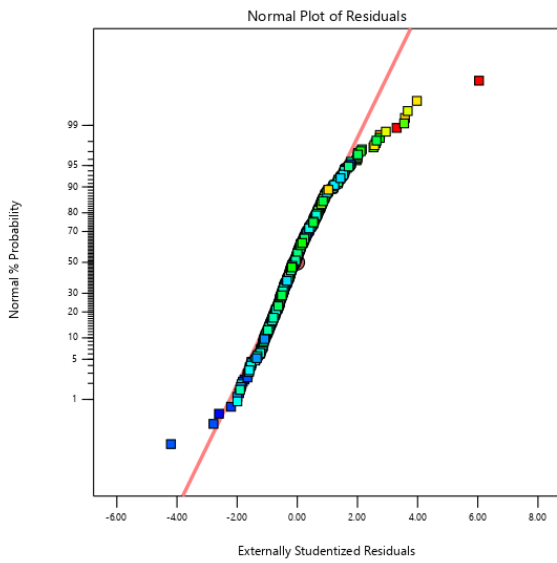


Figure A- 15. Normal Plot of Residuals for NOx Model

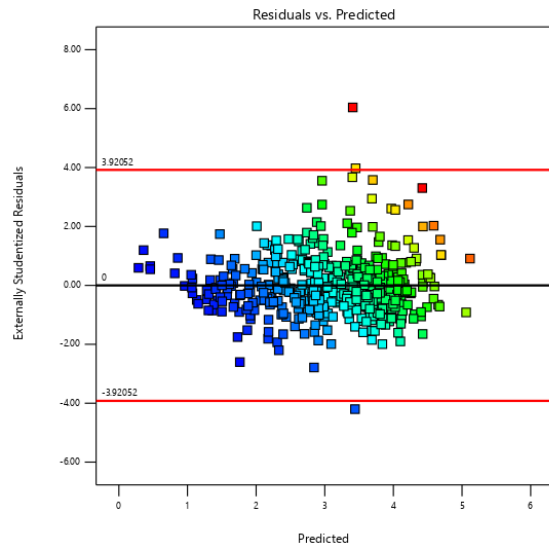


Figure A- 16. Residuals vs. Predicted for NOx Model

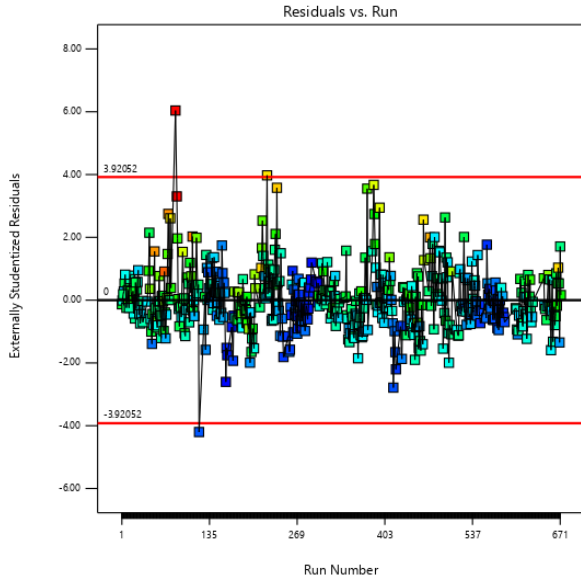


Figure A- 17. Residuals vs. Run for NOx Model

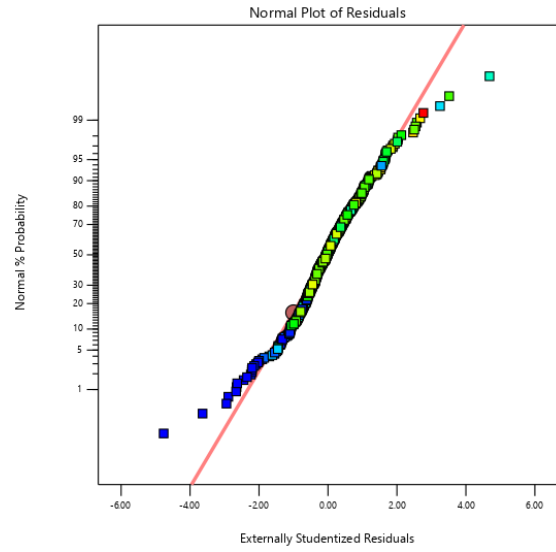


Figure A- 18. Normal Plot of Residuals for NO/NOx Model

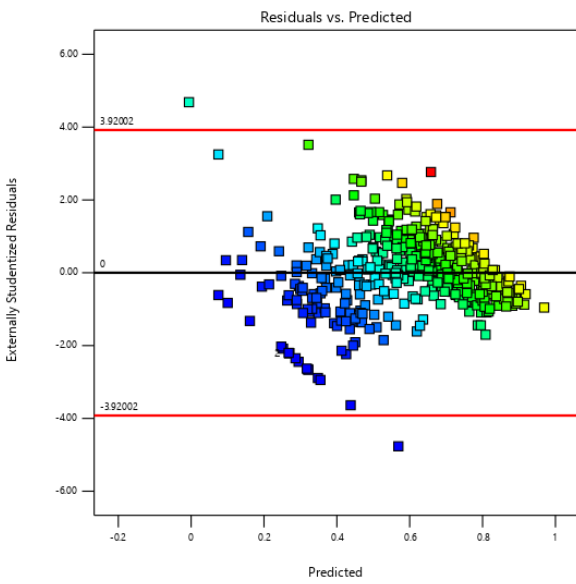


Figure A- 19. Residuals vs. Predicted for NO/NOx Model

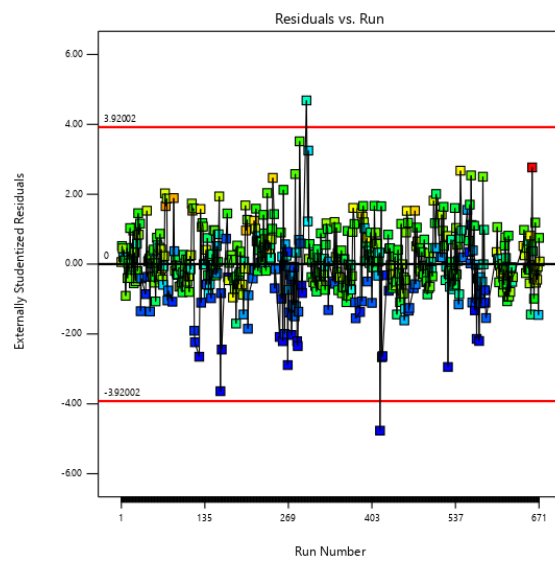


Figure A- 20. Residuals vs. Run for NO/NOx Model

Table A- 31. CO Emissions Experimental vs. CHEMKIN, 15% O2 ppmvd

STD Order	15% O2 ppmvd		
	Measured	CHEMKIN	Deviation, %
1	21.30	87.00	308%
2	31.90	126.22	296%
3	27.80	83.80	201%

4	26.20	92.22	252%
5	775.00	368.26	-52%
6	1.10	0.00	-100%
7	36.70	78.20	113%
8	1.00	0.00	-100%
9	102.00	263.00	158%
10	133.10	330.68	148%
11	16.00	27.10	69%
12	33.00	72.70	120%
13	69.20	128.00	85%
14	36.20	94.40	161%
15	2.80	0.00	-100%
16	-0.04	0.00	-100%
17	38.20	355.00	829%
18	42.30	146.51	246%
19	3.40	0.00	-100%
20	1.40	0.00	-100%
21	194.00	276.00	42%
22	96.40	270.20	180%
23	32.10	69.50	117%
24	19.90	41.10	107%
25	28.50	76.96	170%
26	83.00	369.00	345%
27	75.40	184.00	144%
28	2947.00	10022.39	240%
29	2234.00	3622.39	62%
30	3.60	0.00	-100%
31	3.50	0.00	-100%
32	2397.50	9410.00	292%

33	1711.00	3090.00	81%
34	36.20	0.00	-100%
35	3.50	0.00	-100%
36	3553.00	320.13	-91%
37	6640.00	2493.60	-62%
38	0.00	0.00	#DIV/0!
39	0.50	0.00	-100%
40	6264.00	3130.00	-50%
41	3551.40	2550.00	-28%
42	33.20	0.00	-100%
43	16.20	0.00	-100%

Table A- 32. NO Emissions Experimental vs. CHEMKIN, 15% O2 ppmvd

STD Order	15% O2 ppmvd		
	Measured	CHEMKIN	Deviation, %
1	3.52	6.06	-72%
2	1.79	5.50	-207%
3	10.93	6.06	45%
4	6.28	5.89	6%
5	0.92	1.04	-13%
6	15.10	12.20	19%
7	4.36	7.99	-83%
8	15.53	28.21	-82%
9	6.05	1.74	71%
10	2.68	1.57	41%
11	7.74	8.03	-4%
12	4.72	9.02	-91%
13	1.20	4.49	-274%

14	5.65	4.59	19%
15	8.78	12.30	-40%
16	26.47	29.60	-12%
17	4.14	5.10	-23%
18	2.59	4.67	-80%
19	20.58	26.50	-29%
20	11.42	13.55	-19%
21	1.41	1.47	-4%
22	7.44	1.63	78%
23	3.60	8.91	-148%
24	9.00	8.95	1%
25	4.56	5.49	-20%
26	8.93	76.31	-754%
27	8.40	38.10	-354%
28	-0.14	0.00	100%
29	2.64	0.00	100%
30	0.79	9.13	-1056%
31	0.30	0.44	-47%
32	-0.20	0.00	100%
33	-0.43	0.00	100%
34	-0.03	1.31	4451%
35	0.09	2.86	-3073%
36	0.43	10.42	-2323%
37	0.00	3.47	N/A
38	20.67	21.70	-5%
39	9.85	5.61	43%
40	0.00	3.24	N/A
41	-0.15	3.72	2580%

42	7.80	6.14	21%
43	14.76	7.76	47%

Table A- 33. NOx Emissions Experimental vs. CHEMKIN, 15% O2 ppmvd

STD Order	15% O2 ppmvd		
	Measured	CHEMKIN	Deviation, %
1	6.97	7.10	2%
2	4.66	6.53	40%
3	15.13	7.45	-51%
4	10.96	7.24	-34%
5	6.40	2.51	-61%
6	19.71	13.20	-33%
7	7.89	8.30	5%
8	22.13	29.20	32%
9	10.92	3.16	-71%
10	7.60	3.13	-59%
11	11.86	8.33	-30%
12	8.74	9.35	7%
13	4.31	5.48	27%
14	10.26	5.90	-42%
15	13.97	13.10	-6%
16	34.81	30.75	-12%
17	7.57	6.23	-18%
18	6.10	5.79	-5%
19	27.37	27.50	0%
20	17.44	14.58	-16%
21	5.57	2.85	-49%
22	13.85	3.49	-75%

23	6.90	9.19	33%
24	13.19	9.30	-29%
25	8.52	6.67	-22%
26	13.50	76.60	467%
27	12.29	38.20	211%
28	5.30	0.01	-100%
29	-0.24	0.00	-101%
30	11.34	9.18	-19%
31	4.22	0.79	-81%
32	3.38	0.02	-99%
33	0.91	0.00	-100%
34	5.41	1.62	-70%
35	2.58	3.35	30%
36	8.80	10.64	21%
37	4.46	4.19	-6%
38	24.55	22.89	-7%
39	13.40	6.65	-50%
40	4.07	3.80	-7%
41	5.50	4.56	-17%
42	11.55	7.27	-37%
43	18.02	9.26	-49%

Table A- 34. CO Emissions Experimental vs. CHEMKIN Model, ng/J

STD Order	Ng/J		
	Measured	CHEMKIN	Deviation, %
1	11.65	48.01	312%
2	17.64	69.72	295%
3	18.48	55.79	202%

4	17.18	61.09	256%
5	593.36	285.46	-52%
6	0.76	0.00	-100%
7	18.63	39.96	114%
8	0.54	0.00	-100%
9	76.11	198.25	160%
10	99.32	247.54	149%
11	7.96	13.43	69%
12	16.36	36.02	120%
13	39.23	72.75	85%
14	24.45	64.42	164%
15	1.69	0.00	-100%
16	-0.02	0.00	-100%
17	23.64	220.32	832%
18	25.84	90.95	252%
19	1.87	0.00	-100%
20	0.93	0.00	-100%
21	131.32	186.98	42%
22	80.14	227.33	184%
23	14.67	31.79	117%
24	10.82	22.07	104%
25	17.16	46.44	171%
26	33.53	148.33	342%
27	30.27	73.96	144%
28	6833.57	14888.77	118%
29	6563.46	5384.21	-18%
30	4.95	0.00	-100%
31	4.89	0.00	-100%
32	6033.05	11625.27	93%

33	6358.52	5689.96	-11%
34	42.63	0.00	-100%
35	5.97	0.00	-100%
36	3625.06	325.12	-91%
37	7844.36	2534.07	-68%
38	0.00	0.00	#DIV/0!
39	0.47	0.00	-100%
40	7247.58	2778.23	-62%
41	4313.61	3005.49	-30%
42	27.54	0.00	-100%
43	17.73	0.00	-100%

Table A- 35. NO Emissions Experimental vs. CHEMKIN Model, ng/J

STD Order	Ng/J		
	Measured	CHEMKIN	Deviation, %
1	3.54	6.18	75%
2	1.86	5.60	202%
3	11.07	6.18	-44%
4	6.34	6.01	-5%
5	1.03	1.15	12%
6	11.40	9.27	-19%
7	4.77	8.81	85%
8	11.69	21.43	83%
9	6.17	1.77	-71%
10	2.72	1.60	-41%
11	7.79	8.19	5%
12	4.73	9.20	94%
13	1.20	4.95	312%
14	6.16	5.06	-18%

15	6.63	9.34	41%
16	19.99	22.49	12%
17	4.49	5.63	25%
18	2.85	5.15	81%
19	15.55	20.13	29%
20	8.63	10.29	19%
21	1.39	1.50	8%
22	7.58	1.66	-78%
23	3.63	9.08	150%
24	9.13	9.13	0%
25	4.58	5.60	22%
26	9.02	77.80	763%
27	8.45	38.85	360%
28	-0.25	0.00	-100%
29	2.74	0.00	-100%
30	0.63	6.94	994%
31	0.22	0.34	49%
32	-0.38	0.00	-100%
33	-0.40	0.00	-100%
34	-0.03	0.99	-4027%
35	0.07	2.17	2864%
36	0.36	10.62	2843%
37	0.00	3.54	#DIV/0!
38	16.03	16.48	3%
39	7.51	4.26	-43%
40	0.00	3.30	#DIV/0!
41	-0.20	3.79	-2042%
42	5.96	4.66	-22%

43	11.27	5.90	-48%
----	-------	------	------

Table A- 36. NOx Emissions Experimental vs. CHEMKIN Model, ng/J

STD Order	Ng/J		
	Measured	CHEMKIN	Deviation, %
1	8.82	7.80	-12%
2	6.30	7.21	15%
3	17.45	8.35	-52%
4	13.65	8.10	-41%
5	10.19	3.62	-64%
6	16.72	10.43	-38%
7	10.83	9.34	-14%
8	19.60	22.58	15%
9	13.68	3.99	-71%
10	10.41	4.04	-61%
11	14.26	8.66	-39%
12	10.98	9.71	-12%
13	6.52	6.62	1%
14	13.90	7.27	-48%
15	12.79	10.27	-20%
16	29.43	23.82	-19%
17	10.34	7.53	-27%
18	8.72	7.04	-19%
19	23.56	21.29	-10%
20	15.74	11.50	-27%
21	7.97	3.65	-54%
22	17.53	4.56	-74%

23	8.75	9.52	9%
24	15.73	9.67	-39%
25	10.74	7.44	-31%
26	16.29	78.26	381%
27	14.36	39.00	172%
28	8.23	0.01	-100%
29	-1.64	0.00	-100%
30	13.17	6.99	-47%
31	4.86	0.74	-85%
32	5.57	0.03	-100%
33	1.73	0.00	-100%
34	6.27	1.36	-78%
35	3.07	2.74	-11%
36	13.21	10.96	-17%
37	6.99	4.67	-33%
38	20.49	17.87	-13%
39	11.50	5.47	-52%
40	6.51	4.18	-36%
41	8.73	5.10	-42%
42	10.24	5.98	-42%
43	15.06	7.64	-49%

Table A- 37. Perfectly Premixed CHEMKIN Results

STD Order	15% O2 ppmvd			Ng/J		
	CO	NO	NOx	CO	NO	NOx
1	26.90	2.48	3.01	14.85	2.53	3.36
2	63.00	2.74	3.26	34.80	2.79	3.60

3	21.20	2.50	3.21	14.11	2.55	3.66
4	46.00	2.94	3.61	30.47	3.00	4.04
5	184.00	0.52	1.25	142.63	0.57	1.81
6	0.00	1.44	2.28	0.00	1.09	2.07
7	78.20	7.99	8.30	39.96	8.81	9.34
8	0.00	4.39	4.99	0.00	3.33	4.03
9	107.00	0.66	1.49	80.66	0.68	1.97
10	165.00	0.78	1.56	124.52	0.80	2.01
11	27.10	8.03	8.33	13.43	8.19	8.66
12	72.70	9.02	9.35	36.02	9.20	9.71
13	64.10	2.24	2.73	36.43	2.47	3.30
14	47.10	2.29	2.94	32.14	2.53	3.62
15	0.00	1.72	2.42	0.00	1.31	2.12
16	0.00	4.05	4.78	0.00	3.08	3.92
17	31.20	2.06	2.64	19.36	2.27	3.25
18	73.10	2.33	2.89	45.38	2.57	3.52
19	0.00	3.44	4.10	0.00	2.61	3.38
20	0.00	1.86	2.66	0.00	1.41	2.34
21	138.00	0.73	1.42	93.49	0.75	1.82
22	135.00	0.81	1.74	113.58	0.83	2.27
23	69.50	8.91	9.19	31.79	9.08	9.52
24	41.10	8.95	9.30	22.07	9.13	9.67
25	38.40	2.74	3.33	23.17	2.79	3.71
26	184.00	38.10	38.20	73.96	38.85	39.00
27	184.00	38.10	38.20	73.96	38.85	39.00
28	0.00	0.00	0.00	0.00	0.00	0.00
29	0.00	0.00	0.00	0.00	0.00	0.00
30	0.00	0.00	0.00	0.00	0.00	0.00

31	0.00	0.00	0.00	0.00	0.00	0.00
32	0.00	0.00	0.00	0.00	0.00	0.00
33	0.00	0.00	0.00	0.00	0.00	0.00
34	0.00	0.00	0.00	0.00	0.00	0.00
35	0.00	0.00	0.00	0.00	0.00	0.00
36	0.00	0.00	0.00	0.00	0.00	0.00
37	2440.00	0.05	0.49	2479.60	0.05	0.74
38	0.00	0.19	1.17	0.00	0.15	1.28
39	0.00	0.30	1.27	0.00	0.23	1.36
40	3080.00	0.03	0.35	2733.85	0.03	0.53
41	2510.00	0.04	0.56	2958.35	0.04	0.85
42	0.00	0.26	1.12	0.00	0.20	1.20
43	0.00	0.27	1.41	0.00	0.21	1.53

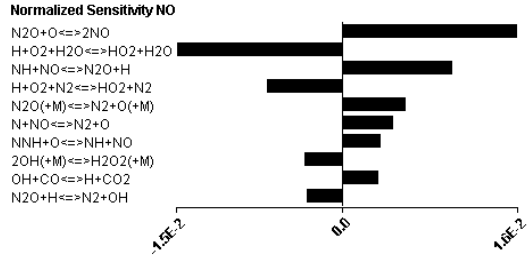


Figure A- 21. NO Normalized Sensitivity for STD 13 (100% CH4) for PFR

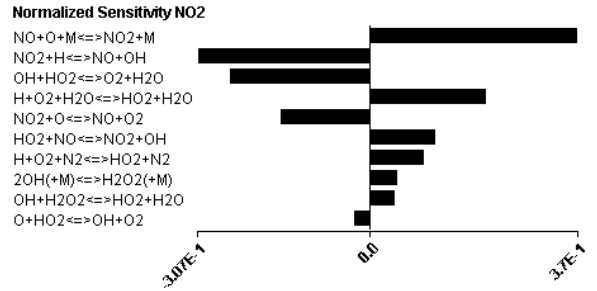


Figure A- 22. NO2 Normalized Sensitivity for STD 13 (100% CH4) for PFR

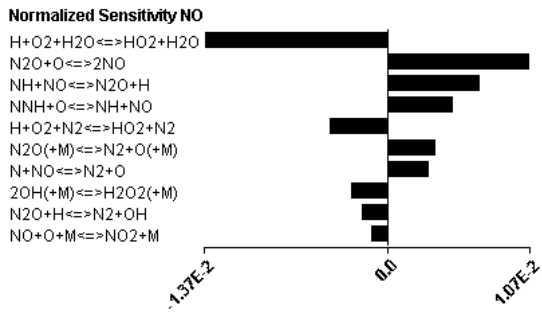


Figure A- 23. NO Normalized Sensitivity for STD 16 (100% H2) for PFR

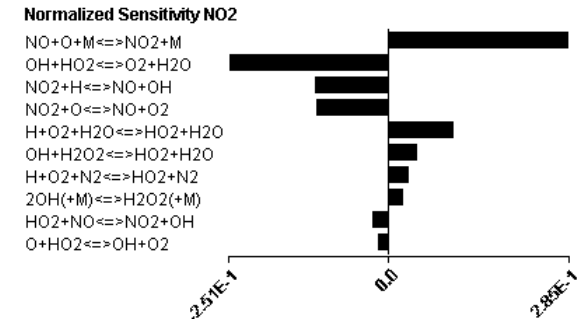


Figure A- 24. NO2 Normalized Sensitivity for STD 16 (100% H2) for PFR

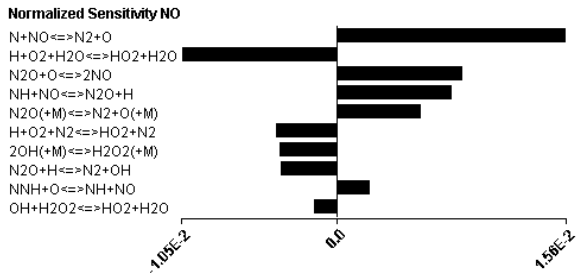


Figure A- 25. NO Normalized Sensitivity for STD 7 (100% CH4) for PFR

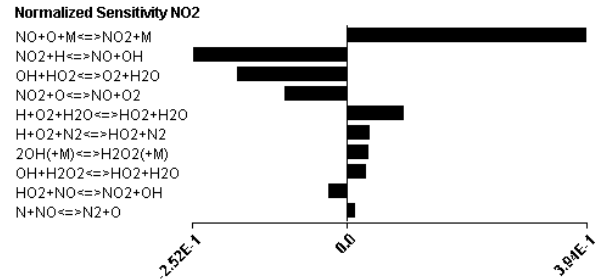


Figure A- 26. NO Normalized Sensitivity for STD 7 (100% CH4) for PFR

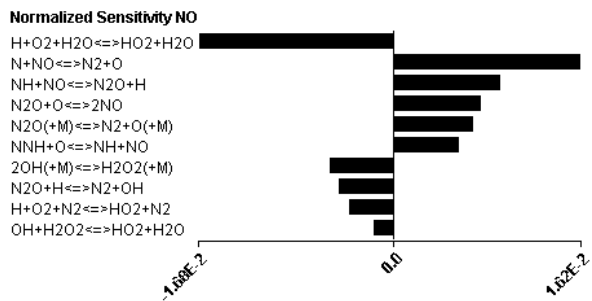


Figure A- 27. NO2 Normalized Sensitivity for STD 8 (100% H2) for PFR

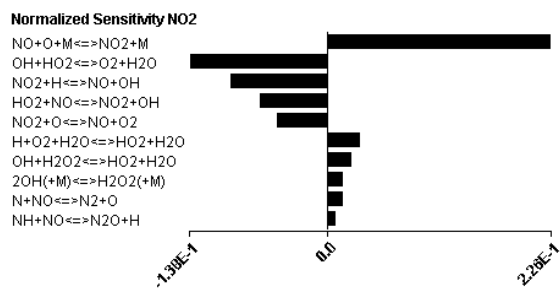


Figure A- 28. NO2 Normalized Sensitivity for STD 8 (100% H2) for PFR

References

- [1] United States Environmental Protection Agency, "Clean Air Act Text," United States Environmental Protection Agency, 24 March 2021. [Online]. Available: <https://www.epa.gov/clean-air-act-overview/clean-air-act-text>. [Accessed 21 April 2022].
- [2] United States Environmental Protection Agency, "Final Rule for Control of Air Pollution From Aircraft and Aircraft Engines; Emission Standards and Test Procedures," Federal Register, Washington, D.C. , 2012.
- [3] United States Environmental Protection Agency, "Milestones in EPA and Environmental History," United States Environmental Protection Agency, 5 May 2021. [Online]. Available: <https://www.epa.gov/history/milestones-epa-and-environmental-history>. [Accessed 21 April 2022].
- [4] N. Rott, "How The EPA Became A Victim Of Its Own Success," National Public Radio (NPR), 17 February 2017. [Online]. Available: <https://www.npr.org/2017/02/17/515748401/how-the-epa-became-a-victim-of-its-own-success>. [Accessed 15 August 2022].
- [5] United States Environmental Protection Agency, "Nitrogen Oxides (NOx) Control Regulations," United States Environmental Protection Agency, 28 March 2022. [Online]. Available: <https://www3.epa.gov/region1/airquality/nox.html>. [Accessed 2022 April 21].
- [6] Mitsubishi Power, "Turbines driven purely by hydrogen in the pipeline," [Online]. Available: <https://www.nature.com/articles/d42473-020-00545-7>. [Accessed 25 November 2022].
- [7] GE (General Electric) Gas Power, "Hydrogen fueled gas turbines," [Online]. Available: <https://www.ge.com/gas-power/future-of-energy/hydrogen-fueled-gas-turbines>. [Accessed 25 November 2022].
- [8] T. Asai, S. Dodo, H. Koizumi, H. Takahashi, S. Yoshida and H. Inoue, "EFFECTS OF MULTIPLE-INJECTION-BURNER CONFIGURATIONS ON COMBUSTION CHARACTERISTICS FOR DRY LOW-NOX COMBUSTION OF HYDROGEN-RICH FUELS," in *Proceedings of ASME Turbo Expo 2011*, Vancouver, British Columbia, Canada, 2011.
- [9] T. Asai, S. Dodo, M. Karishuku, N. Yagi, Y. Akiyaman and A. Hayashi, "Performance of Multiple-Injection Dry Low-NOx Combustors on Hydrogen-Rich Syngas Fuel in an IGCC Pilot Plant," *Journal of Engineering for Gas Turbines and Power* , vol. 137, pp. 1-11, 2015.
- [10] Mitsubishi Power, "Mitsubishi Power to Establish Hydrogen Power Demonstration Facility
] "Takasago Hydrogen Park" at Takasago Machinery Works," 22 February 2022. [Online]. Available: <https://power.mhi.com/regions/amer/news/20220222>. [Accessed 25 Novemeber 2022].
- [11] Clean Air Technology Center, "Nitrogen Oxides (NOx), Why and How They Are Controlled,"
] United States Environmental Protection Agency , Research Triangle Park, NC, 1999.
- [12] B. Fumeya, T. Buetler and U. Vogt, "Ultra-low NOx emissions from catalytic hydrogen
] combustion," *Applied Energy* , vol. 213, pp. 334-342, 2018.

- [13 P. O. Thevenin, P. G. Menon and S. G. Järås, "Catalytic processes to convert methane: partial or
] total oxidation Part II: Catalytic total oxidation of methane," CAT TECH, 2003.
- [14 C. Fenimore, "Formation of Nitric Oxide in Premixed Hydrocarbon Flames," *Symposium
] (International) On Combustion* , vol. 13, no. 1, pp. 373-380, 1970.
- [15 R. PRASAD, L. A. KENNEDY and E. RUCKENSTEIN, "Catalytic Combustion," *Science and
] Engineering*, vol. 26, no. 1, pp. 1-58, 1984.
- [16 Y. Zeldovich, P. Sadovnikov and D. Frank-Kamenetskii, *Oxidation of nitrogen in combustion*,
] Moscow: Academy of Sciences of the USSR, 1947.
- [17 S. R. Turns, *An Introduction to Combustion: Concepts and Applications*, Boston : McGraw Hill,
] 2000.
- [18 A. L. Purohit, A. Nalbandyan, P. C. Malte and I. V. Novosselov, "NNH mechanism in low-NOx
] hydrogen combustion: Experimental and numerical analysis of formation pathways," *Fuel*, vol. 292,
pp. 1-11, 2021.
- [19 S. J. Klippenstein, L. B. Harding, P. Glarborg and J. A. Miller, "The role of NNH in NO formation
] and control," *Combustion and Flame*, vol. 158, pp. 774-789, 2011.
- [20 M. C. Drake and R. J. Blint, "Calculations of NOx Formation Pathways in Propagating Laminar,
] High Pressure Premixed CH₄/Air Flames," *COMBUSTION SCIENCE AND TECHNOLOGY*, vol.
75, pp. 261-285, 1991.
- [21 ANSYS Inc., "13.1 NOx Formation (Theory Guide)," ANSYS Fluent Release 12.0, Canonsburg,
] PA, 2009.
- [22 R. C. Steele, A. C. Jarrett, P. C. Malte, J. H. Tonouchi and D. G. Nicol, "Variables Affecting NOx
] Formation in Lean-Premixed Combustion," *Journal of Engineering for Gas Turbines and Power* ,
vol. 119, pp. 102-107, 1997.
- [23 B. S. Mohammad, K. McManus, A. Brand, A. M. Elkady and D. Cuppoletti, "HYDROGEN
] ENRICHMENT IMPACT ON GAS TURBINE COMBUSTION CHARACTERISTICS," in *ASME
Turbo Expo 2020*, Virtual, Online, 2020.
- [24 New World Encyclopedia , "Combustion," New World Encyclopedia, 2020.
]
- [25 U.S. E.P.A. (United States Environmental Protection Agency) , "What is the average level of carbon
] monoxide in homes?," 30 December 2021. [Online]. Available: <https://www.epa.gov/indoor-air-quality-iaq/what-average-level-carbon-monoxide-homes>. [Accessed 25 November 2022].
- [26 Acurex Environmental Corporation; Edward Aul & Associates, Inc.; E.H. PEchan and Associates,
] Inc., "EMISSION FACTOR DOCUMENTATION FOR AP-42 SECTION 1.5 LIQUEFIED
PETROLEUM GAS COMBUSTION," U.S. Environmental Protection Agency , Research Triangle
Park, NC, 1993.

- [27 National Institute of Standards and Technology , "Thermophysical Properties of Fluid Systems," 2022. [Online]. Available: <https://webbook.nist.gov/chemistry/fluid/>. [Accessed 25 November 2022].
- [28 S. R. Hernandez, Q. Wang, V. McDonell, A. Mansour, E. Steinhorsson and B. Hollon, "MICRO-MIXING FUEL INJECTORS FOR LOW EMISSIONS HYDROGEN COMBUSTION," in *Turbo Expo: Power for Land, Sea, and Air*, Berlin, Germany, 2008.
- [29 E. Æsøy, T. Indlekofer, F. Gant, A. Cuquel, M. R. Bothiena and J. R. Dawson, "The effect of hydrogen enrichment, flame-flame interaction, confinement, and asymmetry on the acoustic response of a model can combustor," *Combustion and Flame*, vol. 242, pp. 1-11, 2022.
- [30 P. Therkelsen, J. Mauzey, V. McDonell and S. Samuelsen, "EVALUATION OF A LOW EMISSION GAS TURBINE OPERATED ON HYDROGEN," in *ASME Turbo Expo 2006: Power for Land, Sea and Air*, Barcelona, Spain, 2006.
- [31 T. Lieuwen, V. McDonell, E. Petersen and D. Santavicca, "Fuel Flexibility Influences on Premixed Combustor Blowout, Flashback, Autoignition, and Stability," *Journal of Engineering for Gas Turbines and Power*, vol. 130, pp. 1-10, 2008.
- [32 D. A. Crowla and Y.-D. Job, "The hazards and risks of hydrogen," *Journal of Loss Prevention in the Process Industries*, vol. 20, pp. 158-164, 2007.
- [33 I. Glassman, *Combustion*, San Diego: Academic Press, 1996.
- [34 A. Lantz, R. Collin, M. Alden, A. Lindholm, J. Larfeldt and D. Lorstad, "Investigation of Hydrogen Enriched Natural Gas Flames in a SGT-700/800 Burner Using OH PLIF and Chemiluminescence Imaging," *Journal of Engineering for Gas Turbines and Power* , vol. 137, pp. 1-8, 2015.
- [35 H. S. Kim, V. K. Arghode and A. K. Gupta, "Flame characteristics of hydrogen-enriched methane-air premixed swirling flames," *International Journal of Hydrogen Energy* , vol. 34, pp. 1063-1073, 2009.
- [36 W. D. York, W. S. Ziminsky and E. Yilmaz, "Development and Testing of a Low NO_x Hydrogen Combustion System for Heavy-Duty Gas Turbines," *Journal of Engineering for Gas Turbines and Power*, vol. 135, pp. 1-8, 2013.
- [37 B. S. Mohammad, N. Magina, B. Volk and K. Mcmanus, "IMPACT OF HIGH HYDROGEN OPERATION ON COMBUSTOR PERFORMANCE," in *Turbomachinery Technical Conference and Exposition* , Rotterdam, The Netherlands, 2022.
- [38 B. Shaffer, Z. Duan and V. McDonell, "Study of Fuel Composition Effects on Flashback Using a Confined Jet Flame Burner," *Journal of Engineering for Gas Turbines and Power*, vol. 135, pp. 1-9, 2013.

- [39 A. Choudhuri, "Effects of Combustion-Induced Vortex Breakdown on Flashback Limits of Syngas-Fueled Gas Turbine Combustors," Center for Space Exploration and Technology Research, El Paso, TX, 2011.
- [40 D. N. Anderson, "EMISSIONS OF OXIDES OF NITROGEN FROM AN EXPERIMENTAL PREMIXED-HYDROGEN BURNER," NASA Lewis Research Center, Cleveland, Ohio, 1976.
- [41 C. T. BOWMAN, "CONTROL OF COMBUSTION-GENERATED NITROGEN OXIDE EMISSIONS: TECHNOLOGY DRIVEN BY REGULATION," *Twenty-Fourth Symposium (International) on Combustion/The Combustion Institute*, pp. 859-878, 1992.
- [42 Clean Air Technology Center, "Nitrogen Oxides (NOx), Why and How They Are Controlled," United States Environmental Protection Agency, Research Triangle Park, North Carolina, 1999.
- [43 S. Hernandez, Q. Wang, H. Lee, V. McDonell, B. Hollon, A. Mansour and E. Steinthorsson, "Micro-mixing Fuel Injection for Low Emission Combustion of Hydrogen for Gas Turbine Applications," in *International Pittsburgh Coal Conference*, Pittsburgh, PA, USA, 2009.
- [44 B. Hollon, E. Steinthorsson, A. Mansour, V. McDonell and H. Lee, "ULTRA-LOW EMISSION HYDROGEN/SYNGAS COMBUSTION WITH A 1.3 MW INJECTOR USING A MICRO-MIXING LEAN-PREMIX SYSTEM," in *ASME Turbo Expo 2011*, Vancouver, British Columbia, Canada, 2011.
- [45 R. Tacina, P. Laing, C. Wey and A. Mansour, "SECTOR TESTS OF A LOW-NOX, LEAN-DIRECT-INJECTION, MULTIPOINT INTEGRATED MODULE COMBUSTOR CONCEPT," in *ASME Turbo Expo 2002*, Amsterdam, the Netherlands, 2002.
- [46 R. Tacina, L. Partelow, A. Mansour and C. Wey, "EXPERIMENTAL SECTOR AND FLAME-TUBE EVALUATIONS OF A MULTIPOINT INTEGRATED MODULE CONCEPT FOR LOW EMISSION COMBUSTORS," in *ASME Turbo Expo 2004, Power for Land, Sea and Air*, Vienna, Austria, 2004.
- [47 M. Hussain, A. Abdelhafez, M. A. Nemitallah and M. A. Habib, "MICROMIXERS AND HYDROGEN ENRICHMENT: THE FUTURE COMBUSTION TECHNOLOGY IN ZERO-EMISSION POWER PLANTS," in *ASME Power Conference*, Online, Virtual , 2020.
- [48 A. H. Ayed, K. Kusterer, H.-W. Funke, J. Keinz, C. Striegan and D. Bohn, "Experimental and numerical investigations of the dry-low-NOx hydrogen micromix combustion chamber of an industrial gas turbine," *Propulsion and Power Research* , vol. 4, no. 3, pp. 123-131, 2015.
- [49 T. A. Satochi Dodo, H. Koizumi, H. Takahashi, S. Yoshida and H. Inoue, "COMBUSTION CHARACTERISTICS OF A MULTIPLE-INJECTION COMBUSTOR FOR DRY LOW-NOX COMBUSTION OF HYDROGEN-RICH FUELS UNDER MEDIUM PRESSURE," in *ASME Turbo Expo 2011*, Vancouver, British Columbia, Canada, 2011.
- [50 H. Lee, S. Hernandez, V. McDonell, E. Steinthorsson, A. Mansour and B. Hollon, "DEVELOPMENT OF FLASHBACK RESISTANT LOW-EMISSION MICRO-MIXING FUEL

INJECTOR FOR 100% HYDROGEN AND SYNGAS FUELS," in *ASME Turbo Expo 2009: Power for Land, Sea and Air*, Orlando, Florida, USA, 2009.

- [51 H. H. W. Funke, N. Beckmann, J. Keinz and S. Abanteriba, "Numerical and Experimental Evaluation of a Dual-Fuel Dry Low-NO_x Micromix Combustor for Industrial Gas Turbine Applications," *Journal of Thermal Science and Engineering Applications*, vol. 11, pp. 1-9, 2019.
- [52 General Electric Gas Power, "GE 7F gas turbine," General Electric Gas Power, [Online]. Available: <https://www.ge.com/gas-power/products/gas-turbines/7f>. [Accessed 29 June 2022].
- [53 General Electric Gas Power, "9F Gas Turbine," General Electric Gas Power, [Online]. Available: <https://www.ge.com/gas-power/products/gas-turbines/9f>. [Accessed 30 July 2022].
- [54 General Electric Gas Power, "6F gas turbine," General Electric Gas Power, [Online]. Available: <https://www.ge.com/gas-power/products/gas-turbines/6f>. [Accessed 30 July 2022].
- [55 The Mitsubishi Heavy Industries Ltd., "Development of Hydrogen and Natural Gas Co-firing Gas Turbine," Mitsubishi Heavy Industries Technical Review, 2018.
- [56 A. Horikawa, K. Okada, M. Yamaguchi, S. Aoki, M. Wirsum, H. H.-W. Funke and K. Kusterer, "COMBUSTOR DEVELOPMENT AND ENGINE DEMONSTRATION OF MICRO-MIX HYDROGEN COMBUSTION APPLIED TO M1A-17 GAS TURBINE," in *Turbomachinery Technical Conference and Exposition*, Online, 2021.
- [57 N. Tekin, M. Ashikaga, A. Horikawa and H. Funke, "Enhancement of fuel flexibility of industrial gas turbines by development of innovative hydrogen combustion systems," *Gas for Energy*, 2018.
- [58 K. B. S. Coogana and D. Teraji, "Micromix combustor for high temperature hybrid gas turbine concentrated solar power systems," *Energy Procedia*, vol. 49, pp. 1298-1307, 2014.
- [59 S. Coogan, K. Brun and D. Teraji, "DESIGN OF A MICROMIX FUEL INJECTOR FOR HIGH TEMPERATURE HYBRID CONCENTRATED SOLAR POWER PLANTS," in *ASME 2014 8th International Conference on Energy Sustainability*, Boston, Massachusetts, USA, 2014.
- [60 X. Lu, B. Forrest, S. Martin and J. Fetvedt, in *ASME Turbo Expo 2016: Turbine Technical Conference and Exposition*, Seoul, South Korea, 2016.
- [61 Kawasaki Heavy Industries, Ltd., "World's First Successful Technology Verification of 100% Hydrogen-fueled Gas Turbine Operation with Dry Low NO_x Combustion Technology," New Energy and Industrial Technology Development Organization (NEDO), Japan, 2020.
- [62 Kawasaki Heavy Industries, Ltd., "Kawasaki Develops Forty-percent-hydrogen Mixed-fuel Technology in Gas Turbine DLE Combustors," Kawasaki Heavy Industries, Ltd., Japan, 2021.
- [63 J. L. Sorrels, "Selective Catalytic Reduction," U.S. Environmental Protection Agency, Research Triangle Park, NC, 2019.
- [64 NO_x CONTROL TECHNICAL DIVISION INSTITUTE OF CLEAN AIR COMPANIES, INC., "SELECTIVE CATALYTIC REDUCTION (SCR) CONTROL OF NO_x EMISSIONS FROM

FOSSIL FUEL-FIRED ELECTRIC POWER PLANTS," INSTITUTE OF CLEAN AIR COMPANIES, INC., 2009.

- [65 H. Sinzenich, "HOW DOES SELECTIVE CATALYTIC REDUCTION WORK?," Mtu a Rolls Royce Solution, 19 May 2014. [Online]. Available: <https://www.mtu-solutions.com/na/en/stories/technology/research-development/how-does-selective-catalytic-reduction-work.html#:~:text=In%20the%20case%20of%20selective,flow%20using%20a%20metering%20module..> [Accessed 29 November 2022].
- [66 J. Holman and W. J. G. Jr., Experimental Methods for Engineers Eighth Edition, New York, New York: McGraw Hill Book Company , 2012.
- [67 C. M. Douglas, S. L. Shaw, T. D. Martz, R. C. Steele, D. R. Noble, B. L. Emerson and T. C. Lieuwen, "Pollutant Emissions Reporting and Performance Considerations for Hydrogen-Hydrocarbon Fuels in Gas Turbines," *Journal of Engineering for Gas Turbines and Power*, vol. 144, pp. 1-7, 2022.
- [68 B. Magnussen and B. Hjertager, "On mathematical modeling of turbulent combustion with special emphasis on soot formation and combustion," *Symposium (International) of Combustion* , vol. 16, no. 1, pp. 719-729, 1977.
- [69 A. Colorado, "Pollutant Emissions and Lean Blowoff Limits of Fuel Flexible Burners Operating on Gaseous Renewable and Fossil Fuels," University of California, Irvine , Irvine , 2016.
- [70 S. Bragg, "Application of Reaction Rate Theory to Combustion Chamber Analysis," Aeronautical Research Council, London (England), 1953.
- [71 A. Colorado and V. McDonell, "REACTOR NETWORK ANALYSIS TO ASSESS FUEL COMPOSITION EFFECTS ON NO_x EMISSIONS FROM A RECUPERATED GAS TURBINE," in *ASME Turbo Expo 2014: Turbine Technical Conference and Exposition*, Düsseldorf, Germany, 2014.
- [72 C. Hernandez, V. McDonell, J. Delimont, G. Oskam and M. Ramotowski, "EXPLORING USE OF HYDROGEN FOR EXTENDING OPERABILITY OF A FULL-SCALE ANNULAR COMBUSTOR," in *ASME Turbo Expo 2021: Turbomachinery Technical Conference and Exposition*, Online, 2021.
- [73 T. Rutar and P. Malte, "NO_x Formation in High-Pressure Jet-Stirred Reactors With Significance to Lean-Premixed Combustion Turbines," *Journal of Engineering for Gas Turbines and Power* , vol. 124, pp. 776-783, 2002.
- [74 Reaction Design , "ANSYS Chemkin Theory Manual 17.0," San Diego , 2016.
- [75 G. Leonard and J. Stegmaier, "Development of an Aeroderivative Gas Turbine Dry Low Emissions Combustion System," *Journal of Engineering for Gas Turbines and Power*, vol. 116, pp. 542-546, 1994.

- [76 F. Barbir, "Transition to Renewable Energy Systems with Hydrogen as an Energy Carrier," *Energy*, pp. 308-312, 2009.
- [77 J. OGDEN, "High Hopes for HYDROGEN," *Scientific American*, vol. 295, no. 3, pp. 94-101, 2006.
- [78 S. Singh, S. Jain, V. PS, A. K. Tiwari, M. R. NouniJitendra, J. K. Pandey and S. Goel, "Hydrogen: A sustainable fuel for future of the transport sector," *Renewable and Sustainable Energy Reviews*, vol. 51, pp. 623-633, 2015.
- [79 J. Li, H. Huang, N. Kobayashi, Z. He and Y. Nagai, "Study on using hydrogen and ammonia as fuels: Combustion characteristics and NOx formation," *International Journal of Energy Research*, vol. 38, pp. 1214-1223, 2014.
- [80 S. R. Bell and M. Gupta, "Extension of the Lean Operating Limit for Natural," *Combustion Science and Technology*, vol. 123, pp. 23-48, 1997.
- [81 M. Momirlan and T. Veziroglu, "The properties of hydrogen as fuel tomorrow in sustainable energy system for a cleaner planet," *International Journal of Hydrogen Energy*, vol. 30, pp. 795-802, 2005.
- [82 D. L. Daggett, L. Fucke, R. C. Hendricks and D. J. Eames, "Water Injection on Commercial Aircraft to Reduce Airport Nitrogen Oxides," NASA Glenn Research Center, Cleveland, Ohio, 2004.
- [83 D. N. Anderson, R. R. Tacina and T. S. Mroz, "PERFORMANCE OF A CATALYTIC REACTOR AT SIMULATED GAS TURBINE COMBUSTOR OPERATING CONDITIONS," NASA Lewis Research Center, Cleveland, Ohio, 1975.
- [84 w. s. BLAZOWSKI and D. E. WALSH, "Catalytic Combustion: An Important Consideration for Future Applications," *Combustion Science and Technology*, vol. 10, pp. 223-244, 1975.
- [85 A. C. MAURO A. GALBIATI, A. EFFUGGI, D. GELOSA and R. ROTA, "MILD COMBUSTION FOR FUEL-NOX REDUCTION," *Combustion, Science and Technology*, vol. 176, pp. 1035-1054, 2004.
- [86 T. J. ROSFJORD, "CATALYTIC COMBUSTORS FOR GAS TURBINE ENGINES," in *American Institute of Aeronautics and Astronautics*, Washington, DC, 1976.
- [87 V. J. Siminski and H. Shaw, "DEVELOPMENT OF A CATALYTIC COMBUSTOR FOR AIRCRAFT GAS TURBINE ENGINES," EXXON RESEARCH AND ENGINEERING COMPANY, Linden, New Jersey, 1976.
- [88 B. Tran, "Pre-Evaluating Emissions from an Aero Engine Injector," University of California, Irvine, Irvine, CA, 2022.
- [89 C. Clifford, "Hydrogen power is gaining momentum, but critics say it's neither efficient nor green enough," CNBC, 6 January 2021. [Online]. Available: <https://www.cnbc.com/2022/01/06/what-is-green-hydrogen-vs-blue-hydrogen-and-why-it-matters.html>. [Accessed 2 July 2022].

[90 U. Bossel and B. Eliasson, "Energy and the Hydrogen Economy," U.S. Department of Energy:
] Energy Efficiency and Renewable Energy .